COMPUTER SIMULATION OF IMPACT BEHAVIOUR OF SPHERICAL AGGLOMERATES USING DISTINCT ELEMENT METHOD

by

Roberto Moreno

A thesis submitted for the degree of

Doctor of Philosophy

at the

University of Surrey

Guildford, Surrey, GU2 7XH

March 2003

To God

" Love your neighbour as you love yourself "

The Bible

Matthew, chapter 22, verse 40

ABSTRACT

Chemical, pharmaceutical and food industries amongst many others, use agglomerates either as intermediate or manufactured products. The mechanical strength of agglomerates under impact or shear deformation during handling and processing is of great interest to these industries for optimising product specification and functionality.

This thesis focuses on the analysis of agglomerate behaviour under impact using Distinct Element Analysis (DEA). Special attention has been paid to the influence of the interface energy representing the inter-particle bond strength, the impact angle and the agglomerate size on the breakage of the agglomerate.

A model based on the hypothesis that the work expended in the breakage of contacts is proportional to the incident kinetic energy has been developed in order to predict the influence of the interface energy on the number of contacts broken upon impact. The agglomerate breakage pattern is also influenced by the interface energy. At sufficiently low values of the interface energy agglomerates fail by disintegrating into small fragments without any evidence of crack propagation. When the interface energy is increased the agglomerates show crack propagation accompanied by the disintegration of the contact area into small fragments.

The analysis of the effect of the agglomerate size on the breakage pattern shows an increase in the tendency to fragmentation into a large number of pieces as the agglomerate size is increased.

The investigations on the effect of the impact angle show that the number of broken contacts depends only on the normal component of the impact velocity. However, for the same number of broken contacts but different impact angles, the fragmentation pattern is different, clearly indicating the influence of the impact angle on the breakage pattern.

This work has produced a better understanding of some of the factors that affect the agglomerate strength. However many other factors, such as elastic modulus, strain rate effect of bond breakage and method of agglomerate preparation, influence the breakage of agglomerates and therefore their analysis should be addressed in the future.

ACKNOWLEDGEMENTS

I would like to acknowledge the work of my supervisor Prof. Mojtaba Ghadiri for his help in forming me as a researcher and as a person which beyond any doubt will help me in my future career. He has also taught me that a scientist should be able to transmit and diffuse his knowledge to others. Finally I would like to thank him for his deep and constructive criticism of my dissertation.

I would also like to express my acknowledgment to my supervisor at the University of Surrey Dr. Adel Sharif for his help especially during the last days of my PhD period. Alongside Dr. Sharif I want also to give thanks to the other project members Drs J.A.S. Cleaver, S. J. Antony, C. Hodges, L. Looi and H. Ahmed for the interaction and friendly relationship.

I want to express my gratitude to ICI and EPSRC for their financial support of my project and very specially to Prof. R. Oliver and Dr. D. Sutton, who coordinated the project at ICI.

Thanks to Dr. C. Thornton for allowing the use of the computer code TRUBAL within our group and for the comments on the development of the mechanistic model presented in this work.

I cannot forget my special thanks to Mr. Dennis Golchert for his scientific and grammatical comments on my dissertation. I also want to acknowledge my colleagues and friends for the technical discussions and support during my PhD. I mention them in alphabetical order Mr. P. Brumby, Mr. Y. Chen, Dr. J. Eow, Mr. A. Hassanpour, Dr. S. Hou, Dr. A. Khan, Miss C.C. Kwan, Mr. H. Mio, Mr. A. Samimi, Mr. A. Santomaso.

To my parents Antonio and Lucía and my brother Juan Antonio for their love, support and encouragement. To them all my love and thanks.

Finally, to my beloved and future wife Frances Neville for all her love, patience and support in every moment during the large process of the development of the PhD. In addition, for her help in the learning of the English language which has been invaluable and for her comments on my dissertation.

CONTENTS

NOTATION

Latin characters

A	Hamaker constant	J
A_C	Area of a contact	m^2
a	Contact area radius	m
a_0	Contact area radius at the initial contact point	m
a_y	Contact area radius at yield point	m
c	Crack length	m
c_d	Velocity of propagation of compressive waves	m/s
c_s	Velocity of propagation of shear waves	m/s
d	Distance between spheres	m
D	Particle diameter	m
D_{mp}	Damping coefficient	$kg/sm^{1/4}$
D_R	Damage ratio	-
E_K	Incident kinetic energy of an agglomerate	J
e	Electron charge	C
e_n	Normal restitution coefficient	-
e_t	Tangential restitution coefficient	-
E	Elastic modulus	Pa
F	Force between dipoles	N
F_a	Interparticle bond force	N
F_{cl}	Force to cause lateral fracture	N
F_N	Normal force in a contact	N
F_{ND}	Normal damping force	N
F_{TD}	Tangential damping force	N
G	Shear modulus	Pa
g	gravity	m/s^2
H	Hardness	Pa
h	Mean curvature of a liquid bridge	m^{-1}
I	Momentum of inertia	$kg\ m^2$
K	Boltzman constant	J/K

K_c	Fracture toughness	$Pa\ m^{1/2}$
K_h	Hertz constant	$N/m^{3/2}$
k_n	Normal stifness	N/m
k_t	Tangential stifness	N/m
M	Momentum of a force	J
m	Particle mass	kg
m_B	Mass of one solid bridge	kg
N	Number of particles in an agglomerate	-
N_B	Number of broken contacts	-
N_0	Initial number of bonds in an agglomerate	-
N_p	Number of particles detached from the agglomerate	-
P	External load in a contact	N
P_E	Equivalent elastic force during plastic deformation	N
P_{EFF}	Effective force in JKR model	N
P_{OFF}	Force to break a contact	N
P_y	Force to cause yield	N
q	Density of atoms in a material	cm^{-3}
R	Particle radius	M
R_P	Equivalent elastic radius during unloading with plastic deformation	m
r	Distance from the center of the contact area between particles	m
r_{c1}, r_{c2}	Main curvature radius of a liquid bridge	M
R_B	Breakage energy	
R_p	Equivalent elastic curvature radius	M
T	Tangential force	N
T_{peel}	Maximum tangential force during peeling	N
t	time	s
T_{abs}	Absolute temperature	K
U	Total energy of a solid	J
U_E	Elastic strain energy	J
U_S	Energy expended in creating new surfaces	J
V	Particle velocity	m/s
V_0	Velocity under which no contacts are broken in agglomerates	m/s

V_R	Velocity of propagation of Rayleigh waves	m/s
V_y	Velocity at yield point	m/s
W	Work made by external forces	J
W_C	Work for breaking one contact	J
W_e	Weber Number	-
W'_e	Modified Weber number	-
Z	Coordination number	-
z	Ion valence	-

Greek characters

α	Attrition propensity parameter	-
α_g	Global damping coefficient	kg/s
α_r	Angle of rotation of a particle	Rad
β	Liquid solid contact angle	rad
β_d	Damping ratio	--
Γ	Interface energy	J/m^2
Γ_C	Fracture energy	J/m^2
γ	Surface energy	J/m^2
γ_T	Surface tension	N/m
ΔP_h	Hydrostatic pressure	N/m^2
δ	Agglomerate deformation	m
δ_n	Normal displacement	M
δ_t	Tangential displacement	M
ε	Porosity	-
θ	Impact angle	Rad
θ^*	Parameter in the model of Thornton and Randall	--
θ'	Critical impact angle in the model of Ning and Thornton	Rad
λ	London-van der Waals	J/C^2
μ	Friction coefficient	-
ν	Poisson's ratio	-
ρ	Particle density	kg/m^3

ρ_B	Solid bridge density	kg/m^3
ρ_T	Target density in a impact process	kg/m^3
σ	Strength	Pa
σ_B	Strength of a solid bridge	Pa
σ_y	Yield stress	Pa
σ^S_Y	Static yield stress	Pa
σ^D_Y	Dynamic yield stress	Pa
σ_r	Pressure distribution within the contact area	Pa
Φ	Packing fraction	-
Ω	Half filling angle	Rad

LIST OF TABLES

LIST OF FIGURES

INTRODUCTION

Medicines, foods, paints and many other products which are used daily contain agglomerates. The properties of the primary particles as well as the agglomeration method and the binders used in the process of agglomeration strongly influence the agglomerate functionality and characteristics such as packing, density, structure, and dissolution rate.

Agglomerate strength is an important feature in handling and processing as it should not give rise to excessive attrition and breakage but it should, at the same time, allow dispersion when desired. Therefore agglomerate strength has been the subject of many studies. Agglomerates usually suffer attrition due to collisions with walls during transportation. The strength shown by agglomerates when collided depends not only on the material properties and agglomerate formation process but on factors such as impact velocity, impact angle and wall properties. The agglomerate breakage is undesirable in these cases and it is of interest for many industries to avoid it.

A large number of parameters affect the mechanical strength resistance of agglomerates and this makes the study of agglomerate behaviour very difficult. A systematic mapping out of the influence of all parameters that affect the agglomerate breakage is of great interest for many industries. However, from an experimental point of view this is difficult since the analysis of the influence of one property on agglomerate breakage may change some of the other properties. In contrast, the isolation of only one property for studying its influence on the agglomerate breakage is much more easily achieved by computer simulation.

The objective of this thesis is to analyse the factors that influence agglomerate breakage. However, the analysis of all factors is not possible within the time scale of a thesis due to the extensive computational time required for the formation of agglomerates. Therefore, some of the factors that influence agglomerate breakage have been selected considering their potential importance and the lack of conclusive or extensive results in the literature on the same topics. The content of this thesis can be summarised as follows:

- Chapter 1 presents a review of the influence of the interparticle bonds on agglomerate strength, the characterisation of agglomerate properties, the mode of failure of solid particles and a comparison with the mode of failure of agglomerates. In addition, the models of contact deformation of a single particle are reviewed since they are incorporated into the computer code used in the research carried out in this thesis. The last part of this chapter reviews the most important results of computer simulation of agglomerate impact.

- Chapter 2 shows an analysis of the influence of the agglomeration method on the agglomerate structure. A general description of the impact process is also presented in this chapter and a further comparison between agglomerate and solid particle impact behaviour is carried out.

- Chapter 3 is focused on an investigation of the influence of the bond strength on the breakage of interparticle bonds and mode of failure of agglomerates. This chapter compares the simulation results with the prediction of a new theoretical model which is described in Appendix A.

- Chapter 4 shows an analysis of the effect of the impact angle on the agglomerate breakage pattern. An analysis of the influence of the normal and tangential components of the impact velocity on the breakage of contacts is carried out.

- Chapter 5 presents a comparative analysis of the breakage of contacts and breakage pattern of agglomerates of different sized agglomerates made with the same material properties.

- Chapter 6 shows a detailed analysis of the evolution of the compressive and tensile contacts of the agglomerate during impact. In addition, the analysis of the breakage of contacts that originate the detachment of the largest fragment has been analysed. Finally, impact and compression processes are compared in terms of breakage of contacts, force exerted on the walls and breakage pattern.

- Chapter 7 contains the final conclusions of this thesis highlighting the most important achievements and the possibilities of future work.

CHAPTER 1: LITERATURE REVIEW

1.1 Introduction

The agglomerate behaviour under impact conditions has been analysed in the literature by a number of research workers. The agglomerate behaviour depends on the primary particle properties as well as on the particle interactions and the structure of the agglomerates. The inter-relationship is complex and it does not easily allow the agglomerates behaviour to be predicted.

With the objective of clarifying and discerning the key properties that influence the behaviour of agglomerates a literature survey has been carried out focusing on the following points:

- The analysis of the interparticle interactions has been reviewed and where possible attention has been paid to the relationship between agglomerate strength and the characteristics of the bonds.
- The characterisation of geometrical (*e.g.* porosity, packing fraction) and physical and mechanical properties (*e.g.* elasticity, strength) have been reviewed focusing on the mode of failure of agglomerates.
- The models of normal and oblique contact deformations with and without adhesion have been reviewed. The most relevant pieces of work are the analysis of Hertz (1885), Johnson *et al.* (1971), Derjaguin *et al.* (1975), Mindlin and Deresiewicz (1941), Kendall (1971,1977), Savkoor and Briggs (1977). These models have been used in the Distinct Element Method (DEM) to predict the mechanical behaviour of agglomerates based on the single particle properties.
- Finally a critical review on the reported work on the computer simulation of agglomerate impact using DEM has been carried out and where appropriate simulations have been compared with the experimental results.

1.2 General description of agglomeration

Ennis and Litster, (1997) defined agglomeration as a process where particles are brought together to form a large structure called a granule or an agglomerate in which

the original particles are distinguishable. This definition establishes a way for distinguishing agglomerates from single particles whose primary components, usually molecules, can be orders of magnitude smaller than the particles.

The agglomeration process is a balance between attractive and repulsive forces, which control the characteristics of the structure of the agglomerate (Simon, 1996). Sometimes the attractive forces act in short distances around the particles and therefore collisions are required in order to allow the attractive forces to bind the particles together as in the case of van der Waals forces. Capillary and viscous forces are commonly used in the agglomeration process, which is typically carried out in drums or fluidised beds by spraying certain amount of liquid into the bed (Iveson *et al.,* 2001). In other cases, for example in crystallisation the particles can either solidify or form a solid bridge by crystallising (Tardos and Gupta, 1996) .

Agglomerates can suffer a size reduction by collisions with walls or other agglomerates (Subero, 2001) during transportation which is undesirable. The analysis of agglomerate and bulk particle behaviour under different loading conditions has contributed to a better understanding of the mechanical strength of granular materials and the attrition and comminution behaviour (Kafui and Thornton, 1993, Salman *et al.* 1995, Thornton *et al.*, 1996, Ning *et al.* 1997, Couroyer 2001, Antony and Ghadiri, 2001, Hassanpour, 2003, Moreno *et al.* 2003). Therefore the analysis of the agglomerate strength and its relationship with the agglomerate properties is fundamentally important.

1.3 Binding mechanisms

Agglomerates are made of particles joined by bonds. Simons (1996) suggested that the bonds can be classified in terms of their relative magnitude, from more adhesive to less adhesive bonds in solid bridge forces, followed by liquid bridge forces, van der Waals forces, electrostatic and magnetic forces.

1.3.1 Solid bridge forces

Solid bridges between particles can be formed in different ways. Sintering, melting at high temperatures and the diffusion of the material to form a bridge, rubbing of

particles against each other, where melting occurs due to the heat originated by the friction and the contact pressure, crystallisation, precipitation, chemical reaction and deposition of colloidal material are common mechanisms involved in the process (Simons, 1996).

Pietsch (1969) investigated the tensile strength of agglomerates bound by salt bridges and showed that it is proportional to the tensile strength of the average binding material σ_B .

$$\sigma = \frac{m_B \rho}{m \rho_B}(1-\varepsilon)\sigma_B \qquad (1.1)$$

where m_B is the mass of the bridge, m is the mass of the particles, ε is the porosity and ρ and ρ_B the densities of the particles that form the agglomerate and the binding material. The expression of Pietsch is just the ratio between the volume of the binder and the agglomerate volume multiplied by the strength of the solid bridge.

The applicability of the above expression to agglomerates bound by viscoelastic materials is not clear, where the failure is preceded by an extensive elongation of the bridge. The expression of Pietsch (1969) is linear in terms of the packing fraction, in contrast to the models of Rumpf (1969) and Kendall (1988) who proposed a different dependency of the strength on the packing fraction. This point will be addressed later, where the models of Rumpf (1969) and Kendall (1988) are outlined.

Tardos and Gupta (1996) studied experimentally the formation of two kinds of solid bridges. The first type was due to drying of a concentrated polymer solution and the other due to crystallisation of a saturated salt solution. They showed that large attractive forces appeared, of the order of several hundred times the weight of the bridge in the case of a concentrated polymer. In the case of crystallisation of the saturated salt solution, large forces also appeared but they tended to push the particles apart, due to volume changes as a result of crystallisation. These authors did not develop any theoretical expression and limited their study to the experimental measurement of the formation of the bridge.

1.3.2 Liquid bridge forces

In wet granulation a quantity of liquid is introduced to the particle mass, and depending on the liquid loading, this can form bridges between the particles producing a resultant attractive force between the particles. This process is used in the preparation of fertiliser, ceramic, pesticide and detergent granules. The adhesion force depends on the sum of three effects (Fisher, 1926): the liquid surface tension acting at the liquid-solid boundary, the force exerted by the reduced hydrostatic pressure in the bridge itself and the buoyancy force resulting from the partial immersion of the particles (Fisher, 1926).

To evaluate the capillary force it is necessary to solve the Laplace-Young equation, which relates the hydrostatic pressure within the liquid with the principal radii of curvature of the bridge and the surface tension. The hydrostatic pressure can be expressed as follows (Lian *et al.* 1993):

$$\Delta P_h = 2\gamma_T \left(\frac{1}{r_{c1}} + \frac{1}{r_{c2}} \right) = 2\gamma_T h \qquad (1.2)$$

where ΔP_h is the reduced hydrostatic pressure within the liquid bridge, r_{c1} and r_{c2} are the principal radii of curvature, h is the mean curvature and γ_T the liquid surface tension.

The exact expression for the force between two spheres joined by a liquid bridge is the sum between the surface tension and the hydrostatic pressure as given by Lian *et al.* (1993):

$$F = 2\pi\gamma_T R \sin(\Omega + \beta) \sin\Omega + \pi R^2 \Delta P_h \sin^2 \Omega \qquad (1.3)$$

where β is the contact angle between liquid-solid and Ω is the half filling angle and R is the particle radius.

The main problem in the calculation of the liquid bridge force is the evaluation of the principal radius of curvature in the Young-Laplace equation. Fisher (1926) proposed a simple approach to estimate the liquid bridge forces, in which he approximated the shape of the bridge to a toroid, where the shape of the air-liquid interface became circular as a result of the approximation. A circular shape has a constant radius of curvature which simplifies the calculations. However, the other radius of curvature has to be calculated by several methods making approximations. The first one is called the boundary method (Iveson *et al.*, 2001). This method takes the mean radius of curvature as the one along the three phase contact line (Lian *et al.* 1993). The second method is called the gorge or neck method (Iveson *et al.*, 2001) and takes the mean curvature as the minimum curvature of the toroid which is at the neck of the toroid.

Lian *et al.* (1993) solved the equation numerically and compared the exact results with the toroidal approach. The boundary method overpredicted the exact values of the forces. However, the gorge method was in a good agreement at low separation distance, but when the separation distance increased the gorge method underpredicted the values of the forces in the bridge as compared with the numerical results.

Several authors have studied the problem of the rupture of the liquid bridges establishing different criteria about the point at which the liquid bridge is broken. Mason and Clark (1965) measured the forces between spheres joined by a liquid bridge. They measured the rupture distance of the bridge as a function of the volume of liquid. De Bisschop and Rigole (1982) proposed that rupture occurred when the half-filling angle of the liquid bridge is a minimum. This is the angle between the line connecting the centres of the spheres and the line connecting the contact point of the bridge on the surface to the one of the sphere. This criterion results in an underestimation of about 25-30%. Mazzone *et al.* (1986) solved numerically the Laplace-Young equation including the effect of gravity, and compared it with the experimental results of Mason and Clark (1965), for which they found a good agreement. However, they claimed that there was an increasingly large underestimation as the separation distance between particles increased.

By numerical solution of Laplace equation Lian *et al.* (1993) showed that the critical separation distance for the rupture of a liquid bridge is proportional to the solid-liquid contact angle, θ and the cube root of the liquid volume, V.

$$S = \frac{1}{2}(1 + 0.5\beta)V^{1/3} \qquad (1.4)$$

The problem in the analysis of the liquid bridge arises from the difficulty of solving theoretically the exact model. The investigators have all made some approximations which have produced either an underestimation or overestimation of the results. The model of Lian *et al.* (1993) appears to have the best fit, because no drastic approximation has been made as compared to the other models.

Simons *et al.* (1994) developed an expression for a zero contact angle between the liquid bridge and the particle. In contrast, the model of Willett *et al.* (1998) predicted the rupture energy of a liquid bridge for any contact angle. The dependency of the rupture energy on the volume of the bridge is the same for both models. The advantage of the model of Willet *et al.* (1998) obviously arises from the applicability to the whole range of contact angles, in contrast with the previous model of Simon *et al.* (1994) that considered only zero contact angle.

In spite of significant attempts by various authors to calculate the force between particles bound by a liquid bridge or the rupture condition of the bridge, the models of the liquid bridge have not been widely applied to the analysis of agglomerate behaviour except the numerical simulation work of Lian *et al.* (1998) and of course, of the model of Rumpf (1962) in principle applicable to the case of liquid bridges and it will be discussed later.

1.3.3 Van der Waals forces

These are short range forces arising on the microscopic scale from molecular interactions between the electric fields of permanent and induced dipoles. The interaction energy between dipoles decays with the distance in the form d^{-6}. Hamaker (1937) integrated the expression of the interaction energy in order to calculate the

attraction between two spheres of radius R and containing q atoms per cm^3. The interaction energy obtained by Hamaker (1937) for the attraction between spheres decays linearly with the distance, in contrast to the interaction between single dipoles. In this case the force between spheres decays with the distance between particles, d. The force between spheres should decay with the square of the distance. The expression of the force between spheres is given by Hamaker (1937):

$$F = \frac{AR}{12d^2} \tag{1.5}$$

where the Hamaker constant A depends on the material properties through the number of atoms per cm^3, q, and the London-van de Waals constant, λ:

$$A = \pi^2 q^2 \lambda \tag{1.6}$$

Overbeek (1984) provided some the values of the Hamaker constant for several materials. Some of them are summarised in Table 1.1.

Table 1.1 Hamaker constant in air and in water (after Overbeek, 1984)

A (10^{-20})	Air	Water
Water	4.4	0
Hydrocarbons	4-10	0.3-1
Oxides and halides	6-15	0.5-5
Metals	15-50	5-30

Israelachvili (1985) explained the concept of surface energy as the work per unit area required to separate to an infinite distance two planar surfaces, which are under the influence of the van der Waals forces. This work is the sum of the free energy of the two planes and is therefore twice the work of adhesion of the material.

Roberts (1968) and Kendall (1969) observed that the contact area between two rubber particles at low values of the external load was larger than those predicted by Hertz analysis. The two particles were under a strong adhesion due to the van der Waals attraction. Using the experimental observation of Roberts and Kendall and treating the contact geometry as an annular crack Johnson *et al.* (1971) used the concept of linear elastic fracture mechanics of surface energy to describe the Van der Waals forces in a model of contact between elastic particles. Derjaguin, Muller and Toporov (1975) also investigated the effect of the Van der Waals forces in the contact between an elastic sphere and a rigid wall. These two models will be reviewed later in more detail.

1.3.3 Electrostatic forces

When a charged body approaches a medium that is constituted of dipoles, but it is electrically neutral overall, a net charge separation takes place on the surface of the medium. In this case a net force appears between the medium and the body. This is a polarisation force and the charge induced on the surface of the body is called polarisation charge.

When we have a charged surface in contact with a liquid containing ions of the opposite charge, the surface attracts the ions. The final surface charge is balanced by an equal oppositely charged region of counterions, some of which are temporarily bound to the surface within the so-called 'Stern layer' (Stern, 1924). The others form an atmosphere of ions in rapid thermal motion close to the surface, known as the diffuse electric double layer. This structure was studied first by Gouy (1910) and Chapman (1913).

The Poisson-Boltzmann equation gives the distribution of counterions inside the double layer between two surfaces and can be expressed by

$$\frac{d^2\psi}{dx^2} = -\left(\frac{ze\rho_0}{\varepsilon\varepsilon_0}\right)e^{-ze\psi/KT} \qquad (1.7)$$

where ψ is the potential, z is the ion valence, e is the electron charge , ρ_0 is the counterion density at the middle point of the layer, K is the Boltzmann constant, T is the absolute temperature and ε is the relative permeability of the medium (Israelachvili, 1985).

The DLVO theory (Derjaguin and Landau, 1941, Verwey and Overbeek, 1948) describes the interaction between particles considering two components, one attractive due to the Van der Waals forces and another repulsive due to the interaction of the electrical double layer. Bowen and Sharif (1998) solved the Poisson-Boltzmann equation to calculate the interaction between two spheres confined in a long, charged cylindrical tube. The authors showed that it was possible to obtain attractive forces between two spheres as evidenced in recent experiments and without the need of revising the previous concepts. This attraction is due to the redistribution of the electric double layer of ions and counterions in solution around the spheres caused by the presence of the walls.

In this work the focus is on the solid bridges forces and therefore the applications of electrostatic forces is not consider further.

1.3.4 Discussion

- Binding mechanisms play an important role in the strength of agglomerates. Van der Waals forces allow the sliding of bodies which is otherwise not possible if the particles are bound by solid bridges. This is shown by the work of Ning *et al.* (1996) where extensive agglomerate deformation is observed in agglomerates whose particles are joined by van der Waals forces. Liquid bridges allow the elongation of the bond before rupture. Some types of solid bonds such as viscoelastic bonds also exhibit the same behaviour. The influence of these constrictions in the movement of the particles, due to the bond characteristic on the agglomerate strength, has not been analysed so far.

1.4 Macroscopic characterisation of agglomerates

Agglomerates can be characterised for geometric and physical properties. Important geometric features are packing fraction porosity, volume and number of particles forming the agglomerate. Important physical properties are strength, stiffness, density, shear modulus, toughness and hardness of the agglomerate.

1.4.1 Packing fraction, porosity, contact number, coordination number

Porosity ε is commonly defined as the fraction of voids in a material. Packing fraction is therefore $1-\varepsilon$. For a simple cubic structure (SC) the packing fraction is 0.52 and for a face centred cubic structure (FCC) it is 0.74 for monosize spheres.

The contact number is the number of contacts established in the assembly. The coordination number is the average contact number for each particle in the assembly. As an example the coordination numbers are six and twelve in a simple cubic packing and in a face-centred cubic packing, respectively. Packing fraction and coordination number are expected to be related to each other since an increase in the packing fraction will produce an increase in the number of contacts for every particle. This fact does not follow any mathematical relationship for the case of random assemblies of particles.

Mishra and Thornton (2001) showed that the fragmentation pattern observed in the impact of two agglomerates with the same packing fraction and different coordination number was different. The agglomerate with a higher coordination number showed a more brittle behaviour (evidence of crack propagation) than the agglomerate with a lower coordination number (disintegration of the agglomerate and no evidence of fragmentation). Mishra and Thornton (2001) suggested that the pattern of force propagation depended on the coordination number.

Ghadiri and Subero (1997) and Subero *et al.* (1999) studied experimentally and by computer simulation the effect of size and number of macro-voids on the strength of agglomerates. Agglomerates with a similar macrovoid size but different number of

macrovoids and therefore different total porosity behaved in a similar way at high impact velocities (Subero, 2001). He observed that agglomerates with a larger size of macrovoids were weaker than agglomerates with a larger number of macrovoids. In this study, although the variation of the total packing fraction of the agglomerate was very low the results of Subero *et* al. (1999) showed clearly the effect of the voids. Subero (2001) evaluated the models of Kendall (1988) and Rumpf (1962) for which the dependency of the agglomerate strength on the packing fraction, ϕ, is in the forms of ϕ^4 and $\phi/(1-\phi)$, respectively. Subero (2001) showed that within the range of practical porosities, these functional relationships have very close values and in any case cannot adequately describe the agglomerate behaviour as a function of porosity because the size of the voids has a stronger effect than the number of voids. However, this was not successful. One of the explanations given by Subero (2001) was that the above mentioned discrepancies with the models in the literature were originated by the fact that such models were developed for tensile fields and did not readily apply to the impact case as was the case in the work of Subero.

Mishra and Thornton (2001) observed that there was a transition of the mode of failure of the agglomerate as a function of the packing fraction. At low values of the packing fraction (0.537) the agglomerate tended to disintegrate upon impact resulting in one large cluster from which a lot of small debris was detached. When the value of the packing fraction increased until 0.571 the agglomerate behaviour was different for different values of the coordination number. In the case when the value of the coordination number was 3.308, agglomerate fragmentation took place. With the same value of packing fraction (0.571) and the value of the coordination number of 3.061 the agglomerate did not fragment. This evidence clearly suggested the importance of the path of propagation of forces on the agglomerate strength. When the packing fraction of the agglomerate was increased to 0.602 the agglomerate fragmented at impact velocities of 1.5 m/s and 2.0 m/s.

The coordination number used by Mishra and Thornton (2001) for a packing fraction of 0.537 is 3.308 which is exceptionally low as compared with the coordination number of other structures with similar values of packing fraction (*i.e. simple cubic:* packing fraction 0.52, coordination number 6.0; random packing reported by Ning *et al.*

(1997): packing fraction 0.522 and coordination number 5.4). Therefore, the comparison of the computer simulation results with any experimental data could be a difficult objective to achieve. In addition, such a low value of the coordination number used by Mishra and Thornton (2001) might influence the range of packing fraction where fragmentation is observed.

1.4.2 Elasticity and surface energy

For assemblies made of well-packed fine particles, the primary particles may be cohesive and the assembly may exhibit elastic properties. Interface energy is defined as the work per unit area needed to separate two surfaces to an infinite distance. This definition of interface energy, Γ, can be expressed by the Dupré equation (Israelachvili, 1985).

$$\Gamma = \gamma_1 + \gamma_2 - \gamma_{12} \qquad (1.8)$$

where γ_1 and γ_2 are the surface energies of the two surfaces and γ_{12} an interaction term between both surfaces.

Kendall *et al.* (1987) developed an expression for the elastic modulus, E^*, (Young's modulus) of a cubic assembly of spheres of diameter, D, as a function of the packing fraction, ϕ, Young's modulus of the particles E and interface energy:

$$E^* = 17.1\phi^4 \left[\frac{\Gamma E^2}{D}\right]^{1/3} \qquad (1.9)$$

Kendall *et al.* (1987) extended the applicability of the above equation to random packings of uniform spheres. When they compared their predictions with the experimental results for titania, zirconia and silica measured experimentally they found that the values obtained in experiments were lower than those predicted by the theory. This observation was attributed to the presence of impurities on the samples. However, Thornton (1993) developed an alternative model in which he included the stiffness of the tangential contact and produced a model which was dependent on Poisson's ratio. The expression of Thornton has the same dependencies on the elastic modulus of single

particles, interface energy and particle diameter as the model of Kendall *et al.* (1987) (Eq. 1.9).

$$E^* = 17.61\left(\frac{\chi}{(2+\chi)}\right)(1-\nu^2)^{-2/3}\left(\frac{E^2\Gamma}{D}\right)^{1/3} \tag{1.10}$$

where χ is the ratio between tangential and normal stiffnesses:

$$\chi = \frac{(1-\nu)}{0.3(2-\nu)} \tag{1.11}$$

The results obtained by Thornton (1993) are one order of magnitude lower than those obtained by Kendall *et al.* (1987). Thornton therefore concluded that the differences between the experiment and theory found by Kendall *et al.* (1987) could not be attributed only to surface contamination.

Subero *et al.* (1999) have studied the effect of the surface energy on the strength of agglomerates by performing simulations for different values of the surface energy. They confirmed the previous observations made by Kafui and Thornton (1993) and Thornton *et al.* (1996), that the effect of interface energy on agglomerate damage diminishes as impact velocity increases and that the agglomerate strength increases when the interface energy increases.

1.4.3 Strength and fracture

Agglomerates can suffer mechanical damage during processing or transport. The damage can be by wear of the surface or by fragmentation of the agglomerate. Agglomerates may also be deliberately broken down such as in milling processes. Therefore the strength and fracture of agglomerates is of paramount importance. There are two classical pieces of work reported in the literature, one by Rumpf (1962) based on a simple force balance and another by Kendall (1988) based on fracture mechanics.

Rumpf (1962) developed a theory for agglomerate strength based on the equation for the London-Van der Waals (London, 1937) attractive force between two spherical particles. The expression given by Rumpf of the agglomerate strength is based on the consideration that failure occurs on a plane when the two parts of an agglomerate are pulled apart. A force balance relates the macroscopic tensile force to the microscopic interparticle force on the failure plane. The model of Rumpf (1962) is based on the following hypotheses:

(a) the number of bonds in the cross section is very high;
(b) the bonds are statistically distributed and orientated across the section;
(c) the spheres are statistically distributed in the granule and therefore the cross section is homogenous;
(d) the effective bonding forces are distributed around a mean value;
(e) the breakage of all bonds occurs simultaneously.

Hypotheses (d) and (e) imply that the force to rupture all bonds, σ can be written as the product of the number of bonds on the plane of fracture, n, multiplied by the average force of each bond, $F_{a,}$.

$$\sigma = nF_a \tag{1.12}$$

Once the number of bonds in the failure plane is estimated based on geometrical considerations, the final expression given by Rumpf (1962) for the agglomerate strength is

$$\sigma = \frac{1.1\phi A}{(1-\phi)24d^2 D} \tag{1.13}$$

where ϕ is the packing fraction of the assembly, D the diameter of the spheres and d is the distance between the spheres.

Rumpf (1962) assumed that failure occurs simultaneously across the agglomerate, *i.e.* the crack appears when all the bonds are broken at the same time. Rumpf's theory does not consider the possibility of a pre-existing flaw in the material, and it produces an

overestimate of the energy required to fracture the agglomerate, as compared to the actual process of crack propagation (Kendall, 1988).

Kendall (1988) proposed an alternative approach based on the fracture mechanics principles, where the work done for crack propagation is furnished by the elastic strain energy stored within the agglomerate. To study the crack propagation phenomenon, Kendall considered the agglomerate as an elastic body that satisfies the Griffith criterion of fracture (Griffith, 1920). Griffith consider that a crack is about to propagate when there is no change in the sum of the mechanical and surface energy of the system as the crack length varies, *i.e.* the total energy of the system is a minimum (Eq. 1.14).

$$\frac{dU}{dc} = 0 \qquad (1.14)$$

When a crack propagates there is a release of strain energy, U_E. This energy released by the system plus the work carried out by the external forces, W, are spent in separating the two surfaces beyond the attractive distance of the interparticle forces. The sum of the work of the external applied forces on the system, W, the elastic strain energy, U_E and the energy required to create new surfaces, U_S, is the total energy of the system.

$$\frac{d(W + U_E)}{dc} + \frac{dU_S}{dc} = 0 \qquad (1.15)$$

Kendall (1988) showed that the breakage energy, R_B, of agglomerates depends on the fourth power of the packing fraction and on the 5/3 power of the fracture energy, Γ_C.

$$R_B = 56\,\phi^4 \left[\frac{\Gamma_c^5}{E^2 D^2}\right]^{1/3} \qquad (1.16)$$

where E is the Young's modulus of the particles and D the particle diameter, Γ_C is the fracture energy or energy per unit area required to break the interparticle bonds. In the case of alumina, the fracture energy is 21 J/m^2 when the equilibrium value (interface energy) is just 0.58 J/m^2. According to Kendall (1988) the differences are due to the loss in energy that appears in experiments.

Kendall (1988) calculated the agglomerate strength, σ^* as a function of the fracture toughness K_C and using the expression previously calculated for the breakage energy

$$\sigma = 0.893 K_C (\pi c)^{-1/2} \tag{1.17}$$

$$K^*_{1C} = 31\phi^4 \, \Gamma_C^{5/6} \Gamma^{1/6} D^{-1/2} \tag{1.18}$$

The expression obtained by Kendall (1988) is obviously very different from the expression obtained by Rumpf (Eq. 1.13). Kendall (1988) assumed a pre-existing flaw of size c to which the strength is related. This assumption makes the expression of Kendall (1988) to be applicable for a brittle or semibrittle failure. Kendall's expression requires the knowledge the internal distribution and sizes of flaws in the agglomerates in order to make a prediction of the agglomerate strength. In contrast, the model of Rumpf (1962) does not require the existence of any flaw and the applicability of this expression is more suitable for a ductile failure of materials.

The expressions of Kendall (1988) and Rumpf (1962) cannot predict the pattern of breakage as it is going to depend on the type of test carried out in the agglomerate and its structure. The prediction of the breakage pattern would require a detailed knowledge of the orientation of contacts with and the loading conditions as well as bond characteristics. It is extremely difficult to develop a model that predicts the agglomerate breakage patterns and hence the lack of theoretical models in literature on this topic.

1.4.4 Modes of failure

Failure is the loss of structural integrity in materials. Depending on the form in which the material could fail, *i.e.* elastic and/or plastic, the failure mode can be classified as

brittle, semi-brittle or ductile. Brittle failure is caused by fracture with little or no plastic deformation. If plastic deformation precedes the fracture the mode of failure is referred to as semi-brittle. In contrast, ductile failure is dominated by extensive plastic flow that is responsible for the rupture of the material with no crack propagation.

Generically, materials are called brittle, semibrittle and ductile depending on the way in which they fail. In the literature a different terminology sometimes appears that applies the term 'brittle' to brittle and semibrittle materials and the term 'non-brittle' to ductile materials. In these cases when the authors want to mention a brittle material with the meaning used in this review, brittle materials are named 'highly brittle materials' (Lawn and Wilshaw, 1975).

Ghadiri (1999) summarised the failure mode of a number of materials which he had tested previously and this is reproduced in Table 1.2. However, materials cannot always be easily included in one of the three modes since they fail exhibiting mixed properties. This problem has been discussed by Lawn (1993). They quantified the brittleness of materials based on a brittleness index defined as the ratio between hardness and fracture toughness (H/K_C). The ratio of these two parameters is the ratio between the resistance to plastic deformation and the resistance to crack propagation. The brittleness index of a number of materials is given in Table 1.3.

Table 1.2 Mode of failure of different materials (Ghadiri, 1999)

Brittle	**Semibrittle**	**Ductile**
Porous silica beads	NaCl	Weak agglomerates
Porous alumina beads	KCl	PMMA (Polymethyl methacrylate)
Al_2O_3 crystals	MgO	Polystyrene
Agglomerates	$Na_2CO_3 \cdot 3H_2O$	
FCC	$B_2O_3 \cdot 5H_2O$	
	NH_4NO_3	
	Lactose	
	Paracetamol	

Table 1.3 Hardness, toughness and brittleness index (data from Lawn, 1993).

Material	**H (GPa)**	**K_C (MPa $m^{1/2}$)**	**Brit. Index (H/K_c)**
Diamond	80	4	20
Silicon	10	0.7	14
Magnesium oxide	9	0.9	10
Silica (glass)	6	0.75	8
Sapphire	20	3	7
Zirconia	12	3	4
Tungsten carbide	20	13	1.5

In addition, the type of test influences the mode of failure. If a material is indented with a sharp indenter, the solid is going to show a large amount of plastic deformation under the indentation zone. In contrast, if the indenter is spherical the plastic deformation is going to be small. However, to overload a spherical indenter can originate a zone of inelastic deformation making the behaviour becoming similar to a sharp indentation. (Lawn and Wilshaw, 1975).

1.4.4.1 Brittle Failure Mode

This mode of failure is due to the presence of preexisting internal or surface flaws (Griffith 1920, Lawn and Wilshaw, 1975). In their absence, particles are strong and can only fail in this mode when shear deformations can generate microcracks which are the origin of larger cracks. This mode of failure is observed in indentation made by large spherical indenters.

When a spherical indenter is pressed against a brittle material a ring crack is formed surrounding the contact area. The radius of the ring crack is between two and three times the radius of the contact area. The ring crack follows the path of the hoop stresses produced by the indentation (Lawn and Wilshaw, 1975). The distance to the centre of the contact will depend on the population of microcracks in the material prior to the indentation, but it is usual to find this ring crack between one and two times the radius of the contact area (Wilshaw, 1971). The formation of the ring crack is followed by

the propagation of the crack downward and perpendicular to the surface until it is finally deflected and forms a cone which is known as Hertzian cone.

The path followed by the crack is related to the stress distribution of the material since such a path approximately follows the trajectories of the principal stresses. The solution to this problem is given by Wilshaw (1971) who provides an analytical solution based on the hypothesis that the material deformation is linear elastic and isotropic and that cracks do not perturb the initial elastic stress field.

In the impact testing of sapphire and glass against hard targets, Shipway and Hutchings (1993 a,b) observed that fragments of spheres tended to be hemispherical or in the wedge-shaped form. Shipway and Hutchings presented a theoretical experimental study of the fracture of brittle spheres under uniaxial compression and impact. Their theoretical analysis shows that the stress distributions in elastic spheres are broadly similar under both quasistatic and impact conditions, thus indicating the insensitivity of brittle failure to the strain rate.

The theory of Kendall (1988) for agglomerate strength assumes the existence of flaws in the material. Therefore, this theory is applicable to brittle materials since they fail by the propagation of microscopic cracks.

1.4.4.2 Semibrittle Failure Mode

Semibrittle failure is characterised by plastic deformation, which precedes crack propagation. This mode of failure is typically observed when solids are subjected to an indentation process by sharp indenters such as Vickers type indenters.

The indenter deforms the zone around its tip once the stress reaches the yield stress of the material. From this plastic deformation zone three types of cracks are observed to propagate: median, radial and lateral cracks (Evans and Wilshaw, 1976). Median cracks appear during loading in contrast to radial and lateral cracks that appear during unloading (Hagan and Swain, 1978).

Lawn and Swain (1975) described the microfracture patterns around infinitely small sharp points. Median cracks have a penny shape and appear beneath the plastic zone propagating perpendicularly to the maximum tensile stresses which are parallel to the surface of the material. If the indentation is made with a Vickers indenter then median cracks connect the opposite corners of the indentation (Hagan and Swain, 1978).

It was observed by Hagan and Swain (1978) that in the cases in which the load of the indenter is not high enough to produce a median crack, radial cracks appear during unloading. These authors suggested that such radial cracks were due to the removal of stresses during unloading although no verification of their suggestion was presented in their paper.

Lateral cracks are observed during unloading of the material. They usually propagate from intersection points of shear lines within the plastic deformation zone having this common characteristic with median cracks. In contrast to the median cracks, the propagation of the lateral cracks seems to be triggered by the release of residual tensile stresses.

When a semibrittle material is impacted, it shows two regimes of breakage: chipping and fragmentation. Chipping is characterised by the detachment of small clusters from the sides of the particle due to the propagation of lateral cracks. Fragmentation is characterised by the propagation of radial or median cracks that divide the particle into two or more large clusters. The tendency to generate lateral cracks is greater in hard materials than in soft materials because the former can store greater residual stresses.

Arbiter *et al.* (1969) investigated the fracture of sand-cement spheres and glass spheres in a free-fall impact. They showed that fracture starts from the region of contact with the plate and propagates through the sphere while further fracture planes are developed. In most cases, breakage by oblique fracture planes seems to have been preceded by at least one meridian fracture plane dividing the sphere into nearly equal parts.

Arbiter *et al.* (1969) observed that when failure occurs, it starts along a conical surface. The base of the cone corresponds approximately to the area of contact of the specimen and the plate at the instant of failure. The surface of the cone is covered by a layer of pulverised materials while the cone remains free of damage as it is under hydrostatic pressure. Cracking in semibrittle materials occurs more extensively at high impact velocities, however there is no theory that can relate the product size distribution to the impact conditions and material properties in a predictive way.

Ghadiri and Zhang (2002) developed a model of attrition due to chipping based on the propagation of sub-surface lateral cracks. In their model, the extent of breakage, ξ depends on the fracture toughness, K_C, and the hardness of the material, H.

$$\xi = \alpha \frac{\rho V^2 DH}{K_C^2} \qquad (1.19)$$

where ρ is the density of the material, V is the impact velocity, D is the diameter of the particle, and α is the proportionality factor which depends on particle shape and impact geometry and is determined experimentally.

Thornton *et al.* (1995), by using computer simulations of agglomerate impact breakage, also showed that there was a linear relationship between the extent of breakage calculated as the ratio between the mass of debris to initial mass of the agglomerate and the Weber number in the chipping regime.

Marshall *et al.* (1982) have shown that there is a critical load applied by a sharp rigid indenter, F_{cl}, to cause lateral fracture on a semibrittle material. This is a function of the elastic modulus, E, the fracture toughness K_C and the hardness, H, given by

$$F_{cl} \propto E\left(\frac{K_c}{H}\right)^4 \qquad (1.20)$$

Under impact conditions the force generated depends on the impact velocity and the particle size and it is possible to state that there is a minimum velocity to cause lateral

fracture. Hutchings (1992) reported an expression for this velocity V_{ch} showing a dependence on the density ρ, fracture toughness K_C, hardness, H and diameter of the particles, D.

$$V_{ch} \alpha \left(\frac{K_c}{H} \right)^4 \frac{E}{H^{1/2}} \rho^{-1/2} D^{-2} \qquad (1.21)$$

Hutchings (1992) also showed that there is a critical particle size below which no fragmentation of the impacting particle occurs. He used the model of Hagan (1984) who reported an expression for the critical load for producing fragmentation. In this model a threshold velocity, V_{fr} for fragmenting the particle also exists and it is given by

$$V_{fr} \alpha \left(\frac{K_c}{H} \right)^4 H^{1/2} \rho^{-1/2} D^{-2} \qquad (1.22)$$

In their computer simulations, Thornton *et al.* (1996) observed a semibrittle behaviour of agglomerates. A plastic behaviour in the impact region followed by crack propagation from this part to the agglomerate boundary was observed. These results are consistent with the observation of Arbiter *et al.* (1969) who showed that the crack is propagated from the region with the highest level of stresses in this case the boundaries of the contact area.

1.4.4.3 Ductile Failure Mode

This failure mode normally prevails in metals and polymers. Hutchings (1992) analysed the wear mechanisms of ductile materials when they were impacted by a hard particle. This process is controlled by plastic deformation. The study of Hutchings (1992) of the oblique impact of single particles on metals revealed three different types of damage called ploughing, type I cutting and type II cutting. In ploughing, the material is displaced to the side and to the front of the particle. If an angular impact is carried out the deformation depends on whether the particle rolls forwards or backwards during contact. In the type I cutting the particle rolls forward and the

material is raised forming a lip, similar to post-indentation surfaces. In type II, the particle rolls backwards producing the detachment of a chip from the surface. These three ways of wearing a surface are restricted to spherical shapes. Irregular particles with prominent corners act in more different ways and they are more difficult to classify.

In contrast, when the impact is perpendicular to the target the previous type of damage does not apply (Hutchings, 1993). In normal impact the material is detached when the plastic deformation reaches a certain level of strain (Hutchings, 1981). This level of strain is reached usually by repeated impacts of the material (Hutchings, 1981). Hutching also developed a model that predicts the mass eroded from the particle. This model predicts a dependency of the eroded mass, M_E on the cube of the impact velocity, V^3, and on exponent 3/2 of the hardness of the material, H:

$$M_E \propto \frac{\rho {\rho_T}^{1/2} V^3}{{\varepsilon_r}^2 H^{3/2}} \qquad (1.23)$$

where ρ is the density of the particle, ρ the density of the target, and ε_r the 'erosion ductility' which is the maximum strain supported by the material. It is interesting to observe that the eroded mass depends on the impact velocity with a higher exponent than the one provided by the input kinetic energy.

The previous analysis has been made for the impact of rigid particles into ductile materials. In a study of weak agglomerates breakage Ning *et al.* (1996) found ductile behaviour since this type of structure could not store significant elastic strain energy before breaking and consequently no crack propagation appeared. Extensive plastic deformation preceded the breakage of agglomerates. In this case material was always detached from the plastic zone which spread upwards from the contact area and its volume increased with the impact velocity. Ning *et al.* (1996) showed clearly the ductility of a lactose agglomerate using visual observations and analysing the product size distribution.

Ghadiri and Subero, (1997) simulated several agglomerates that exhibited a ductile behaviour, *i.e.* plastic deformation preceding the failure. Their results are in agreement with the observations of Ning *et al.* (1996).

The comparison of the simulation works above described with the work of Hutchings is difficult due to the differences among the systems. In the case of Hutchings the ductile material is the target and not the impacting body which is a single particle for the case studied by Hutching and an agglomerate in the works of Ning *et al.* (1996) and Ghadiri and Subero (1997). However there is a common factor in all cases. The failure of the material was preceded by an extensive deformation without any evidence of crack propagation at the impact site.

1.4.4.4 General conclusions for the three failure modes

- The analysis of Kendall (1988) is based on the crack propagation in a material failing in the brittle or semibrittle mode.
- Rumpf's analysis (Rumpf, 1962) is a simple force balance and it may be more suited to the ductile failure mode.
- The actual mode of failure of single particles is described by a parameter such as brittleness index (Table 1.3).
- The mode of failure of an agglomerate is related to the forces that join the particles together and the structure of the agglomerate. However the relationships between the mode of failure of bonds and agglomerates have not been systematically investigated.
- The extension of the modes of failure of single particles does not follow straight into the mode of failure of agglomerates. However, some similarities have been found between the behaviour of these two different structures.

1.5 Review of single particle impact

Since Hertz (1882) pioneered the classical analysis of contact between two frictionless elastic bodies, the interaction laws of two non-conforming contacting bodies have been extended to include aspects such as the influence of tangential loading (Mindlin and

Deresiewicz, 1953), sliding contact and the effect of surface energy (Johnson *et al* 1971, Savkoor and Briggs, 1977) and elasto-plastic deformation (Thornton and Ning, 1998).

1.5.1 Elastic normal loading without adhesion: the Hertz analysis

Hertz (1882) analysed the contact between two frictionless elastic spheres. His analysis was based on the following assumptions: the deformation area is small compared with the dimension of each body, the surfaces are frictionless and the energy absorbed in the wave motion is negligible so that the deformation is perfectly reversible. In Hertz analysis, the radius of the contact, a_0, is given by

$$a^3 = \frac{3\,R^*\,P}{4\;\;E^*} \tag{1.24}$$

where P is the external load, E^* is the reduced elastic modulus, and R^* is the reduced radius of two spheres.

This model provides a pressure distribution that is zero at the boundaries of the contact area and the pressure at any point in the contact area at a distance, r, from the centre of the contact area is given by:

$$\sigma_r = \frac{3P}{2\pi a^2}\left(1-\frac{r^2}{a^2}\right)^{1/2} \tag{1.25}$$

Hertz (1882) verified his analysis experimentally using an optical microscope to measure the contact between glass spheres.

The Hertz theory was developed for quasi-static conditions. This limitation of Hertz analysis should be taken into account when single particles are impacted at a high velocity since for having a quasi-static approach the speed of the impact should be less than the sound speed in the material. In this case, the deformation of the real particles

could be very different from the deformation predicted by Hertz analysis (Johnson, 1985).

1.5.2 Interaction of adhesive elastic spheres

Roberts (1968) and Kendall (1969) noted that at low loads the contact areas between two bodies were considerably larger than those predicted by Hertz (1882) and approached to a constant finite value as the load was reduced to zero. Strong adhesion was observed if the surfaces were clean and dry. At high loads, the results closely fitted the Hertz Theory.

Johnson *et al.* (1971) extended the Hertz analysis to two elastic adhesive spheres by using a fracture mechanics approach (JKR model). The total energy associated with loading can be divided into stored elastic energy, the mechanical work and the surface energy. A crack is at the point of propagation when the rate of change of energy with crack extension is zero. The exact analysis made by Johnson *et al.* (1971) expresses the contact radius in the same form as in the Hertzian model but substituting the external load for an effective external load which depends on the surface energy.

$$a^3 = \frac{3}{4}\frac{R^*}{E^*}\left\{P + 3\gamma\pi R^* + \sqrt{\left[6\gamma\pi R^* P + (3\gamma\pi R^*)^2\right]}\right\} = \frac{3}{4}\frac{R^* P_{EFF}}{E^*} \qquad (1.26)$$

This equation is in good agreement with the observations made by the same authors on spherical and flat surfaces made of rubber and gelatine (Johnson *et al.* 1971).

The pressure distribution provided by the model of Johnson *et al.* (1971) has the inconvenience that it tends to infinity at the perimeter of the contact area. This is in contrast to the Hertzian model, which predicts a zero pressure distribution at the boundary of the contact area.

$$\sigma_r = \left(\frac{2aE^*}{\pi R^*}\right)\left(1 - \frac{r^2}{a^2}\right)^{1/2} - \left(\frac{4\gamma E^*}{\pi a}\right)^{1/2}\left(1 - \frac{r^2}{a^2}\right)^{-1/2} \qquad (1.27)$$

The infinite value of the pressure distribution at the boundary of the contact area is in agreement with the observations of Arbiter (1969) who found that the value of stresses at the boundary of the contact area was a maximum.

The JKR model predicted that the force required to break a contact is independent of the external load and therefore of the deformation of the contact. This force to break a contact is given by

$$P_{OFF} = 3\pi\gamma R^* \qquad (1.28)$$

Derjaguin *et al.* (1975) (DMT model) studied the contact between an elastic ball and a hard wall. These authors considered the case in which the ball has a very large elastic modulus, so that the molecular attraction forces would not be able to change its shape appreciably outside the contact area (rigid body). Under this hypothesis they calculate the force required to break an adhesive contact. The pull-off force predicted by DMT model shows the same dependency in the particle radius and surface energy than the pull-off force predicted by JKR model. The pull-off force given in DMT model is

$$P_{OFF} = 4\pi\gamma R^* \qquad (1.29)$$

The constant part of the pull-off force in Eqs 1.28 and 1.29 is different in both models. Among other reasons the effect of the molecular attraction outside the contact area as considered in DMT model is one of the contributing factors for this difference. Maugis (1991) developed an intermediate model in which there is a dimensionless parameter λ that controls the behaviour of the system. When this parameter is increased from zero to infinity there is a continuous transition from the DMT approximation to the JKR approximation. This model shows the underlying consideration of the JKR model that the Van der Waals forces are not considered outside the contact area and so the pressure distribution at the boundaries of the contact area tends to infinity. Maugis (1991) did not clarify the significance of the parameter of his theory to provide a better understanding of his model.

These models as well as the model of Hertz were developed for quasi-static conditions. In real experiments the propagation of elastic waves causes energy dissipation. In addition, there exists a strain-rate dependency of the adhesion forces which has not been considered and therefore JKR and DMT models are limited to quasi-static loading.

1.5.3 Tangential stiffness of elastic spheres without adhesion

The analysis of the effect of a tangential force on the contact between elastic bodies was initiated by Mindlin (1949). Mindlin calculated the stiffness of the tangential contact deformation when the normal force is kept constant (no-slip solution of Mindlin). In this case the contact stiffness, k_t, is defined as

$$k_t = \frac{dF_t}{d\delta_t} = 8G^* a \tag{1.30}$$

where F_t and δ_t are the tangential force and displacements respectively and G^* is the shear modulus of the material and a the contact area radius.

The above expression was obtained by Mindlin (1949) for tangential stress that tends to infinity at the boundary of the contact area. Mindlin supposed that no slip occurs between the two particles in contact. He further assumed that at any point of the contact area the stress could be larger than the product between the friction coefficient and the normal stress. Lastly, he assumed that an annulus of slip is developed and it propagates radially inwards. When the total tangential force reaches the product of the friction coefficient and the normal load gross sliding occurs. The tangential stiffness in presence of slip is calculated as

$$k_t = 8G^* a\left(1 - \frac{T}{\mu P}\right)^{1/3} \tag{1.31}$$

From Eq. 1.31 is obvious that the relationship between tangential force and displacement is no longer linear as for the no-slip solution of Mindlin, assuming a normal constant force.

Johnson (1954) verified Eq. 1.31 for the case in which a tangential force was applied to a steel ball in contact with a steel surface. The comparison between the experimental curves of Johnson (1954) and the model of Mindlin (1949) showed a large agreement.

Mindlin and Deresiewicz (1953) extended the study of Mindlin (1949) for the case in which the normal applied force was not kept constant. They showed that the relationship between tangential force and deformation was dependent on the history of the loading forces. However, in spite of the important predictions of this model, Mindlin and Deresiewicz (1953) did not validate their theory experimentally.

Thornton and Randall (1988) expressed the tangential stiffness of a contact during loading, unloading, and reloading of the tangential force. The tangential stiffness can be expressed as a function of the friction coefficient, μ, the normal load, P, and a parameter θ^* which has different values in each one of the three stages and depends on the shear modulus, G^*, where the sign minus should be for unloading,

$$k^t = 8G^* a \pm \mu(1-\theta^*)\frac{\Delta P}{\Delta \delta_t} \tag{1.32}$$

where θ^* is defined for loading, unloading and reloading, respectively, as follows:

$$\theta^{*3} = 1 - \frac{T + \mu \Delta P}{\mu P} \tag{1.33}$$

$$\theta^{*3} = 1 - \frac{T^* - T + 2\mu \Delta P}{2\mu P} \tag{1.34}$$

$$\theta^{*3} = 1 - \frac{T - T^{**} + 2\mu \Delta P}{2\mu P} \tag{1.35}$$

where T^* and T^{**} are the values of the tangential force at which unloading and reloading starts, and ΔP is the incremental normal force.

Johnson (1985) investigated the relationship between tangential traction and normal load showing that the tangential traction has a negligible effect on the normal force and therefore the JKR model for normal adhesive contact can still be used.

Thornton and Yin (1991) reported computer simulations of oblique impacts of two elastic spheres at different impact angles. The angle of impact in the simulation of Thornton and Yin (1991) was defined as the angle between the incident direction and the normal to the plane. They showed that if the impact angle was larger than the angle of internal friction, sliding of the bodies occurred from the beginning of the impact.

During impact the kinetic energy passes trough a minimum value depending on the impact angle. At zero impact angle the minimum kinetic energy is zero as the particles change direction during impact. However, the minimum kinetic energy increases as the impact angle is increased because of the tangential velocity (Thornton and Yin, 1991).

As the angle of impact increased, the loss in translational kinetic energy and the gain in the rotational kinetic energy increased until the impact angle was sufficiently large to produce rigid body sliding throughout the impact. Further increases in the impact angle result in reduction in the rotational kinetic energy and corresponding smaller losses in linear kinetic energy.

For large impact angles, there is sliding throughout the whole impact. In this case, there is no observed recovery of the kinetic energy during the rebound stage (Thornton and Yin, 1991). In this case the sliding of the particles dissipates a large amount of energy due to friction.

The extension of the observations of Thornton and Yin (1991) to the agglomerate behaviour is not straightforward since agglomerates can suffer from extensive damage during impact and the input kinetic energy could be spent in the breakage of bonds. However, the analysis is applicable to the primary particles of agglomerates.

1.5.4 Tangential stiffness in presence of adhesion

Savkoor and Briggs (1977) extended the JKR analysis to account for the effect of oblique loading in the presence of adhesion and showed that the area of contact between two surfaces decreased when the tangential force was increased due to a 'peeling mechanism'. The contact radius, *a,* (Eq. 1.34) reduces as the tangential force, *T*, is increased until a critical value T_C is reached, ($T=T_c$) beyond which the behaviour depends on the value of T_c, although the original paper by Savkoor and Briggs did not analyse the behaviour after peeling. During peeling the contact radius can be expressed as follows:

$$a^3 = \frac{3R^*}{4E^*}\left\{P + 2P_{OFF} + \sqrt{\left[4P_{OFF}P + 4P_{OFF}{}^2 - \frac{T^2E^*}{4G^*}\right]}\right\} \qquad (1.36)$$

where P_{OFF} is the pull-off force and G^* the reduced shear modulus.

Thornton and Yin (1991) proposed that when $T = T_c$ there is a smooth transition from peeling to sliding in which the contact area is subjected to an equivalent Hertzian-like normal stress distribution. The problem of this criterion is that it does not fit well for negative normal loads. Thornton and Yin (1991) proposed an alternative sliding criterion based on the hypothesis that peeling occurs until a critical value of the contact radius is reached. This criterion has a better fit over the complete range of experimental results even for negative loads, compared to the criterion of Savkoor and Briggs (1977).

$$T = \mu P_{EFF}\left[\frac{(2P_{EFF} + P)}{3P_{EFF}}\right]^{3/2} \qquad (1.37)$$

where P_{EFF} is the effective normal force defined in the model of Johnson *et al.* (1971).

$$P_{EFF} = (P + 2P_{OFF} + (4PP_{OFF} + 4P_{OFF}^2)^{1/2} \qquad (1.38)$$

When the normal applied force is much larger that the van der Waals forces the effective force is approximately the normal load and therefore the expression of Thornton and Yin adopts the form of Amonton's law, $T=\mu P$.

1.5.5 Elasto-plastic impact without adhesion

As described by Bitter (1963) the process of an elastic-plastic impact can be divided into three stages.

(i) The first stage of interaction between the bodies starts at the moment of initial contact of the bodies and ends when the peak pressure reaches the elastic yield limit of the softer of the two bodies.

(ii) The second stage commences at the onset of plastic deformation and ends when the impact bodies have zero relative velocity.

(iii) In the third stage of impact the stored elastic energy is recovered and the rebound of the particle depends on the incident velocity, surface adhesion, surface roughness, etc.

Davies (1949) calculated the yield velocity and the contact radius at the yield point showing the velocity at the yield point depends on the power 5/2 of the yield stress.

$$V_Y = 1.56\left(\frac{\sigma_Y^5}{E^{*4}\rho}\right)^{1/2} \tag{1.39}$$

Ning and Thornton (1993) calculated the normal force after the initial yield. They assumed a Hertzian pressure distribution with a cut-off corresponding to the contact yield stress, and therefore the plastic zone of the contact area is subjected to a contact yield pressure.

$$P = P_E - 2\pi \int_0^{a_P} \left(\sigma_r(r) - p_Y\right) dr \tag{1.40}$$

Integrating and using the expressions of Hertz model (Hertz, 1889), they obtained

$$P = P_Y + \pi p_Y (a^2 - a_Y^2) \tag{1.41}$$

where a is the radius of the contact area at the applied force P, a_Y, P_y, and p_Y are the values of the radius, force and pressure at the yield point. The contact area is surrounded by an annulus of elastic pressure distribution. Bitter (1963) and later Ning and Thornton (1993) showed that the area of the elastic annulus is equal to the contact area at initial yield.

When plastic deformation occurs the actual contact area radius is the same that is produced by an elastic force, P_E, with a curvature radius R. During unloading the force-displacement behaviour is assumed to be elastic. Therefore the contact area radius can be also calculated, in terms of the actual force P and an equivalent elastic curvature radius, R_P (Thornton and Ning, 1998).

$$R_P P = R P_E \tag{1.42}$$

As radius R_P is larger than the actual radius R, the deformation provided by the elastic equation is smaller than the actual deformation. Therefore, at zero applied force the real deformation of the material is different from that predicted by the Hertz analysis. The non-zero deformation at zero load corresponds to a permanent deformation in the material.

1.5.5.1 Coefficient of restitution

The coefficient of restitution, e, in an impact process is defined as the ratio between the rebound velocity and the impact velocity. For the case of a perfectly plastic impact of a sphere impacting on a plane surface Johnson (1985) developed an expression for the restitution coefficient that shows a power dependence -1/4 on the impact velocity.

$$e_n = 1.324 \left(\frac{p_Y^5}{E^{*4} \rho} \right)^{1/8} V^{-1/4} \tag{1.43}$$

Thornton and Ning (1994) obtained a similar expression, but with a different proportionality factor because the normal stiffness used was double of that used by Thornton and Ning (1994).

For oblique impacts of elasto-plastic spheres Ning and Thornton (1993) observed that there was an impact angle, θ, at which the tangential coefficient of restitution is minimum and independent of the friction coefficient. The tangential coefficient of restitution was defined as the ratio between the incident and the rebound tangential velocities. They then developed expressions for the tangential coefficient of restitution based on the optimum and the actual impact angles,

$$e_t = 1-(1-e_{t\,min})\sin\left(\frac{\pi\theta}{2\theta'}\right) \tag{1.44}$$

where $e_{t\,min}$ is defined as

$$e_{t\,min} = \frac{5}{7} - \frac{2}{7}\frac{e_N}{\left(\sqrt{3}\tan\theta'\right)} \tag{1.45}$$

and

$$\tan\theta' = \frac{\mu E^*}{4G^*}\left(\frac{7E^*}{4G^*} - 3\right) \tag{1.46}$$

It is noteworthy that the tangential coefficient of restitution depends on the normal coefficient of restitution which depends on the particle properties and on the incident and rebound particle properties.

1.5.6 Elasto-plastic impact with adhesion

Rogers and Reed (1984) developed a model for the elasto-plastic impact for which the effect of adhesion was considered only during the unloading stage. The deformation

due to impact takes the form of a central area of plastic deformation surrounded by an annulus of elastic deformation. They also established a criterion for the particle rebound considering that the plastic deformation is the only energy loss mechanism. This criterion established that the difference between the kinetic energy and the energy dissipated by plastic deformation has to be greater than or equal to the total adhesive energy available at the end of the impact for the particle rebound to occur.

Wall *et al.* (1989) compared their experimental measurements of the coefficient of restitution with the theoretical model of Rogers and Reed (1984). Wall *et al.* (1989) observed that yield started at higher values of impact velocities than those predicted by Rogers and Reed (1984). Wall *et al.* (1989) attributed this to the fact that the model considered a constant yield limit independent of the impact velocity. When the model of Rogers and Reed was modified including a dynamic yield limit, a better agreement with the experimental results was shown.

Ning and Thornton (1993) combined the JKR model with their theory of elasto-plastic impact to model the combined effect of plastic deformation and adhesion. The pressure distribution was assumed to be adhesive with a cut-off pressure. The model is similar to that of elasto-plastic deformation with no adhesion.

$$P = P_Y + \pi p_Y (a^2 - a_Y^2) - a_Y (8\pi\Gamma E^* a)^{1/2} \qquad (1.47)$$

In the unloading stage, an elastic process is assumed and the behaviour is described by the JKR theory.

The coefficient of restitution is clearly influenced by the surface energy. At velocities higher than the yield velocity the curves corresponding to different values of the surface energy overlap each other. In this region, the power law index for the impact velocity changes from -1/4 in the case of no-adhesion to -1/6 for the case of adhesion.

In the case of adhesive impact, a critical velocity, V_C, is defined below which no rebound would occur and the particle would get stuck due to adhesion. In the computer simulation of impact of soft elasto-plastic spheres carried out by Ning and Thornton

(1993) a comparison was made with the experimental data of Wall *et al.* (1989), who reported results of ammonium fluorescein particles impacting on a silicon target. It could be seen that for impact velocities greater than the critical velocity V_c which is due to the adhesion of the materials, the simulated results largely underpredicted the coefficient of restitution. In order to solve the above discrepancies a dynamical yield point depending on the impact velocity was proposed.

$$\sigma_Y^D = \sigma_Y^S \left(1 + A \ln\left(\frac{V_i}{V_C} \right) \right) \tag{1.48}$$

where V_i is the impact velocity and σ_Y^S the static yield point. In order to fit the constant, A, a new series of impact simulations was performed by Ning and Thornton (1993) and their results were compared with the results of Wall *et al.* (1989).

1.6 Computer simulation of agglomerate impact

1.6.1 General description of the simulations

In a series of simulations Thornton and co-workers investigated agglomerate strength using an extended version of the program TRUBAL. TRUBAL is a computer program for the modelling of mechanics of particle systems. The technique has become known as the using Distinct Element Method (DEM), which is a numerical method capable of describing the mechanical behaviour of assemblies of discs or spheres. It was originally developed by Cundall (1971) for the analysis of rock mechanics problems.

In DEM, forces, accelerations, velocities and positions are calculated and updated cyclically. The interparticle force increments within a time Δt are calculated at all contacts from the relative displacements of the contacting particles using a finite form of the force-displacements law provided by contact mechanics. The interparticle forces and momentum acting on the particles are calculated. From these forces and momentums the new particle accelerations (both linear and rotational) are obtained using Newton's second law of motion. Then the accelerations are used to update the velocities. Further numerical integration provides displacement increments from which

the new particle coordinates are obtained. After that the computer code recalculates the force increments again and the cycle is repeated.

The models of normal and tangential forces incorporated in TRUBAL, for the case of no adhesion, are based on Hertz analysis (1882) and Mindlin and Deresiewicz (1953), respectively. In the presence of adhesion the JKR model (Johnson *et al.,* 1971) is used for the normal contact deformation while the tangential behaviour is governed according to Savkoor and Briggs (1977) for the adhesion case and Thornton (1991) when there is sliding of the particles. In the simulations particles only interact when they are in contact. Particles are modelled as elastic spheres with both interparticle friction and adhesion. The time step used is a function of the Rayleigh wave speed through the solid particles and the average particle radius (Ning 1995).

The agglomeration method followed by Thornton and co-workers can be summarised as follows: the primary particles of the agglomerate are randomly generated within a spherical volume and a centripetal gravity force is applied at the centre of the particles in order to bring the particles together (Thornton *et al.* 1999, Subero *et al.* 1999). The formation method has the advantage of producing homogenous and spherical agglomerates in an easy way (Moreno *et al.* 2001) and it is able to produce agglomerates with different physical properties changing the material of the primary particles and controlling the agglomeration method.

1.6.2 Bond breakage

Kafui and Thornton (1993) expressed the extent of damage as the fraction of initial primary particle contacts that are broken as a result of the impact and called it the damage ratio. The damage ratio expresses the extent of damage imparted to an agglomerate due to an impact.

Kafui and Thornton (1993) and later Subero *et al.* (1999) have observed a threshold velocity under which no breakage of bonds is observed. The threshold velocity increases exponentially with the surface energy as reported by Thornton *et al.* (1996) for a 2-D agglomerate. However the Kafui and Thornton (2000) found the following

power law for the threshold velocity as a function of the interface energy Γ for the impact of a 3-D crystalline agglomerate:

$$V_0 = 0.17\Gamma^{1.5} \tag{1.49}$$

The differences between the two trends cannot be easily explained, but it could be due to either a narrow range of interface energies investigated or the lack of a statistical average since the results belong to just one agglomerate.

When the surface energy is increased, more kinetic energy is required to produce the same number of broken contacts. The agglomerate strength is obviously a function of the interparticle bond strength which is characterised by the interface energy, $\Gamma=2\gamma$ for the case of spheres made of the same material properties and whose surface energy is γ.

Kafui and Thornton (1993) proposed that the damage ratio is a function of Weber Number, *We*, which describes the ratio of input energy to the average bond strength (Kafui and Thornton, 1993).

$$We = \frac{\rho V^2 D}{\Gamma} \tag{1.50}$$

where ρ is the particle density, V is the impact velocity, D the diameter of the particles and Γ the interface energy. Note that no agglomerate size appears in this relationship.

Thornton *et al.* (1996) later modified the Weber Number including the velocity under which no damage was produced, V_0. With this new Weber Number, a better fit was obtained.

$$W_e' = \frac{\rho (V - V_0)^2 D}{\Gamma} \tag{1.51}$$

where V is the impact velocity, D the diameter of the particles, Γ the interface energy.

Subero *et al.* (1999) found that for the simulation of agglomerate impact the damage ratio *vs.* W'_e varies linearly at low values of the Weber number but above a critical velocity, the trend starts approaching an asymptotic value. This behaviour agrees with the previous results of Kafui and Thornton (1993), who compared the results of impact breakage of FCC and BCC packing. They showed an approximate linear relationship between damage ratio and Weber Number.

Kafui and Thornton (1993) compared the behaviour of different assemblies as a function of the packing fraction. Their analysis revealed that the behaviour of assemblies with lower packing fraction (like *e.g.* of BCC) suffered less breakage of contacts at the same value of impact velocities as compared to an FCC agglomerate. According to the authors, the most porous agglomerate accommodated better the transmitted energy in the impact process.

In order to understand the effect of impact on the agglomerate breakage it is necessary to analyse not just the number of broken bonds but the mechanism of bond rupture. Regarding this issue point, two important pieces of work should be noted, the first by Thornton *et al.* (1996) and the second by Ning *et al.* (1996). Thornton *et al.* (1996) observed that when the impact wave propagates through the agglomerate, contacts bearing tensile forces are mainly orientated in two different directions in contrast to the random orientation of the tensile contacts before impact. The broken contacts from the beginning of the impact were also orientated in the same direction as the tensile contacts. These observations were corroborated by the work of Ning *et al.* (1996) who provided a more detailed explanation of the mechanism of rupture of bonds. They observed that the compressive contacts during impact were orientated following the lines of maximum compression, which depart almost radially from the contact area. The tensile contacts were perpendicularly orientated to the lines of maximum compression. Finally the broken contacts were orientated in the same directions as the tensile contacts which confirmed the observations of Thornton *et al.* (1996).

The analysis of the breakage of contacts in agglomerates as well as the mechanism of bond failure has been successfully treated in the literature and a large agreement exists among different authors regarding the influence of the impact velocity and interface

energy. However, there remain many other factors to be investigated such as the influence of the elastic modulus, the dissipative mechanisms (due to friction and damping) on the breakage of contacts of agglomerates upon impact, strain rate dependency on the breakage of contacts and bond failure mechanism, *i.e.* ductile, brittle or semibrittle.

1.6.3 Failure of agglomerates

An important part of the analysis of the damage suffered by agglomerates during impact is the one related to the mode of failure of agglomerates. To determine how and under which conditions the agglomerate fails is probably best done by the use of DEM as a tool in the investigation of agglomerate behaviour. The influence of impact velocity, interface energy and packing fraction on the agglomerate failure will be reviewed in the following sections.

1.6.3.1 Influence of the impact velocity

Thornton *et al.* (1996) have presented an analysis of the influence of the impact velocity on the breakage of the agglomerate. At high impact velocity the damage suffered by agglomerates affects the whole assembly. At low impact velocities the damage is usually localised at the impact site. At medium impact velocities would be the intermediate cases between low and high impact velocity. The high, medium and low velocities apply only to the specific agglomerates generated in the simulations and it will not be possible at this stage to quantify what constitutes high, medium and low velocity as the damage depends also on other factors such as surface energy and particle size. It is perhaps more useful to consider the type of damage caused at different velocities and this is addressed in the following.

Thornton *et al.* (1996) observed that at high impact velocities, the compressive wave originated by the collision between the agglomerate and the target deformed the whole agglomerate producing a flattening of the structure. Simultaneously, the propagated force produced a shear effect. The particles localised in the contact region slowed down their movement whilst the adjacent particles continued their trajectory towards the target. This produced a crack in the agglomerate that divided the structure into two

large portions (Thornton *et al.,* 1998). However, the tail-end of the compressive waves continued travelling through the agglomerate breaking more contacts and shattering the agglomerate.

Thornton *et al.* (1998) described the shattering regime as a process in which the agglomerate fragmented into many medium-size fragments which subsequently lost particles from their surfaces.

In the case of weak agglomerates (Ning *et al.,* 1997) extensive plastic flow precedes the shattering of the whole structure into small clusters depending on the impact velocity. Similar results to those of Ning *et al.* (1996) were found by Subero (2001) when the agglomerates were impacted at a high velocity.

There is an important difference between the work of Ning *et al.* (1996), Subero *et al.* (1999) and those of Thornton and co-workers. In the work of Thornton and co-workers, the shattering of the agglomerate starts with the development of a meridian crack that initially divides the agglomerate. However, neither Ning *et al.* (1996) nor Subero (2000) reported the propagation of cracks preceding the shattering of the agglomerate. Therefore, it seems that this is the behaviour of two different types of structure, which may have been formed in different ways.

As the impact velocity is lowered, the force generated on impact also lowered and so the effect of the impact on the breakage of the agglomerate is also smaller (Thornton *et al.*, 1996). The decrease in the intensity of the impact restricts the plastic deformation zone to regions close to the contact between agglomerate and target. According to Thornton *et al.* (1996) cracks are initiated at the perimeter of the plastic deformation zone and they propagate vertically (meridian) and radially. This is a typical behaviour of semibrittle materials. This kind of pattern has also been observed by Subero *et al.* (1999) in the experiments of agglomerate impacts using glass ballotini and by Arbiter *et al.* (1969) with sand-cement spheres.

Arbiter *et al.* (1969) observed experimentally that a conical region developed at the impact site and meridian fracture planes formed from this region. When the impact velocity was increased it was found that the number of such meridian planes increased.

The base of the cone was approximately equal to the contact area between the agglomerate and the impact plate. In addition, oblique fracture planes formed accompanied by an increase in damage to the conical region which was covered by pulverised material at relatively moderate velocities. All fracture planes followed trajectories of maximum compression. This type of behaviour corresponds to the behaviour of semibrittle materials where cracks are preceded by plastic deformation.

Both, Ning *et al.* (1996) and Subero *et al.* (1999) observed the rupture of bonds but without crack propagation and an extensive flattening of the simulated agglomerates. The flattening was accompanied by the detachment of particles from the same flattened region.

For solid materials failing in the semibrittle mode Ghadiri and Zhang (2002) showed that the fractional mass of debris detaching from a particle as a result of impact is proportional to the square of the impact velocity. This is for the case where the mother particle survives the impact but small debris is detached from the impact region (chipping regime). The relationship between the extent of breakage and the square of the impact velocity was also observed by Thornton *et al.* (1995) in the computer simulation of agglomerate breakage. This indicates that certain similarities exist between the impact behaviour of agglomerates and single particles.

At sufficiently low velocity the agglomerate rebounds with no crack formation. However, the damage may be produced as a result of localised plastic deformation adjacent to the contact wall.

Thornton *et al.* (1999) have shown that at low impact velocities, the damage ratio is initially very small until the platen force reaches its maximum value and then it increases rapidly until the end of the impact. The debris is mainly concentrated near the agglomerate-platen interface and only a few primary particles are detached in the top half of the agglomerate.

Little information has been reported of the behaviour at low impact velocity. Nevertheless, it could be of great interest to determine the velocity corresponding to elastic-plastic transition as a function of the agglomerate size and properties.

Several features are note worthy on the effect of the impact velocity on the agglomerate breakage:

- it is obvious that impact velocity has a drastic effect on agglomerate breakage. The increase in impact velocity produces a change in the breakage pattern of agglomerates.
- The agglomerates simulated do not exhibit a purely brittle mode of failure in agglomerates. The origin of this problem could be due to several reasons but one in particular seems to be important. The structure deforms easily and it does not store significant elastic energy required for crack propagation.

1.6.3.2 Interface energy

In the simulations reported here, bonds are broken when the force in the contact reaches the value of the pull-off force established in the model of Johnson *et al.* (1971). This pull-off force is directly proportional to the interface energy. Therefore, the change in interface energy affects the values of the impact velocity at which bonds are broken and this may affect the mode of failure of agglomerates.

Ghadiri *et al.* (2001) showed that the interface energy can influence the breakage pattern of agglomerates. It was shown that when the interface energy was decreased by one order of magnitude, the fragmentation of the agglomerate was observed in the presence of a large amount of debris as a result of local disintegration of the impact site. These results are compatible with the simulations of Ning *et al.* (1997) who used a lower value of interface energy.

Ning *et al.* (1997) did not observe any crack propagation in the computer simulations of the impact of lactose agglomerate which corroborated with the experimental results for the same material. These agglomerates suffered extensive plastic deformation

before failing. The simulation results of Ghadiri *et al.* (2001) are consistent with those of Thornton *et al.* (1999). However, there are differences between these simulations and those of Subero *et al.* (1999) who report massive breakage into small clusters when the agglomerate impacted at a high velocity. They used the term "expanded disintegration" to describe the mode of failure of their agglomerates. It was suggested by the authors that during the formation process, their agglomerate did not gain sufficient rigidity in order to store strain energy to make crack propagation possible. There may also be other factors influencing the structure of the particles such as the presence of residual stresses in the agglomerate formed as a result of the agglomerate preparation method. Golchert (2003) has shown using computer simulations that the agglomerate state depends on the preparation method due to the presence of residual stresses, formed at the preparation stage.

From previous work two important features are noteworthy:

- There is no systematic work that analyses the influence of the interface energy in a wide range of values of this parameter. This is required in order to adequately establish the influence of the interface energy on the breakage of agglomerates.
- It is difficult to compare agglomerates made by different authors since the agglomerates could have been formed in slightly different ways making the structure and residual stresses within them different from each other.

1.6.3.3 Packing fraction

Ciomocos (1996) observed that the agglomerates of low packing fraction did not propagate any cracks. However, two agglomerates with larger packing fractions seemed to fail propagating cracks in the material. These observations that are consistent with the recent work of Mishra and Thornton (2001) clarified the observations of Ciomocos (1996) as they showed that the failure pattern of agglomerates also depended upon the packing fraction. At low values of packing fraction the agglomerates did not fragment. At high values of packing fraction their agglomerates fragmented into several pieces of comparable sizes. Finally at the intermediate values of packing fraction the agglomerates, when impacted at different orientations, showed different behaviour - in some orientations the agglomerates fragmented and in the others they did not fragment.

The results of Mishra and Thornton (2001) agreed qualitatively with the work of Subero (2001) who analysed experimentally the effect of porosity on the agglomerate breakage. The experimental results were previously reviewed in Section 1.4.1. The simulation showed that agglomerates with higher numbers of voids produced a larger amount of debris. He reported that for apparently the same porosity two types of agglomerate breakage may be observed, (i) extensive local disintegration with no crack propagation, (ii) local disintegration plus fragmentation due to crack propagation.

The main important feature can be summarised in the following point:

- A systematic analysis of the effect of the packing on the agglomerate breakage is recommended. It would also require a detailed analysis of the propagation of forces that could explain the observations of the authors aforementioned.

1.6.3.4 Impact angle

Data on the effect of the impact angle are scarce in the literature and inconsistent amongst the work reported. Vervoorn (1986) studied the effect of repeated impact of cylindrical alumina for normal and oblique impact. Vervoorn observed that the data of the probability of fracture of alumina as a function of the normal component of the impact velocity (for oblique impacts) were distributed around the lines that represented the data of the probability of fracture for normal impact velocity. Therefore Vervoorn concluded that the normal component of the impact velocity had a stronger effect on the particle breakage than the tangential component. Furthermore, Vervoorn observed that when the tangential component became equal to or greater than the normal component of the impact velocity, the impacting particle could roll and slide producing an increase in the abrasion of the particle and consequently in the mass lost per impact. Therefore, the tangential component of the impact velocity influenced the particle behaviour when it became larger than the normal component.

Hutchings (1981) reviewed the factors that influence the wear of materials. He reported that metals which fail in ductile mode, tend to suffer most severe wear at 20°

and 30°. In contrast, materials that fail in brittle mode, such as ceramics, tend to suffer the maximum wear at 90°.

Hutchings (1992) analysed the impact of flat targets by hard spherical particles. He observed that there is a critical impact angle at which a transition in the behaviour of the target material occurred. Over the transition angle, large lateral chips were detached from the target. Below the critical angle of transition the material suffered from extensive plastic deformation and the amount of material removed from the target was much smaller.

Salman *et al.* (1995) and Salman *et al.* (2003) reported on the oblique impacts of aluminium oxide spheres (solid particles) and a fertiliser. They observed that the probability of breakage increased as the impact angle was increased although the probability of breakage varied very slowly between 90° and 50°. For impact angles less than 20° for aluminium oxide spheres and 10° for the fertiliser the probability of breakage became negligible.

Samimi (2003) suggested that both the normal and tangential component of the impact velocity influenced the extent of damage of agglomerates. When the chipping regimes dominated, the normal component of the impact velocity determined the extent of breakage independent of the impact angle. However, in the fragmentation regime the tangential component of the impact velocity controlled the agglomerate behaviour.

Moreno *et al.* (2003) analysed the oblique impact of agglomerates. They found that the number of broken contacts decreased with decreasing impact angle when the impact velocity was kept constant. In addition, the number of contacts broken in the agglomerate was roughly the same for all impact angles when the normal component of the impact velocity was kept constant. However, the tangential component of the impact velocity seemed to influence the location of the contacts broken upon impact. When the impact angle was 90° (perpendicular to the target) the broken contacts seemed to be more uniformly spread through the agglomerate showing certain symmetry with respect to the perpendicular of the wall. However, at 30° impact (measured from the target), the broken contacts were more localised in one side of the

agglomerates (the side of the target from which the agglomerate moves to impact the wall). This change in the location of broken contacts concentrates the small debris produced upon impact in the same side as the broken contacts.

A detailed analysis of the propagation of forces within the agglomerate should be carried out in future. It would help in the explanation of the different behaviour observed by the different authors.

1.7 Conclusions

In this literature survey the fundamental concepts of agglomerate characterisation, contact mechanics and the results of computer simulation of agglomerate impact have been reviewed.

From this review we can conclude:

- The comparison between computer simulations and experiments as far as the modes of failure of agglomerates are concerned, has demonstrated the usefulness of the Distinct Element Method in gaining a better understanding of the agglomerate behaviour.
- Contact mechanics is an important feature of the simulation of agglomerates since several models (Hertz, JKR, DMT, Mindlin and Deresiewicz, Savkoor and Briggs, Thornton and Ning) are included into the TRUBAL software in order to reproduce the behaviour observed in experiments.
- The TRUBAL code is capable of simulating a wide variety of agglomerates by changing the physical properties of the constituent single particles.

The limitations of computer simulation found in the papers are listed below.

- So far, relationships between interparticle forces and geometric properties of agglomerates such as the fractal dimension, shape, or porosity have not been adequately developed.

- There are no mathematical expressions that relate modes of failure of agglomerates with single particle properties, agglomerate properties or interparticle bonds.
- In addition, there is no model that predicts the failure patterns of agglomerates.
- So far, the simulations carried out by TRUBAL are very restricted in agglomeration formation and other methods of preparation should be explored.

CHAPTER 2: CHARACTERISTICS OF THE AGGLOMERATION AND IMPACT PROCESSES

The procedure for the preparation of the agglomerates and the method of carrying out the impact process are described in this chapter. The structural features of the agglomerates such as the isotropy, density, coordination number and residual stress distribution have been analysed.

The impact process has also been analysed and the stress propagation within the agglomerate and the target force have been quantified and contrasted with the model predictions for solid particles based on Hertz analysis. Based on this analysis the Young's modulus of the agglomerate has been calculated and compared with the models available in the literature.

2.1 Agglomeration

The agglomeration method, the evolving properties and structure of the agglomerates are described in this section. In particular the influence of the agglomeration method on the structure of the agglomerate and the effect of the method of introducing the surface energy on the characteristics of the agglomerate are addressed.

2.1.1 Description of the agglomeration method

Geometrical and physical properties of agglomerates are characteristics that are dependent on factors such as single particle properties, the interaction between them and the way agglomerates are formed.

The agglomeration method used in the simulations can be described as follows:

(a) The dimensions of the space in which the agglomerate is created (working space) are specified and the space is divided into boxes in order to track the movement of the particles. This arrangement does not have any influence on the structure of the final agglomerate although the computational time required to form the agglomerate is

strongly affected. This is due to the searching required to check potential and real contacts between particles within a box.

(b) A spherical volume is specified inside the working space. This spherical volume should be sufficiently large to allow the creation of all particles that will form the agglomerate. In order to save computational time in the agglomeration process, the particles will be created randomly as close as possible to each other but without overlapping.

(c) Physical properties, such as Young's modulus, Poisson's ratio and density, are assigned to the particles according to the specific material to be simulated. In the simulations reported here particles are allowed to deform elastically but not plastically and so no yield modulus has been assigned.

(d) Damping is used in order to simulate energy dissipation due to interparticle and particle-boundary interactions. Two types of damping are used: global damping acting on all the particles and local damping acting on each contact. The contact damping simulates energy losses due to collisions and it has been used in all the simulations reported here. The global damping has not been used during the impact of agglomerates but during the formation process.

(e) In order to bring the particles together a centripetal force with an acceleration of 9.8 m/s^2 is directed to the centre of the spherical space. This force acts at the centre of every particle accelerating them to the centre of the spherical space. The particles positions' are calculated according to the equations given in Appendix A. The spherical symmetry of the centripetal force produces spherical agglomerates.

(f) Once the centripetal force is applied, the contact number (defined as the average number of contacts per particle) increases until a steady state is reached. As it will be shown in the following section, the introduction of surface energy at different stages of the agglomeration process produces agglomerates with different packing fractions. To create very well-packed structures, friction and surface energy are applied once the coordination number has reached a steady state. Friction and surface

energy are applied in small increments to avoid the accumulation of high residual stresses in the contacts. The introduction of cohesive interactions between particles produces a new increase in the coordination number of the assembly. This continues until the coordination number reaches a new steady state. The agglomerate has then been formed.

2.1.2 Influence of the agglomeration method on the structure of the agglomerate

In the agglomeration method used here a number of parameters can be varied to control the final state of the agglomerate. These are the centripetal acceleration, the time at which the interaction between particles is introduced, the values of the global and contact damping parameters and the size of the initial volume where the particles are created. However, the effect of the variation of these parameters has not been extensively investigated due to the significant amount of time required for this purpose. The parameter that has been addressed in some depth in this work is the time at which the interaction between particles is introduced. This is addressed later in this chapter.

2.1.2.1 Effect of the initial spatial distribution of particles

The creation of particles close to each other as described in Section 2.1.1 may influence the size and distribution of pores found in the agglomerate. In some way, this limits the accessible positions for particles. In the tight space available, the particle positioning in a specific place could be affected by its neighbouring particles that are competing for the same position at the same time. This could result in no particles accessing that position due to mechanical arching and a large pore would be created. It would be more appropriate to create particles far away from each other. This method would make the simulation process extremely long and for that reason has not been followed in this work. However, in spite of the shortcoming presented above, it will be shown that the agglomerates formed are quite well packed with random distribution of spheres.

2.1.2.2 Effect of the introduction of the surface energy in the agglomeration process

The surface energy is introduced once the assembly reaches a steady state in terms of the coordination number. The reason for this is to obtain very well-packed structures. The application of the surface energy at different stages of the agglomeration process produces structures with different packing fractions. If the surface energy is applied at the same time as the assembly is compressed a very loose agglomerate is created. In Table 2.1 the differences in structures are compared as a function of the moment at which the adhesive interaction between particles at the value of surface energy of 3.5 J/m^2 is introduced. The agglomerates reported in Table 2.1 are made of 3000 primary particles whose density and elastic modulus are 2000 kg/m^3 and 31 GPa, respectively. The later the surface energy is introduced the higher is the resultant packing fraction and consequently the smaller is the agglomerate and the higher is the density of the agglomerate. The differences in density, packing fraction and coordination number observed when the interaction between particles is introduced at different stages of the agglomeration process provide a way of controlling the agglomerate structure. The agglomerates made in this work are very well-packed since the interaction between particles is introduced at a very late stage of the agglomeration process.

Table 2.1 Effect of the instant at which the introduction of surface energy is made on the structure and properties of agglomerates.

Label	Time (ms)	Packing Fraction	Coordin. Number	Agglomerate Radius (mm)	Density (kg/m^3)
A	0.00	0.385	2.00	1.016	769.8
B	10.80	0.469	3.06	0.953	938.6
C	16.31	0.531	4.66	0.916	1061
D	23.11	0.543	4.89	0.909	1085.2
E	48.60	0.546	5.63	0.908	1091.4
F	89.00	0.546	5.62	0.908	1091.2

If the packing fraction is plotted as a function of the moment at which the adhesive interaction is introduced it is possible to observe that the packing fraction reaches a plateau (see Table 2.1 and Fig. 2.1). This imposes a limit on the packing fraction that can be obtained and hence on the characteristic of the assembly. The main question arising from Fig. 2.1 is the nature of the plateau and whether the maximum value of 0.546 in the packing fraction obtained for the agglomerate is dependent on the agglomeration method or on the physical properties of the particles.

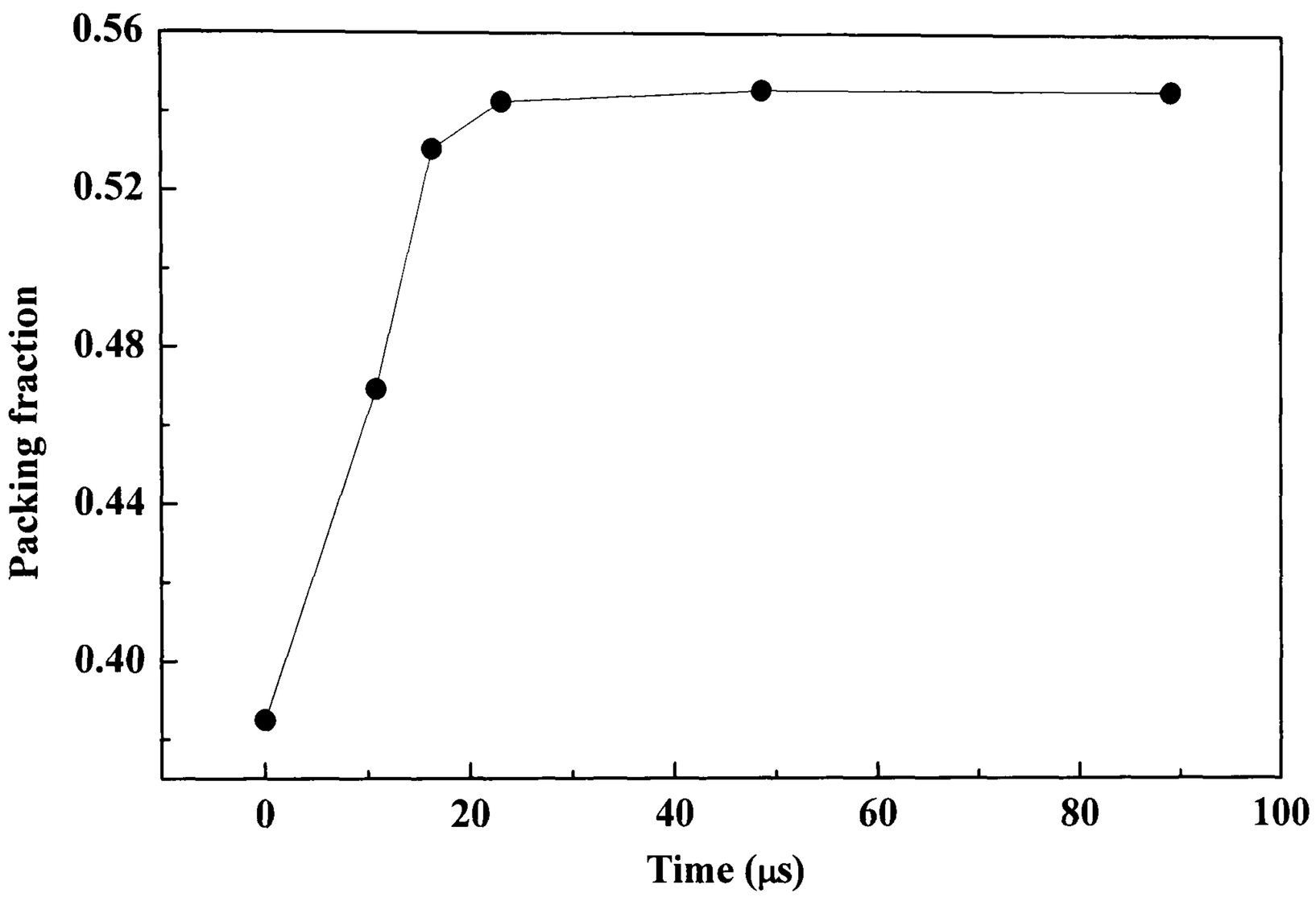

Figure 2.1 Dependency of the packing fraction on the moment at which the surface energy is introduced.

The analysis of the agglomerate labelled F (c.f. Table 2.1) reveals that the packing fraction within a radius 0.8 mm from the centre is 0.646 whilst that of the whole agglomerate is 0.546. This difference arises from the surface roughness. The packing fraction is defined as the ratio of the volume of all particles to the volume occupied by the agglomerates. It is difficult to estimate the volume occupied by the agglomerate since the external surface of the agglomerate is not smooth. For calculating the volume occupied by the material the agglomerate is considered perfectly spherical and its radius is the distance, *RCM*, from the mass centre of the agglomerate, *CM*, to the centre of the outer particle, CP, plus half of the radius of that particle (R_{CM} +0.5R) as shown in Fig. 2.2. The objective of this way of

measuring the volume occupied by the agglomerate is to correct for the roughness of the external surface.

$$V_{OCCUPIED} = \frac{4}{3}\pi(R_{CM} + 0.5R_P)^3$$

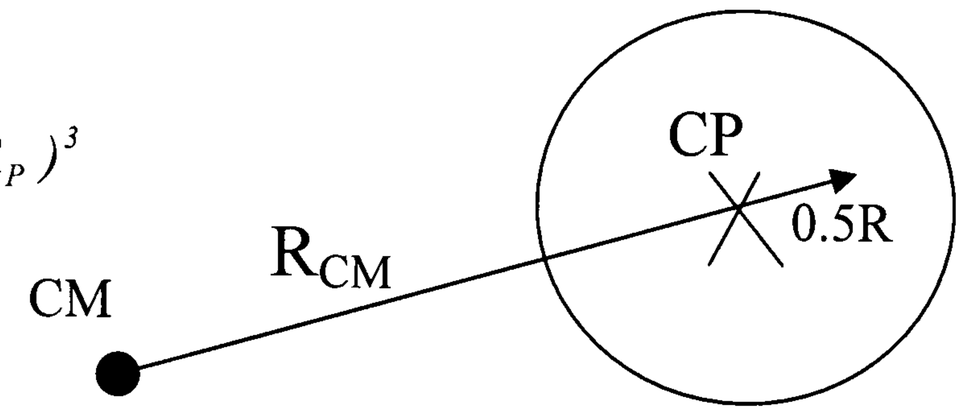

Figure 2.2 Method of calculating the packing fraction of agglomerates.

2.1.3 Analysis of the structure of the agglomerates

The intention of this work is to analyse the strength of spherical agglomerates with a constant mass distribution and coordination number inside the agglomerate. A gradient in the distribution of mass would clearly produce a different type of agglomerate. The analysis of the structure was made by studying the radial distribution of the mass and coordination number. An analysis of the angular mass distribution does not seem to be necessary since the initial distribution of particle is random and the centripetal force is by definition spherically symmetric. The analysis carried out can be described in the following:

- a spherical volume of radius *r* with its centre at the mass centre of the agglomerate *CM* is taken (Fig. 2.3).
- inside the spherical space and a spherical layer of 50 μm thickness (Fig. 2.3) the mass, coordination number and contact number are analysed.
- if a particle is intersected by the surface of a spherical volume of radius *r*, the volume of the particle radius within the spherical space is calculated by integration.

Figure 2.4 shows the mass of the agglomerate inside a volume of radius *r*, plotted as a function of the radius *r*. The data obtained from the simulation are well fitted to a straight line on a log-log scale. Hence, the mass distribution can be described by the following equation:

$$M \propto (r)^{3.00} \qquad (2.1)$$

where M is the mass of the agglomerate within a spherical space of radius r. According to this relationship the fractional exponent is 3.00, which implies that the agglomerate has a spherical distribution of particles.

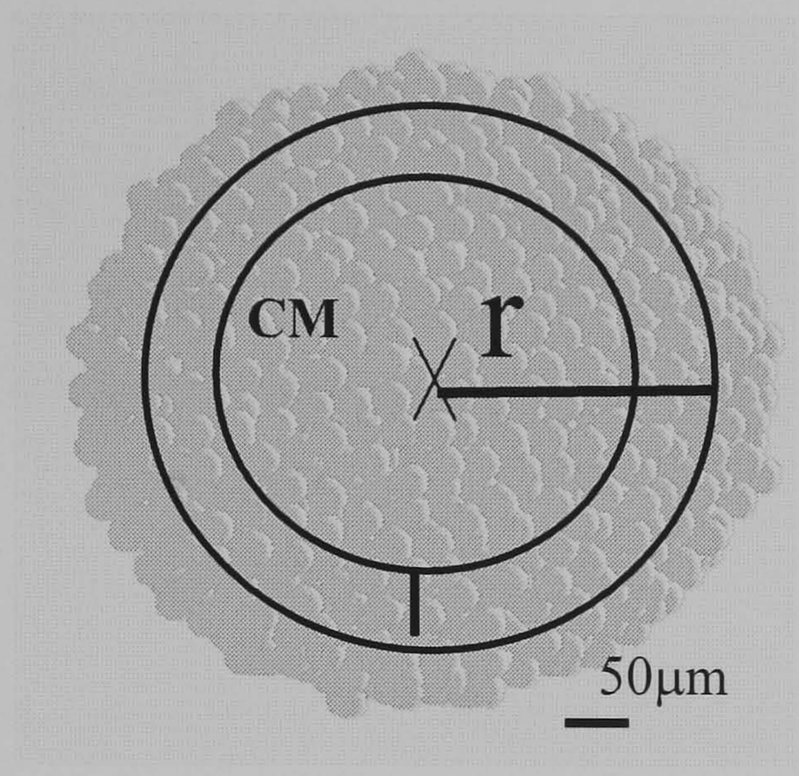

Figure 2.3 Spherical agglomerate.

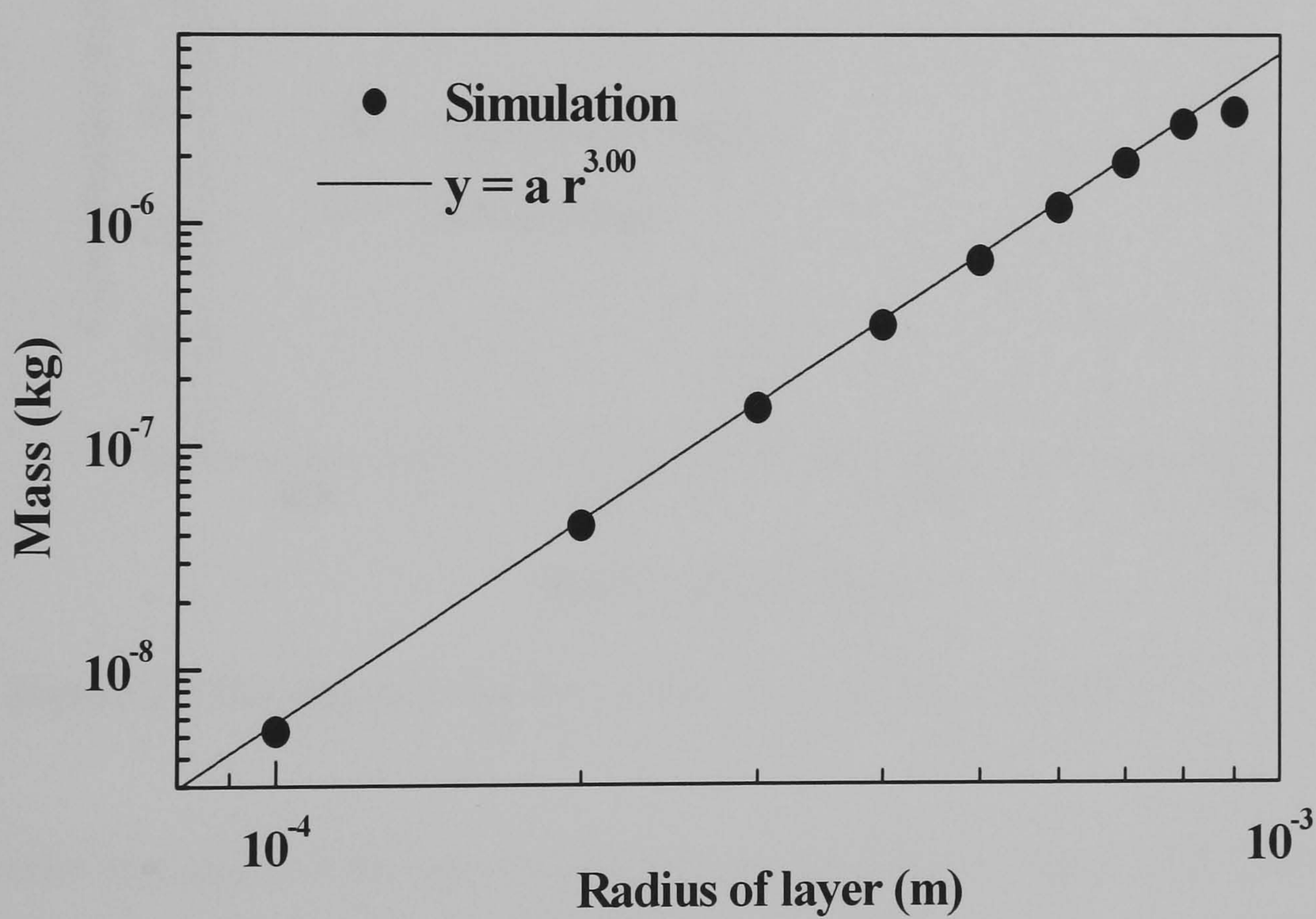

Figure 2.4 Mass distribution within Agglomerate F (Table 2.1).

The contact distribution of particles within the agglomerate was analysed by (i) plotting the coordination number within spheres centred at the mass centre of the agglomerate as a function of the radius *r*, and (ii) by plotting the coordination number within spherical layers (100 μm each) of the agglomerate as a function of the distance between the layer and the mass centre of the agglomerate. The results are shown in Fig. 2.6. The coordination number within the spherical layer as a function of the distance from the mass centre has a constant value throughout the agglomerate. Similarly, the coordination number within the spherical space has a constant value (Fig. 2.5). These two characteristics have been found in all agglomerates used in this work.

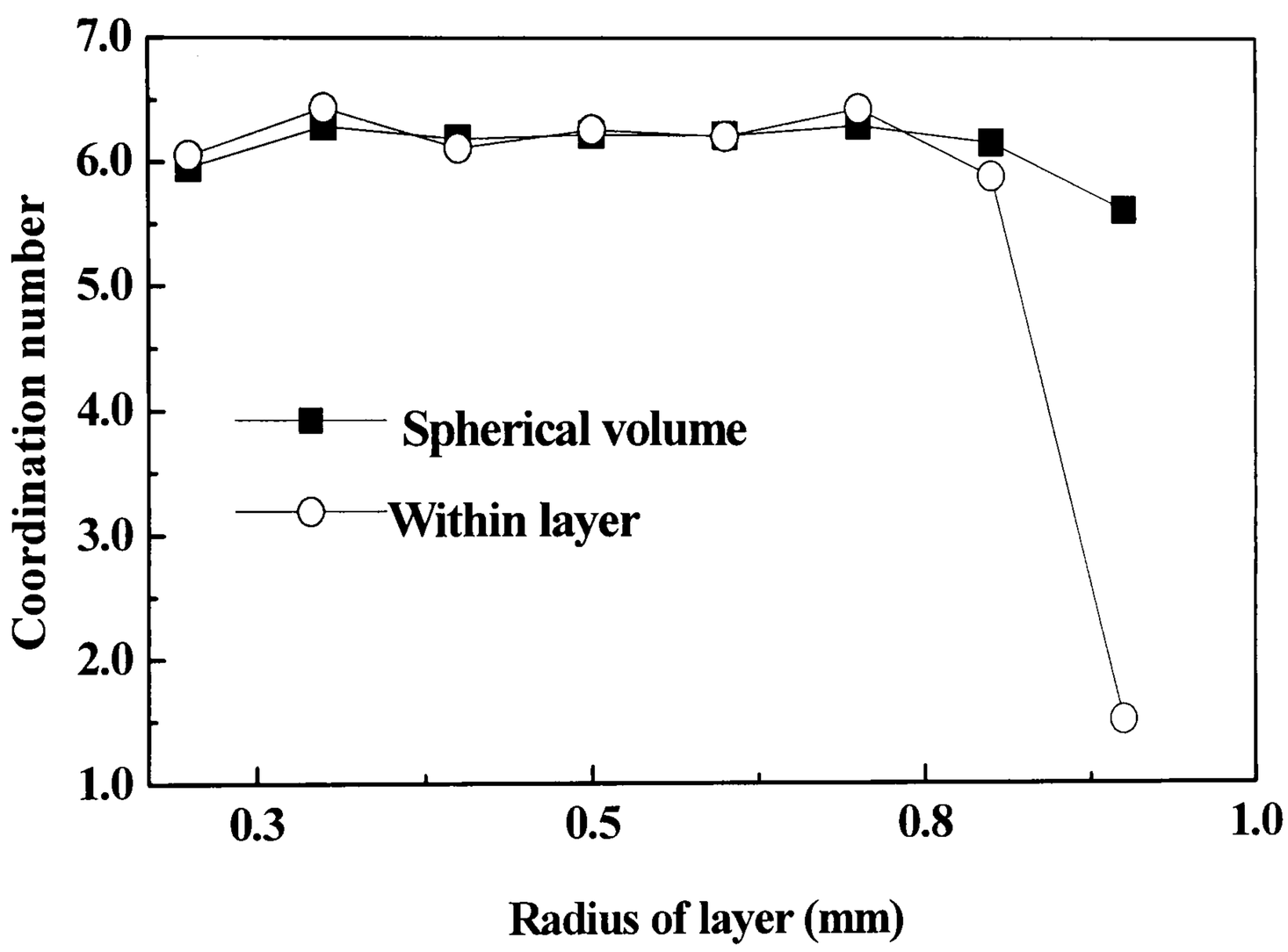

Figure 2.5 Coordination number within Agglomerate F (Table 2.1).

The contact histogram of the agglomerate is shown in Fig. 2.6. Most of the particles have a contact number of around six. The number of particles with just one contact was four and with two contacts was 70. These contacts were located on the external layer of the agglomerate producing the decrease in the coordination number at the boundary as shown in Fig. 2.5 When the agglomerate is impacted these particles are easily detached from the agglomerate and are responsible for the small amount of debris produced at very low impact velocities.

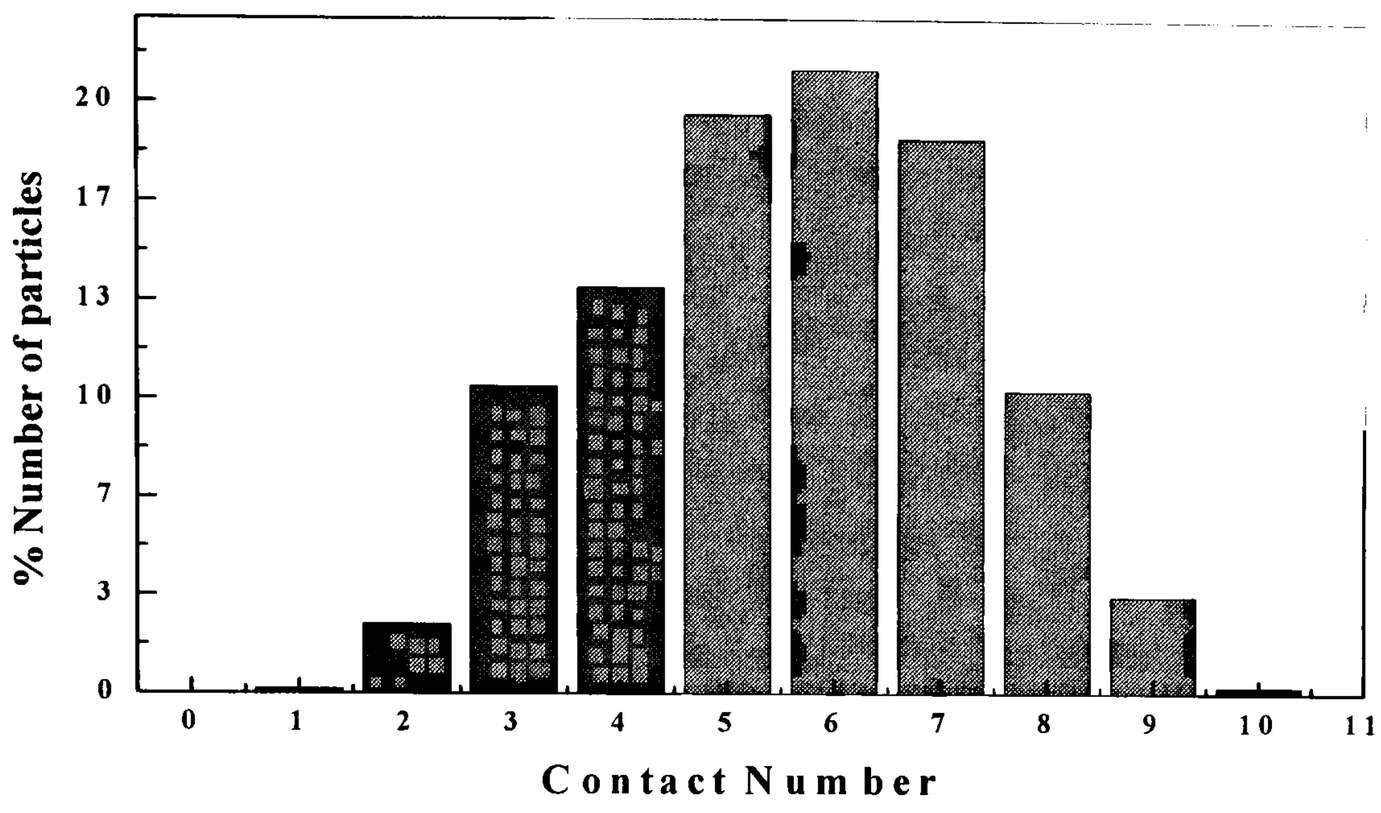

Figure 2.6 Contact histogram for Agglomerate F (Table 2.1).

It is possible to analyse the level of stresses in the contacts between particles following the same method as that used for the analysis of mass and coordination number. The average values of the stresses in the contacts within layers of 50 μm thickness have been plotted in Fig. 2.7 as a function of the distance from the mass centre of the agglomerate to the layer. The values of the compressive and shear stresses in the contacts are fairly constant through the agglomerate. Instead, the level of tensile stresses seems not to be constant near the centre, although the variation is considered to be small. This could be due to the number of tensile contacts in this area of the agglomerate being low, around 10 contacts as compared with the number of compressive contacts which is around 35.

2.1.4 Discussion and conclusion

The agglomeration process produces spherical agglomerates with a constant distribution of mass and coordination number. Similar results have been found in all agglomerates used in this work. However, the roughness of the surface produces a fall in the value of the parameters mentioned above. This decrease is unavoidable. An objective of a future work could be an investigation of the influence of the surface roughness in the mode of failure of agglomerates.

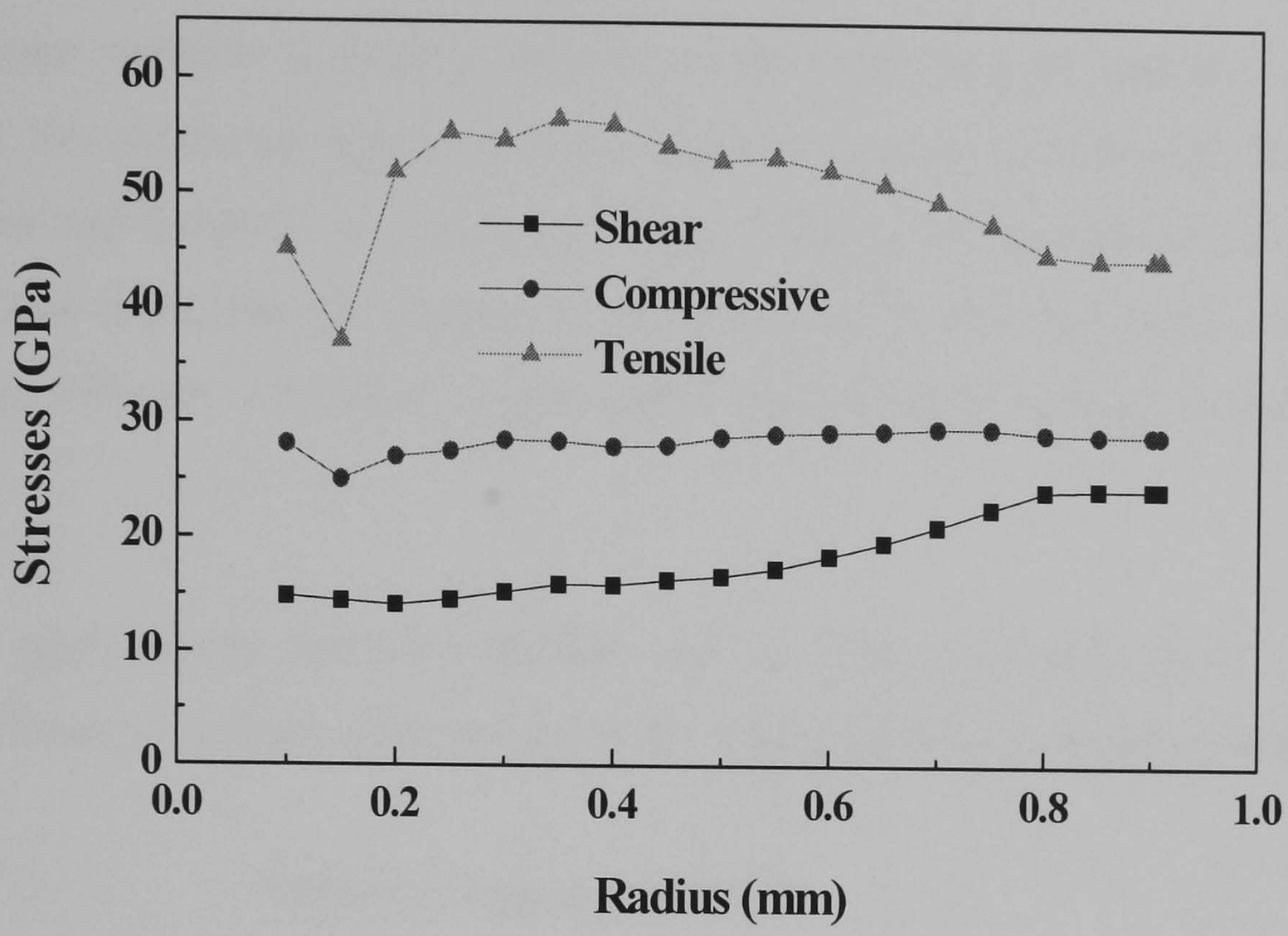

Figure 2.7 Stress distributions at contacts within Agglomerate F (Table 2.1).

It has also been shown that the agglomeration process provides a good control of the packing fraction of the final agglomerate and this is used to produce very well packed agglomerates. However, this method of agglomeration is artificial and cannot be used in real agglomeration processes. It could be useful in future to experiment with different agglomeration methods in order to study the strength of agglomerates created in different ways. Among many possibilities for the preparation of future agglomerates could be to make agglomerates grow by a layering process. Other possibilities could be giving an initial random velocity to the particles at the same time as a centripetal force is applied or agglomerating by simply confining the particles in a decreasing spherical volume.

The agglomeration method followed here has previously been used by other workers such as Subero *et al*. (1999) and Ning *et al.* (1997) who compared their simulation predictions with experimental results and found a good agreement, which provides a base for continuing using this agglomeration method.

2.2 Impact process

2.2.1 Description of the impact process

Agglomerate strength is loosely defined as the resistance of agglomerates to fracture. However, the resistance against fracture depends not only on the particle properties, but also on the test method. A common method to assess the strength of solids is by impact testing. This is because the damage in agglomerates is often due to the collisions with the containing walls or with other agglomerates and hence the interest in the impact testing method.

Once an agglomerate has been formed and its structure analysed, an elastic target is created. Young's modulus and density of the target material correspond to those of steel.

Table 2.2 Target properties

Young's modulus (GPa)	210
Poisson ratio	0.3
Density (kg/m^3)	7800
Surface energy (J/m^2)	0.03
Friction coefficient	0.35

The impact process is implemented according to the following steps:

(a) the agglomerate is initially positioned close to the target. The objective is to save computational time in the time spent in approaching to the target. A typical value used for the initial distance between agglomerate and target is 10 nm which is much smaller than the particle size.

(b) an acceleration along the normal direction of velocity perpendicular to the target with a value of gravity of 9.8 m/s^2 is applied with the objective of reproducing realistic impact conditions.

(c) in the preparation of the agglomerate, global damping is used but in the impact process this is switched off.

(d) Finally, an initial velocity is assigned to all particles. The velocity has the same value for all particles and hence the agglomerate as a whole is directed towards the target. Since the agglomerate is positioned close to the target, the acceleration does not significantly change the impact velocity and thus the initial velocity given can be considered as the impact velocity. For the distance of 10 nm between agglomerate and target the velocity of the agglomerate would be increased by around 0.4 mm/s. The impact angle, θ, can be defined as in Fig. 2.8.

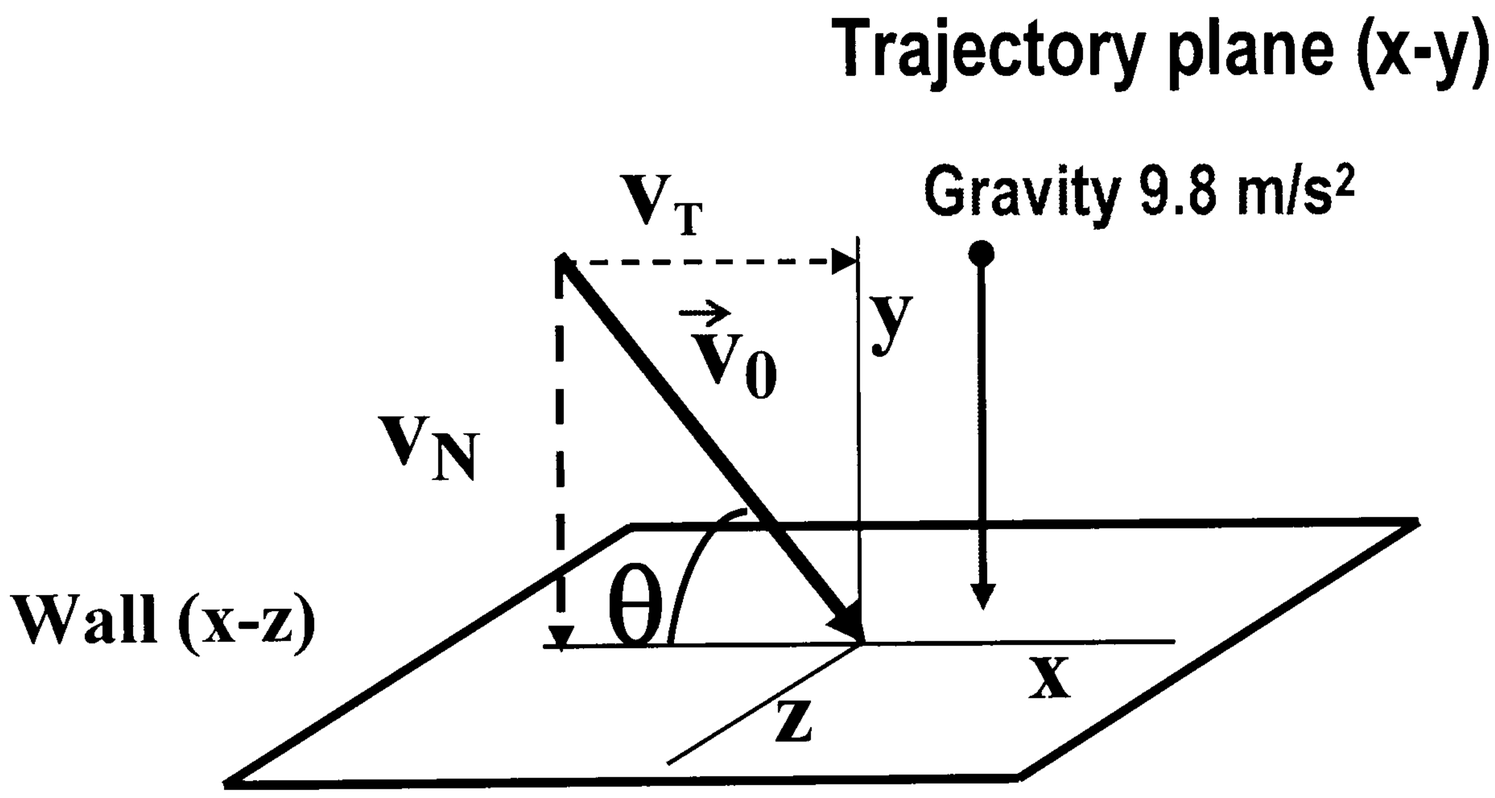

Figure 2.8 Definitions of the impact parameters

The impact of an agglomerate against a target is analysed by monitoring changes in a number of parameters which measure microscopically or macroscopically the damage produced in the agglomerate during impact. These are the number of broken contacts, the number and size of the fragments detached from the agglomerate, the kinetic energy of the particles after impact and the maximum force exerted on the target.

2.2.2 Dynamics of the impact process

The impact process can naturally be divided into two parts: the compression (loading) and the rebound or the deposition of the agglomerate on the target (unloading).

Figures 2.9 and 2.10 show the characteristics of an impact event for Agglomerate F (Table 2.1) on a target at different velocities. During the compression stage the impact force exerted on the target increases (Fig. 2.9), passes through a maximum and then declines. At low impact velocities (0.01-0.05 m/s) the curve of the force versus time is smooth and symmetric with respect to the maximum target force, similar to the behaviour of a spherical solid particle impact (Johnson, 1985). At about 0.5 m/s the curve of the target force versus time is not so smooth any more. At higher impact velocities the curves are asymmetric and are characterised by many secondary maxima. The undulations in these curves are strongly influenced by the rupture of bonds in the assembly and the detachment and further collisions against the target of small debris produced upon impact.

Figure 2.10 shows the evolution of the normalised kinetic energy as a function of time. The kinetic energy first decreases until reaching a minimum value. During this stage the agglomerate is being slowed down. At low impact velocities (*e.g.* 0.01 m/s) the profile of kinetic energy versus time is nearly symmetric as for an elastic solid particle. However, the symmetry is lost at higher impact velocities due to the dissipative mechanisms operating in the system. The loss of energy depends on the impact velocity. At the lowest impact velocity, the kinetic energy recovers to almost 100%. At higher velocities the recovery decreases and furthermore the pattern of the curve changes indicating a significant damage to the agglomerate.

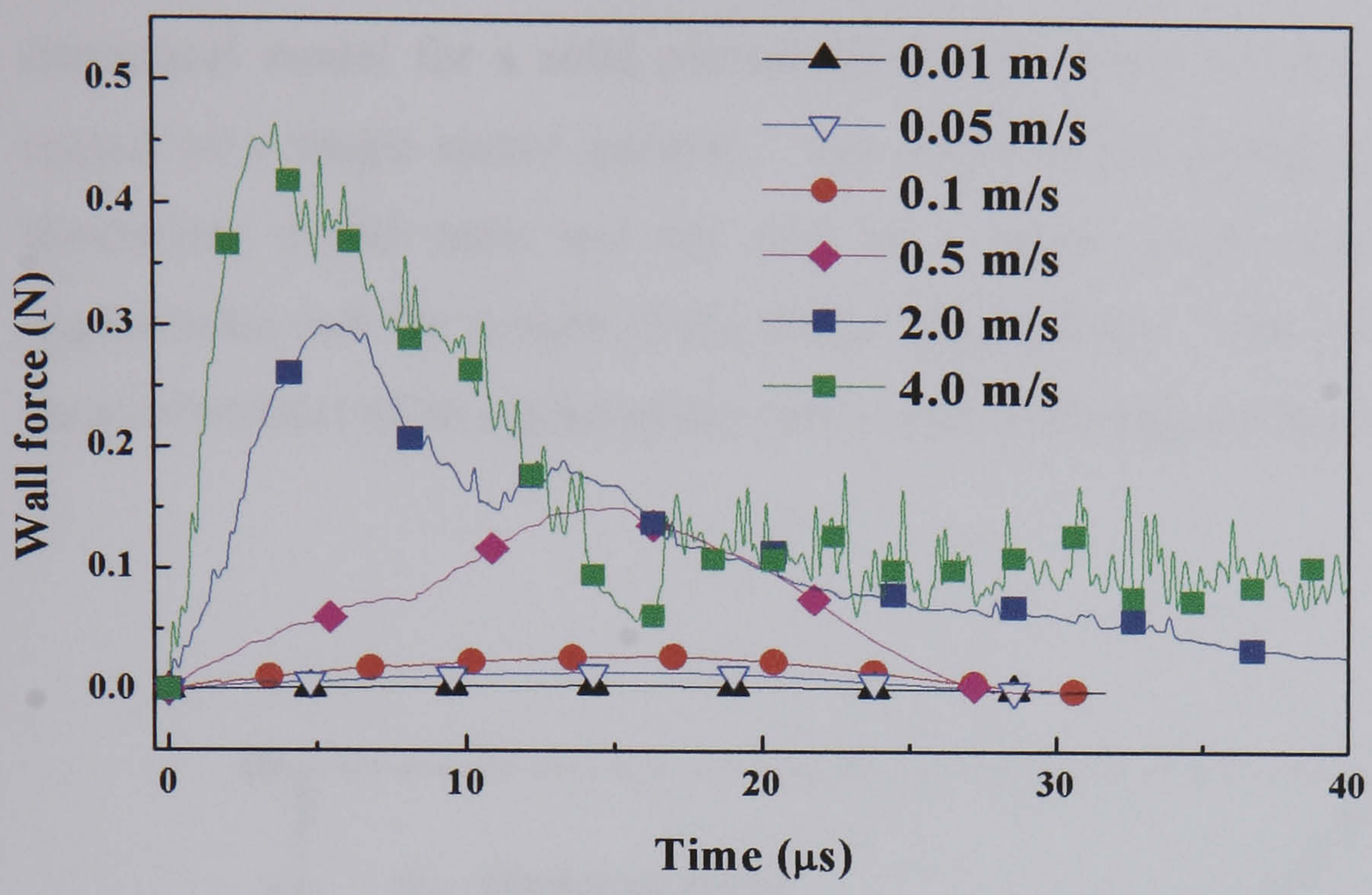

Figure 2.9 Evolution during impact of the force exerted on the target by Agglomerate F (Table 2.1).

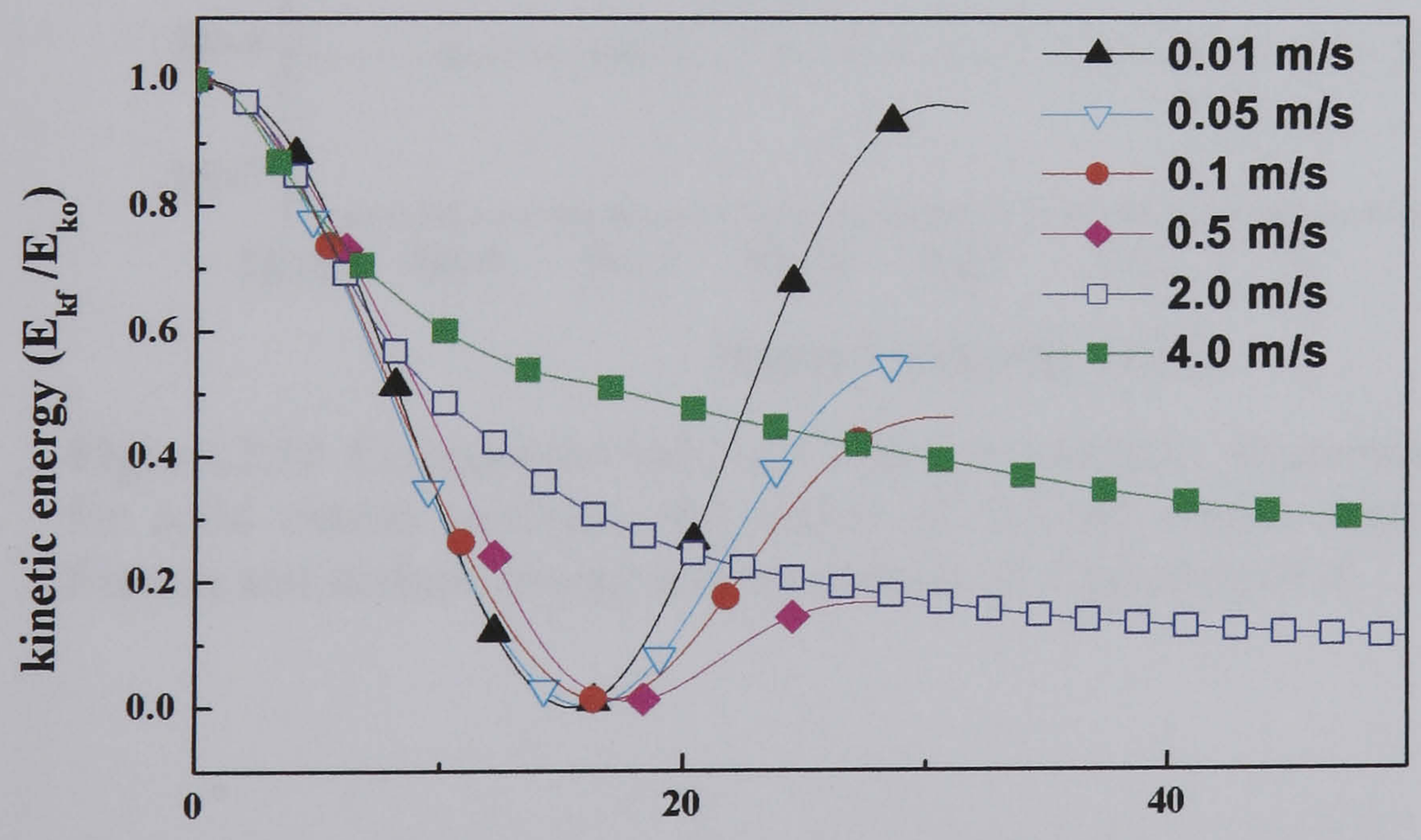

Figure 2.10 Evolution of the kinetic energy during impact of Agglomerate F (Table 2.1).

Figure 2.11 shows a comparison in the maximum target force for an agglomerate, a theoretical model for a solid particle (Johnson, 1985) and the simulation of the impact of a single elastic particle. The elastic solid particle simulation and the theoretical model both use the size of a small single particle forming the agglomerate and the weight of the whole agglomerate. This is because the initial stage of contact of an agglomerate with a wall is through a single primary particle.

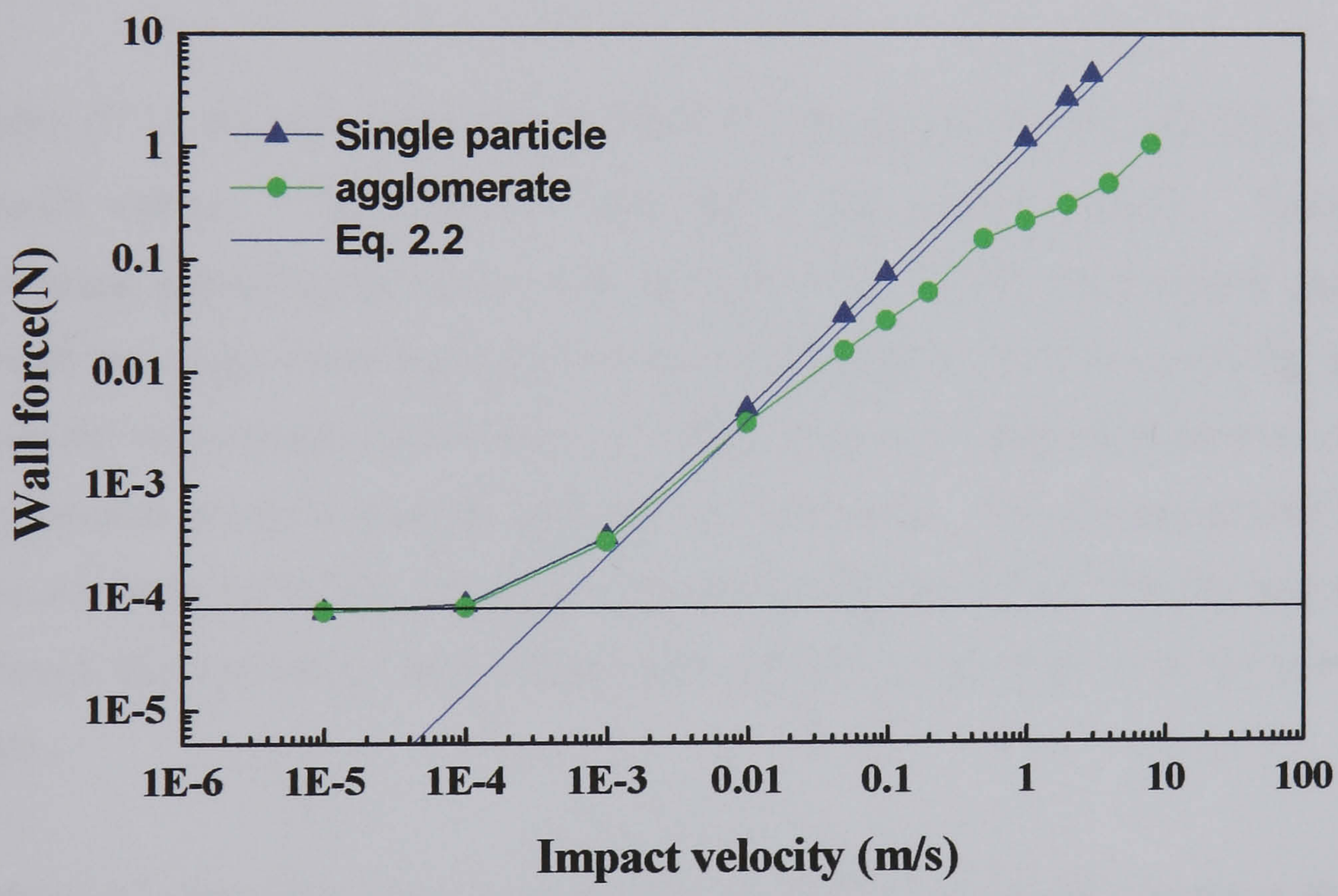

Figure 2.11 Comparison between different models: theoretical model for solid elastic particles, simulation of a small elastic particle with friction and surface energy and simulation of Agglomerate F.

At intermediate velocities, the results for the three cases overlap, but at high impact velocities, the agglomerate behaviour departs from the other cases.

At low impact velocities (less than 0.01 m/s) due to the roughness of the surface there is just a single primary particle of the agglomerate in contact with the target.

This particle deforms and is supporting the whole weight of the agglomerate. The force transmitted to the rest of the agglomerate is transmitted through this particle and therefore the whole deformation of the agglomerate is mainly due to the deformation of this particle.

The expression given by Johnson (1985) is based on Hertz analysis for single elastic particles without adhesion:

$$P = \frac{E^{*2/5} \rho^{3/5} R^{*2} V^{6/5}}{1.27(1-\nu^2)^{2/5}} \qquad (2.2)$$

where E^* is the reduced elastic modulus, ρ the density of the particle, R^* the reduced radius, ν the Poisson's ratio and V the impact velocity. Johnson's expression approximates quite well the behaviour of the solid elastic particle beyond the range where the adhesive forces predominate (>0.01 m/s) (Fig. 2.11). When the impact velocity increases to values close to 0.1 m/s the behaviour of the agglomerate diverges from the solid particle behaviour. The maximum wall force does not seem to follow the same dependency on the impact velocity any more although the number of agglomerate-wall contacts is just one, as in the previous stage.

Figure 2.12 shows the force as a function of deformation for three cases: a particle with the properties of the primary particle of the agglomerate, a particle with the size and elastic modulus of the whole agglomerate and the simulation data for an agglomerate. The agglomerate deformation, δ, is very different from the case of solid elastic particles. For the agglomerate a linear relationship can be fitted. This clearly reflects that the non-linear relationship between force and deformation for the primary particle is absorbed by the discrete nature of the agglomerate and the dynamics of the agglomerate is different from that of solid elastic particles.

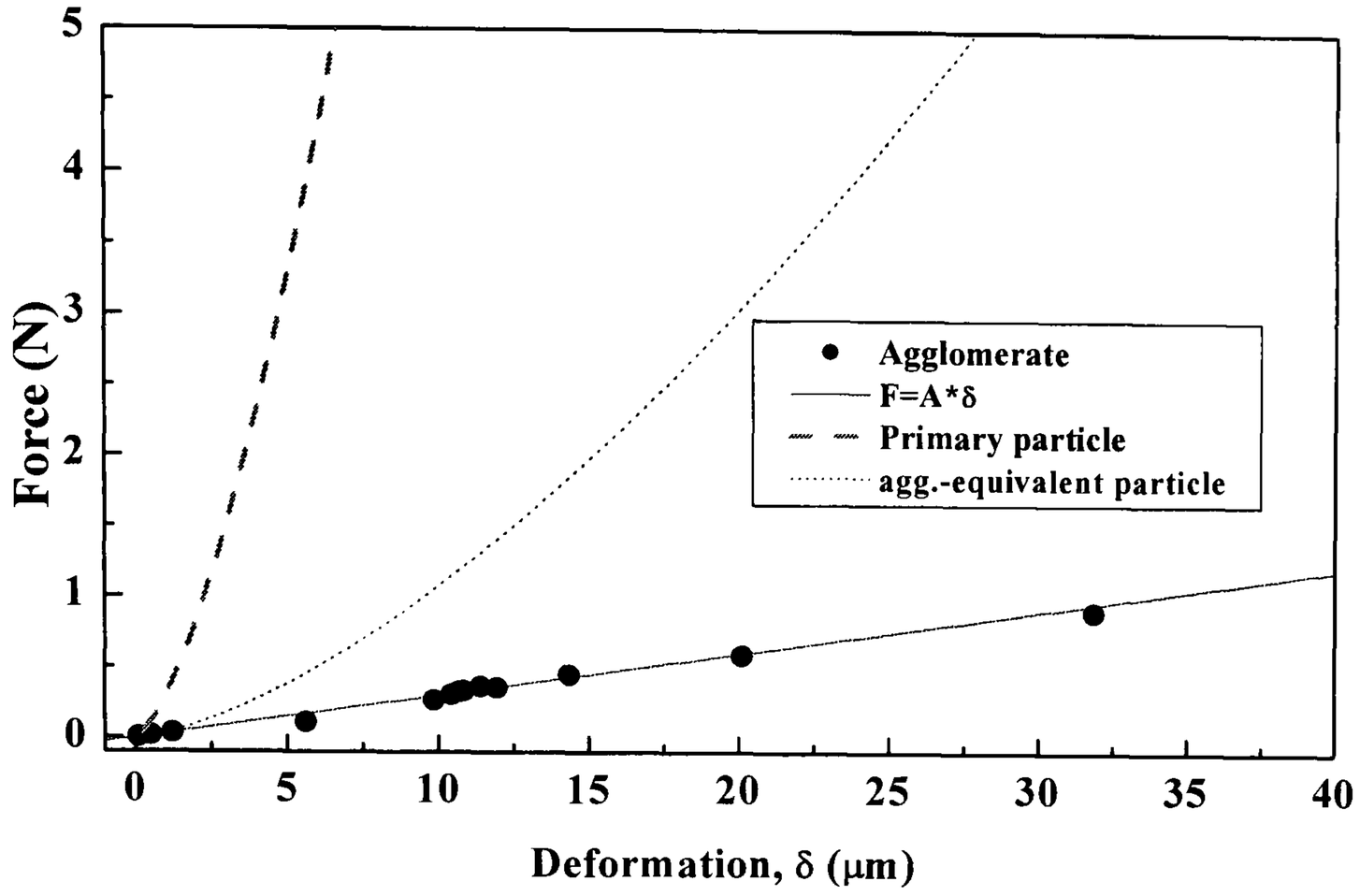

Figure 2.12 Force-deformation relationships for three cases: a particle with the properties of the primary particles of Agglomerate F, a solid particle with the size and elastic modulus of the whole Agglomerate F and the simulation data for Agglomerate F (Table 2.1).

2.2.3 Propagation of the impact force inside the agglomerate

The impact of the agglomerate produces a compressive wave that propagates inside the agglomerate. Figures 2.13(a-d) show the value of the average contact forces within sections of 100 μm thick as a function of the distance to the target and time from the impact moment for four impact velocities. The value of the compressive forces in the contacts during the impact process depends on four factors: the value of the forces in the contact prior to impact, the instant when the values of the forces are measured, the distance from the contact to the wall and the value of the impact velocity. For layers close to the target, the decay of the average contact force with distance can be approximated by a relationship in the form

$$(F - F_0)x^n = constant \qquad (2.3)$$

where x is the layer distance, F_0 the force on the wall for the first layer, F is the average contact force at a distance x from the target and n is an empirical exponent, which has a close fit to the value 2.5. By integrating with respect to the distance, the energy, E, decays inside the agglomerate in the form:

$$Ex^{n-1} = constant \qquad (2.4)$$

If the exponent n had a value of three the energy decays proportionally to the surface area of the wave front (distance square), which is propagating from the contact with the wall to the inside of the agglomerate. However this situation is ideal for non dissipative processes and does not apply to the cases where friction, damping and bond breakage prevail and could explain why the exponent is slightly less than three. Furthermore, this is a simplified explanation since the curves changes with the distance from the impact site at high impact velocities, *e.g.* 5.0 m/s, where the breakage of bonds will be influencing the propagation of force within the assembly of particles.

Thornton and Randall (1988) tested the force attenuation between particles for a system where a particle impacted against a column of single particles. The collision was with the top particle in the column. During the test no friction or damping was applied between the particles. However, they observed that the force was attenuated in the contacts and concluded: "force attenuation through particulate materials is primarily due to the discrete nature of the material and the interactive behaviour at the contacts". In the case studied here the decay of the contact force with the distance to the target cannot therefore be only attributed to the interparticle friction and damping but also to the discrete nature of agglomerates.

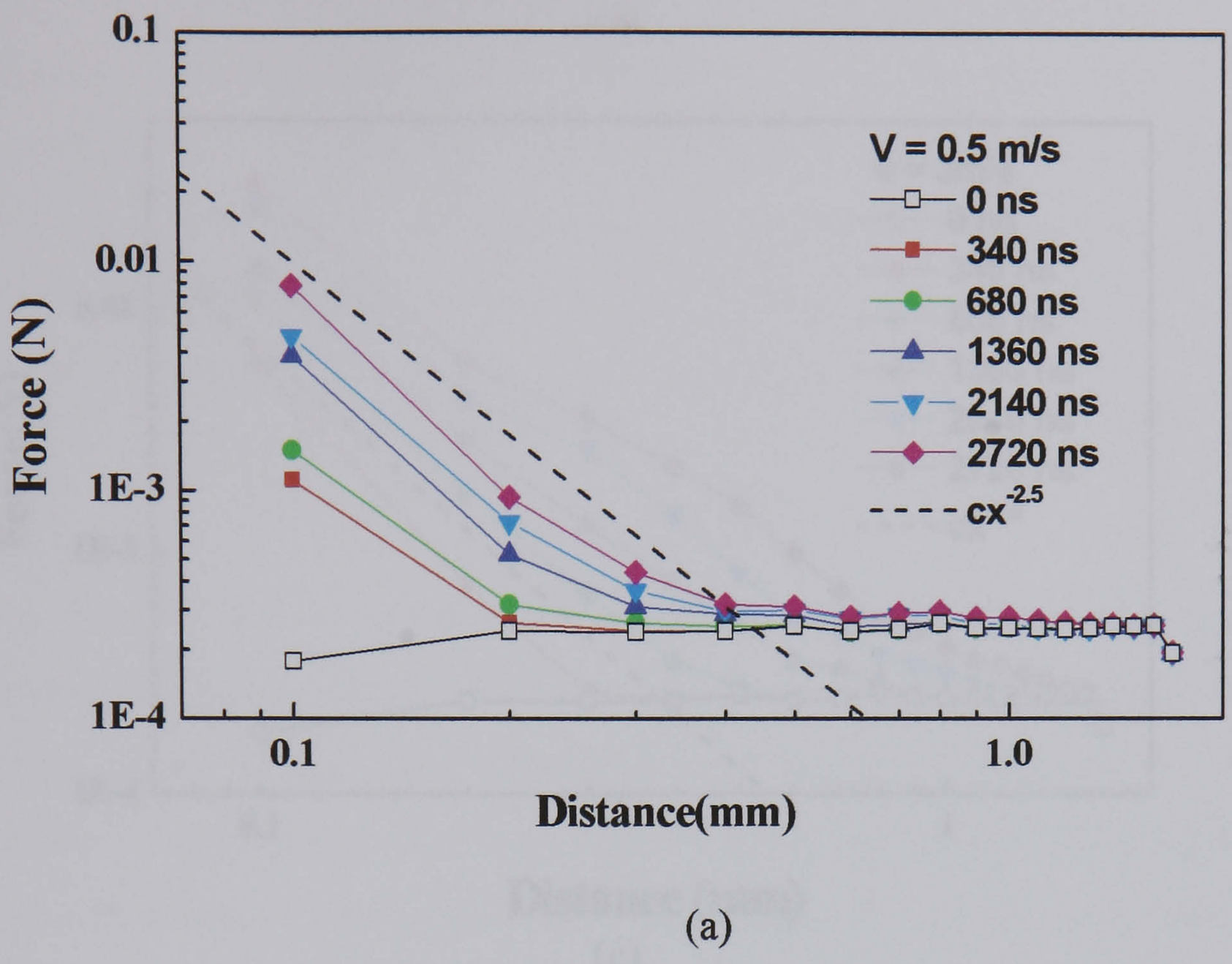
0.1
0.01
1E-3
1E-4
Force (N)
0.1
1.0
Distance(mm)
V = 0.5 m/s
0 ns
340 ns
680 ns
1360 ns
2140 ns
2720 ns
cx-2.5

(a)

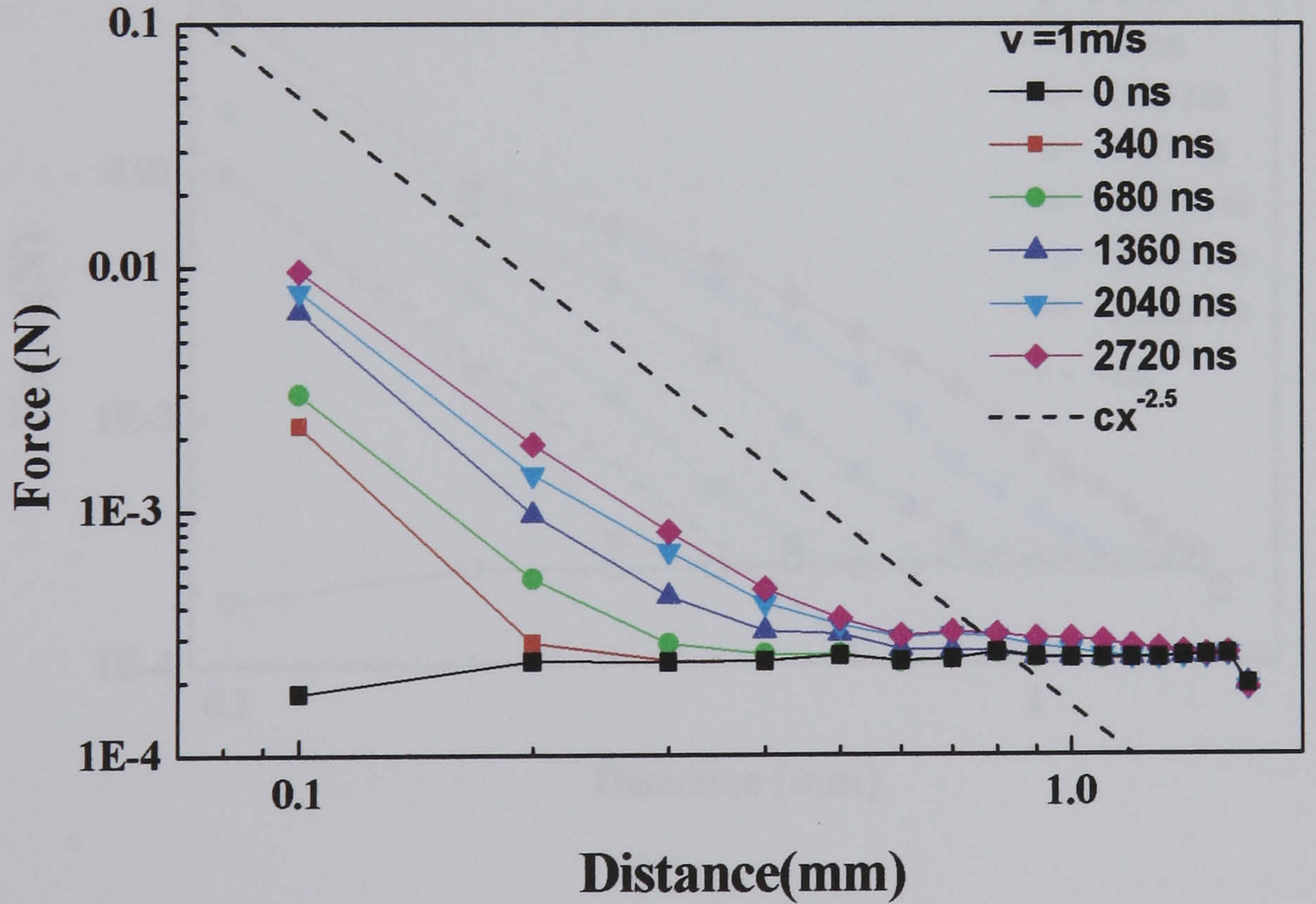
0.1
0.01
1E-3
1E-4
Force (N)
0.1
1.0
Distance(mm)
v =1m/s
0 ns
340 ns
680 ns
1360 ns
2040 ns
2720 ns
cx-2.5

(b)

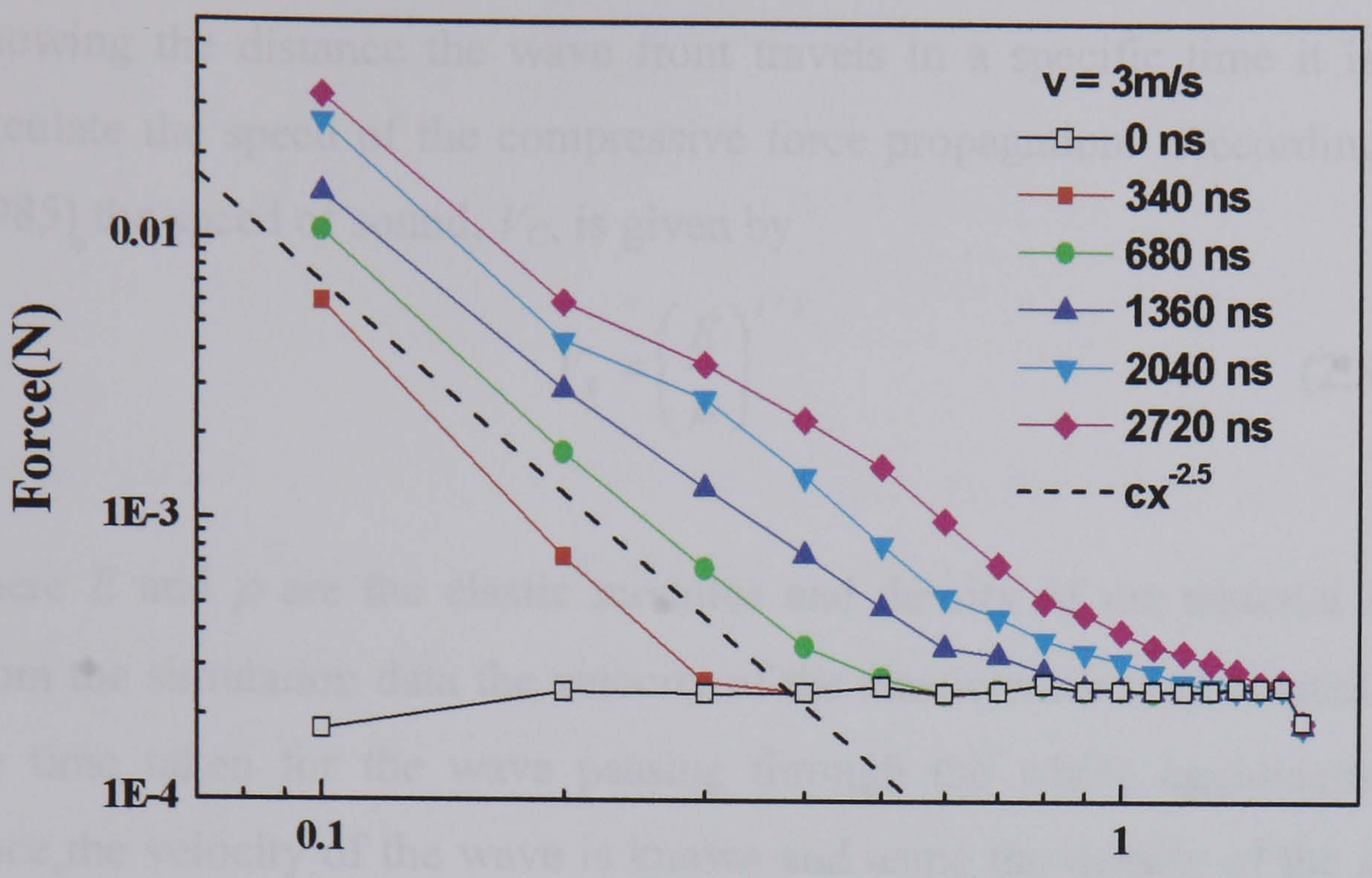

(c)

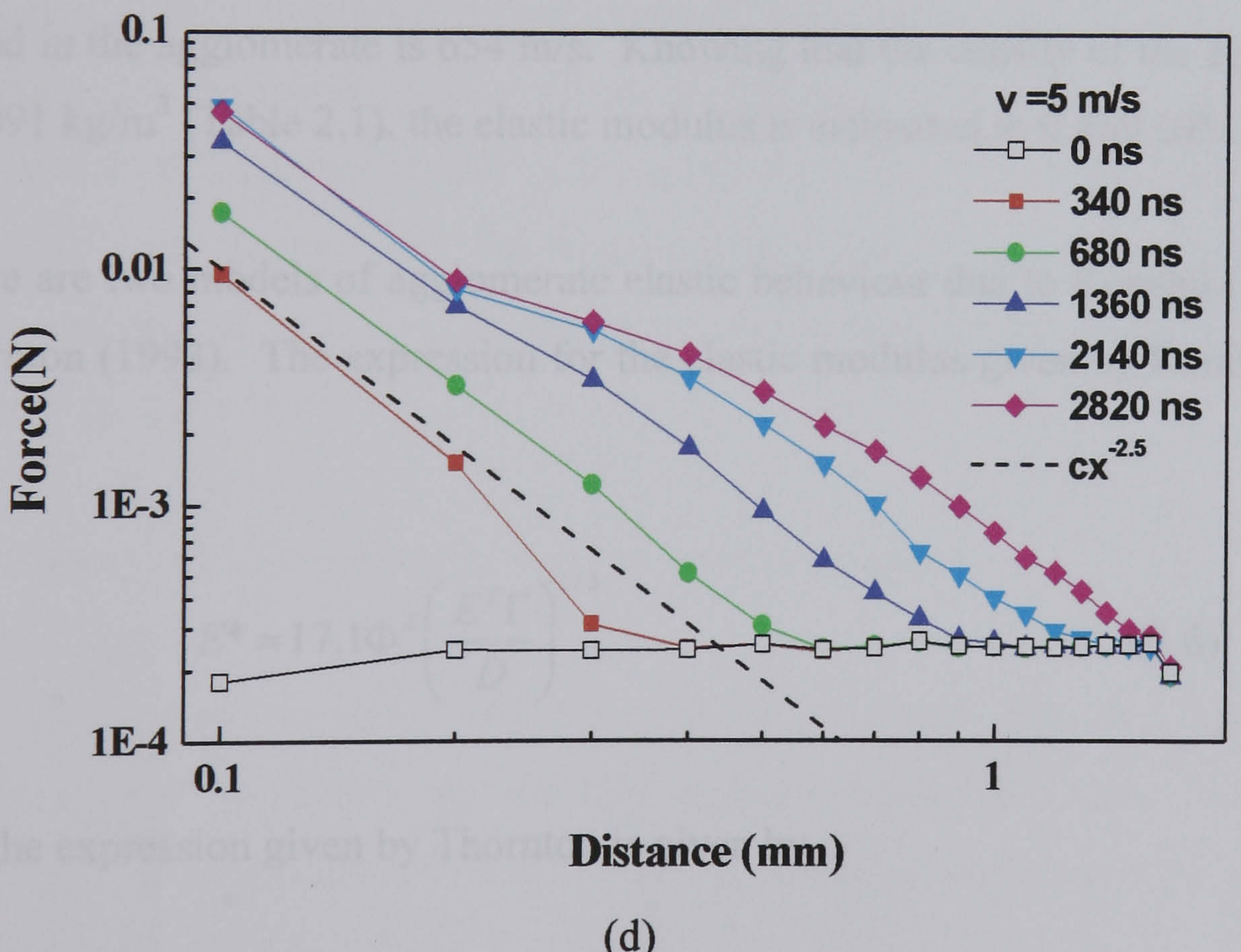

(d)

Figure 2.13 Propagation of the impact force inside Agglomerate F. The dashed line is a power law with exponent -2.5 for comparison with the simulation data.

It would be possible to estimate the elastic modulus of the agglomerate from the propagation speed of the compressive force using the data from Fig. 2.13. Knowing the distance the wave front travels in a specific time it is possible to calculate the speed of the compressive force propagation. According to Johnson (1985) the speed of sound, V_C, is given by

$$V_c = \left(\frac{E}{\rho}\right)^{1/2} \tag{2.5}$$

where E and ρ are the elastic modulus and density of the material respectively. From the simulation data the velocity of the elastic wave is calculated by dividing the time taken for the wave passing through the whole agglomerate diameter. Once the velocity of the wave is known and using the density of the agglomerate, the elastic modulus can be calculated. Applying this procedure to the case of impact velocity 5 m/s and for the data at time equal to 2.140 μs, the velocity of sound in the agglomerate is 654 m/s. Knowing that the density of the agglomerate is 1091 kg/m^3 (Table 2.1), the elastic modulus is estimated as 0.469 GPa.

There are two models of agglomerate elastic behaviour due to Kendall (1988) and Thornton (1993). The expression for the elastic modulus given by Kendall (1988) is

$$E^* = 17.1\Phi^4\left(\frac{E^2\Gamma}{D}\right)^{1/3} \tag{2.6}$$

and the expression given by Thornton is given by

$$E^* = 17.61\Phi^4\left[\frac{\chi}{(2+\chi)}\right]\left(1-\nu^2\right)^{-2/3}\left(\frac{E^2\Gamma}{D}\right)^{1/3} \tag{2.7}$$

with χ being defined as

$$\chi = \frac{1-\nu}{0.3(2-\nu)} \tag{2.8}$$

Simulation	Thornton (1993)	Kendall (1988)
0.469 GPa	0.249 GPa	0.554 GPa

Kendall (1988) and Thornton (1993) apply their analysis to the agglomerate before impact only. During impact the elastic modulus changes since it is a function of the distribution of contact stiffnesses and then depends on contact forces. The contact forces are heterogeneously distributed through the agglomerate being higher near the contact point of impact. However, the simulation results agree reasonably well with both models albeit closer to that of Kendall (1988).

Thornton (1993) has previously suggested that the model of Kendall (1988) overestimates the results but this is not corroborated by the results obtained here. The model of Thornton (1993) is more rigorous than that of Kendall (1988) as Thornton takes into account the tangential stiffness of the contacts. A more in-depth analysis of both models and comparisons with simulated agglomerates is required in future work.

2.2.4 Summary and conclusions of the impact process

The impact force on the wall at low impact velocity follows closely elastic behaviour, but it departs significantly at high impact velocities due to bond breakage. The agglomerate deformation is found to be linear with the impact force.

The dynamics of the agglomerate behaviour under impact are determined by the propagation of the compressive waves produced by the impact of the agglomerate against a target. This compressive wave propagates through the agglomerate,

modifying the contact forces. The influence of this compressive wave decays with the distance following a power law with exponent 2.5.

The propagation of the compressive waves within the agglomerate provides a way of calculating an effective elastic modulus for the assembly of particles. This elastic modulus is in reasonable agreement with the theoretical expressions of Thornton (1993) and Kendall (1974).

In general it is concluded that the discrete nature of agglomerates makes their behaviour very different from that of a solid particle. New models should be developed to predict the dynamics of the agglomerate impact.

CHAPTER 3: EFFECT OF THE INTERFACE ENERGY ON THE IMPACT BEHAVIOUR OF AGGLOMERATES

3.1 Introduction

There are many factors that influence agglomerate strength but probably one of the most important is the interface energy. An increase in bond strength produces an increase in the strength of the agglomerate as demonstrated by experimental work and numerical simulations (Subero *et al*. 1999, Kafui and Thornton, 1993).

The most important theoretical models relating the interface energy and strength of particulate materials are due to Kendall (1988) and Rumpf (1962). Kendall defined agglomerate strength as the resistance of the agglomerate to fracture by means of crack propagation. In contrast, Rumpf considered a plane of failure and defined the strength as the force required to break all contacts simultaneously on that plane. However, there is no theoretical model that relates agglomerate strength under impact to the interface energy. Furthermore, the concept of strength is loosely defined as an agglomerate can suffer size reduction in the form of detachment of small debris and not necessarily by fragmentation as it was considered by Kendall and Rumpf. Therefore it seems more appropriate to define the strength of agglomerates based on the type of damage incurred.

Kafui and Thornton (1993), using computer simulations, analysed the effect of the interface energy on the strength of regular packed agglomerates (FCC and BCC). They related the breakage of contacts to the Weber Number, *We,* defined by

$$We = \frac{\rho D V^2}{\Gamma} \tag{3.1}$$

where ρ is the particle density, D the particle diameter, V the impact velocity and Γ is the interface energy which is defined in terms of the Dupré equation (Israelachvili, 1985) as:

$$\Gamma = \gamma_A + \gamma_B - \gamma_{AB} \qquad (3.2)$$

where γ_A and γ_B are the surface energies of the two surfaces of different materials, A and B, and γ_{AB} is the interaction energy. For surfaces of the same material γ_{AB} is zero and therefore $\Gamma=2\gamma$.

When Kafui and Thornton (1993) plotted the breakage of contacts as a function of the Weber Number they found that the curves corresponding to different values of surface energy were unified.

Subero *et al.* (1999) analysed the effect of the interface energy in randomly packed agglomerates and found that the breakage of contacts decreases with interface energy, indicating the increase of the agglomerate strength in agreement with the work of Kafui and Thornton (1993).

The aforementioned works were focused on the effect of the interface energy on the breakage of contacts and no attention was paid to the influence of the interface energy on the breakage pattern of agglomerates. Furthermore, they were only carried out for one agglomerate in every case and therefore their results are subjected to statistical errors. In this chapter, the relationship between the number of broken contacts and interface energy is analysed, as well as the effect of the interface energy on the breakage pattern of agglomerates.

3.2 Simulation details

In order to analyse the effect of interface energy on the agglomerate behaviour four agglomerates of 3000 particles have been produced in exactly the same way, but with different initial configuration of the primary particle positions. The physical properties of the particles are those used previously by Subero *et al.* (1999) and Subero (2001) as given in Table 3.1. The size and properties of the four agglomerates are given in Table 3.2. The interface energy is given within brackets next to the words "Cont. No." (contact number) and the coordination number is given within brackets next to the

value of the contact number. The surface energy was varied in a range of two orders of magnitude.

Table 3.1 Single particle properties.

Young's modulus (GPa)	31
Poisson ratio	0.3
Density (kg/m^3)	2000
Friction	0.35
Particle radius (μm)	50

Table 3.2 Agglomerate properties.

Agglomerate	**A**	**B**	**C**	**D**
Aggl. radius (mm)	0.902	0.922	0.921	0.912
Packing fraction	0.555	0.520	0.522	0.537
Cont. No. (35 J/m^2)	9151 (6.10)	9061 (6.04)	9102 (6.07)	9093 (6.06)
Cont. No. (3.5 J/m^2)	8932 (5.96)	8796 (5.86)	8836 (5.89)	8854(5.90)
Cont. No. (0.35 J/m^2)	8718 (5.81)	8513 (5.68)	8560 (5.71)	8621(5.75)

Each agglomerate was impacted at a specified velocity and the number of broken contacts was evaluated. For each impact velocity, four agglomerates were tested and the mean and standard deviation of the number of broken contacts was determined. At low surface energy, the pattern of breakage of the agglomerates was similar for all agglomerates. The breakage pattern of agglomerates having a high surface energy shows more diversity than those with a low surface energy. Consequently for a better statistical reliability of the results a fifth agglomerate (labelled E) with similar primary particle properties to the other four assemblies and packing fraction 0.546 was created.

It has been observed that the behaviour of different agglomerates with the same value of interface energy impacted at the same range of impact velocities is quite often very

similar. In these cases only one of these agglomerates is selected to show their behaviour and it will be specified when applicable.

3.3 Analysis of the number of broken contacts in the agglomerates

The first feature analysed was the effect of impact velocity and surface energy on the number of broken contacts. Figure 3.1 show the average of the damage ratio obtained in the impact of the four agglomerates of Table 3.2. The results obtained here are in agreement with Subero *et al*. (1999), and Thornton *et al*. (1996) since similar trends are observed in Fig. 3.1. An increase in the impact velocity implies an increase in the input energy and consequently more energy is available in the system for breaking contacts. However, the number of contacts in the assembly is finite which implies that the rate of breakage of contacts follows a sigmoidal trend.

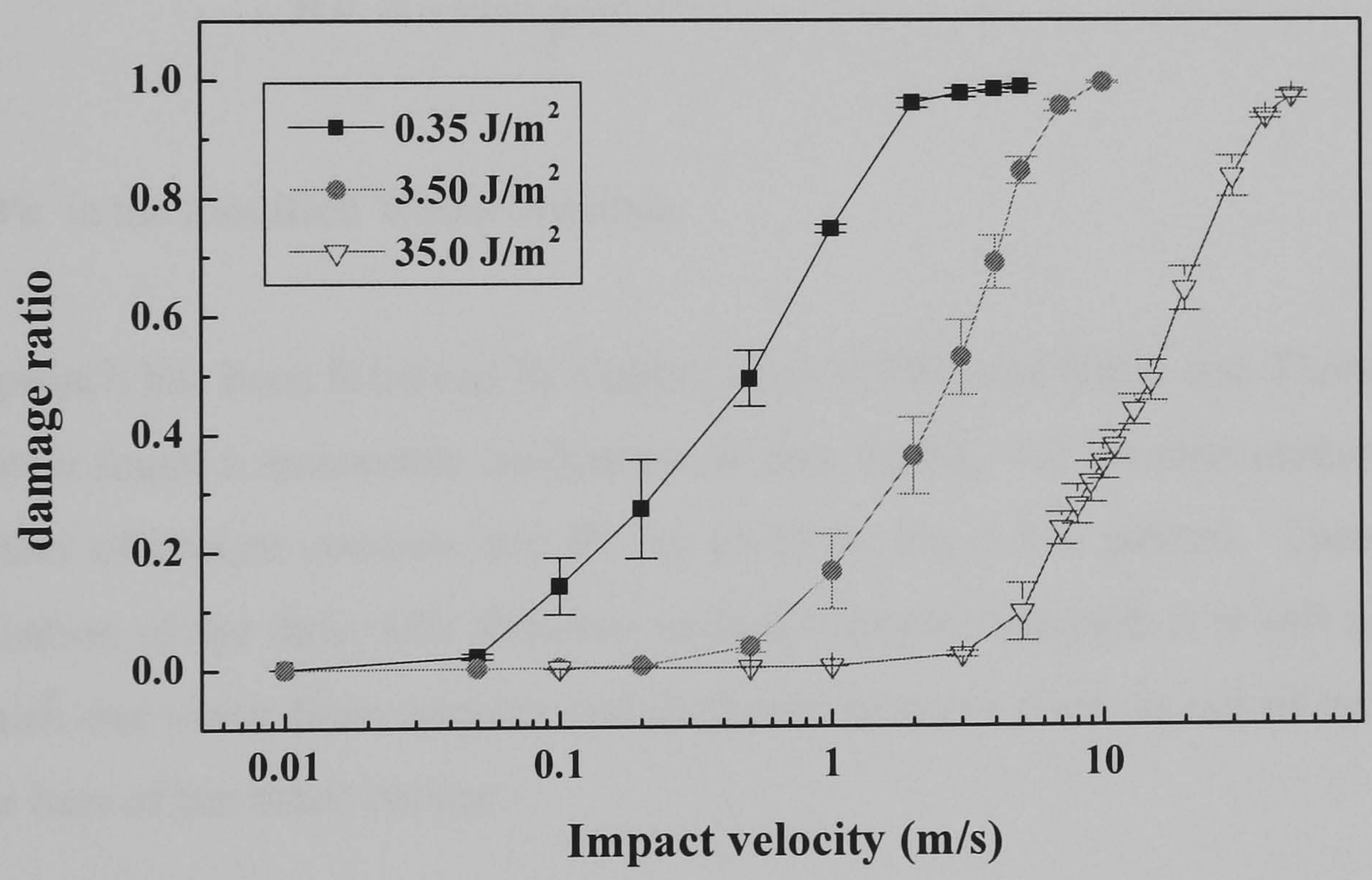

Figure 3.1 Relationship between damage ratio and impact velocity for different values of surface energy. The data points correspond to the average of the damage ratio of the impact of Agglomerates A-D reported in Table 3.2.

In Figure 3.1, for a given impact velocity the damage ratio, defined as the ratio of broken contacts to the initial number of bonds, decreases as the surface energy is increased. This is consistent with the previous works reported by Kafui and Thornton

(1993) and Subero *et al.* (1999). This is due to linear dependency between the force required to break a contact and the surface energy. The lower the surface energy, the lower the force required to break the contacts and therefore the lower the input kinetic energy required to break the same number of contacts. At low impact velocities (Fig. 3.1), the damage ratio is not sensitive to the impact velocity, but once a threshold velocity is exceeded the damage ratio quickly rises and eventually approaches unity in an asymptotic way.

Quantitatively the breakage of contacts has been traditionally associated with the Weber Number which was initially used by Kafui and Thornton (1993) (Eq. 3.1) to unify the data. In a later publication, Thornton *et al.* (1996) found a better fit by substituting the impact velocity, V, by the difference between impact velocity and the velocity under which no damage in the assembly occurs, V_0

$$We' = \frac{\rho D(V - V_0)^2}{\Gamma} \tag{3.3}$$

where We' is the modified Weber Number.

This approach has been followed by Subero *et al.* (1999) and Kafui and Thornton *et al.* (1996) who found a reasonable unification of data. In Fig. 3.2 the relationship between the number of broken contacts and We' as given by Eq. 3.3 is plotted. There is some normalisation of the data with different surface energies although it is still possible to distinguish one curve from another and furthermore every curve is out of the limits of the error bars of the other curves.

In a new development in this work a more accurate relationship between the number of broken contacts and the interface energy is proposed and this is described in detail in Appendix B. The new model development is based on the hypothesis that the work expended on the breakage of contacts is proportional to the incident kinetic energy. From this energy balance a relationship between the number of broken contacts and interface energy in the form $\Gamma^{-5/3}$ is obtained (see Eq. B.12). However, a rearrangement in terms of the modified Weber Number gives Eq. 3.4.

$$D_R \propto We' \left(\frac{ED}{\Gamma} \right)^{2/3} \qquad (3.4)$$

where E is the primary particle elastic modulus, D is the single particle diameter, Γ is the interface energy, ρ is the density of single particles and V the impact velocity.

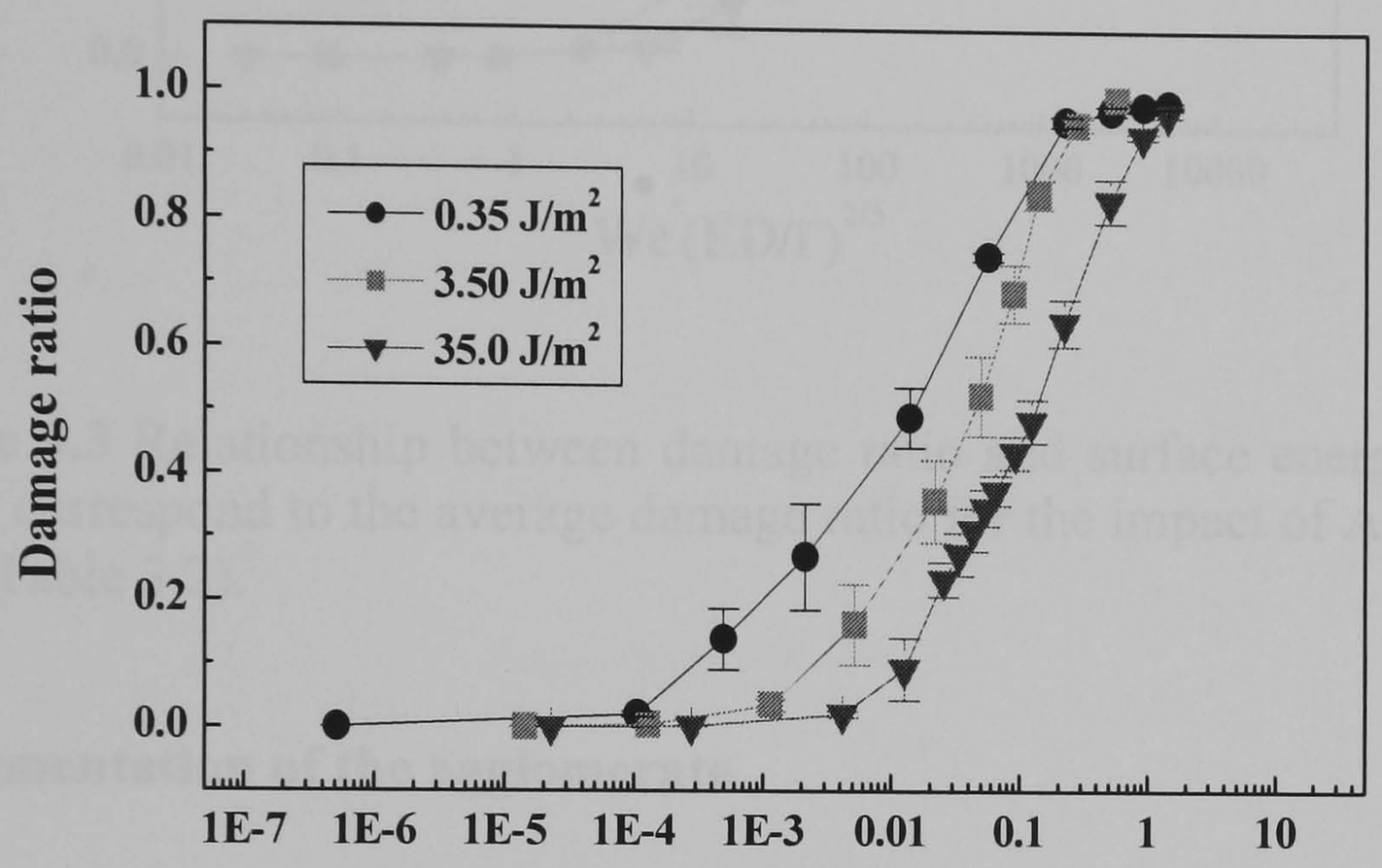

Figure 3.2 Relationship between damage ratio and modified Weber Number. The data points correspond to the average damage ratio for the impact of Agglomerates A-D reported in Table 3.2.

For the data previously presented in Fig. 3.1 the damage ratio is expressed as a function of the new dimensionless group given by Eq. 3.4 and plotted in Fig. 3.3. As it can be seen a better normalisation is obtained as compared to Fig. 3.2. Every curve is now within the error bars of the other curves. However, at high values of the abscissa, the normalisation is not as good as for the rest of the data. This could be due to a number of factors, the most important one being the assumption that the number of broken bonds is proportional to the incident kinetic energy. Further work is needed to refine this model so that the dependency between the number of broken contacts and impact velocities is equally well-predicted even at high values of the impact velocity.

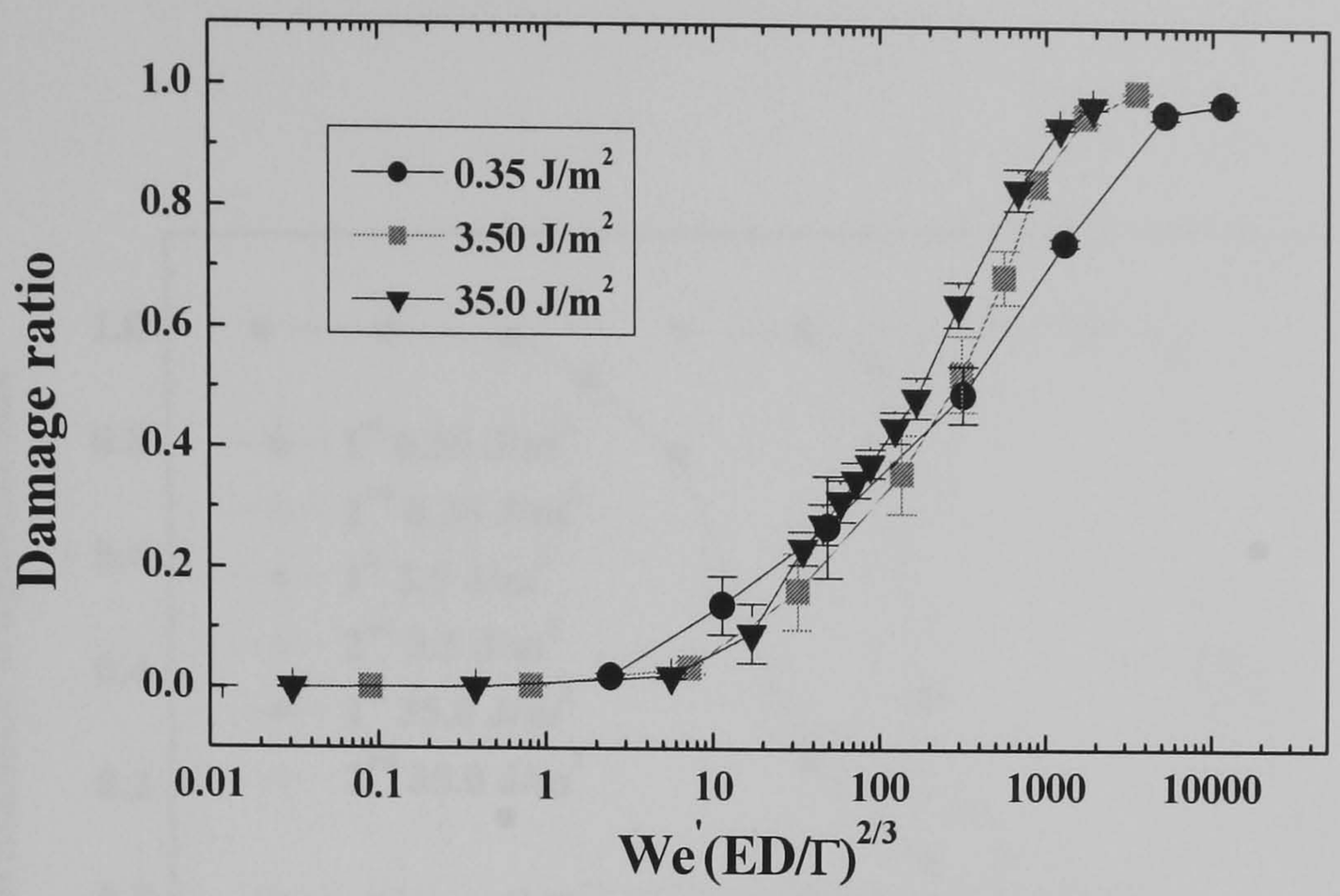

Figure 3.3 Relationship between damage ratio and surface energy. The data points correspond to the average damage ratio for the impact of Agglomerates A-D (Table 3.2).

3.4 Fragmentation of the agglomerate

The damage ratio represents the number of broken bonds but this process does not reflect the formation of debris and fragments. For the study of the latter, the sizes of the two largest fragments produced upon impact are quantified and the results are shown in Figs 3.4(a-d) for different agglomerates. The average number of fragments detached during impact has also been analysed and the results are shown in Fig. 3.5. The impact damage may be classified as follows:

- Regime I: small clusters are detached from the agglomerate and the size of the largest fragment shows a weak dependency on the impact velocity.
- Regime II: this is characterised by a fast decrease of the size of the residual fragment.
- Regime III: the size of the largest fragment is much smaller than the initial agglomerate size and varies slowly with the impact velocity.

The transition velocities between at which a regime change occurs are observed to increase with an increase in the surface energy.

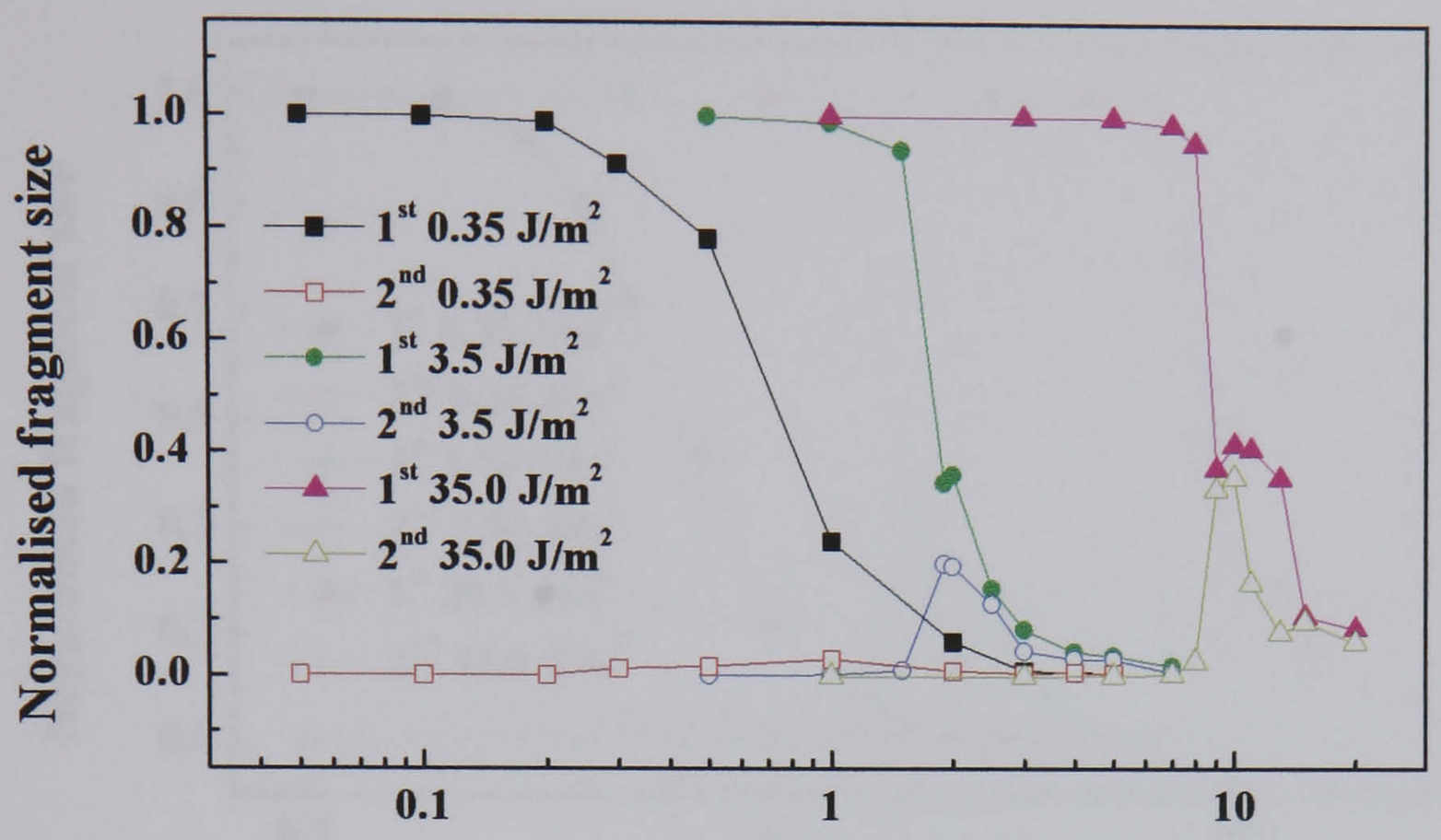

Agglomerate A

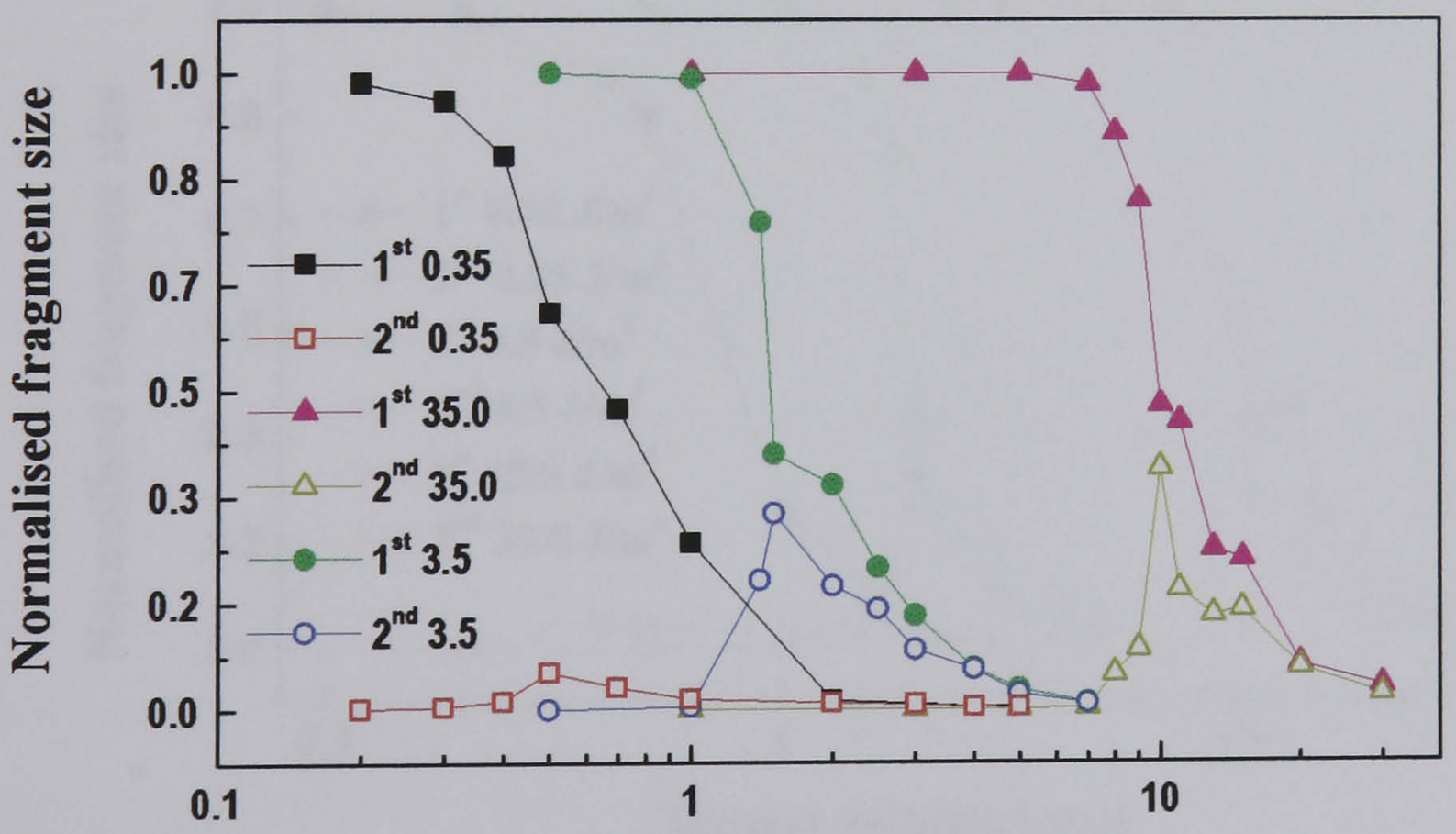

Agglomerate B

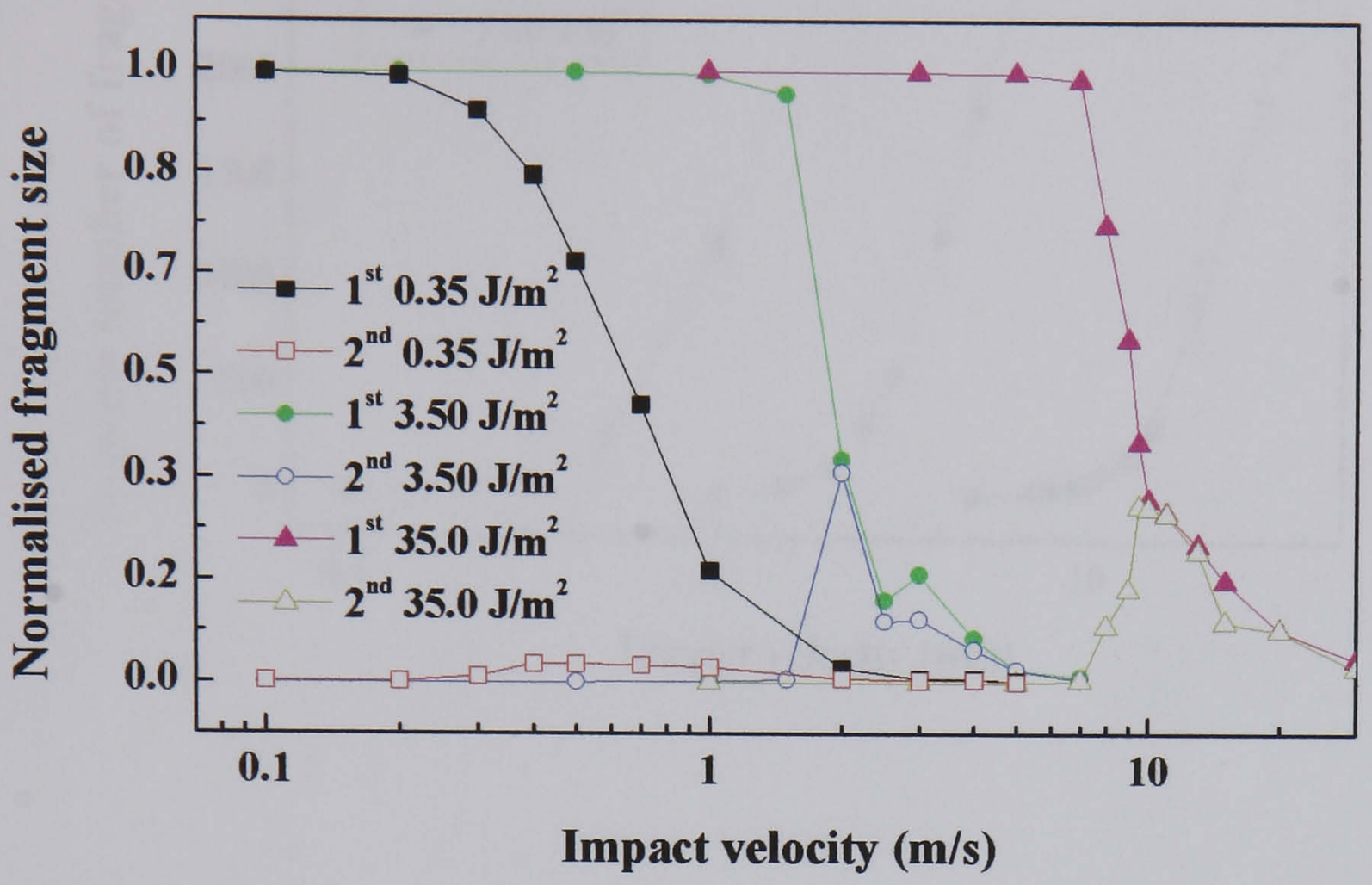

Agglomerate C

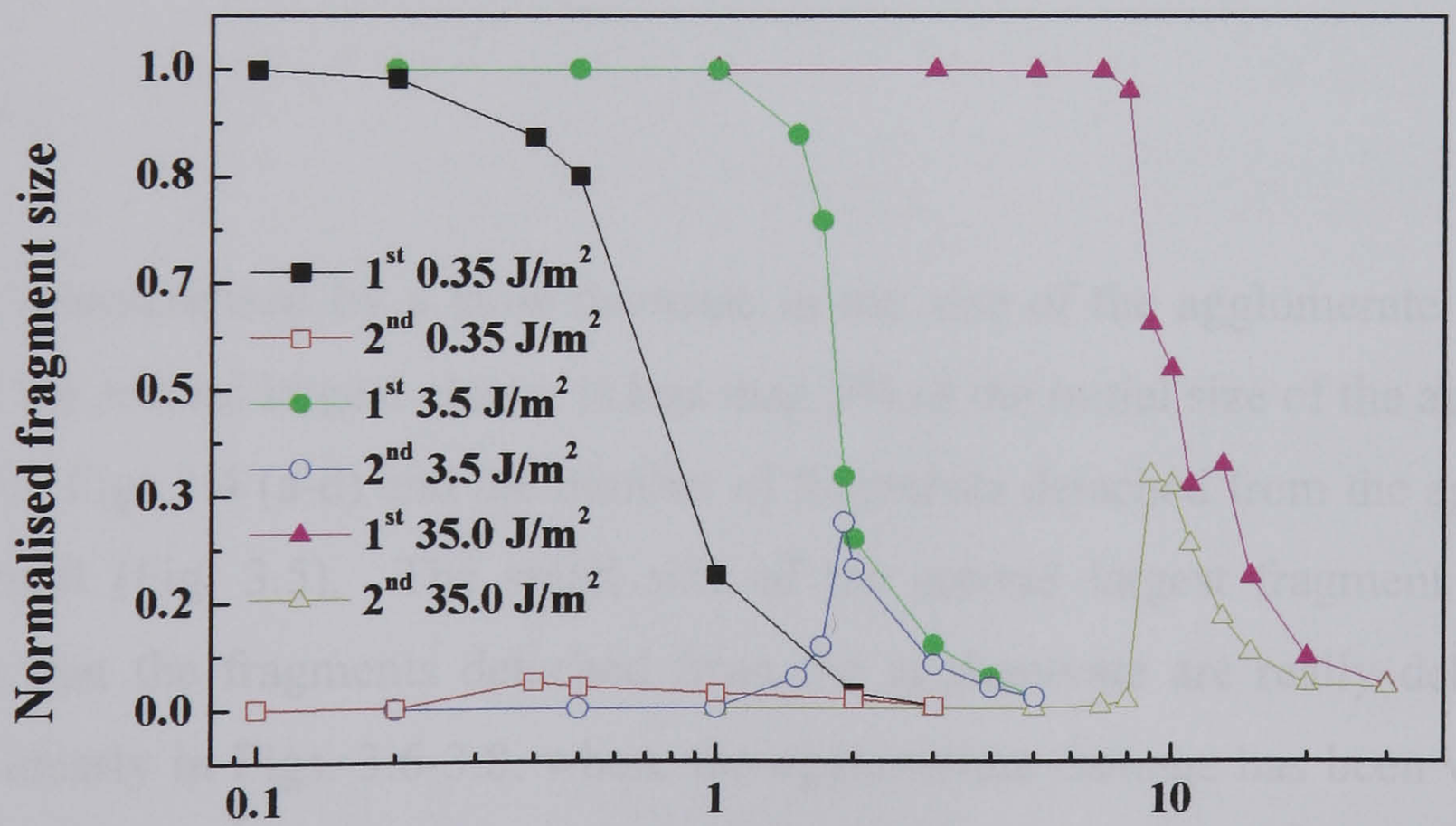

Agglomerate D

Figure 3.4 Size of the two largest fragments as a function of impact velocity for the agglomerates A, B, C and D.

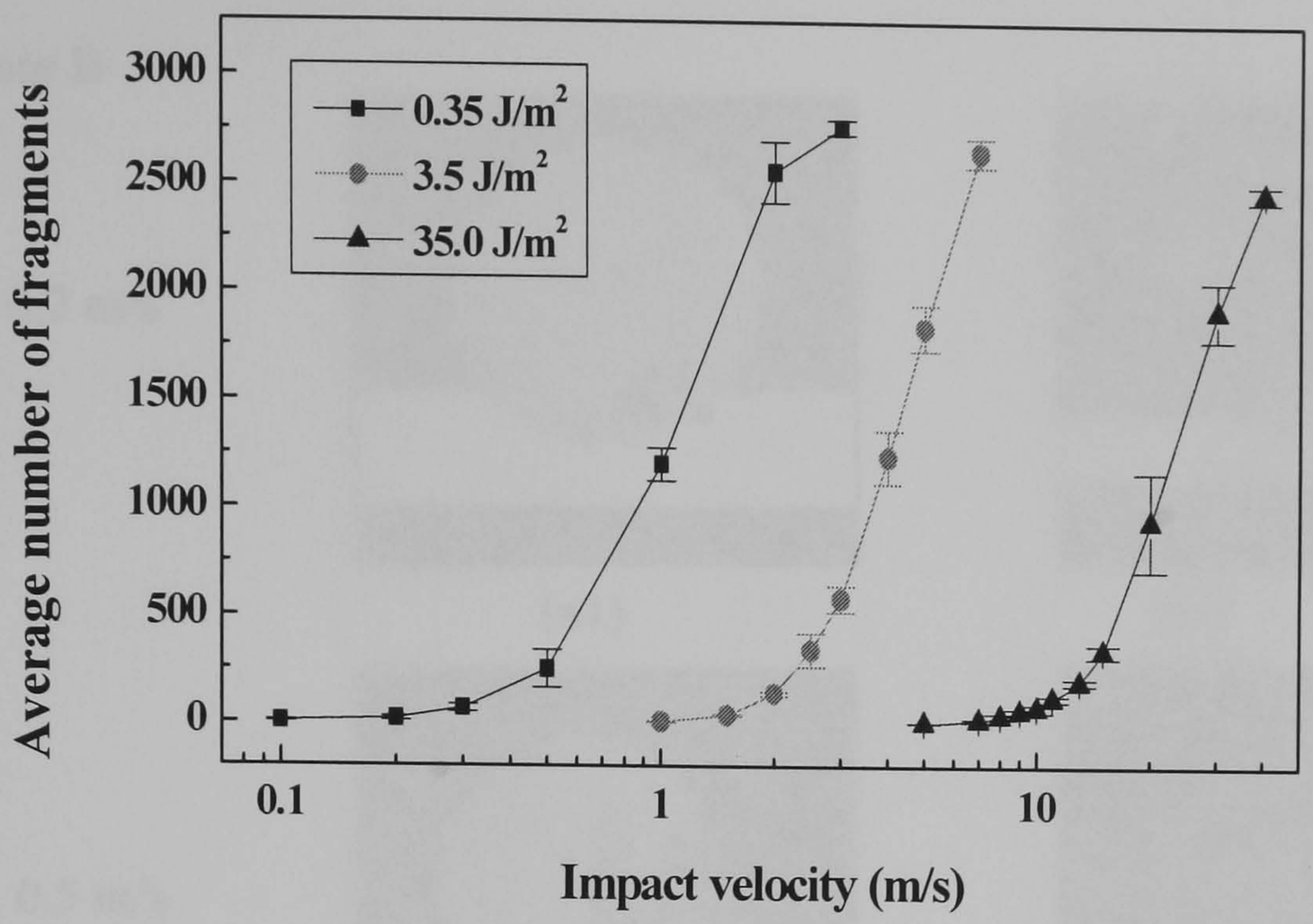

Figure 3.5 Average number of fragments detached after impact for Agglomerates A-D.

Regime I:

This is characterised by a slow decrease in the size of the agglomerate. During this regime the second largest cluster is less than 5% of the initial size of the agglomerate as shown in Figs 3.4 (a-d) and the number of fragments detached from the agglomerate is very small (Fig. 3.5). The small size of the second largest fragment after impact implies that the fragments detached from the agglomerate are really debris. This is shown clearly in Figs. 3.6-3.8, where the agglomerate damage has been visualised for several impact velocities and three surface energies of 0.35 J/m^2, 3.5 J/m^2 and 35.0 J/m^2, respectively. The debris consists of clusters made of less than 10 particles in most cases. Visual observations reveal that the clusters detached from the agglomerates are mainly from the contact area although it is possible to observe them in other parts of the agglomerates.

Agglomerate B

Whole agglomerate **Clusters produced in the impact**

Regime I: 0.2 m/s

(a1) **(a2)**

Regime II: 0.5 m/s

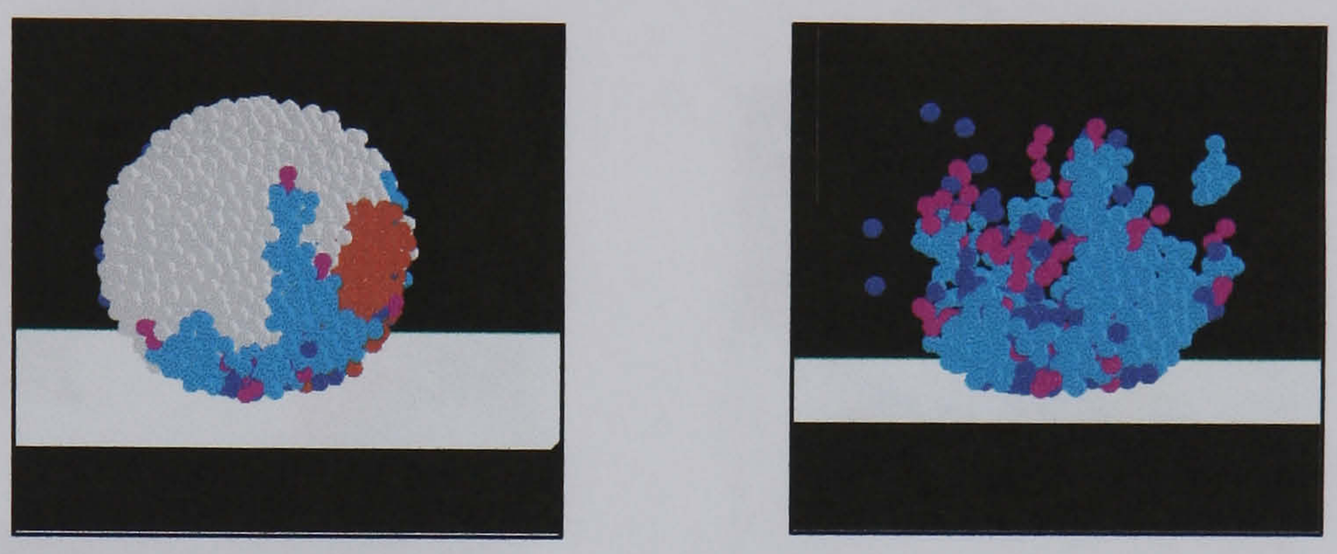

(b1) **(b2)**

Regime II: 1.0 m/s

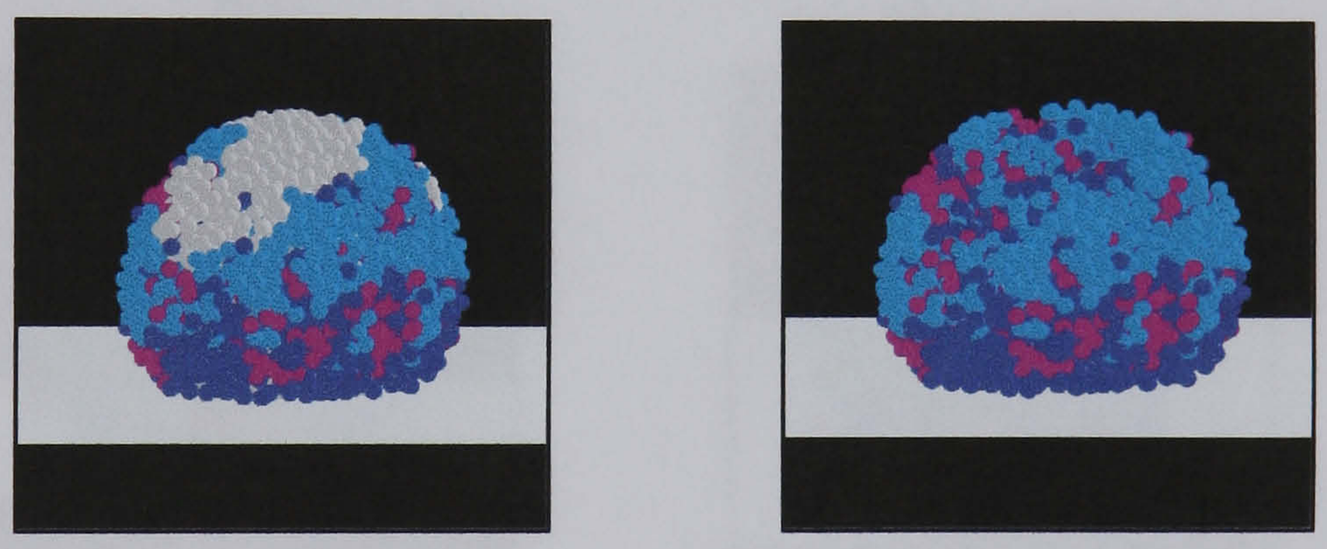

(c1) **(c2)**

Regime III: 2.0 m/s

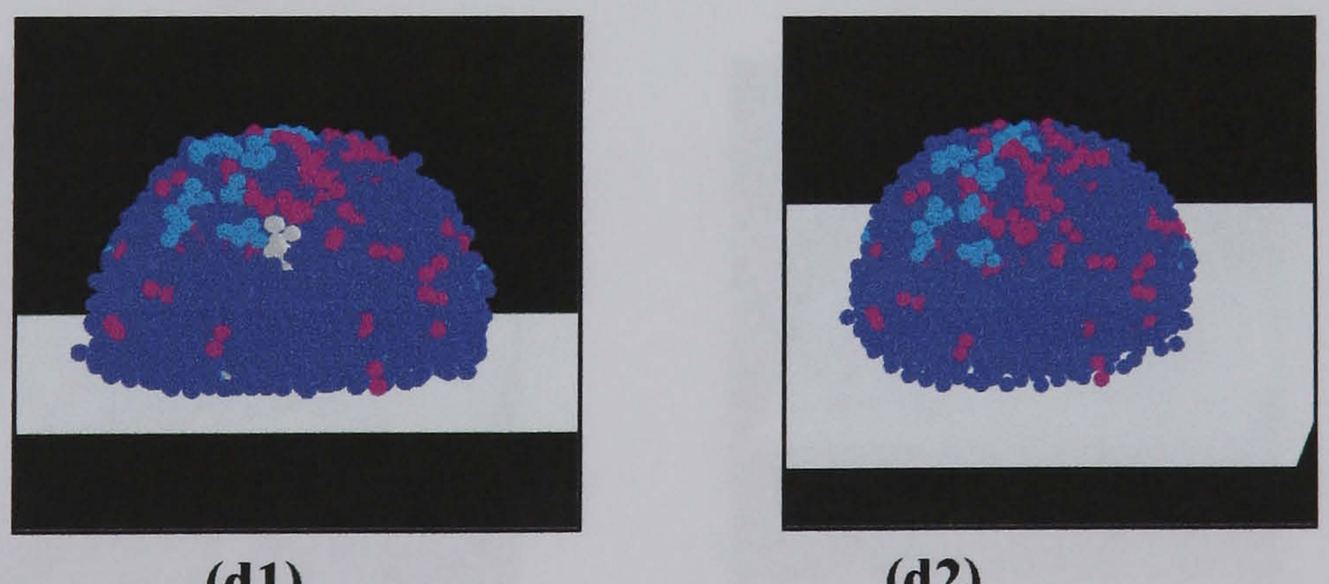

(d1) **(d2)**

Figure 3.6 Agglomerate breakage patterns at various velocities for the surface energy 0.35 J/m^2. Colour coding: white, largest fragment; red, 2nd largest fragment; cyan clusters between 4 and 100 particles; pink, doublets; blue, singlets and the colour white corresponds to the target.

Agglomerate D:

Whole agglomerate **Clusters produced in the impact**

Regime I: 1.3 m/s

(a1) **(a2)**

Regime II: 1.7 m/s

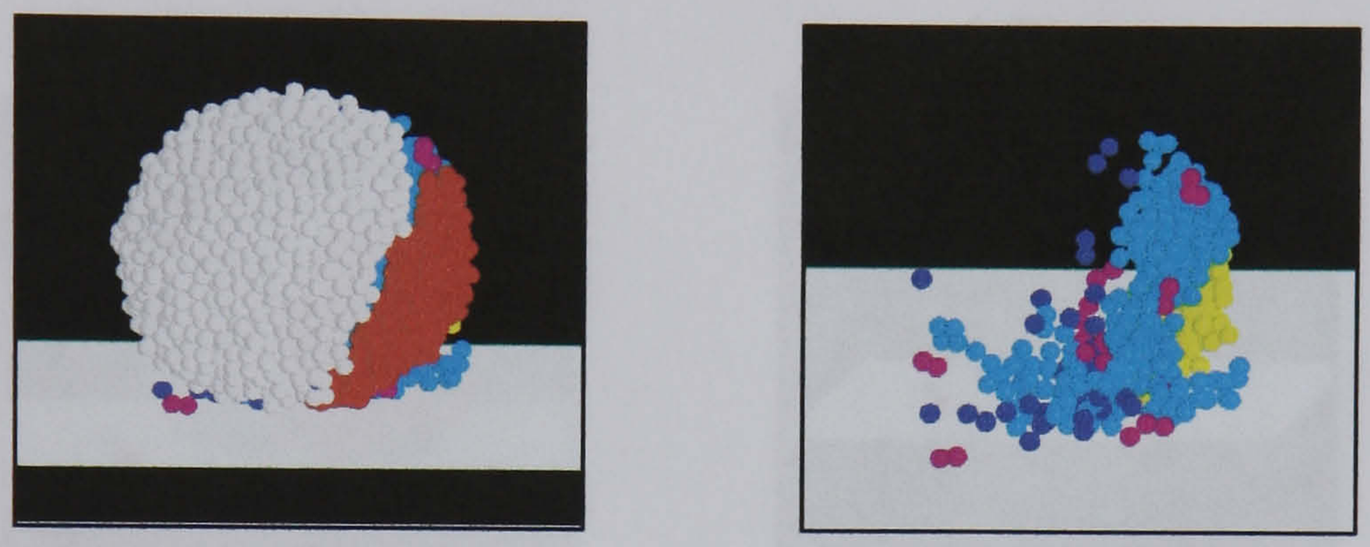

(b1) **(b2)**

Regime II: 2.5m/s

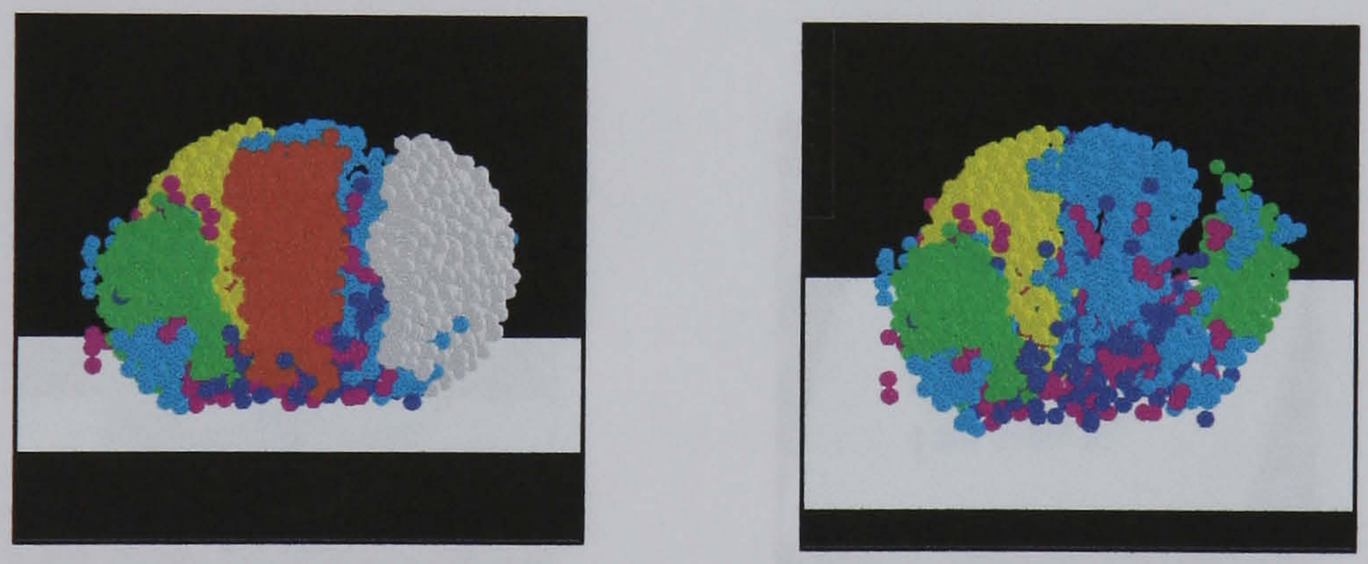

(c1) **(c2)**

Regime III: 3.0 m/s

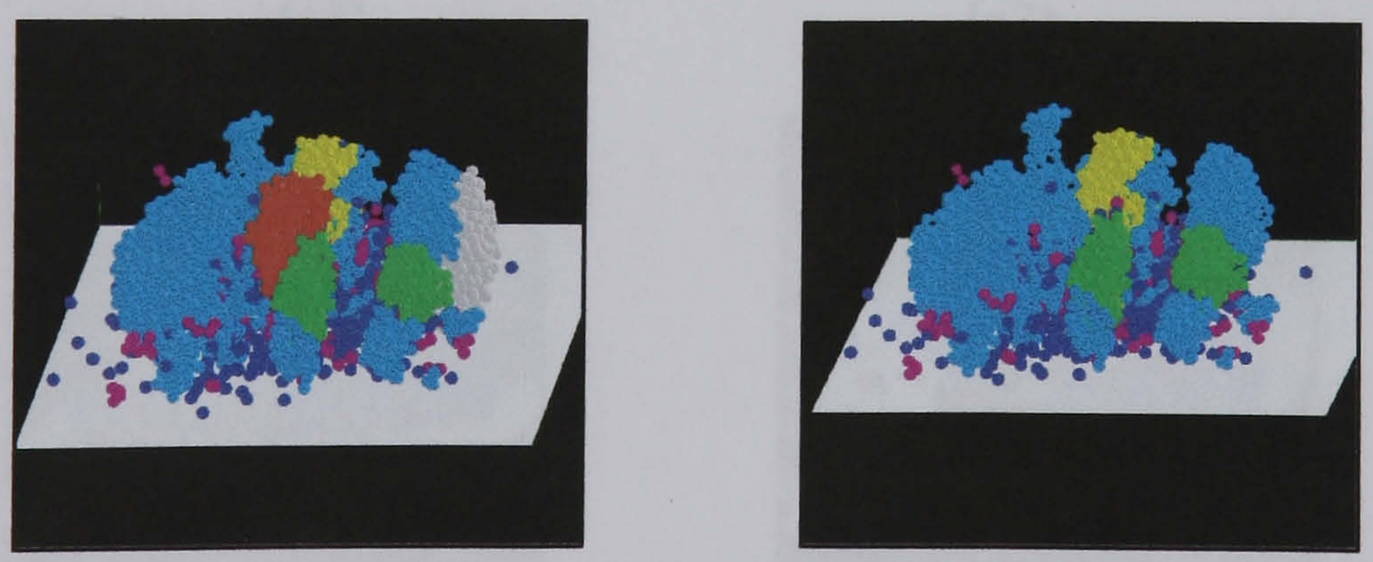

(d1) **(d2)**

Figure 3.7 Agglomerate breakage patterns at various velocities for the surface energy 3.5 J/m^2. Colour coding: light grey, largest fragment; red, 2nd largest fragment, yellow 3rd largest fragment; green, clusters smaller than clusters in yellow and larger than 100 particles; cyan clusters between 4 and 100 particles; pink, doublets; blue, singlets and white, the target.

Whole agglomerate **Clusters produced in the impact**

Agglomerate D:

Regime I: 7.0 m/s

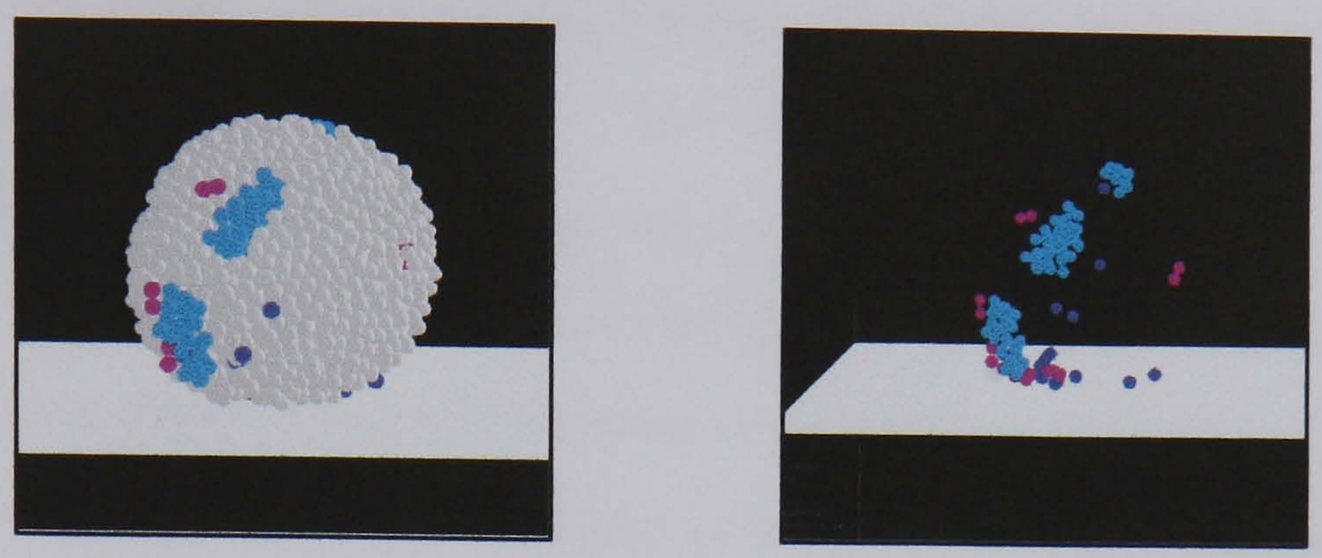

(a1) **(a2)**

Regime II: 9.0 m/s

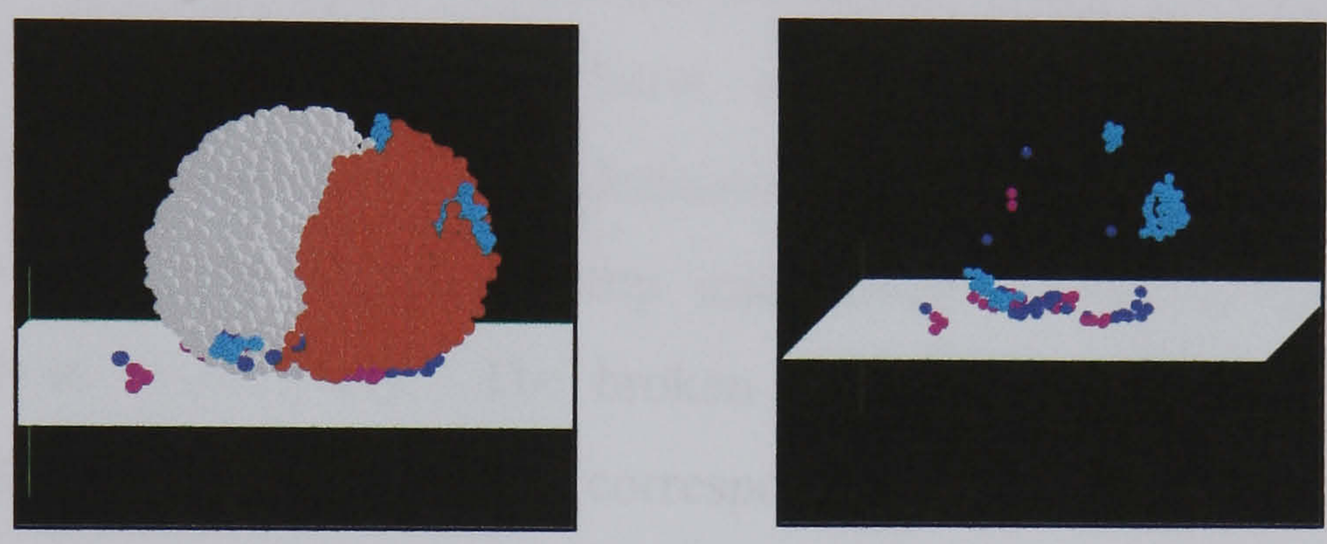

(b1) **(b2)**

Regime II: 11.0 m/s

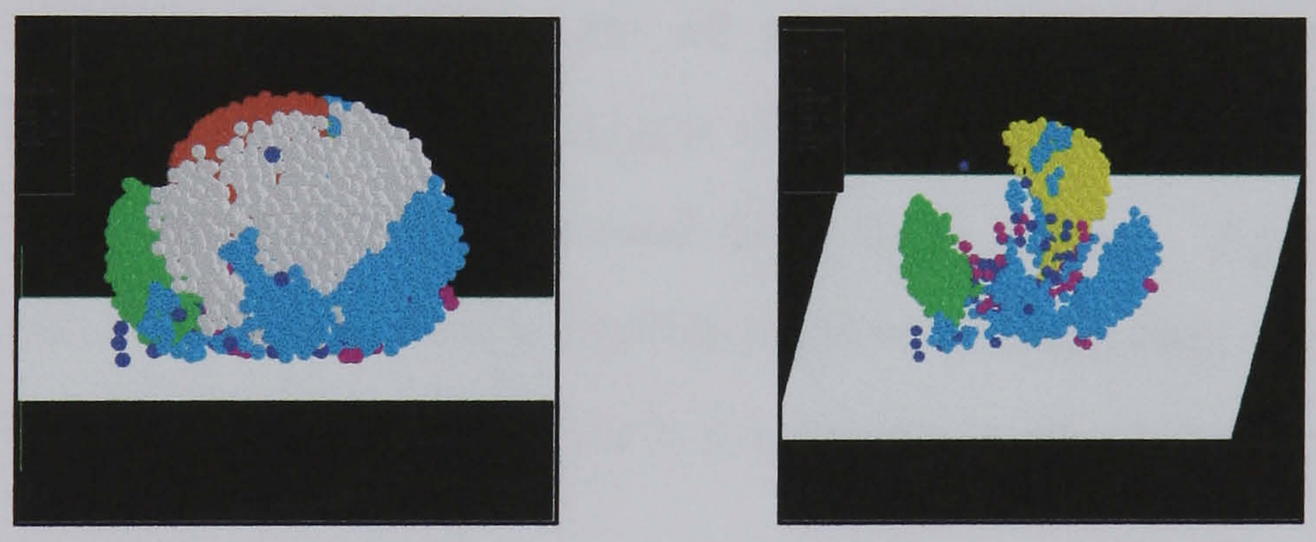

(c1) **(c2)**

Regime III: 15.0 m/s

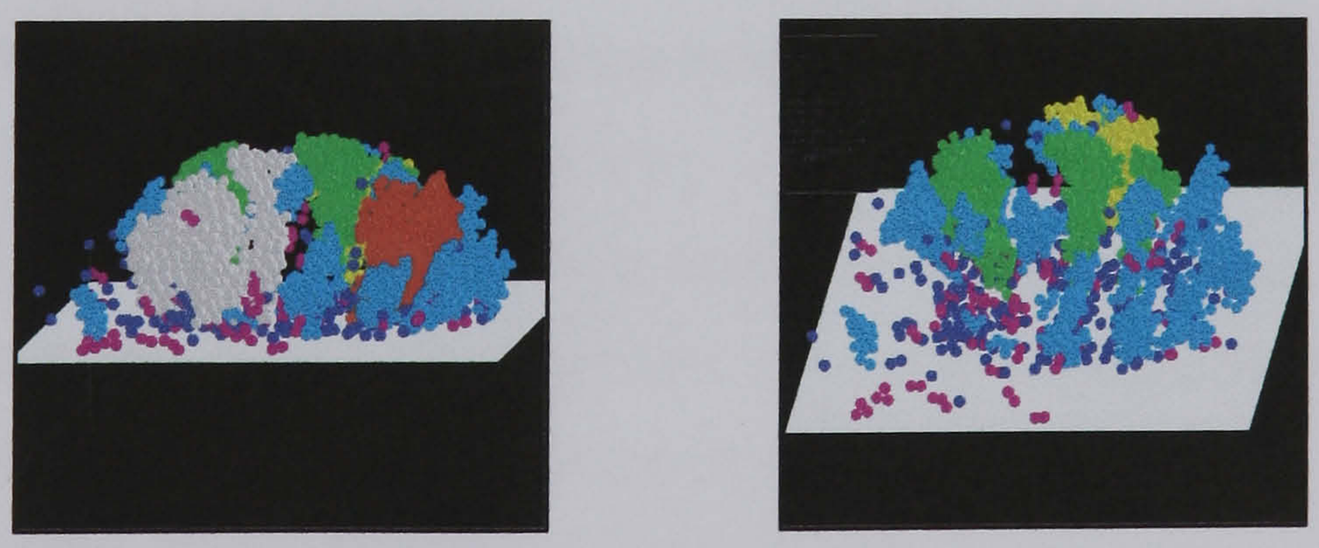

(d1) **(d2)**

Figure 3.8 Agglomerate breakage pattern at various velocities for the surface energy at 35.0 J/m^2. Colour coding: light grey, largest fragment; red, 2nd largest fragment, yellow 3rd largest fragment; green, clusters smaller than clusters in yellow and larger than 100 particles; cyan clusters between 4 and 100 particles; pink, doublets; blue, singlets and white is the target.

Regime II:

In this regime the size of the residual cluster decreases rapidly with the impact velocity (Fig. 3.4) and at the same time the number of fragments detached from the agglomerate increases rapidly (Fig. 3.5.). The size of the second largest cluster increases and passes through a maximum whose magnitude increases when the surface energy is increased (Fig. 3.4). For the case of 0.35 J/m^2, the size of the second largest fragment shows a small maximum which is less than 5% of the initial size. For the surface energy of 3.5 J/m^2 the size of the second largest fragment shows a maximum around 25% of the initial size and for the surface energy of 35.0 J/m^2, this is over 30% of the initial size. In the two latter cases, the maximum in the curves corresponds to the fragmentation of the agglomerates into two fragments. This is shown in Fig. 3.9 and 3.10 where the top and bottom views of the broken agglomerates are given respectively. The broken agglomerates for two levels of surface energy impacted at the velocities corresponding to the maximum of the second largest fragment are visualised. The fragments are coloured coded according to their sizes. The broken agglomerates are all in Regime II and show similar breakage pattern. The presence of the two largest fragments can be seen in all these records. A number of features may be observed from these figures. Agglomerates with the higher surface energy break into a smaller number of fragments and produce a smaller quantity of debris in comparison with the breakage of agglomerates with lower surface energy.

A measure of the size of the fragments detached from the agglomerates can be given by determining the average fragment size in terms of the number of particles in each fragment. In Fig. 3.11 the average fragment size is plotted versus the impact velocity. At low impact velocity the average fragment size is very small indicating that the fragments that are detached from the agglomerates are mainly in the form of small debris. When the impact velocity increases a sharp increase in the average fragment size is observed. The comparison of Figs 3.4(a-d) and 3.11 reveals that the average fragment size reaches its maximum at the value of impact velocity at which the fragmentation is first observed

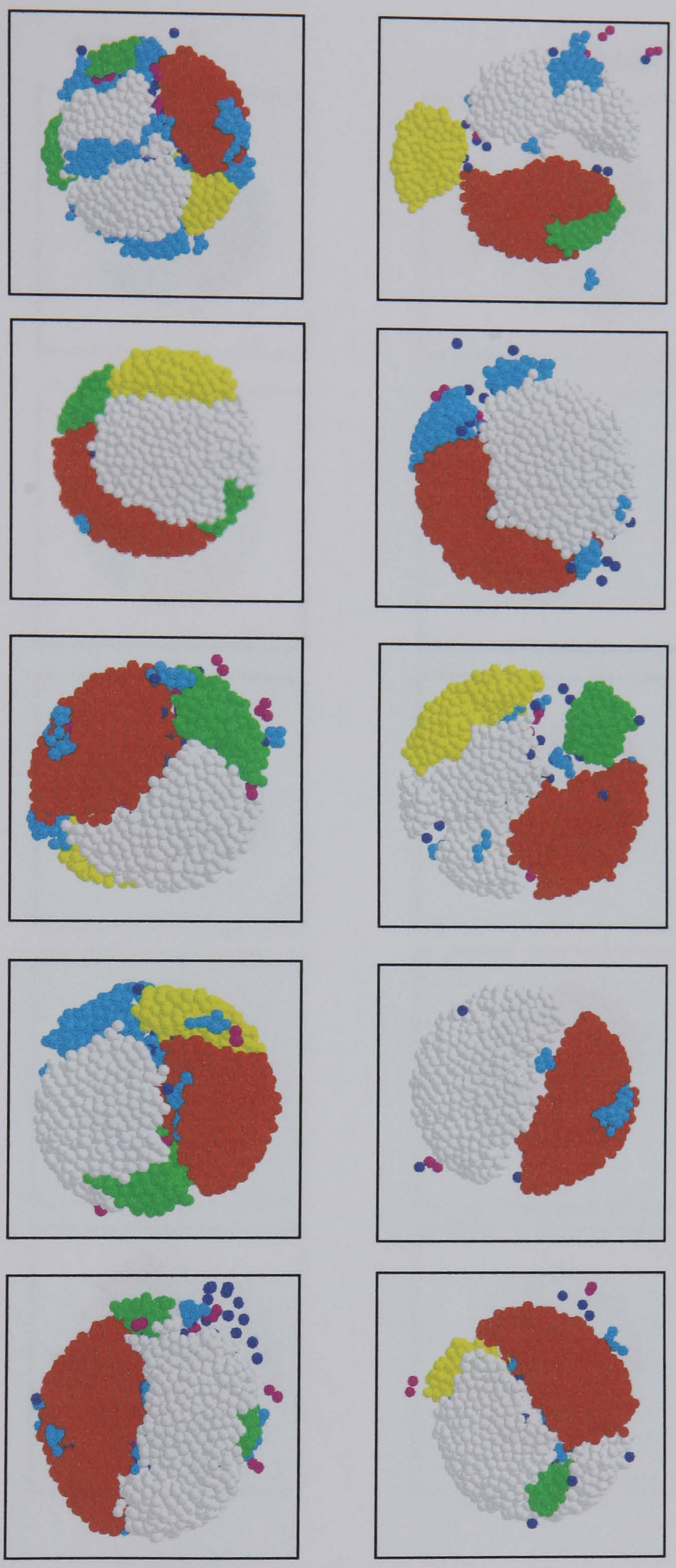

Figure 3.9 Top view of agglomerates impacted at different velocities for two levels of surface energy. Colour coding: light grey, largest fragment; red, second largest fragment, yellow third largest fragment; green, clusters smaller than clusters in yellow and larger than 100 particles; cyan clusters between 4 and 100 particles; pink, doublets; blue, singlets.

Surface energy:	3.50 J/m^2	35.0J/m^2
Agglomerate A 1.9 m/s for 3.5 J/m^2 9.0 m/s for 35.0 J/m^2		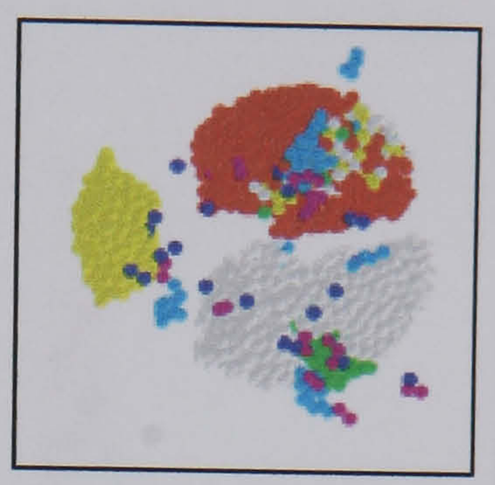
Agglomerate B 1.8 m/s for 3.5 J/m^2 9.0 m/s for 35.0 J/m^2	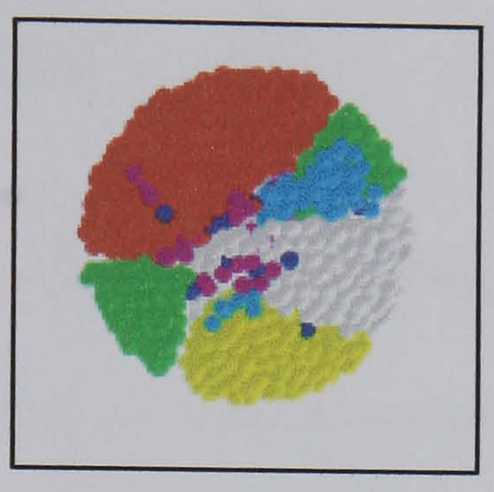	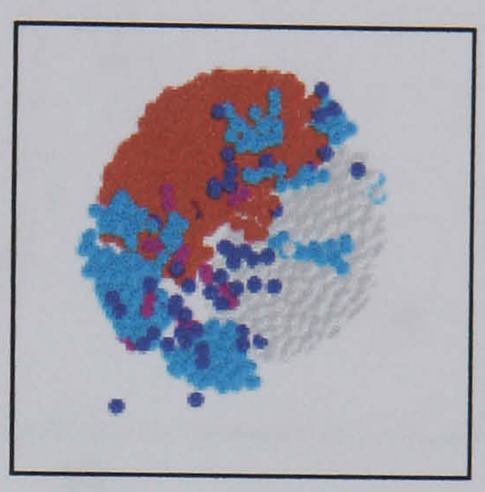
Agglomerate C 2.0 m/s for 3.5 J/m^2 9.0 m/s for 35.0 J/m^2		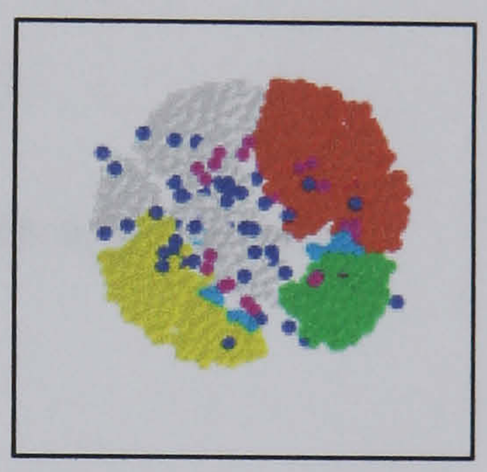
Agglomerate D 1.9 m/s for 3.5 J/m^2 9.5 m/s for 35.0 J/m^2	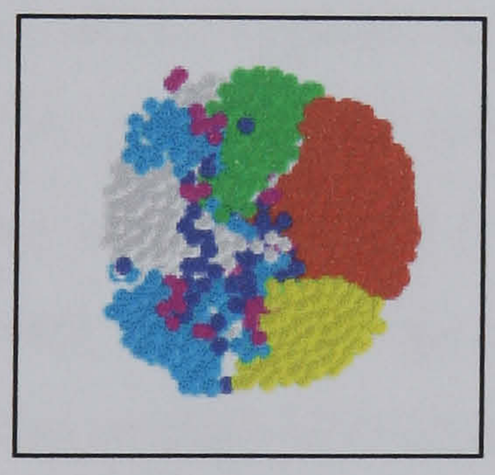	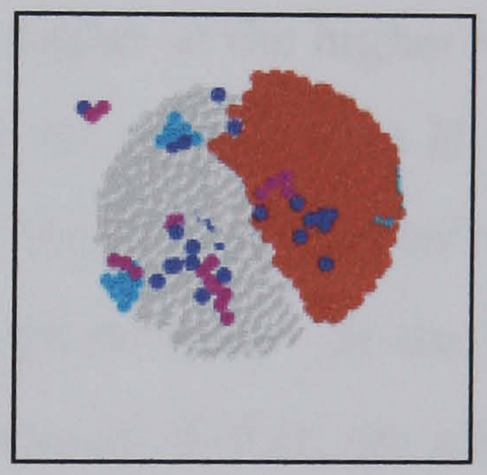
Agglomerate E 2.5 m/s for 3.5 J/m^2 8.0 m/s for 35.0 J/m^2	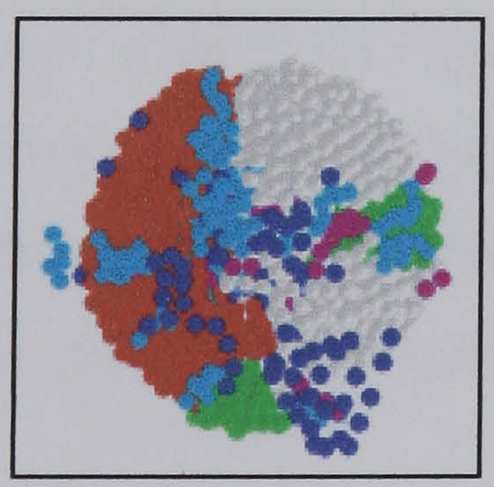	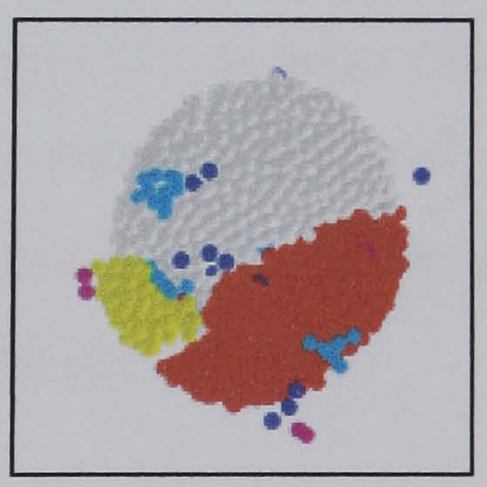

Figure 3.10 Bottom view of agglomerates impacted at different velocities for two levels of surface energy. Colour coding: light grey, largest fragment; red, second largest fragment, yellow third largest fragment; green, clusters smaller than clusters in yellow and larger than 100 particles; cyan clusters between 4 and 100 particles; pink, doublets; blue, singlets.

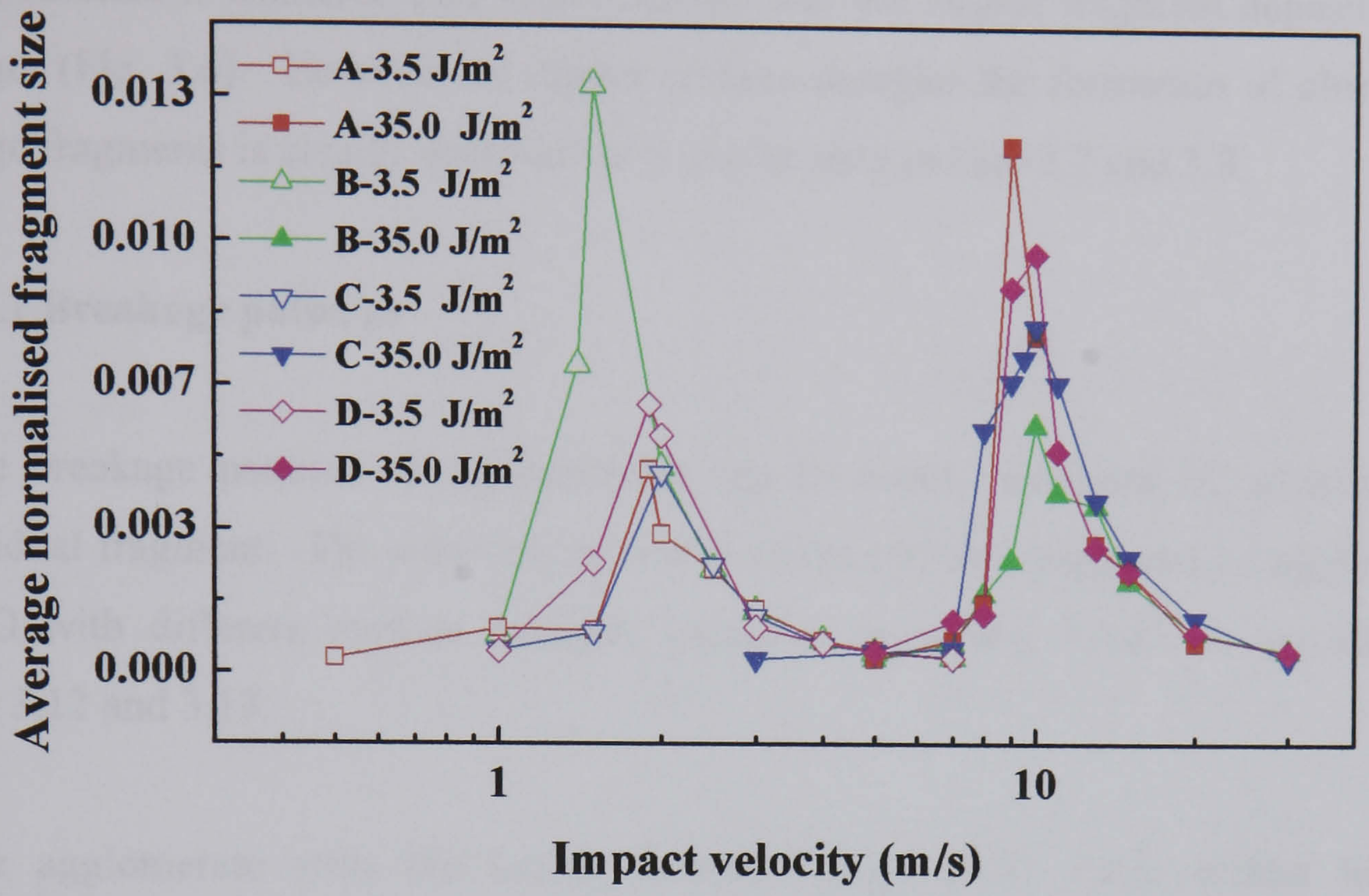

Figure 3.11 Average fragment size in each broken agglomerate.

The peak in the curve of the average fragment is usually higher at the higher values of the surface energy. However, an exception was found for agglomerate B. In this agglomerate the fragmentation is observed at 1.5 m/s for the case of 3.5 J/m^2 which is lower than the value of around 1.9 m/s for the other agglomerates. At the value of impact velocity of 1.5 m/s the number of fragments is around half of the number of fragments produced at 1.9 m/s (Fig. 3.5). Consequently, the average cluster size reaches a higher value than the one for the highest surface energy (35.0 J/m^2) and it is clearly different from the other agglomerates with the same value of impact velocity. The reason for this difference could be attributed to a statistical variation.

Regime III:

In this regime the input kinetic energy that is not dissipated is sufficient to break most of the contacts of the agglomerate and the agglomerate behaviour is clearly characterised by the disintegration of the agglomerate into small fragments as shown

in Figs 3.6, 3.7 and 3.8. However there are differences between the different values of the surface energy. At the lowest value of the surface energy (0.35 J/m^2) the agglomerate is shattered into small clusters and the largest fragment deposits on the target (Fig. 3.6). However, at higher surface energies the formation of clusters and large fragments is clearly observed as it can be seen in Figs 3.7 and 3.8.

3.4.1 Breakage patterns

The breakage patterns of agglomerates can be better visualised by examining the residual fragment. The side and top views of the residual fragments of agglomerates A-D with different surface energies impacted at several velocities are shown in Fig 3.12 and 3.13.

The agglomerate with the lowest surface energy (0.35 J/m^2) suffers from the detachment of small fragments at low impact velocity from the region close to the impact zone (Figs 3.6 a1, a2). When the impact velocity is increased the fragments are detached from regions of the agglomerate further away from the contact area affecting the whole agglomerate as it can be seen for example in the Figs 3.6 b1, b2, c1,c2, and Fig. 3,13.a. The increase in impact velocity produces an increase of the damaged volume around the contact area and the disintegration of the agglomerate into small clusters (Figs 3.6 d1, d2). The residual fragment has a structure with branches and it is irregular in shape (see Figs 3.12 b1, b2, c1, c2 and Figs 3.13 a1, a2, b1, b2). Among possible reasons for the formation of branches is the re-adhesion of the primary particles as there are large fluctuations around a mean in the size of the residual cluster. This occurs for all agglomerates with the lowest value of surface energy and at values of impact velocities between 1.0 and 2.0 m/s. At the value of surface energy 3.50 J/m^2 the breakage of the agglomerate at low impact velocities is similar to that of the agglomerate with value of surface energy of 0.35 J/m^2 (Figs 3.7 a1, a2). The breakage is characterised by the detachment of particles mainly from the contact area although it is possible to observe small fragments in other parts of the agglomerates.

(a) Aggl A (3.5 J/m^2)
V=0.5 m/s

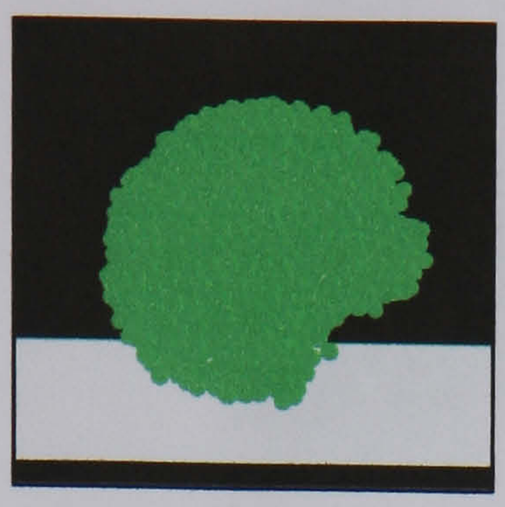

(a)

(b1) Aggl B (0.35 J/m^2).
V = 1 m/s

(b2) Aggl C (0.35 J/m^2)
V = 1.5 m/s

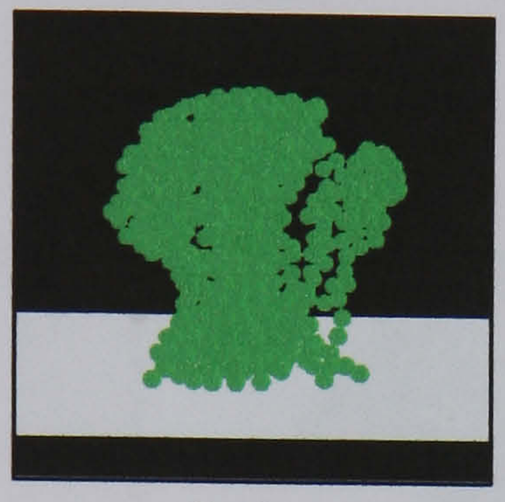

(b1)

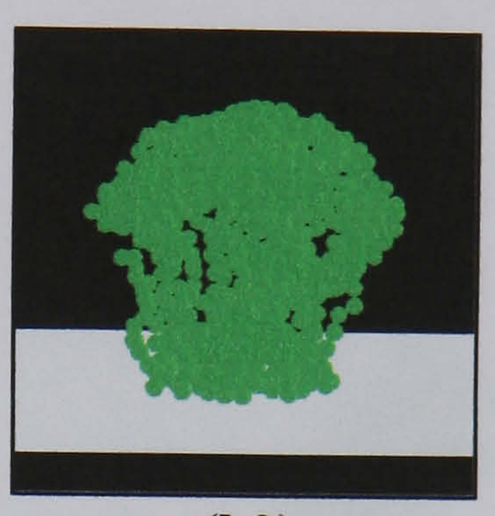

(b2)

(c1) Aggl B (0.35 J/m^2)
V = 2 m/s

(c2) Aggl C (0.35 J/m^2)
V = 2 m/s

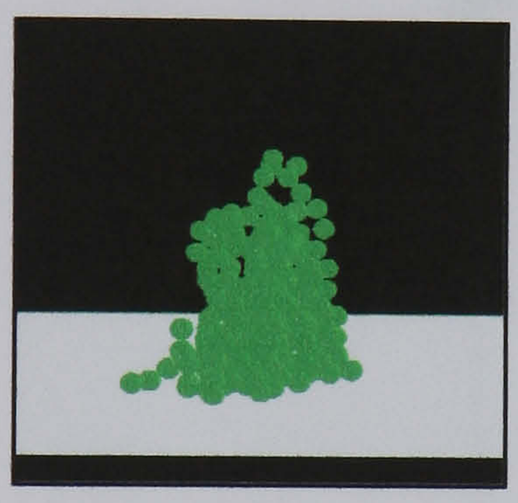

(c1)

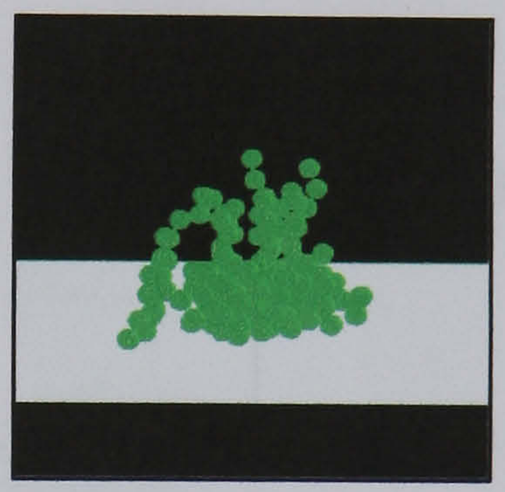

(c2)

(d1) Aggl D (3.5 J/m^2)
V=1.7 m/s

(d2) Aggl D (3.5 J/m^2)
V=2.5 m/s

(d1)

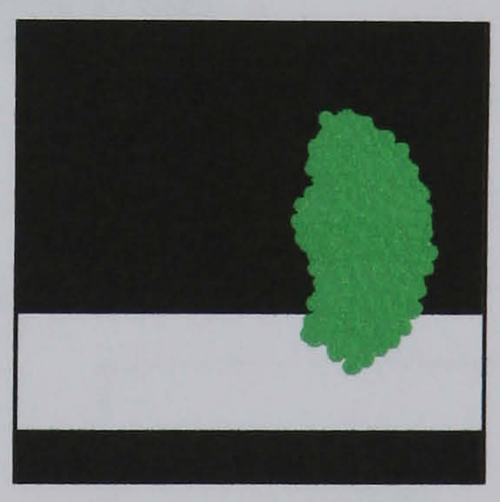

(d2)

(e1) Aggl C (35.0 J/m^2)
V = 11.0 m/s

(e2) Aggl C (35.0 J/m^2)
V = 20.0 m/s

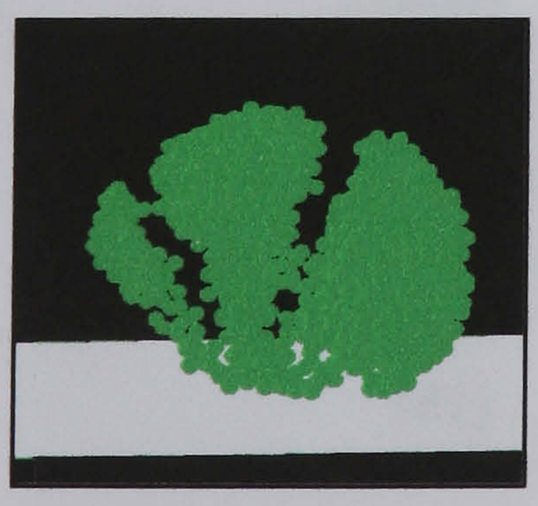

(e1)

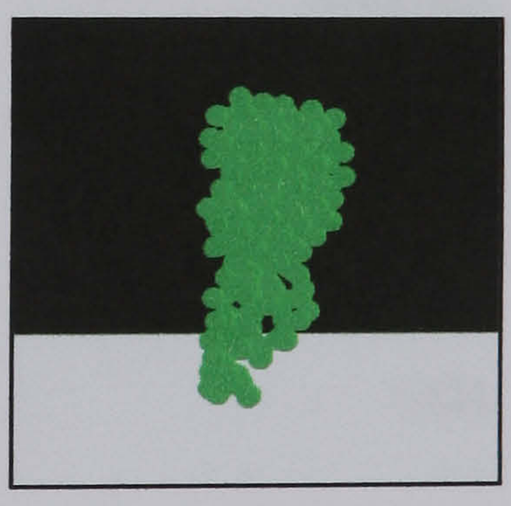

(e2)

Figure 3.12 Side views of the residual fragments. The white colour corresponds to the target.

(a1) Aggl B (0.35 J/m^2).
V = 1 m/s

(a2) Aggl C (0.35 J/m^2)
V = 1.5 m/s

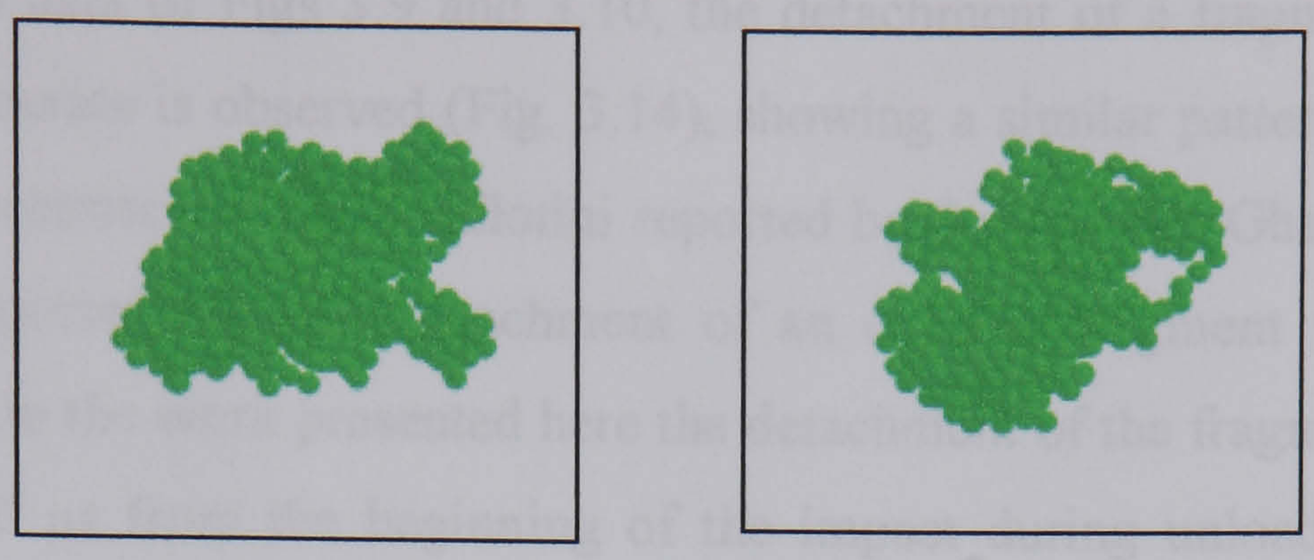

(a1) **(a2)**

(b1) Aggl B (0.35 J/m^2)
V = 2 m/s

(b2) Aggl C (0.35 J/m^2)
V = 2 m/s

(b1) **(b2)**

(c) Aggl D (3.5 J/m^2)
V=2.5 m/s

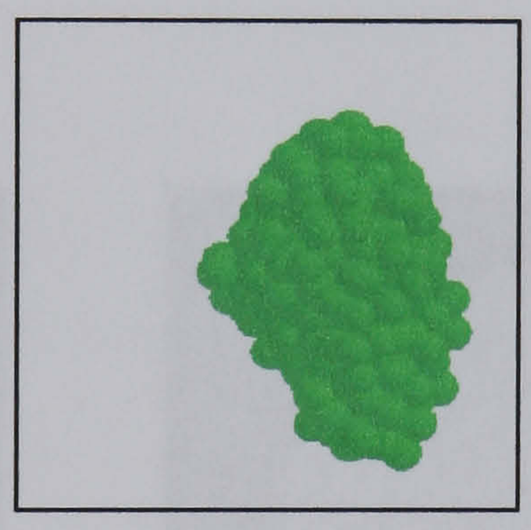

(c)

(d1) Aggl C (35.0 J/m^2)
V = 11.0 m/s

(d2) Aggl C (35.0 J/m^2)
V = 20.0 m/s

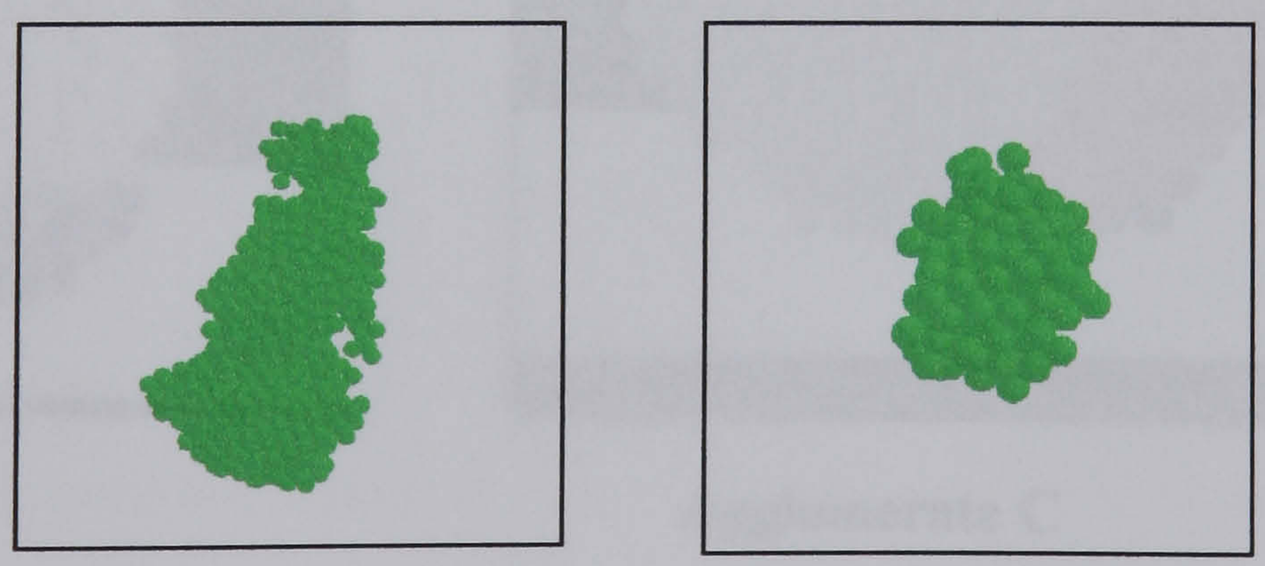

(d1) **(d2)**

Figure 3.13 Top views of the residual fragments. The white colour corresponds to the target.

For 3.5 J/m^2 surface energy, when the impact velocity increases but before reaching the levels prevailing in the data of Figs 3.9 and 3.10, the detachment of a fragment from the side of the agglomerate is observed (Fig. 3.14), showing a similar pattern to that of the impact of agglomerates of glass ballotini reported by Subero and Ghadiri (2001). These authors reported that the detachment of an oblique fragment was produced during loading. In the work presented here the detachment of the fragment was observed at about 300 μs from the beginning of the impact during unloading which had started at about 50 μs from the beginning of the impact. This difference suggests that probably the same pattern has been originated in a different way. When the impact velocity is increased the fragmentation of the residual cluster into two pieces of comparable sizes is observed (see Figs. 3.9 and 3.10). In Fig. 3.15 the two largest fragments of agglomerate D impacted at 2.0 m/s are shown. It is possible to observe that the particles at the bottom and in one of the sides have been detached in the form of small clusters.

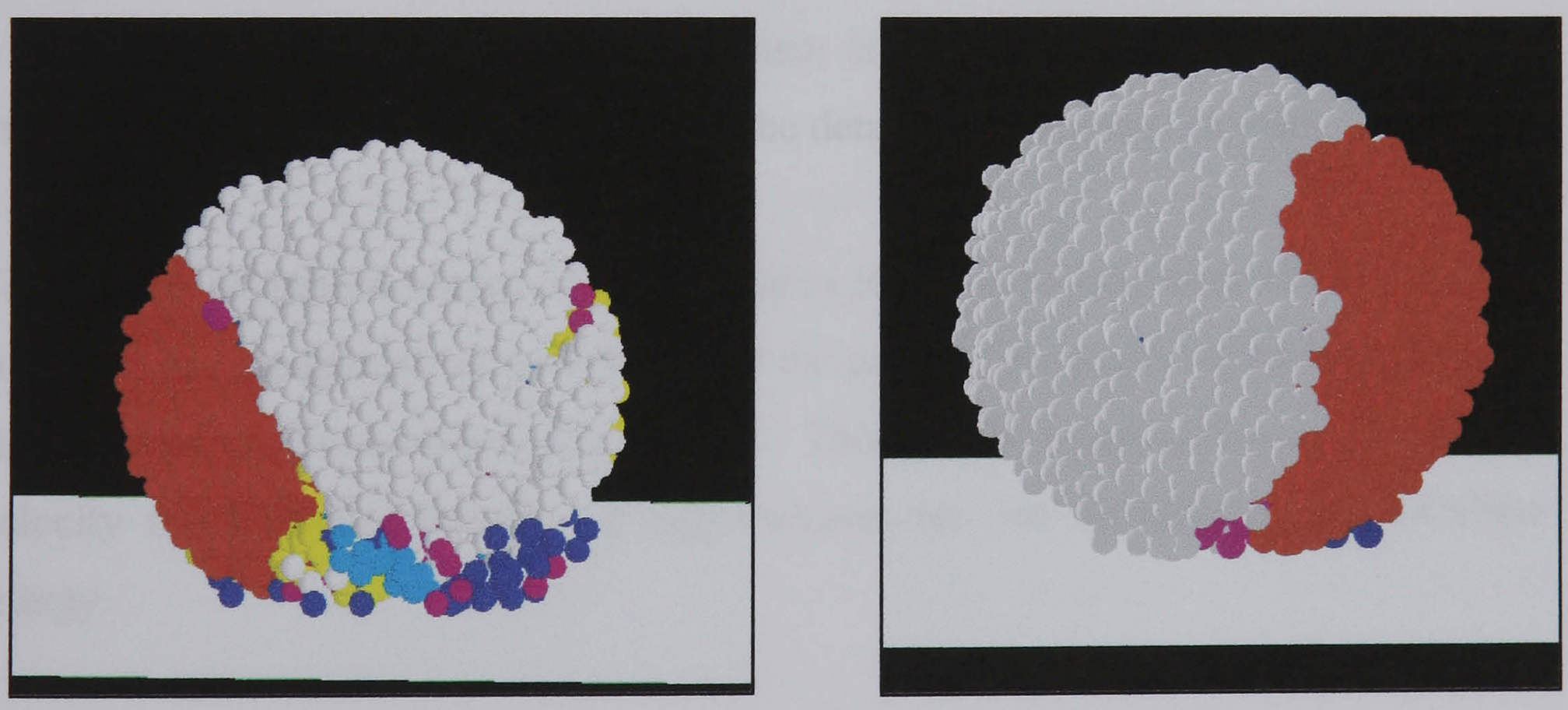

Agglomerate E **Agglomerate C**

Figure 3.14 Detachment of a fragment for Agglomerates E and C impacted at 2.4 m/s and 1.8 m/s respectively. Light grey: largest fragment; red: second largest fragment; white (background): target.

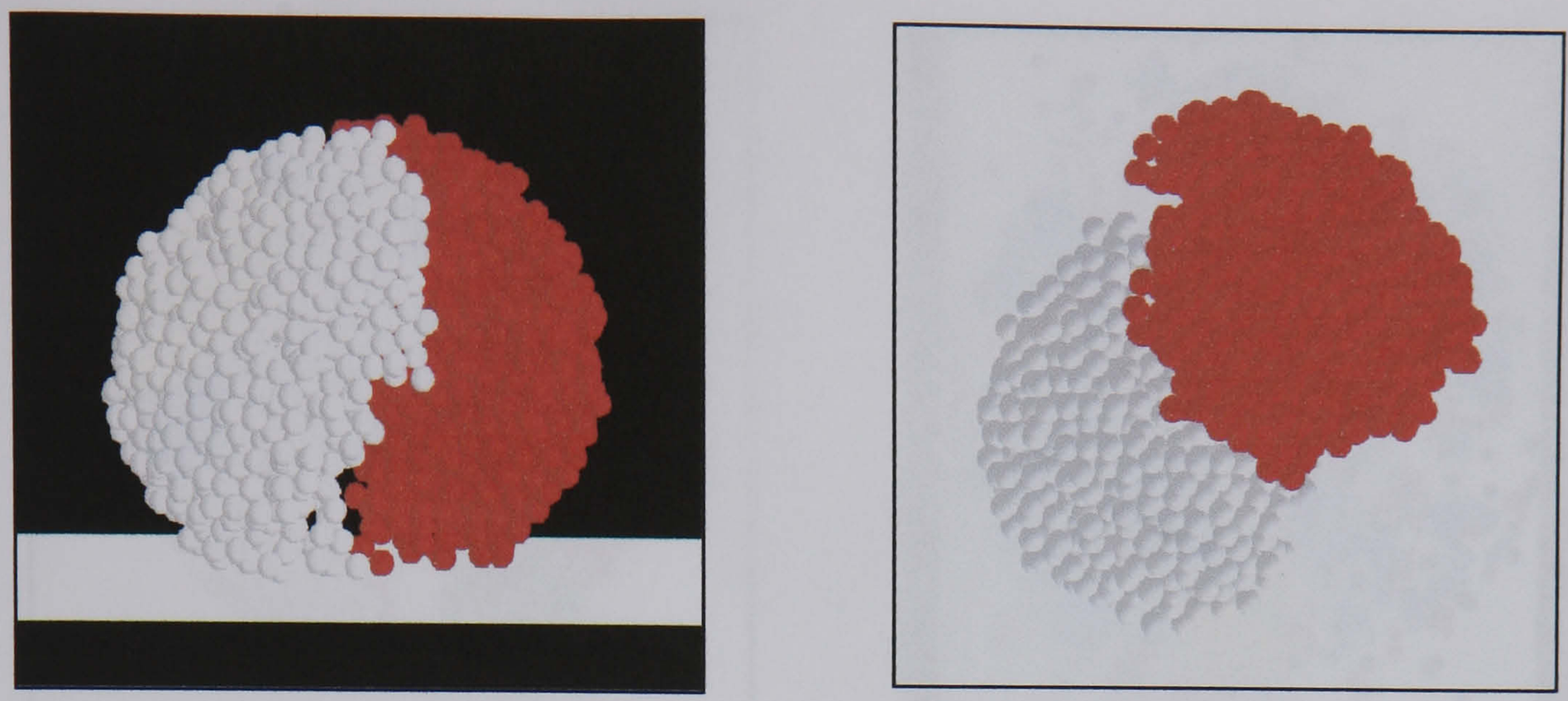

Side **Top**

Figure 3.15 Side and top view of Agglomerate D impacting at 2.0 m/s. Light grey: largest fragment; red: second largest fragment, white (background) target.

At impact velocity of 2.5 m/s it is possible to observe that the residual fragment of the agglomerate D with surface energy of 3.5 J/m^2 shows smoother profiles (Figs 3.12 d1, d2 and Fig. 3.13 c) than those of Agglomerate B and C with the surface energy of 0.35 J/m^2 (see Figs. 3.12 and 3.13). This observation suggests that fragmentation is the predominant mechanism in the failure of the agglomerate with the surface energy of 3.5 J/m^2 rather than the detachment of small clusters.

For the case of surface energy 35.0 J/m^2 and as for the previous cases of lower surface energies, the detachment of particles from the parts of the agglomerate including the contact area has been observed (Fig. 3.8). This clearly suggests that at low impact velocity the breakage patterns of agglomerates are not sensitive to the interface energy.

If the impact velocity is increased the fragmentation of the agglomerate is observed. The fragmentation pattern varies from one agglomerate to another (Figs. 3.10 and 3.11): agglomerate E is divided into two symmetric halves, agglomerate C is divided into two large fragments but not symmetrically, agglomerate B is divided into two large fragments and one slightly smaller one and agglomerate D is divided into three large fragments and one smaller one. It is worth noting that little debris is produced.

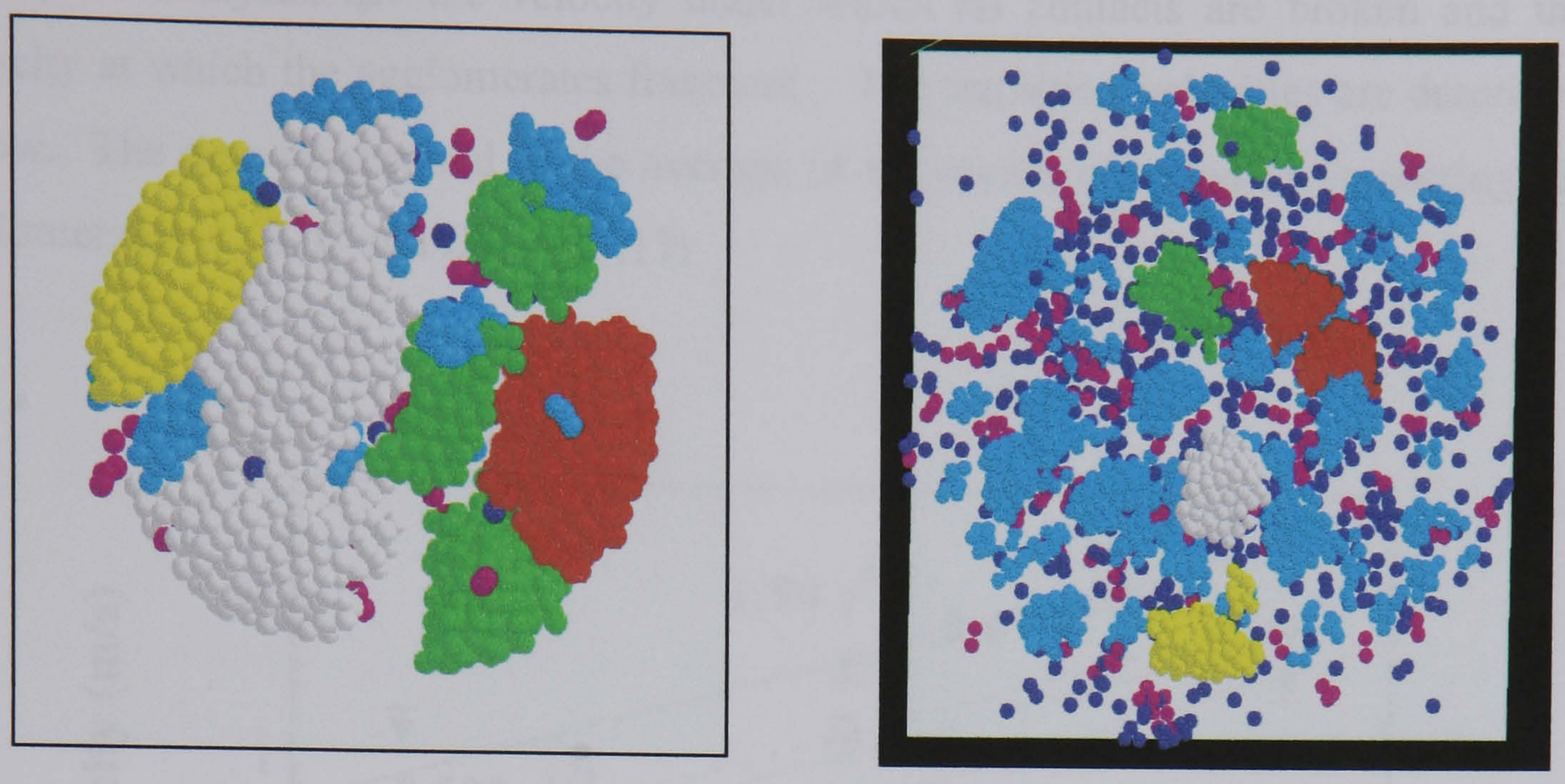

V=11 m/s **V=20 m/s**

Figure 3.16 Top view of agglomerate C after impact at 11.0 m/s and 20 m/s for the value of surface energy of 35.0 J/m^2. Colour coding: light grey: largest fragment; red: second largest fragment, yellow: third largest fragment, green: intermediate clusters; cyan: clusters between 4 and 100 particles; pink: doublets, blue singlets and white the target.

When the impact velocity increases it is possible to observe that the number of fragments increases (Figs 3.8, and 3.16). The largest cluster is not a structure that has been deposited over the contact area like in the case of 0.35 J/m^2 (Fig. 3.16).

There are differences in the breakage pattern for different agglomerates impacted at the same impact velocity and with the same interface energy. The origin of the differences observed in the pattern of breakage can be attributed to a statistical behaviour due to the random distribution of contacts and particles.

3.5 Transition velocities

As shown in the previous section there are several regimes of breakage depending on the impact velocity and surface energy. These regimes are separated by transition velocities from one regime to the other. There are also two other velocities that are

worthy of analysis, *i.e.* the velocity under which no contacts are broken and the velocity at which the agglomerates fragment. The transition velocities are described below. The data correspond to the average of the results obtained by impacting the agglomerates A, B, C and D (Fig. 3.17)

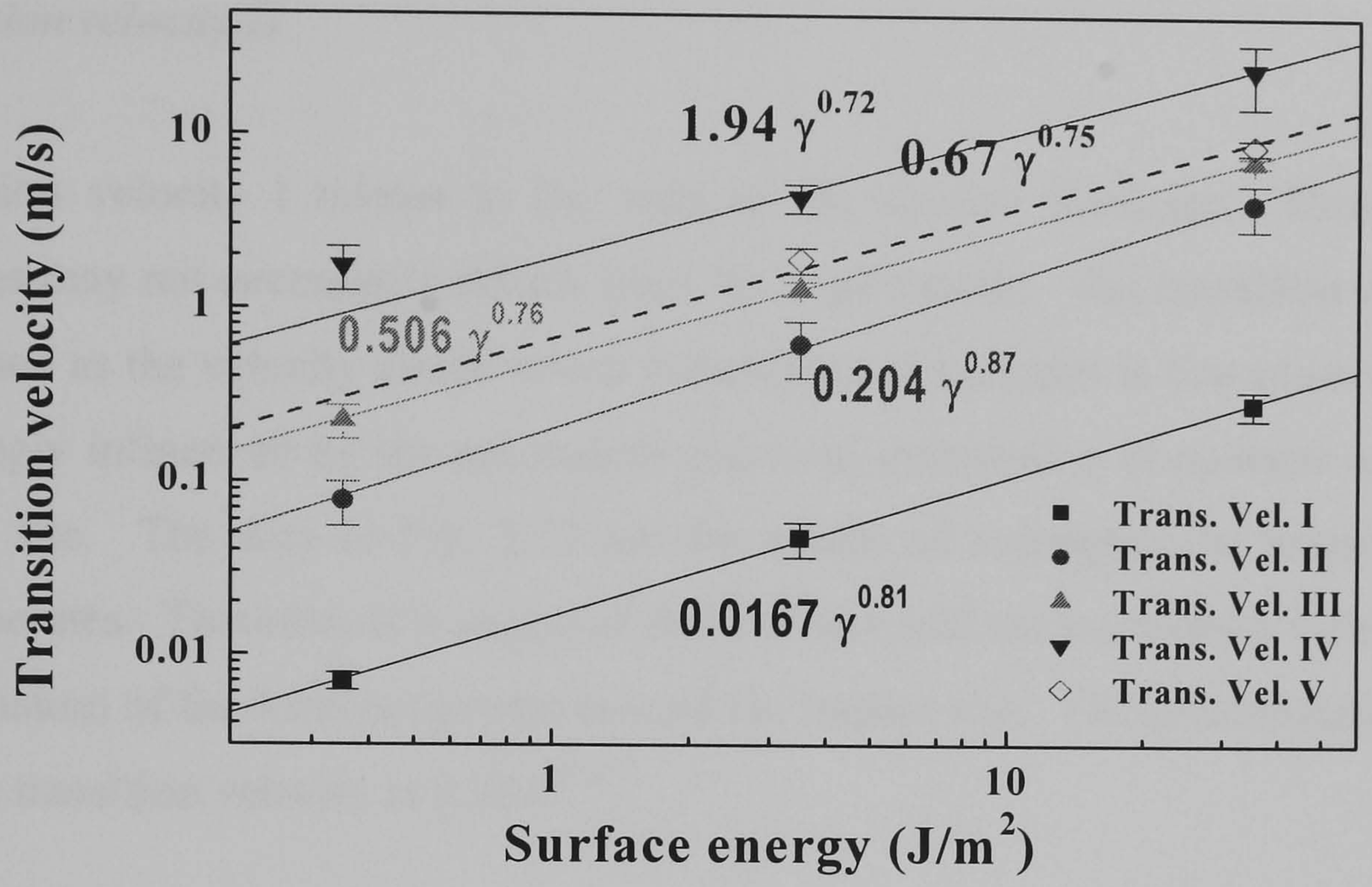

Figure 3.17 Dependence of the transition velocities on the surface energy

Transition velocity I

This transition velocity is the maximum velocity under which no contact breakage is observed, *i.e.* the impact is fully elastic. This velocity is obviously a function of the surface energy for which power law relationships with different exponents have been proposed by Thornton *et al.* (1996), who proposed the relationship $0.0025exp(0.98\gamma)$ for a two-dimensional agglomerate with random packing. For an agglomerate with an ordered structure Kafui and Thornton (2000) proposed a dependence proportional to $\gamma^{1.5}$ for an agglomerate with an ordered structure. For the agglomerates studied here a dependency on the surface energy in the form $\gamma^{0.81}$ fits well with the simulation data. This is shown in Fig. 3.17 where the transition velocities are plotted as a function of the surface energy. The differences between the results presented here and those

reported by Thornton and co-workers could be due to several factors, *e.g.* the difference in the structure and the method of agglomerate preparation and the statistical variations between agglomerates. In this work four different agglomerates were tested but the previous works tested just one agglomerate. In addition, the results of a random packing cannot be easily compared with those of regular packing.

Transition velocity II

Transition velocity I relates to the start of the contact breakage. However, the particles may not necessarily detach from the agglomerate. The transition velocity II is defined as the velocity above which detachment of particles is first observed. This is strongly influenced by the orientation and local distribution of contacts around the impact site. The data in Fig. 3.17 are the results of averaging the impact of four agglomerates. Therefore it is expected that the data will not be strongly influenced by the variation of the local properties around the impact site. The relationship obtained for this transition velocity is $0.204\gamma^{0.87}$.

Transition velocity III

As shown previously in section 3.4 agglomerate breakage occurs in three different regimes depending on the impact velocity. In regime I only local damage occurs. In regime II, the extent of local damage increases and fragmentation starts to occur. In regime III extensive fragmentation and total disintegration of the agglomerate occurs. The second regime was characterised by a fast decrease in the size of the residual cluster. Transition velocity III separates regime I from regime II. A quantitative criterion has been established for identifying the transition velocity: the size of the residual cluster is less than 95% of the initial agglomerate size. A power law relationship is found in the form $0.506\gamma^{0.76}$.

Transition velocity IV

This is the velocity at which fragmentation is first observed. This velocity corresponds to the maximum of the second largest fragment size (see Fig. 3.4 for agglomerates A-D). Agglomerates with the lowest surface energy do not fragment, therefore we have just two data points to obtain the fit for an expression $y=A\gamma^{\alpha}$ which is obviously not very reliable but the exponent is not far different from the previous cases. The relationship obtained here is $y=0.67\gamma^{0.75}$. Data corresponding to the intermediate values of surface energy would be required in future in order to predict a more accurate relationship between this transition velocity and the surface energy.

Transition velocity V

This is the transition between regimes II and III and it is defined as the velocity over which the maximum fragment size is less than 5% of the initial agglomerate size. The data points fit well to the equation $1.94\ \gamma^{0.72}$. The power law index is slightly less than in the previous cases since the data point for low surface energy is too high. The readhesion of the material may influence the agglomerate behaviour at low surface energies. In simulations where no re-adhesion is allowed and at sufficiently high impact velocities the agglomerates are disintegrated into singlets. Now, allowing for particle re-adhesion the fragment size increases. This effect has been observed to be large in agglomerates with low surface energy and at velocities at which the agglomerate is disintegrated into small fragments.

All relationships between transition velocity and surface energy show exponents between 0.75 and 0.87 which may be approximated to 5/6 (0.83). Based on this value the relationship between surface energy and the square of the velocity V^2,has as an exponent -5/3. The analysis of bond breakage based on the energy balance approach outlined in Appendix B shows that the relationship between the number of broken contacts and surface energy is made through the term $V^2/\gamma^{5/3}$. This similarity between both exponents is indeed very interesting and suggests that the agglomerate properties scale with the exponent 5/3 of the surface energy (Section 3.1).

3.6 Conclusions

An analysis of the agglomerate behaviour under impact conditions has been presented here. From this study important conclusions can be obtained and are listed below:

(i) the breakage of interparticle bonds as defined by the damage ratio depends on the surface energy with the exponent -5/3.

(ii) the transition velocities separating the different regimes of behaviour of the agglomerates depend on the surface energy in the form $\gamma^{-5/6}$.

(iii) agglomerates show extensive deformation under impact at the lowest value of the surface energy (0.35 J/m^2) and no evidence of fragmentation was found for any value of impact velocity. In this case the agglomerates behaved macroscopically in a ductile mode.

(iv) at higher values of surface energy (3.5 J/m^2 and 35.0 J/m^2) the agglomerates fragmented at the same time as local damage around the impact site occurred. This type of behaviour is typical of semi-brittle materials.

(v) the amount of debris produced at the impact site when the agglomerates fragmented was smaller at the highest value of surface energy (35.0 J/m^2).

(vi) following on from the three previous points, a transition in the mode of failure of agglomerates is observed when the interface energy is varied. At low surface energies the agglomerate behaves in a ductile mode. When the surface energy is increased the behaviour is more semibrittle. It is not clear if such a transition is gradual or occurs sharply at a specific value of the surface energy.

CHAPTER 4: EFFECT OF THE IMPACT ANGLE ON THE BREAKAGE OF AGGLOMERATES

4.1 Introduction

In this chapter the results of the simulations of oblique impacts of agglomerates are reported. Oblique impact on walls is a common damage process during, for example, pneumatic conveying and size reduction in pin mills. Literature addressing the oblique impact of agglomerates against walls or even single particles is scarce. Vervoorn (1986) studied the effect of repeated impact of cylindrical alumina as a function of the impact angle and velocity. Vervoorn (1986) observed that when the results were plotted in terms of the percentage of broken particles as a function of the normal component of the impact velocity, the experimental data for all angles were fairly unified. Therefore, he concluded that the normal component of the impact velocity was the dominating factor that influenced the breakage. However, Vervoorn (1986) also observed that the tangential component of the impact velocity influenced the mass loss per impact for the case of impact damage by wear, erosion or chipping when the tangential component of the velocity became greater than the normal component.

Hutchings (1992) observed that there was a critical impact angle that separated two different regimes of breakage of a target made of silicate glass-ceramic when impacted by a hard particle. Over the critical impact angle large chips were detached from the target. However, below the critical impact angle the target suffered from plastic deformation with little loss of material.

Salman *et al.*(1995) and Salman *et al.*(2002) reported on the oblique impacts of aluminium oxide spheres (solid particles) and fertiliser granules, respectively. They observed that the probability of breakage was relatively constant in the range 50°-90° (increasing very slightly as the impact angle was increased), but it decreased rapidly below 50°. For impact angles of less than 20° for aluminium oxide spheres and 10° for the fertiliser granules the probability of breakage became negligible.

Thornton *et al.* (1995) reported on simulation of the oblique impact of two agglomerates against each other, each one made of 4000 particles. They found that for relative impact velocity of 1.0 m/s and impact angles of less than 45° little damage was produced in the assembly of particles. They found a linear relationship between the mass of fines produced and the Weber Number that was based on the normal component of the impact velocity.

In spite of the significant differences between the systems analysed by Salman *et al.* (2000) and Thornton *et al.* (1995) common features can be found between them. Normal impact seems to produce the largest damage in both agglomerates and solid particles. When the impact angle is reduced from 90° (perpendicular to the target) the damage of the assemblies or single particles is also reduced.

Samimi (2003) finds that for detergent based granules both tangential and normal components of the impact velocity influence their breakage. However, these components are predominant in different regimes. The normal component of the impact velocity had a larger influence than the tangential component in the chipping regime. During the fragmentation regime the tangential component was more important that the normal component.

In view of the previous work summarised in the above, computer simulations have been carried out using Distinct Element Method, where the breakage characteristics of oblique impacts have been analysed for isotropic and spherical agglomerates (uniform mass distribution and coordination number within the agglomerate). The results of these simulations are reported in this chapter.

4.2 Computer simulations

The agglomerates studied in this chapter have been formed following the procedure described in Chapter 2. The single particle properties and the agglomerate properties are reported in Tables 4.1 and 4.2 respectively. The main simulations were carried out for agglomerate A. Agglomerate B has exactly the same properties, but was formed with different seeding in the random generation of primary particles. It was used just to

corroborate the behaviour of agglomerate A and to observe some effects of the statistical variations. In the cases where the results of agglomerate B are described, reference will be made to agglomerate B. Otherwise, the results relate to agglomerate A. Several impact angles have been used. The impact angle θ is defined as the angle between the wall plane and the impact direction, measured clockwise as shown in Fig. 2.8. The impact of agglomerates in different orientations has been carried out by rotating the agglomerate 90° and 180° around each coordinate axis as shown in Fig. 2.8.

Table 4.1 Single particle properties.

Young's modulus (GPa)	31.0
Poisson ratio	0.3
Density (kg/m^3)	2000
Surface energy (J/m^2)	3.50
Friction coefficient	0.35
Particle radius (μm)	50

Table 4.2 Agglomerate properties.

Agglomerate label	**A**	**B**
Number of particles	3000	3000
Agglomerate radius (mm)	0.907	0.922
Packing fraction	0.546	0.521
Coordination number	5.617	5.864

4.3 Breakage of contacts

Figure 4.1 shows the damage ratio in the velocity range of 1.15 m/s to 3.41 m/s and impact angles between 30° and 90°. These results have been obtained by keeping the impact velocity constant and varying the impact angle. The following points are noteworthy:

(i) damage ratio increases as the impact velocity increases in the range of velocities investigated for all values of the impact angle;

(ii) when the angle is increased from 30° to 90° a gradual increases in the damage ratio is observed.

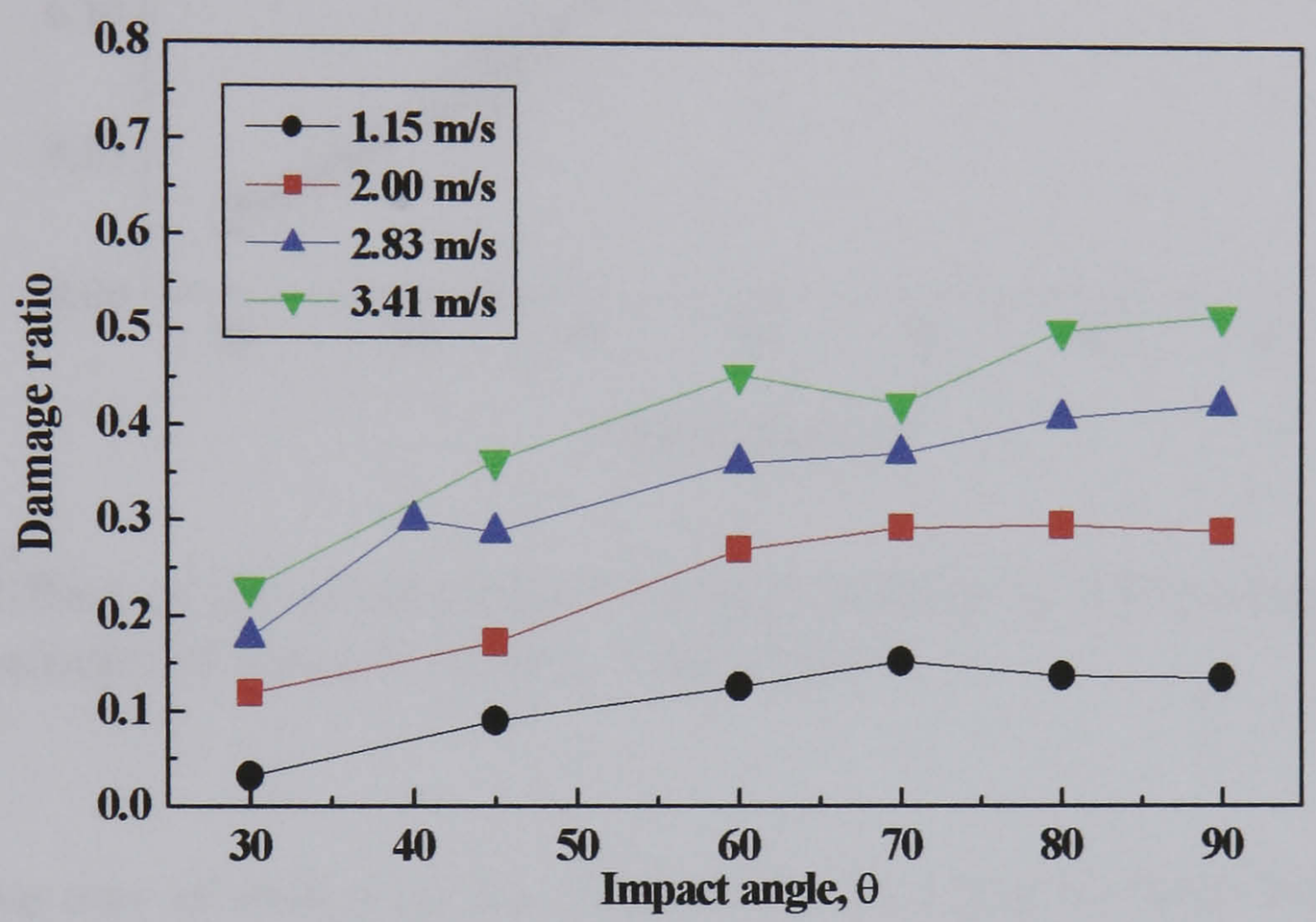

Figure 4.1 Dependency of damage ratio on the impact angle keeping constant the absolute value of the impact velocity.

Figure 4.2 shows the damage ratio at the impact velocity of 2.0 m/s for six different orientations together with the average value and the error bars. The error bars decrease as the impact angle decreases, being around ±10% at 90° and around ±1% at 30°. It is also shown that the curve corresponding to the average of the impact in six different possible orientations is smoother than the curves corresponding to a single impact. This clearly implies that the relative minimum and maximum of the individual curves in Fig. 4.2 are the result of statistical variations.

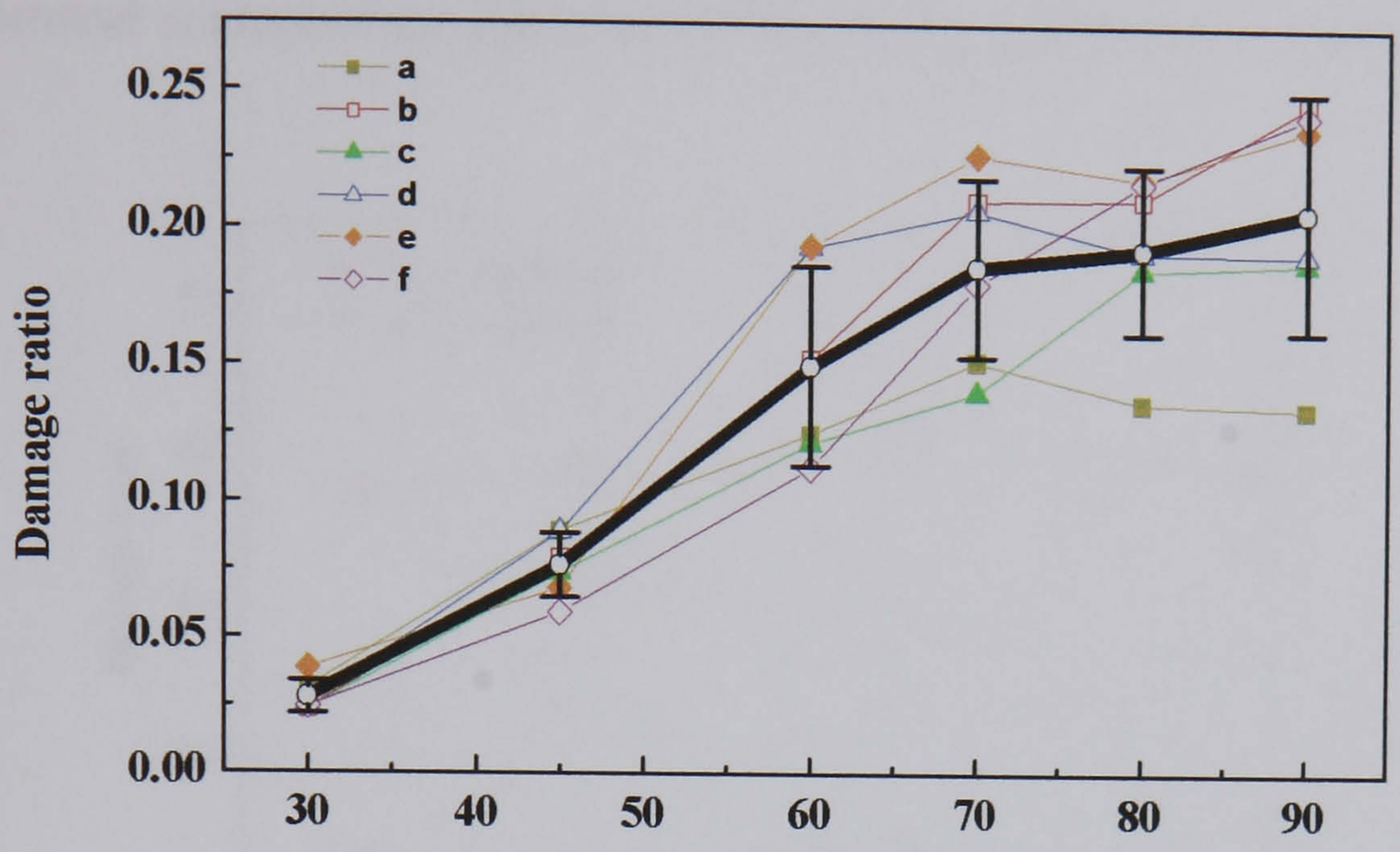

Figure 4.2 Effect of the orientation of the agglomerate on the breakage of bonds at the impact velocity of 2 m/s at various impact angles.

An alternative way of analysing the effect of the impact angle is by keeping the normal component of the impact velocity constant whilst varying the impact angle. Figure 4.3 shows the damage ratio as a function of the impact angle for two values of the normal component of impact velocity. The damage ratio is fairly constant within a margin of 5%. Clearly, in the oblique impact of agglomerates, the damage ratio depends mainly on the normal component of the impact velocity.

The analysis of the wall force supports the above results. When the normal component of the impact velocity is kept constant (for different impact angles), the profiles of the normal wall force F_N as a function of time overlap (Fig. 4.4a). Figure 4.4b shows the influence of the tangential component of the impact velocity for different impact angles. The tangential component of the force, F_X, is surprisingly roughly the same for the two impact angles of 45° and 60°. For the 90° impact case despite zero tangential velocity before impact, it has nevertheless a small peak, although it quickly goes down to zero. The reasons for the presence of a tangential force component for the 90°

impact are unclear and require further investigations, although it is likely that unsymmetrical contact of the particles and the ensuing damage are contributory factors.

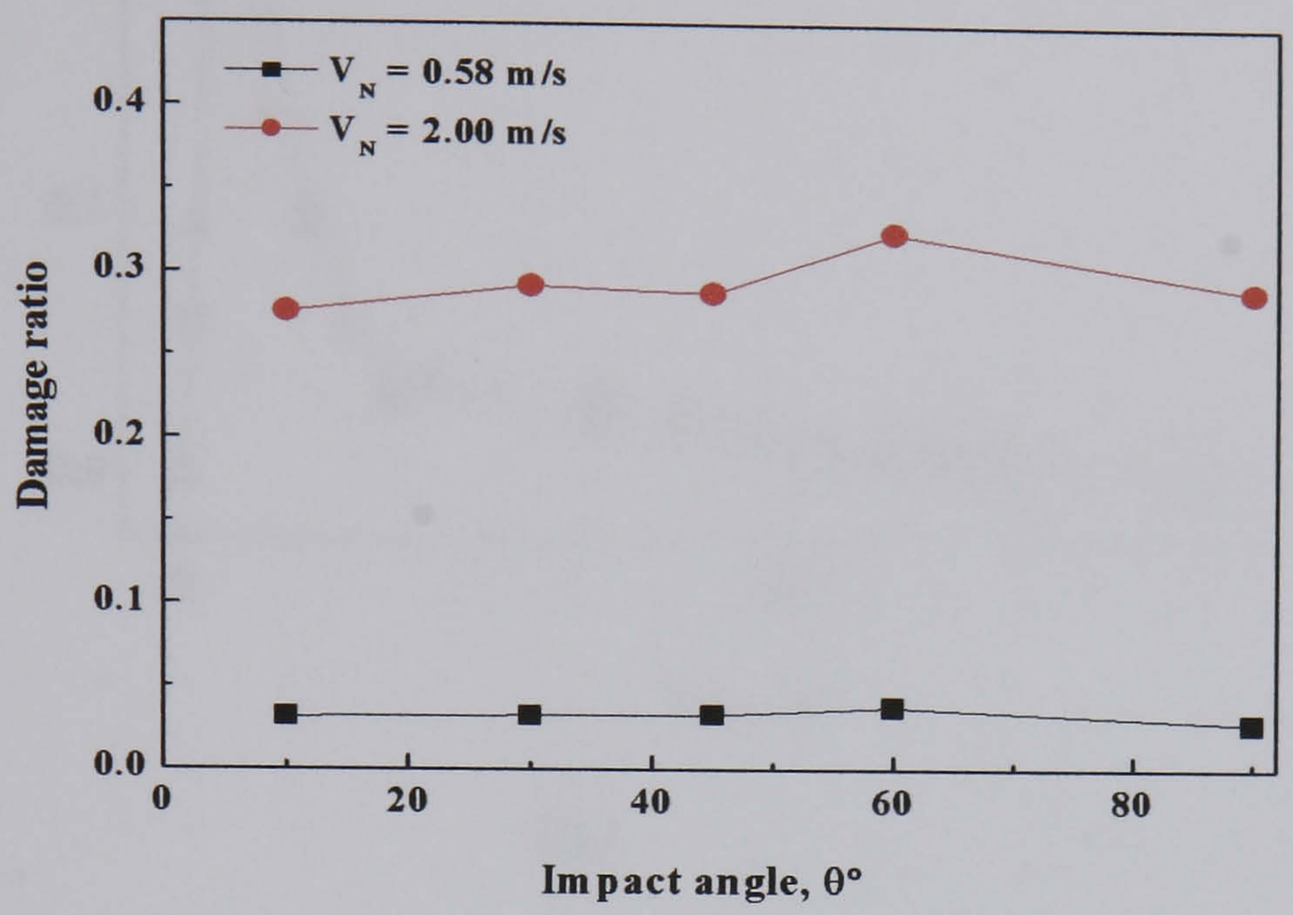

Figure 4.3 Dependency of damage ratio on the normal component of the impact velocity.

4.4 Breakage pattern

4.4.1 Fragment size distribution

An analysis of the cumulative mass fraction undersize as a function of the cluster size is presented in Figs. 4.5(a,b). The cluster size is represented by the number of primary particles, N_p, forming the cluster normalised by the number of particles of the whole agglomerate, N. The results for the case of an impact at 2.8 m/s at different impact angles are presented in Fig. 4.5 (a). We can clearly observe the reduction in the production of fragments and debris when the impact angle is reduced from 90° to 30°.

The results for the case in which the normal component of the impact velocity is kept constant are shown in Fig. 4.5 (b). The proximity between the different curves once again shows that the normal component of impact velocity is the main factor in the breakage of agglomerates under impact for the type of agglomerates examined here.

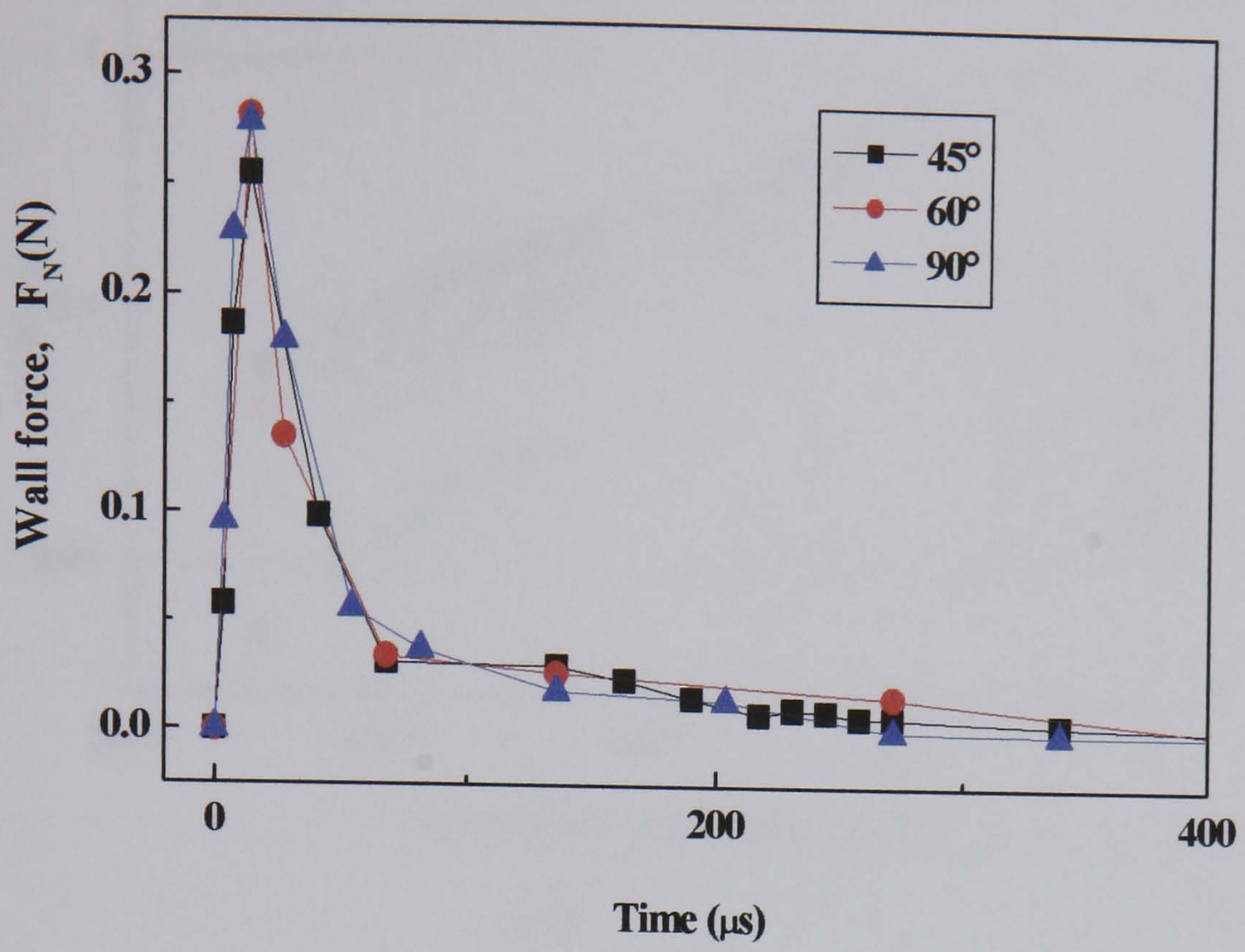

(a)

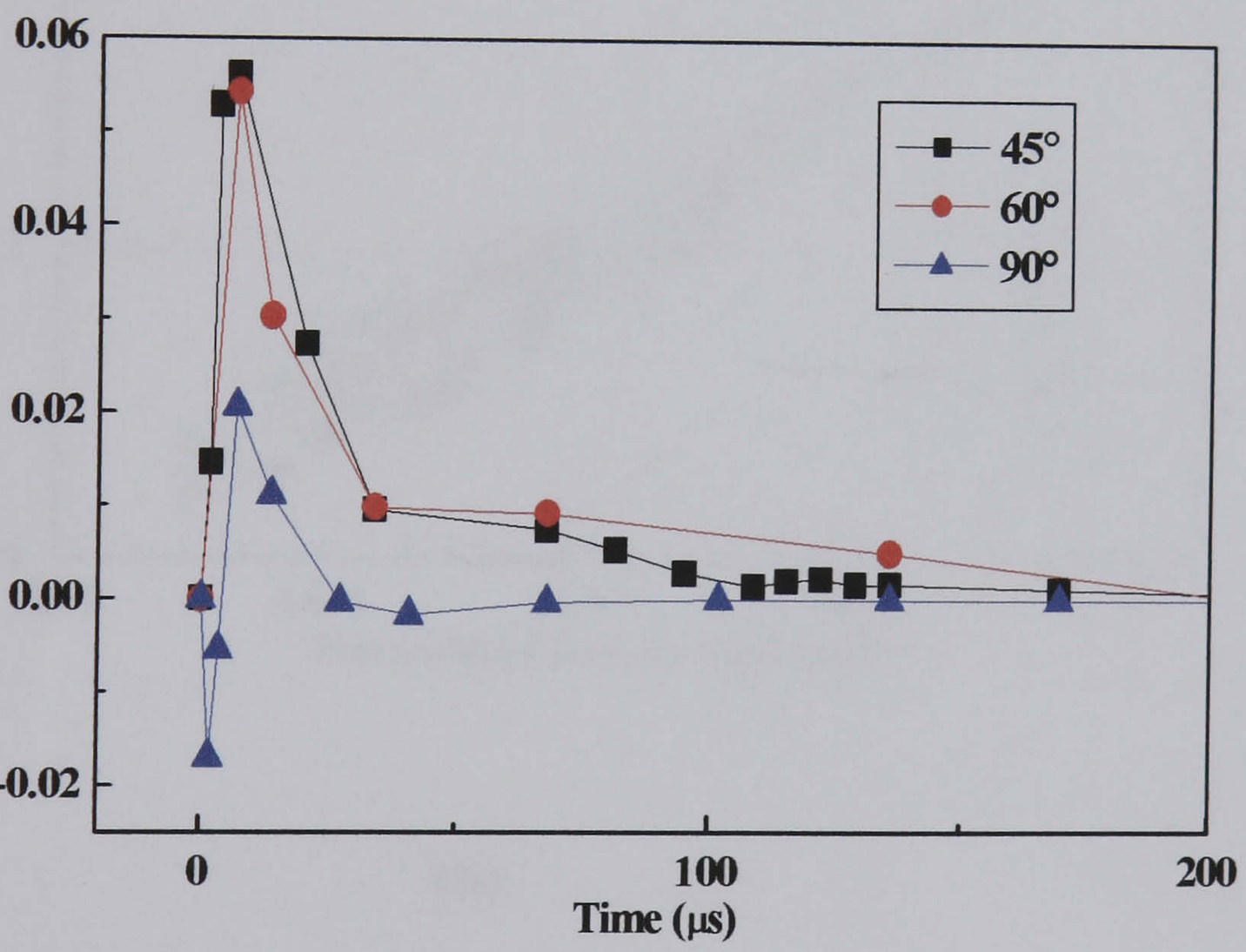

(b)

Figure 4.4 Wall force profiles during impacts at a constant normal component of the impact velocity (2.0 m/s): a) normal component and b) tangential component of the force.

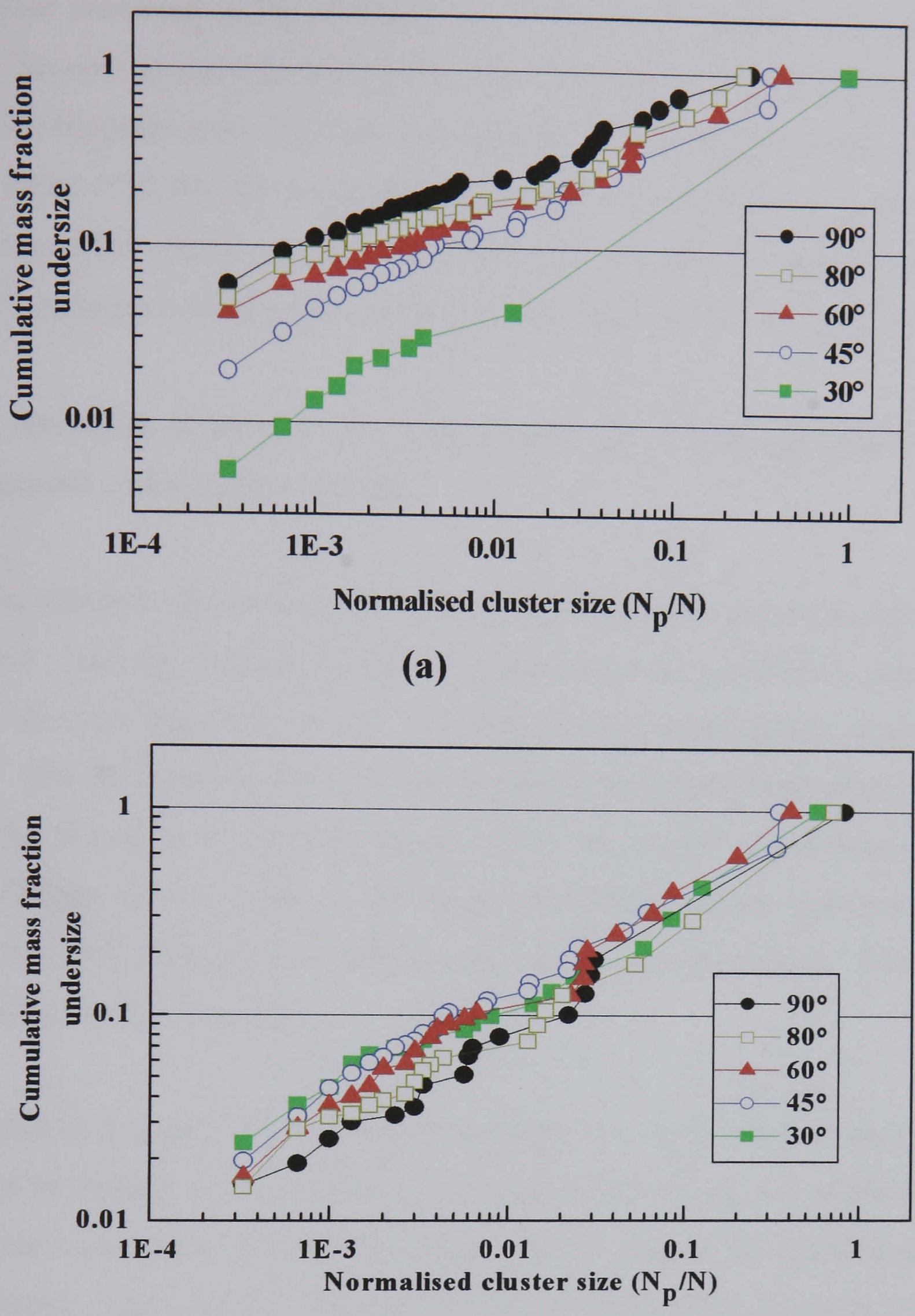

(a)

(b)

Figure 4.5 Cumulative mass fraction undersize for: (a) constant impact velocity at 2.8 m/s and (b) constant normal component of the impact velocity at 2.0 m/s.

The data presented in Fig. 4.5(b) are on a logarithmic scale. The differences in the mass fraction between the size distribution curves for different impact angles increase with the fragment size. The spread in data for the normalised cluster size 0.001 is less than about 0.03, for the normalised cluster size less than 0.01 it is about 0.07 and for the normalised cluster size 0.1 it is about 0.2. Therefore it appears that the fragment size distribution is affected by the tangential component of the impact velocity.

4.4.2 Breakage pattern of the agglomerates at a constant value of the normal component of the impact velocity

Figure 4.6 shows the breakage pattern at the normal component of impact velocity of 2.0 m/s. The top, bottom and side views are shown for different impact angles and hence absolute impact velocities. The impact direction on the side views is from left to right. The different fragments are distinguished by different colour coding. Light grey particles belong to the residual cluster, red is the second largest cluster, yellow is the third largest cluster, cyan is the colour presenting clusters between four and 100 particles, pink particles are doublets and singlets are shown blue. The grey colour in the background is the target.

For oblique impacts, the debris and fragments are more concentrated in the regions behind the impact zone as shown in the bottom view of Fig. 4.6 where more fragments and debris are seen on the left hand side. For 90° impact, the debris is more randomly distributed. The normal component of impact velocity has been kept constant for all the cases shown in Fig. 4.6. The damage ratio is roughly the same for all of them (Fig. 4.3). This implies that the impact angle strongly influences the breakage pattern of agglomerates.

Figure 4.7 shows the breakage pattern of agglomerate B for the impact angles of 30°, 60° and 90° whilst keeping the normal component of impact velocity at the value of 1.7 m/s constant. The damage ratios for all cases shown in Fig. 4.7 are not significantly different. This trend confirms that the normal component of impact velocity is the main factor that influences the number of broken contacts in agglomerates, as shown in Fig. 4.3 for agglomerate A. Figure 4.7 also shows that the

breakage pattern of agglomerates is influenced by the impact angle. The debris is more concentrated in the regions behind the impact zone corroborating the results obtained for agglomerate A as shown in Fig. 4.6.

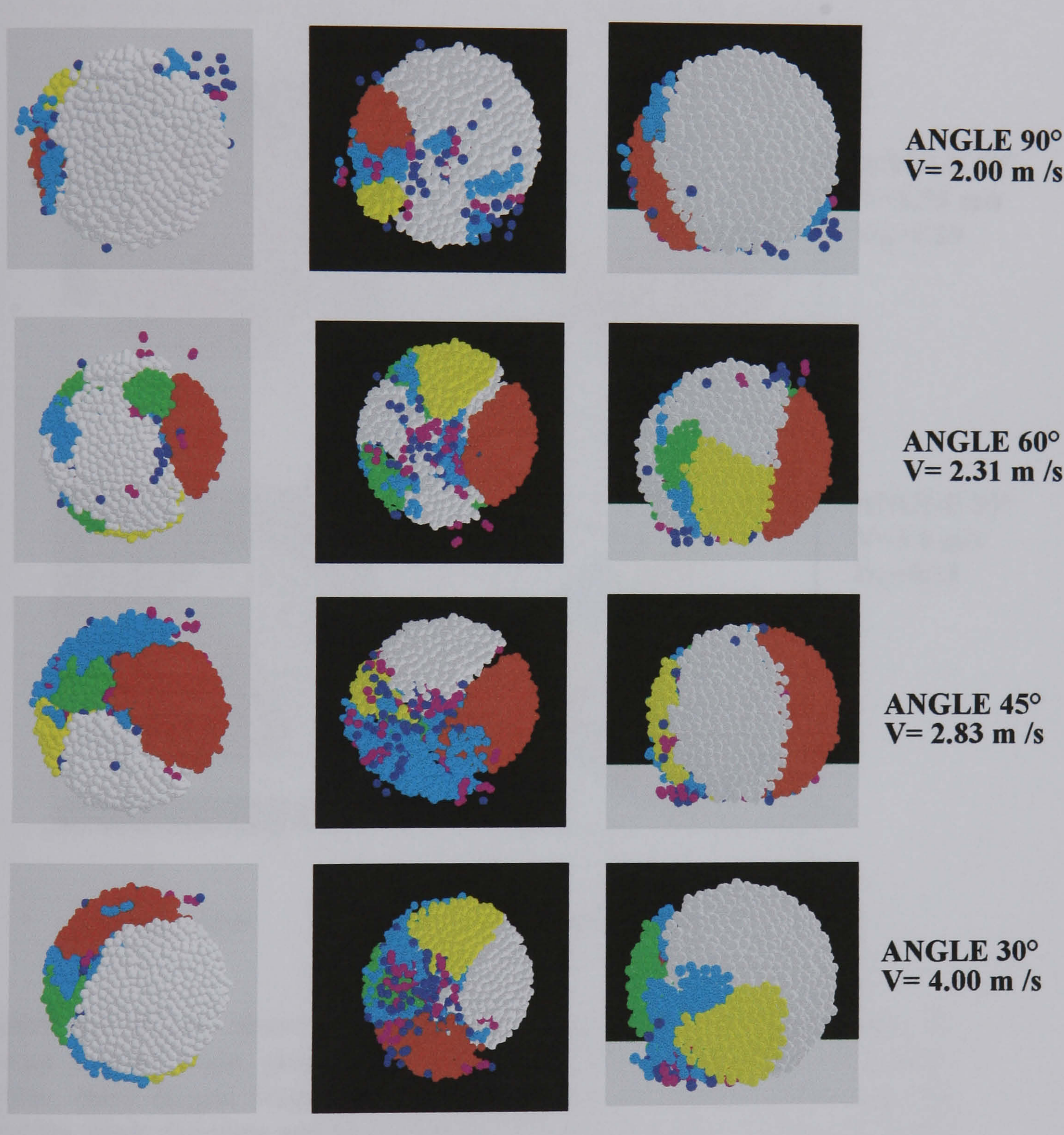

Figure 4.6 Visual observations of the oblique impact of Agglomerate A. Colour coding: light grey: residual cluster, red: second largest fragment, yellow: third largest fragment, cyan: clusters sized between four and 100 particles, pink: doublets and blue singlets. The grey colour in the background corresponds to the target.

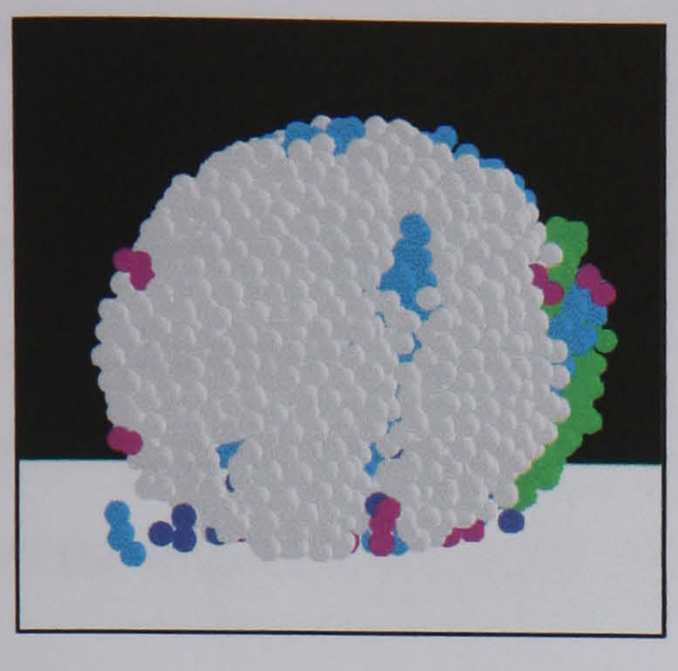

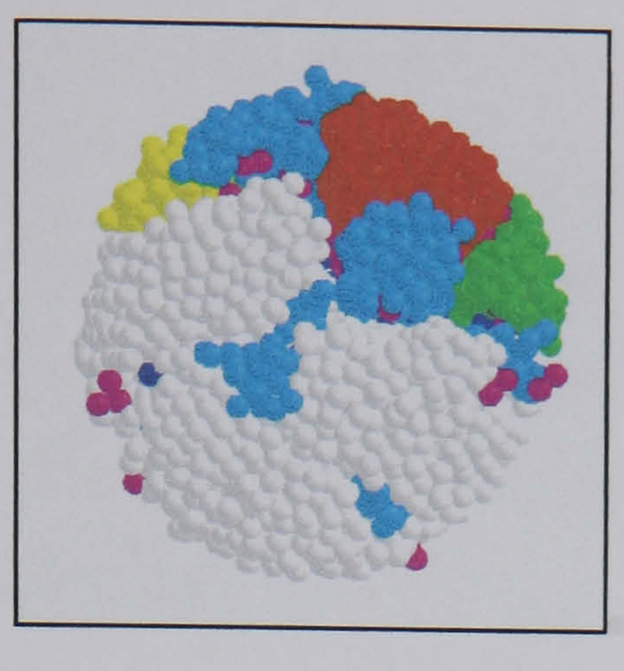

ANGLE 90°
V=1.7 m/s
D_R=0.39

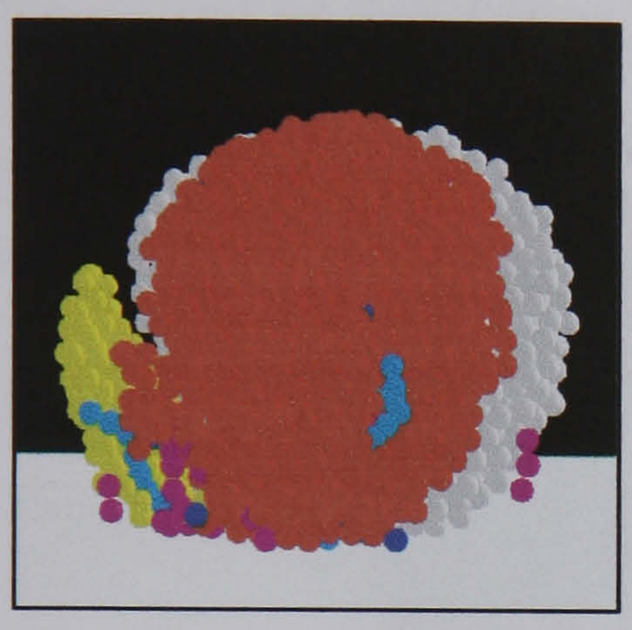

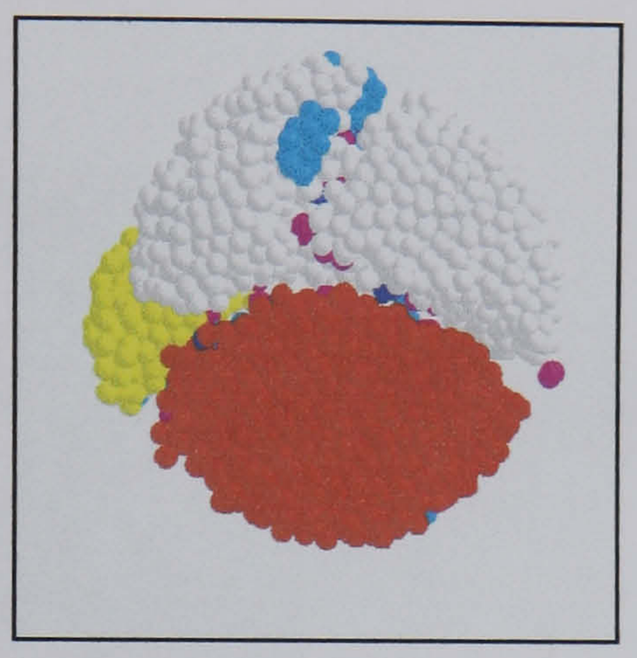

ANGLE 60°
V=1.96 m/s
D_R=0.29

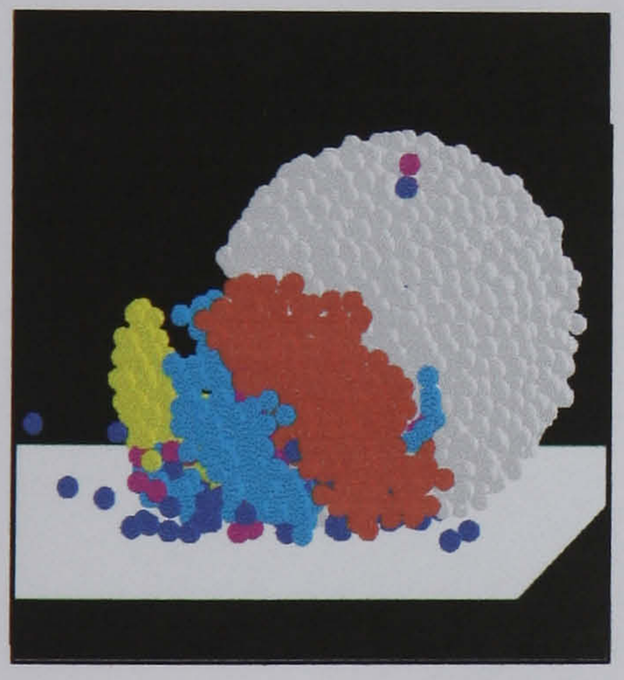

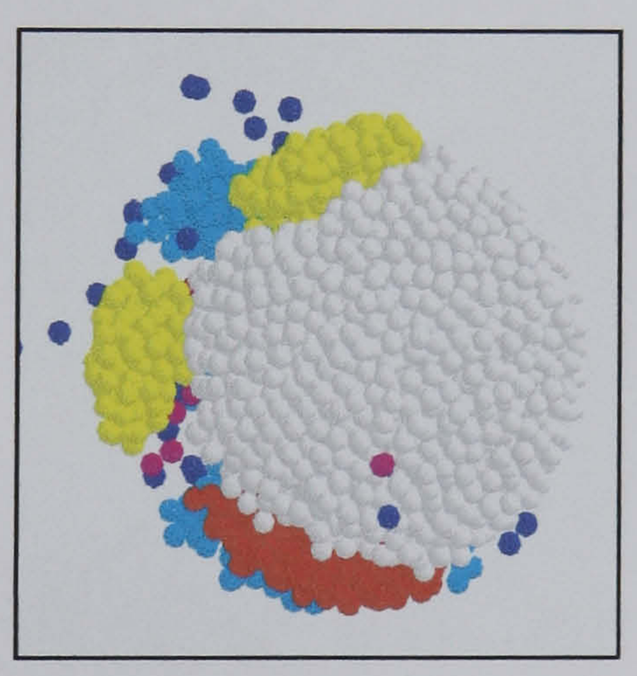

ANGLE 30°
V=3.4 m/s
D_R=0.31

Side view

Top view

Figure 4.7 Visual observations of the oblique impact of Agglomerate B. Colour coding: light grey: residual cluster, red: second largest fragment, yellow: third largest fragment, cyan: clusters sized between four and 100 particles, pink: doublets and blue singlets. The white colour corresponds to the target.

Figure 4.8 shows the pattern of broken contacts for the 30° and 90° angles relating to the Fig. 4.6 as viewed from the top. The effect of the impact angle on the spatial distribution of broken contacts can be clearly seen. Surprisingly, the damage ratio is the same for both cases. At 90° the broken contacts are spread more uniformly within the agglomerate. Figure 4.9 shows that the number of fragments including singlets detached from the agglomerate reduces with an increase in the impact angle confirming that the impact angle affects the size distribution.

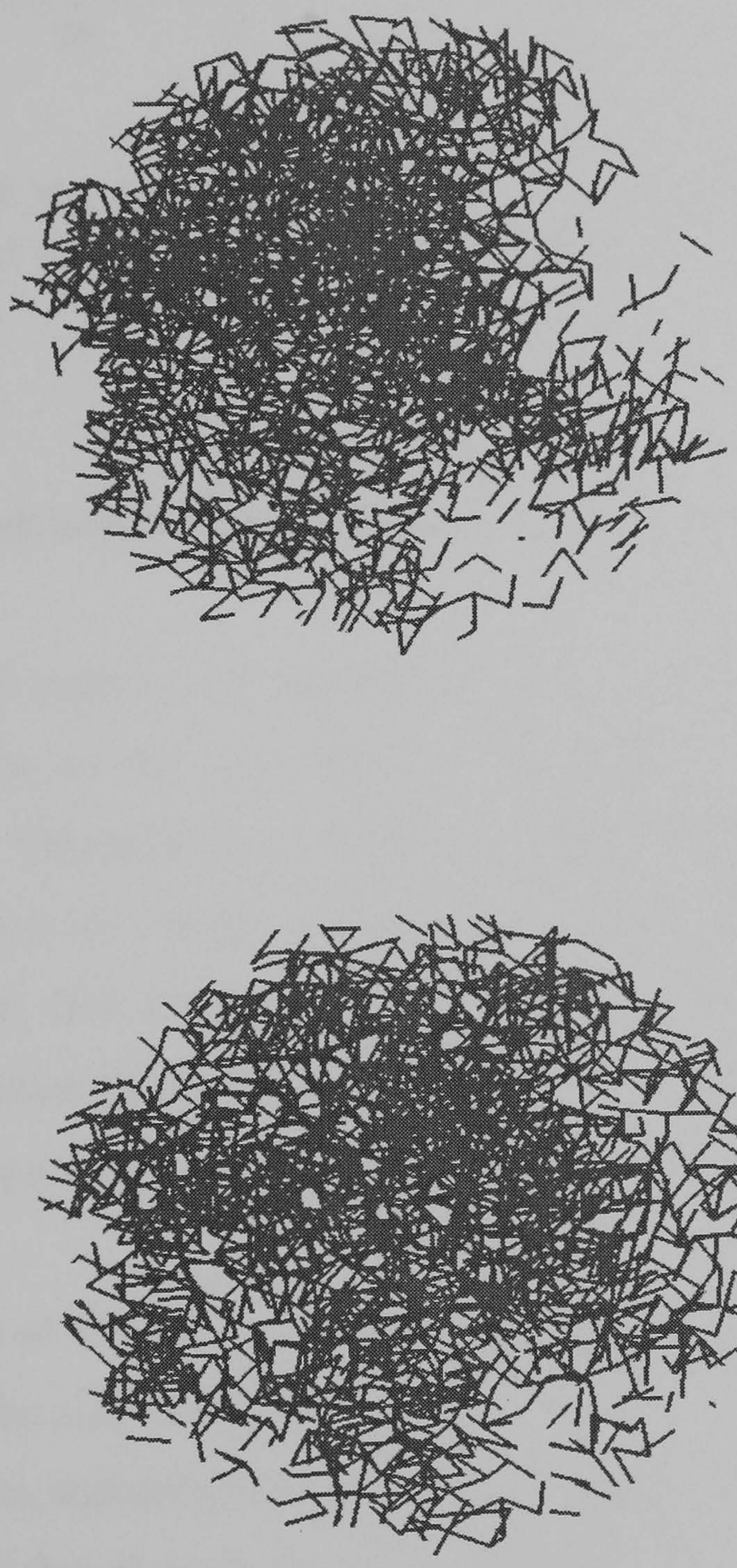

Figure 4.8 Pattern of broken contacts at 30° and 90° impact angle.

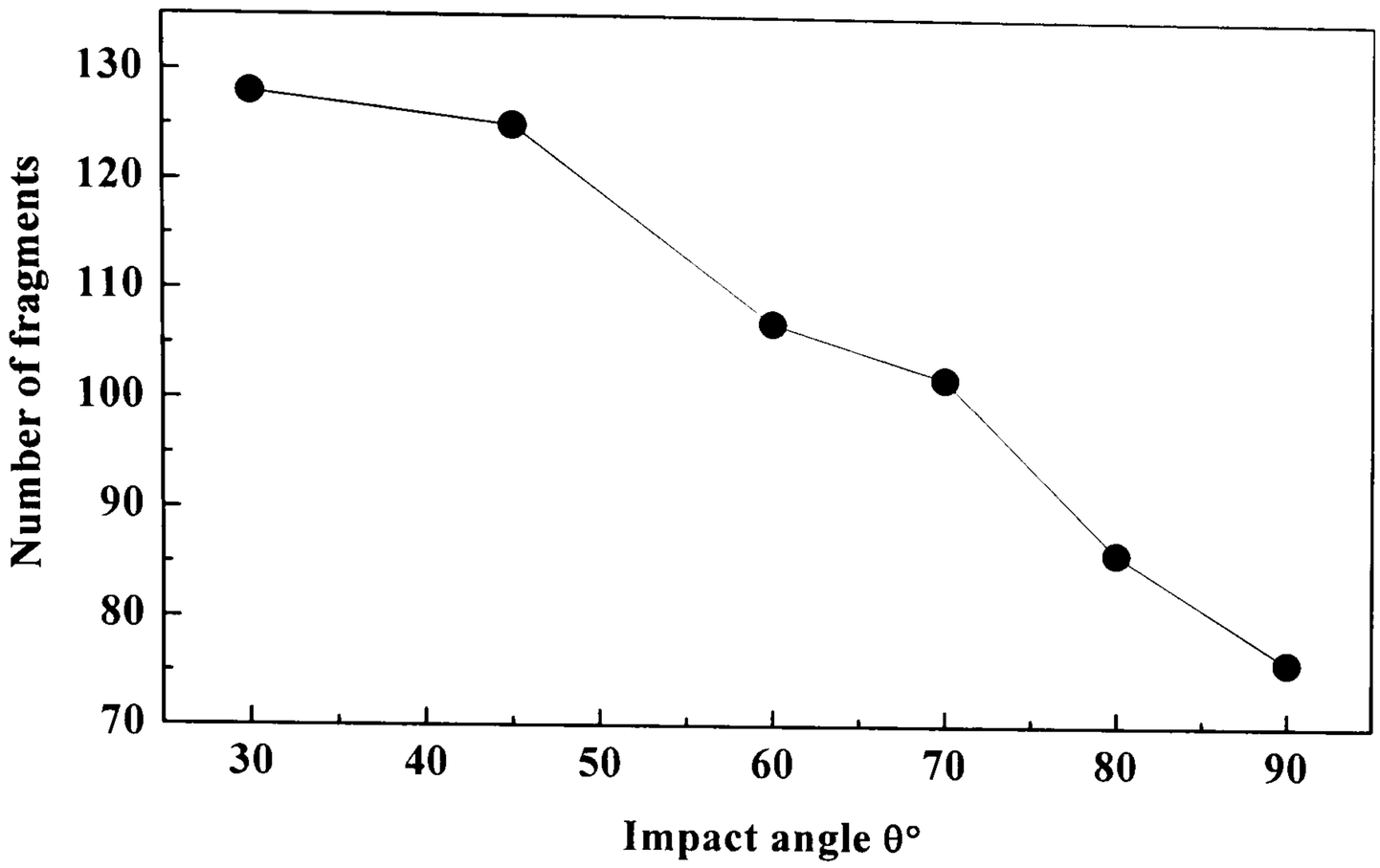

Figure 4.9 Number of fragments detached from Agglomerate A as a function of the impact angle at the value of $V_N = 2.0$ m/s.

4.4.3 Effect of impact velocity on the breakage pattern at constant impact angle

The breakage patterns of Agglomerate A as affected by the impact velocity for the impact angles of 45° and 90° are shown in Fig. 4.10. Previous work (Subero *et al.*, 1999, Thornton *et al.*, 1999) has shown that the agglomerate breakage pattern can be divided into three classes depending on impact velocity: local disintegration, fragmentation and shattering. This trend is confirmed by Fig. 4.10, where at low impact velocities the agglomerate rebounds with a small percentage of broken contacts. When the impact velocity increases the largest cluster size reduces.

For the case of 90°, the size of the largest fragment decreases as the impact velocity increases. The size of the second biggest cluster remains initially nearly constant, but it then increases, indicating the process of fragmentation. Increasing the velocity further, the sizes of the clusters approach each other indicating the predominance of the shattering in the damage process.

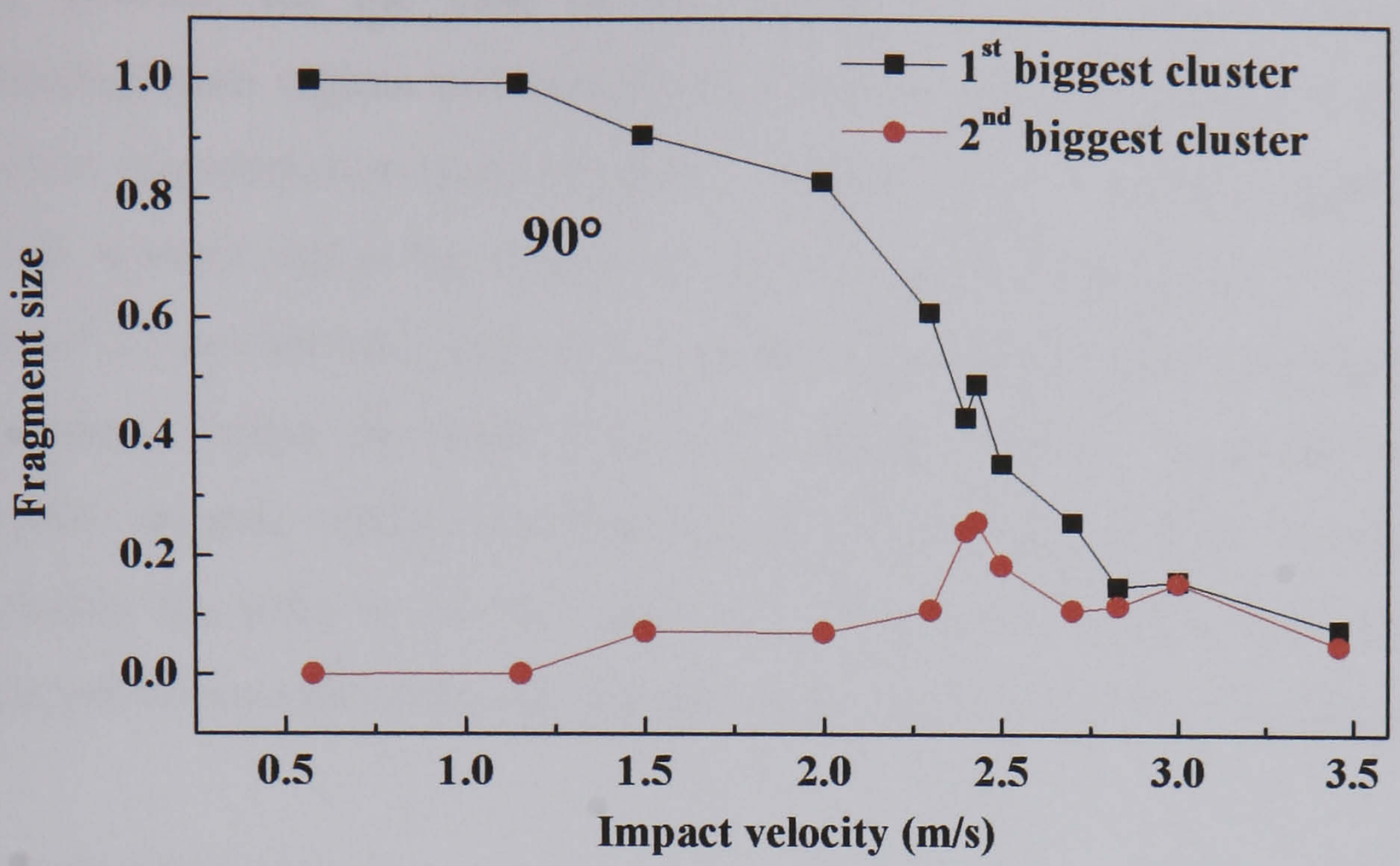

(a)

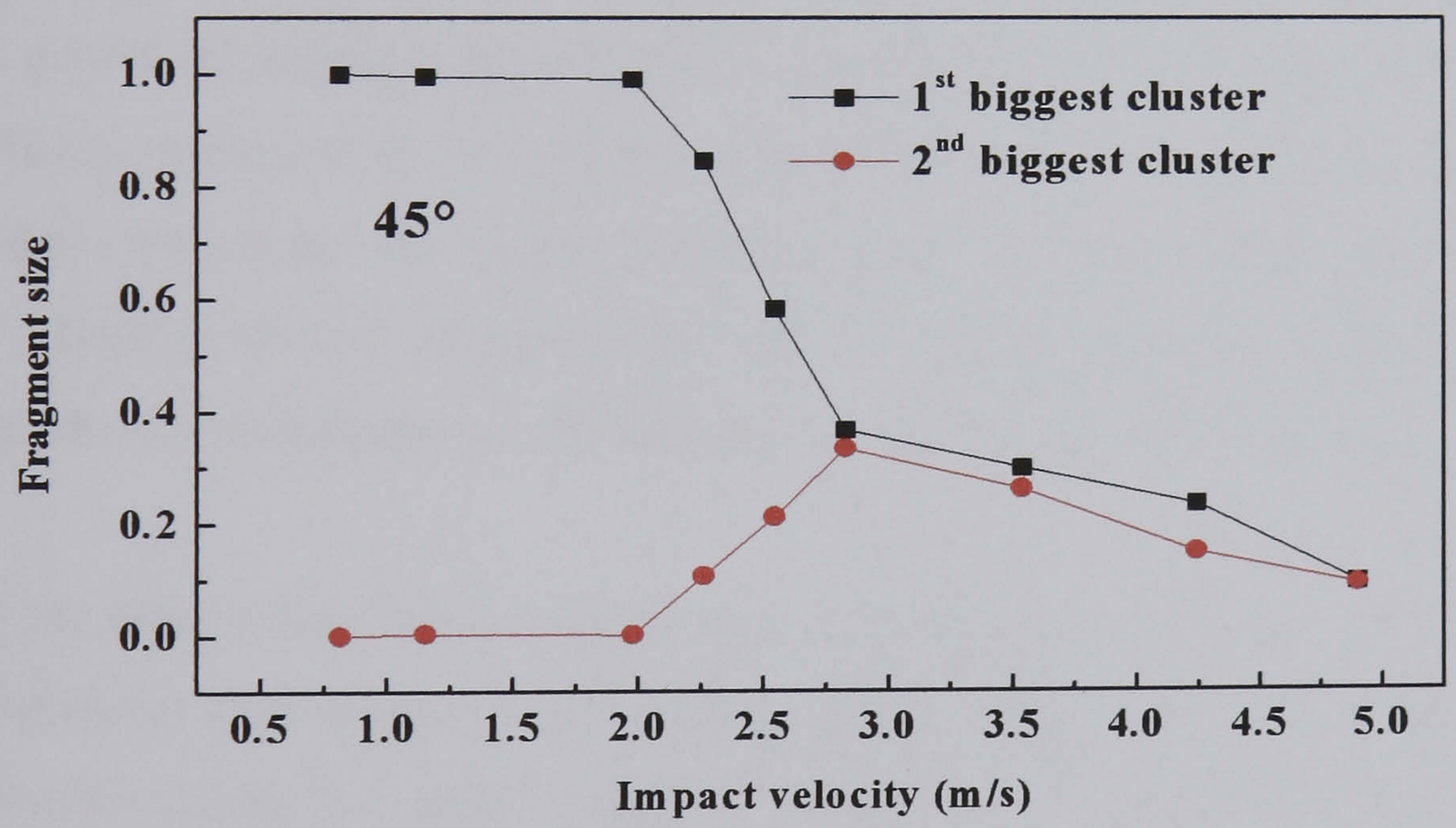

(b)

Figure 4.10 Size of the two biggest fragments for the impact angles of (a) 90° and (b) 45°.

In contrast, for the case of 45° impact the agglomerate remains in the local disintegration regime until the impact velocity exceeds about 2.0 m/s (V_N = 1.8m/s), where fragmentation starts to occur. The size of the second biggest cluster increases with velocity and at the same time the size of the biggest cluster is reduced. Beyond about 2.7 m/s the two biggest clusters have comparable sizes. As the impact velocity is increased further the size of the two biggest clusters is gradually reduced. For an impact velocity with a normal component of 2 m/s the number of broken contacts is the roughly the same as for the case of 2 m/s normal impact. However the number of fragments detached from the agglomerate is significantly less for the case of 90°.

4.5 Conclusions

The influence of the impact angle on the breakage characteristics of spherical agglomerates has been investigated using Distinct Element Analysis. For the impact angle and velocity regimes considered in this investigation, it has been observed that the extent of damage, expressed in terms of the damage ratio, is a function of the normal component of the impact velocity only. However, the spatial distribution of broken contacts as well as the location of the fragments detached from the agglomerate are sensitive to the impact angle and are more prevalent in the back side of the agglomerate with respect to the direction of the impact with the wall.

For the same value of the damage ratio, the agglomerate experiences different patterns of breakage depending on the impact angle. The size distribution of the fragments is also affected by the impact angle. The tangential component of the impact velocity influences the breakage pattern, although further work is needed to elucidate the cause of the difference of breakage patterns for different impact angles.

There are some common features and differences between this work and the previous work that are noteworthy. Vervoorn (1986) observed that the normal component of the impact velocity is the predominant factor in the breakage of particles. However, the results of the simulation reported here show that the breakage of contacts is the only parameter that is influenced by the normal component of the impact velocity and not the breakage pattern. The latter is influenced by both normal and tangential

components of the impact velocity. In some respects, the results reported here agreed qualitatively with the results of Samimi (2003) who observed experimentally the influence of both tangential and normal component of the impact velocity.

At present, there is no theory or observations that can explain the discrepancies amongst the published works. A more in-depth analysis should be carried out to simulate exactly experiments and to use the simulations as a tool for analysing the force propagation within the agglomerates, which would help in the understanding of the influence of the impact angle on the breakage of agglomerates and single particles.

CHAPTER 5: INFLUENCE OF AGGLOMERATE SIZE ON BREAKAGE

5.1 Introduction

Agglomerate properties such as porosity, size and interparticle bond strength strongly influence the agglomerate strength as it has been mentioned throughout this work. Subero (2000) studied the effect of porosity on the agglomerate strength. Ciomocos (1996) and Mishra and Thornton (2000) analysed the effect of the coordination number on the agglomerate breakage. However, the analysis of the influence of the size of the agglomerate on breakage has so far not appeared in the literature.

For solid particles with a semi-brittle failure mode Ghadiri and Zhang (2002) developed a model of impact damage due to chipping, in which the mass lost per impact, ξ, was related to a dimensionless group representing the breakage propensity of the particles. This group is given in Eq. 5.1:

$$\xi = \alpha \frac{\rho V^2 DH}{K_c^2} \tag{5.1}$$

where α is a proportionality factor which is determined experimentally, V is the impact velocity, D is the particle diameter, H is the hardness of the material and K_C is the fracture toughness.

Hutchings (1992), deduced an expression for the minimum velocity below which fragmentation of an spherical particle impacting a target does not occur. This velocity was proportional to D^{-2}.

It is of great interest to extend the models of single particle breakage behaviour to agglomerates or alternatively to find new relationships that express the breakage of the agglomerate as a function of the agglomerate size. In the following sections the

breakage of contacts within an agglomerate and the mode of breakage as a function of the agglomerate size will be addressed.

5.2 Simulation details

The simulations were carried out using 8 agglomerates of different sizes but with the same particle properties and interface energy. The agglomerate sizes in terms of the number of primary particles ranged between 500 and 10000 particles. The properties of the primary particles are shown in Table 5.1 and the properties of the agglomerates such as the agglomerate diameter, packing fraction, coordination number and average residual compressive and tensile forces in the contacts are given in Table 5.2. All agglomerates were selected in such a way that before impact the coordination number is similar in all assemblies. Other agglomerates were created but their coordination number was very different from those given above and therefore no analysis was carried out on these agglomerates. Every agglomerate was impacted at six different orientations, each direction being perpendicular to the other directions. In some cases more than one agglomerate of a specific size was used. The results presented here are the average of all values obtained for the impact of every agglomerate with the same size and for the six different orientations. Due to the extensive computational time it was only possible to create one agglomerate of 6000 particles and one of 10000 particles. The other smaller agglomerates were created in order to get a better average.

Table 5.1 Single particle properties

Elastic modulus	31.0
Density	2000
Poisson Ratio	0.3
Friction	0.3
Surface Energy (J/m^2)	3.5
Particle radius (μm)	50

Table 5.2 Agglomerate properties. Number of particles, agglomerate diameter, packing fraction, coordination number and residual compressive and tensile forces.

	A	B	C	D	E	F	G	H
No. of Particles	500	500	1000	1000	3000	3000	6000	10000
Aggl. Diam. (mm)	1.03	1.027	1.293	1.293	1.844	1.805	2.266	2.65
Packing Fraction	0.52	0.54	0.52	0.52	0.52	0.56	0.55	0.57
Coord. Number	5.82	5.94	6.00	6.00	5.86	5.96	5.87	5.96
Com. Force (mN)	0.19	0.13	0.09	0.05	0.14	0.17	0.10	0.14
Tens. Force (mN)	0.33	0.26	0.18	0.05	0.29	0.32	0.22	0.29

5.3 Breakage of contacts

The kinetic energy of the agglomerate before impact is only partially used in the contact breakage since different dissipation mechanisms such as friction and damping consume a part of the incident energy. It is consequently of importance to determine the relationship between the input kinetic energy and bond breakage.

The analysis of breakage of bonds has been carried out using the concept of damage ratio initially defined by Kafui and Thornton (1993) and later used by Subero *et al.* (1999). Kafui and Thornton (1993) compared the behaviour of three different agglomerates, two of which were agglomerates with FCC packing. The primary particle size of these agglomerates was different, but the two agglomerates had the same diameter and therefore there were a different number of particles in each agglomerate. The third agglomerate had a BCC regular packing but with different number of particles than the other two agglomerates. The comparison of the extent of damage among all these agglomerates were made by relating the damage ratio to the Weber Number and the differences in behaviour were attributed to the differences in packing fractions. However, it was implicitly assumed that any possible influence of the number of particles of the agglomerate on the breakage of contacts is account for by the use of the damage ratio. In the work reported here their approach has been verified by examining the number of broken contacts for different agglomerates sizes and impact velocities as detailed below.

In Fig. 5.1 the number of interparticle bonds broken upon impact is shown for different agglomerate sizes as a function of the impact velocity. However, more information can be obtained by plotting the number of broken contacts as a function of the number of particles in the agglomerate for all impact velocities (Fig. 5.2).

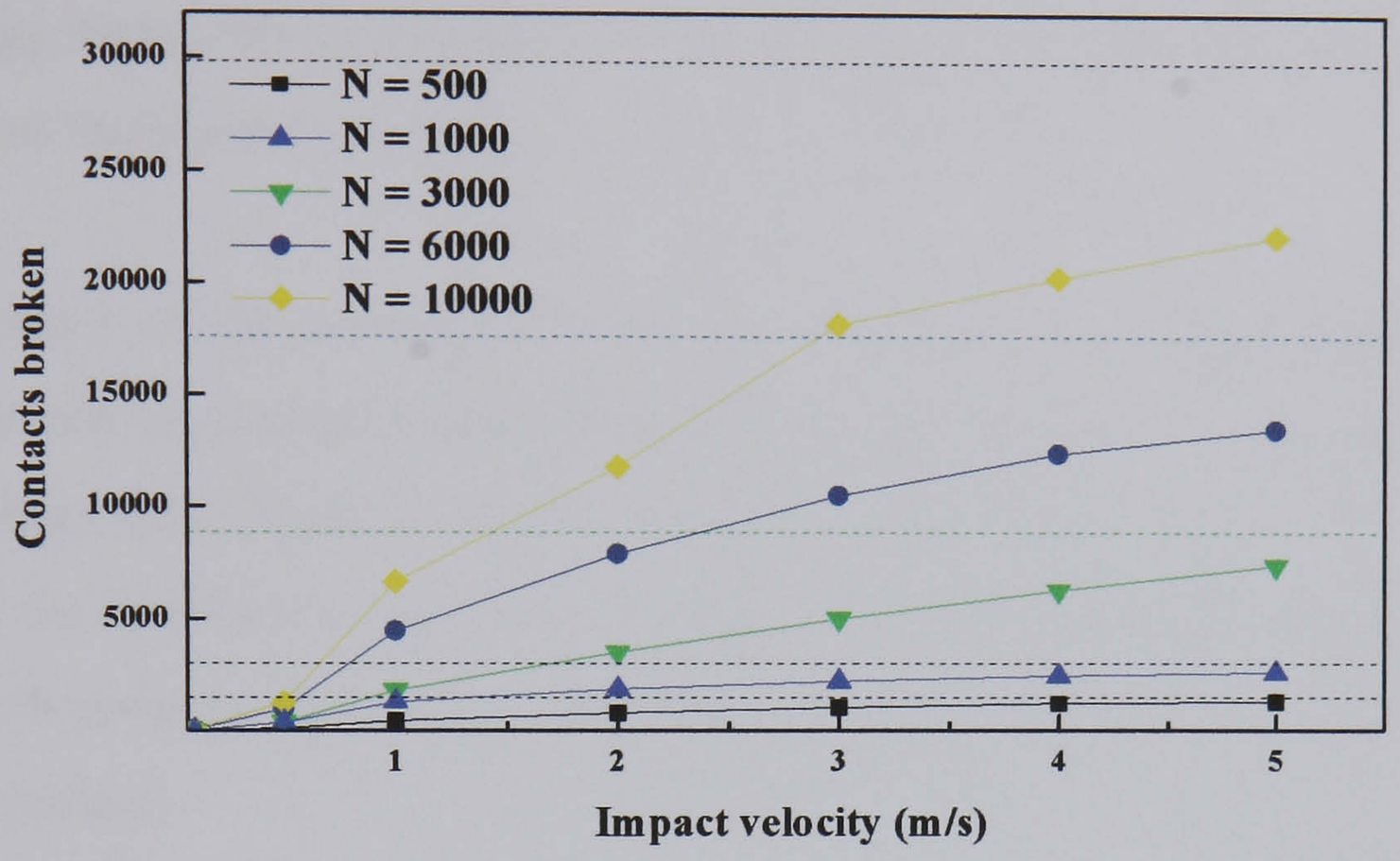

Figure 5.1 Dependency of the number of broken contacts on the impact velocity.

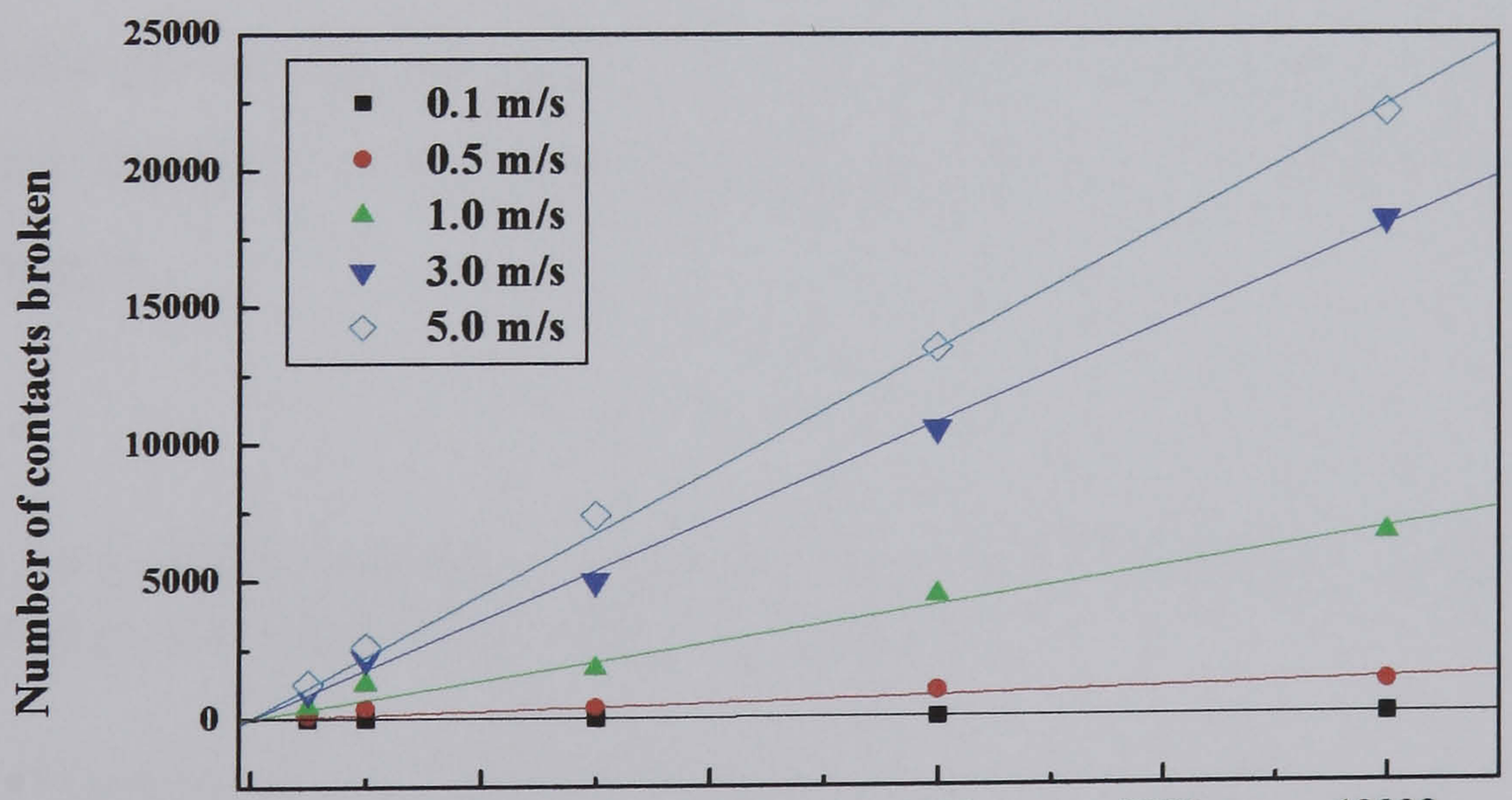

Figure 5.2 Number of broken contacts versus number of particles in the agglomerate

In Fig. 5.2 the data can be fitted to different straight lines depending on the impact velocity which indicates a linear relationship between the number of broken contacts and the number of particles in the agglomerate. The slopes of the curves, correlation coefficients and the average percentage of broken contacts are given in Table 5.3. The correlation coefficients are very high indicating a good fit of the results. However, there is a slight tendency of the correlation coefficients to increase with the impact velocity suggesting certain sensitivity of the breakage of contacts to the impact site at low values of the impact velocity.

The dependency of the number of broken contacts on the number of particles in the agglomerate can be analysed using an energy balance approach. In Appendix B a new model has been developed in order to predict the dependency of the number of broken contacts on the interface energy. In this model it is assumed that the work for breaking N_B contacts is proportional to the incident kinetic energy. From this energy balance the Eq. 5.2 is obtained.

$$N_B = k \frac{2^{2/3}}{3^{7/3}\pi^{2/3}} N \frac{\rho D^{5/3} V^2}{\Gamma^{5/3}} E^{2/3} \qquad (5.2)$$

where D is the primary particle diameter, Γ the interface energy, E the elastic modulus, V the impact velocity, k is a proportionality factor and N is the number of particles in the agglomerate.

Table 5.3 Fit of the breakage of contacts versus number of primary particles of the agglomerates and for different impact velocities.

Velocity (m/s)	0.1	0.5	1.0	2.0	3.0	5.0
Slope	0.004	0.135	0.685	1.21	1.794	2.238
Correlation Coefficient	0.938	0.957	0.991	0.993	0.999	0.999
Average Brok. Cont. (%)	1.12 %	4.9 %	24.3 %	42.6%	61 %	81 %

The above assumption leads to the conclusion that the number of broken contacts is proportional to the number of particles in the agglomerates, N. This relationship has been corroborated by the simulation data presented in Figs 5.2 (a,b).

Alternatively, using the coordination number, Z, we can express the initial number of particles in the agglomerate, N, as a function of the initial number of bonds, N_0:

$$N_B = k \frac{2^{2/3}}{3^{1/3}\pi^{2/3}} \frac{2N_0}{Z} \frac{\rho D^{5/3} V^2}{\Gamma^{5/3}} E^{2/3} \qquad (5.3)$$

Therefore, damage ratio, D_R can be expressed as:

$$D_R = k \frac{2^{5/3}}{3^{1/3}\pi^{2/3}} \frac{1}{Z} \frac{\rho D^{5/3} V^2}{\Gamma^{5/3}} E^{2/3} \qquad (5.4)$$

It is worth noting that Eq. 5.4 does not depend on the number of particles in the agglomerate. It justifies the possibility of using damage ratio for systems with very different number of particles.

In order to investigate the relationship between breakage of contacts and impact velocity, the slopes of the relationships between number of broken contacts and number of particles in the agglomerate given in Table 5.1, have been plotted as a function of the impact velocity in Fig. 5.3. The slope contains the proportionality factor k, the square of the impact velocity and the interface energy amongst other factors, as it is the right hand side of Eq. 5.3 except the number of particles in the agglomerate, N.

Figure 5.3 shows the slopes of the straight lines that represent the number of broken contact versus the number of particles in the agglomerates, the relationship that fits all data points in the whole range of impact velocity and an approximation to a relationship in the form V^2. The best fit for all data points has been found with the relationship

$$M = \frac{0.68V^2}{1 + 0.26V^2} \qquad (5.5)$$

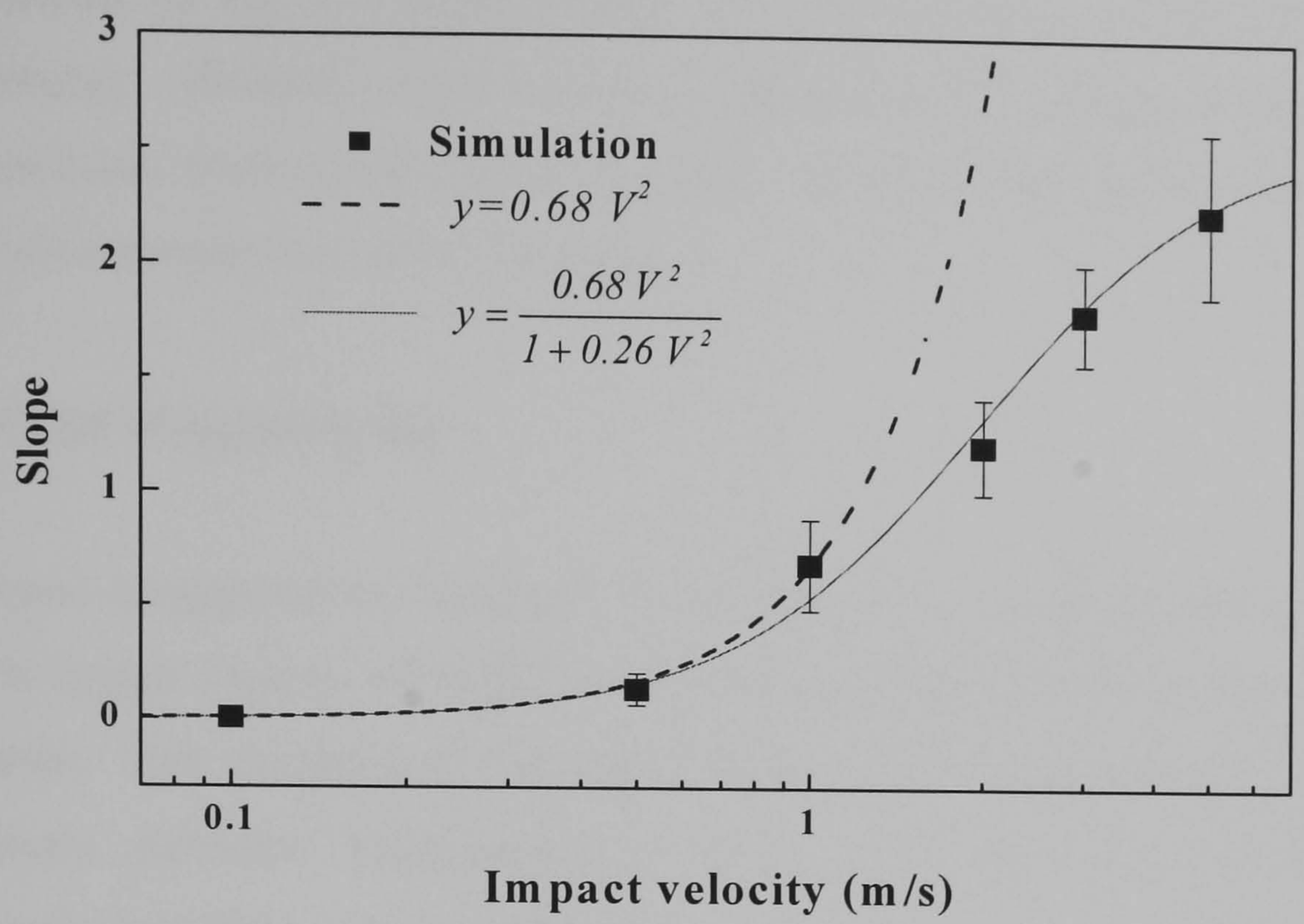

Figure 5.3 Plot of the slopes of the linear relationship between broken contacts and number of particles in the agglomerates versus impact velocity.

It is possible to observe that Eq. 5.5 can be approximated by a relationship with the square of the velocity for impact velocities less than 1.0 m/s. The predicted behaviour given by Eq. 5.3 is a dependency of the slope given in Table 5.3 with the square of the impact velocity. This behaviour is corroborated at low impact velocities. However, at impact velocities higher than 1.0 m/s the curve changes and gets away from the relationship in the form of Eq. 5.3. The expression that fits the curve in the whole range of data points depends on the square of the impact velocity in the numerator. It indicates that the proportionality factor k between the incident kinetic energy and the work for breaking contacts depends on the impact velocity in a form:

$$k = \frac{A}{1 + BV^2} \qquad (5.6)$$

The physical reason that explains Eq. 5.6 is unknown and remains to be investigated. Nevertheless, since the relationship between number of contacts broken and number of particles in the agglomerate is clearly lineal as shown in previous section, the constant k can not depend on the number of particles in the agglomerate. In addition, in

chapter 3 the dependency between number of broken contacts and surface energy was well predicted by Eq. 5.3 which implies that the constant k can not depend on the surface energy. However, it still exist the possibility that k depends on particle size, elastic modulus, friction and contact damping, amongst other factors. These potential dependencies should be analysed in future.

5.4 Breakage of agglomerates

The analysis of agglomerate breakage has been carried out paying attention to the size of the two largest clusters, the total number of fragments and singlets detached from the agglomerate. The simulations have been carried out for Agglomerates A and B with 500 primary particles, Agglomerates E and F with 3000 primary particles and Agglomerate H (10000 primary particles).

The behaviour of the two largest fragments for these agglomerates is shown in Figs. 5.4, 5.5 and 5.6. Not all the results are reported here although all the impacts have been analysed and the results plotted here are representative of all cases.

Figures 5.4, 5.5 and 5.6 show the variation of the size of the two largest fragments of the agglomerates with impact velocity. The size is expressed in the form of a percentage of the initial agglomerate size. Agglomerate breakage patterns are grouped in three different regimes as a function of the impact velocity as described previously in Chapter 3. The first regime is characterised by the detachment of particles or small cluster of particles from the agglomerate. During this regime the size of the residual cluster varies lightly with impact velocity. As the impact velocity is increased, a transition to the second regime occurs and herein the damage is caused by fragmentation. The transition is reflected by a change in the slope of the fragment size with the impact velocity as observed in Figs 5.4, 5.5 and 5.6. The second regime ends when the slope of the curve of the size of the largest fragment starts approaching zero. To quantify this the criterion is that the largest fragment has a size less than 5 % of the initial agglomerate size.

The velocity at which the first fragment is detached is given in Table 5.4 for all agglomerates which are labelled as in Table 5.2. There is no clear trend of this minimum velocity with the agglomerate size despite the differences in the input kinetic energy which is 2000 times smaller for Agglomerate A than for Agglomerate H. It is intuitively expected that the large agglomerate suffers from the detachment of particles at a lower impact velocity as compared to smaller agglomerates. Therefore the lack of any clear trend in Table 5.4 suggests a strong influence of local properties in the impact site and of the external layer of particles. Such an effect is due to the random distribution of properties in the agglomerates which would produce a statistical process. The agglomerates were formed with similar volumetric characteristics in terms of coordination number and void fraction although there was no control of the characteristics of the agglomerate surface.

Table 5.4 Velocity at which the detachment of the first fragment is observed.

Agglomerate	**A**	**B**	**C**	**D**	**E**	**F**	**G**	**H**
No. of Particles	500	500	1000	1000	3000	3000	6000	10000
Velocity (m/s)	0.73	0.61	0.51	0.50	0.59	0.63	0.45	0.525

The velocity at which the second regime starts is approximately the same for all agglomerates (between 1.5 m/s and 2.0 m/s). During the second regime a fast increase in the detachment of fragments is observed. The size of the second largest cluster shows a peak. At this point about 40% of the mass of the agglomerates turns into small clusters from the impact zone and the rest splits into a small number of large fragments as shown in Fig. 5.4, 5.5 and 5.6.

Agglomerate A

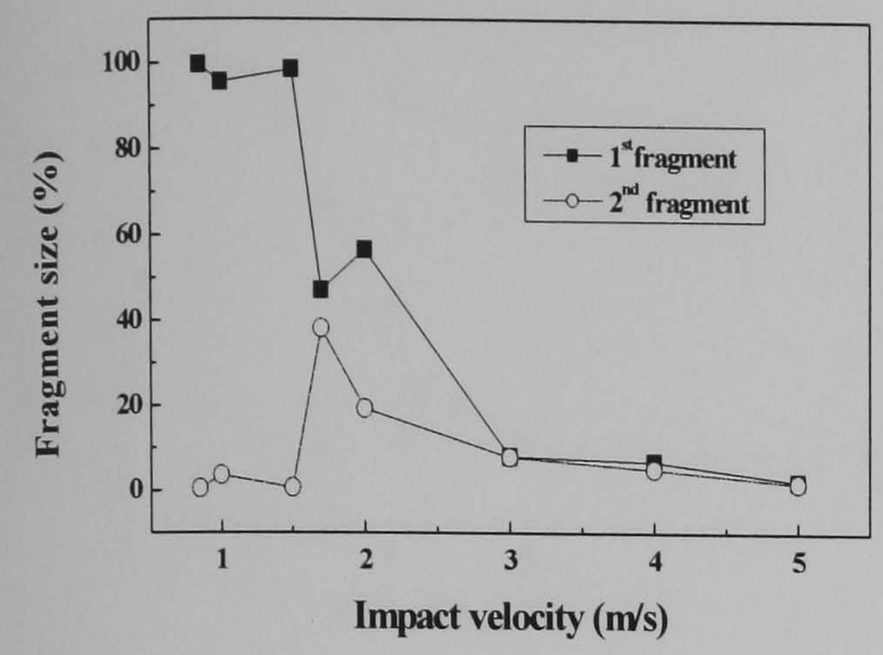

(a1) x-

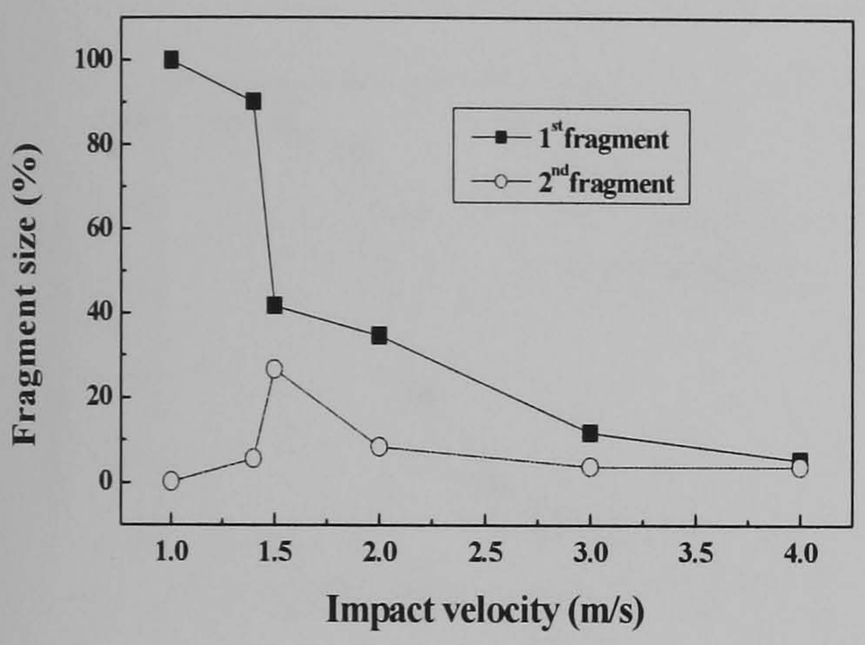

(a2) y-

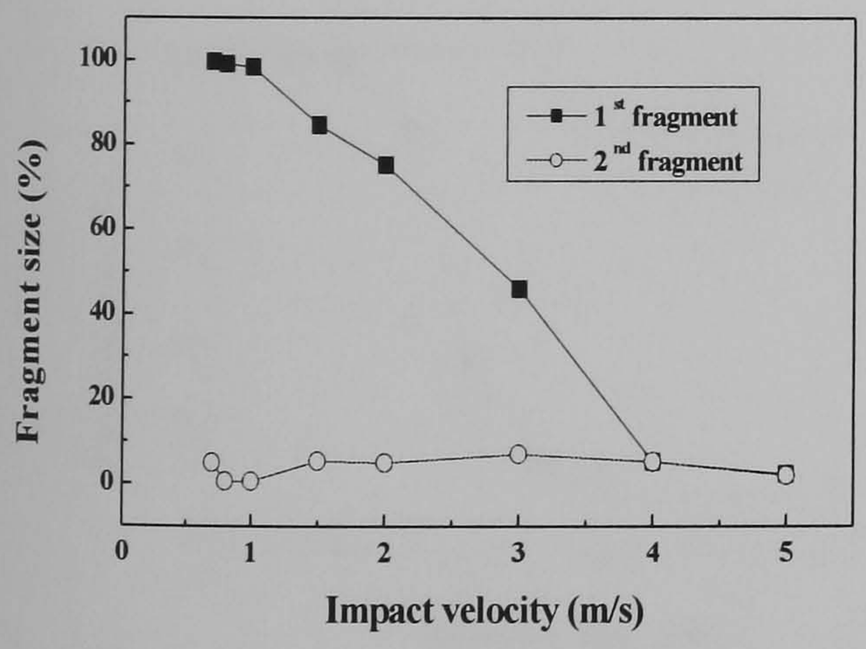

(a3) z-

Agglomerate B

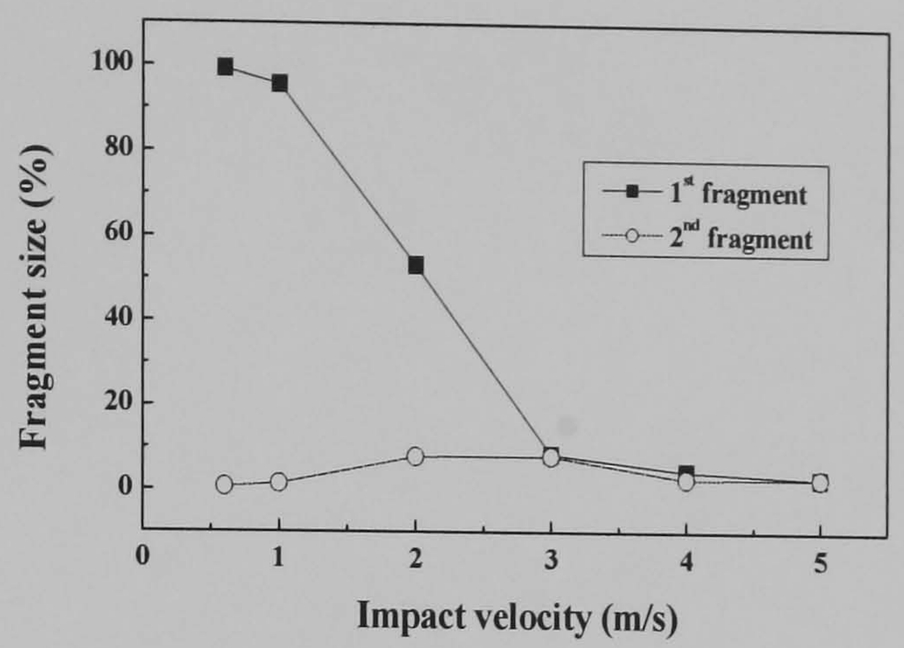

(b1) x-

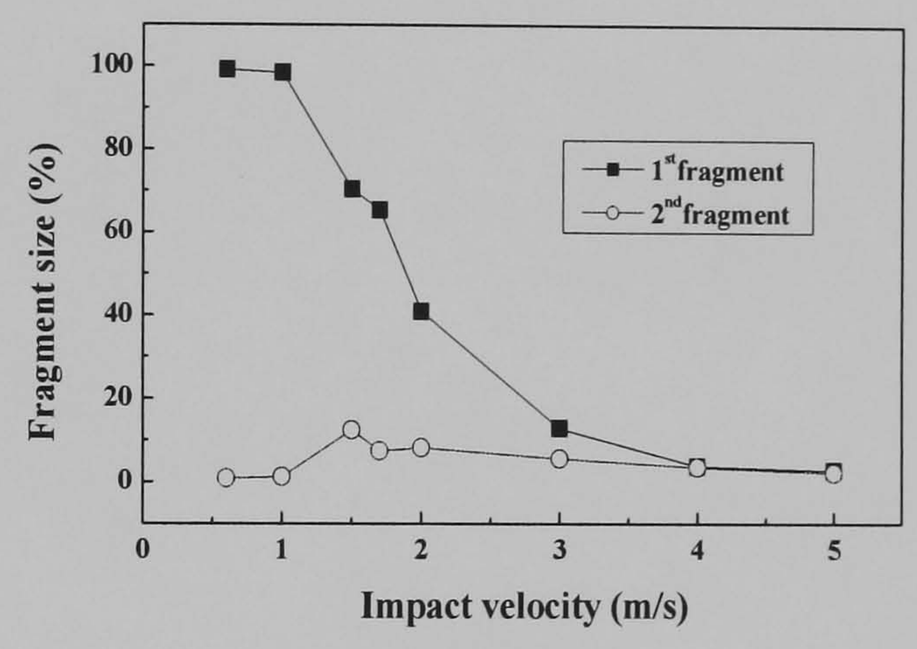

(b2) y-

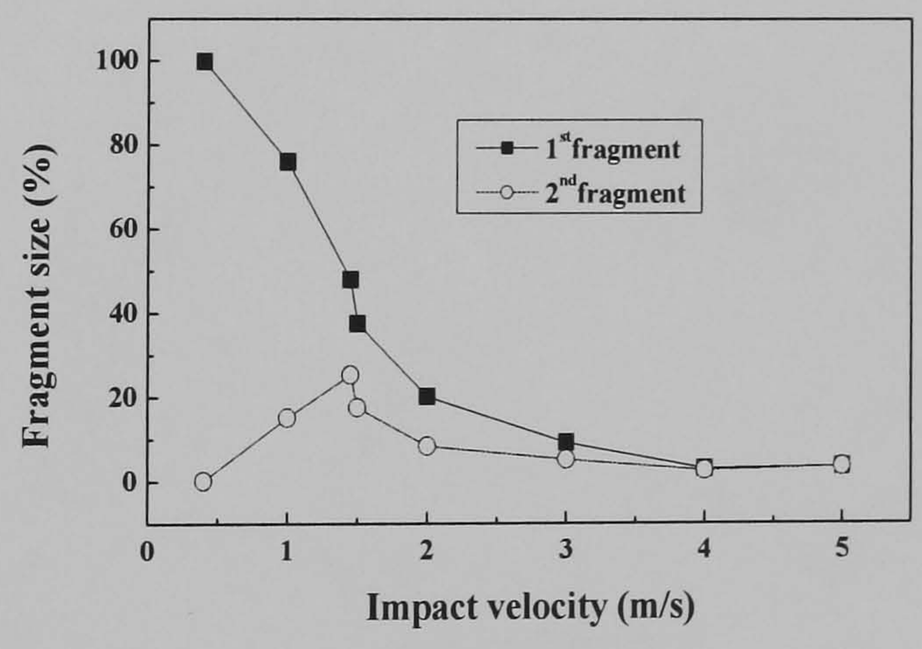

(b3) z-

Figure 5.4 Variation of the two largest fragments of Agglomerate A and Agglomerate B as a function of impact velocity for different impact orientations. The plots from top to bottom are the results for the cases in which the agglomerates have been impacted on the x, y, and z planes with the impact velocity directed along the x-, y- and z- axes, respectively.

Agglomerate E

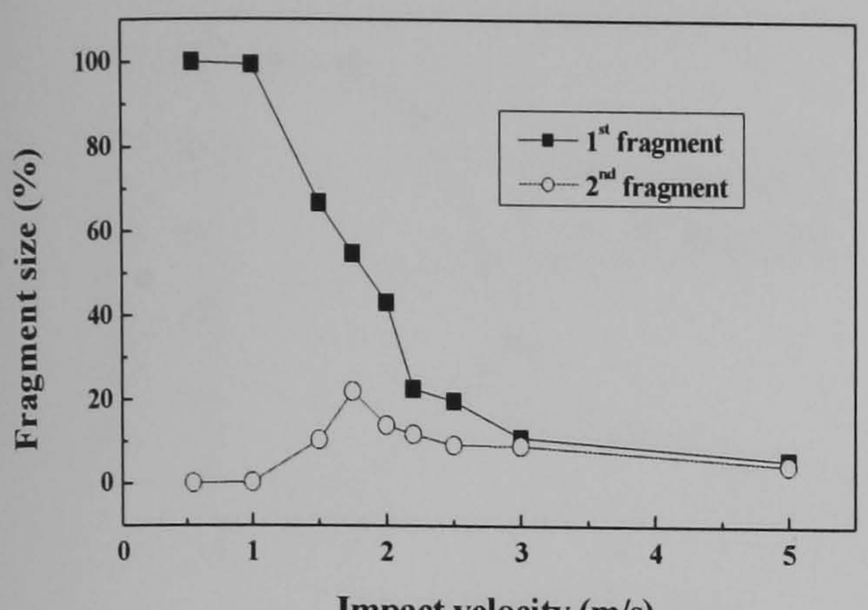

Agglomerate F

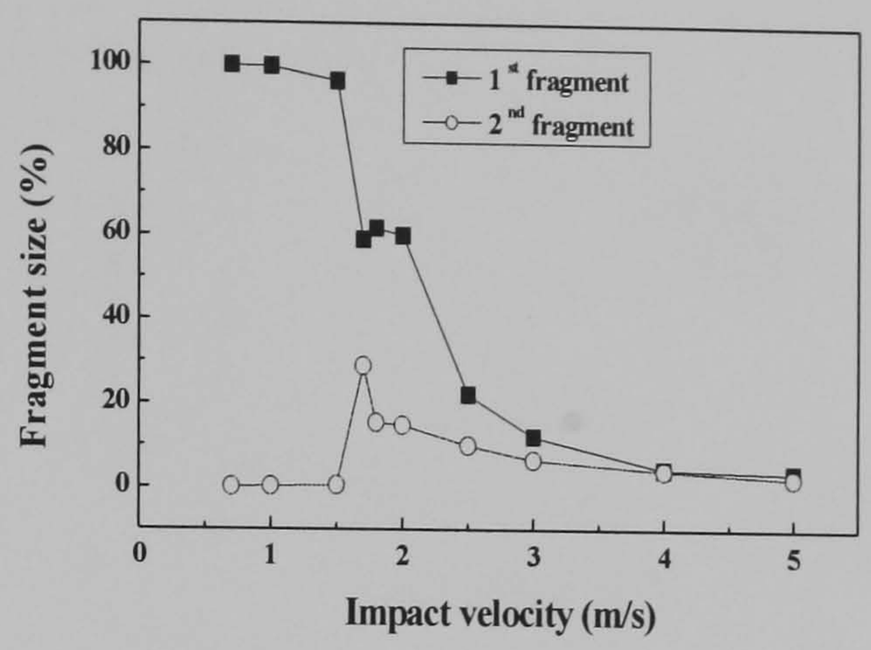

(a1) x-

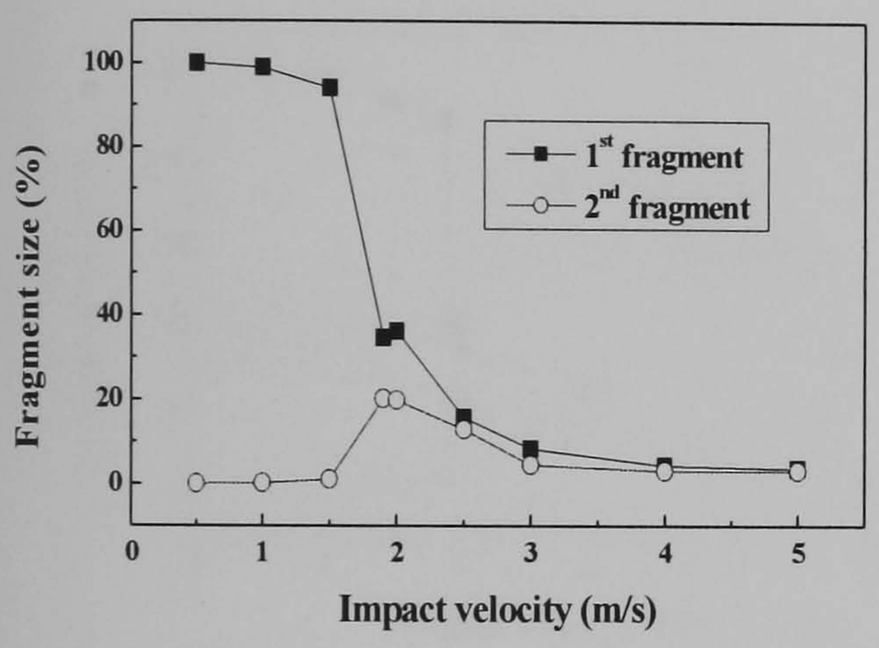

(b1) x-

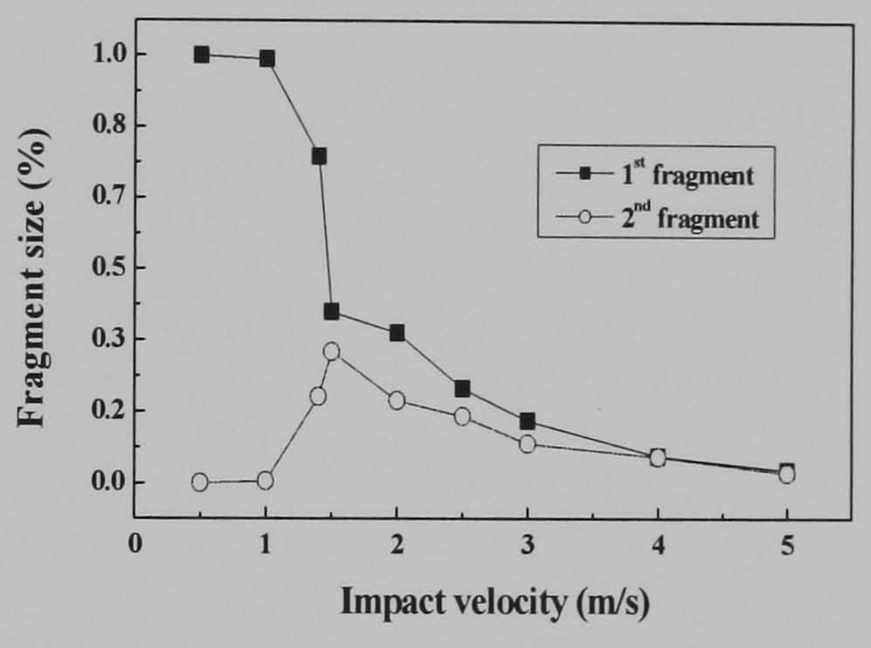

(a2) y-

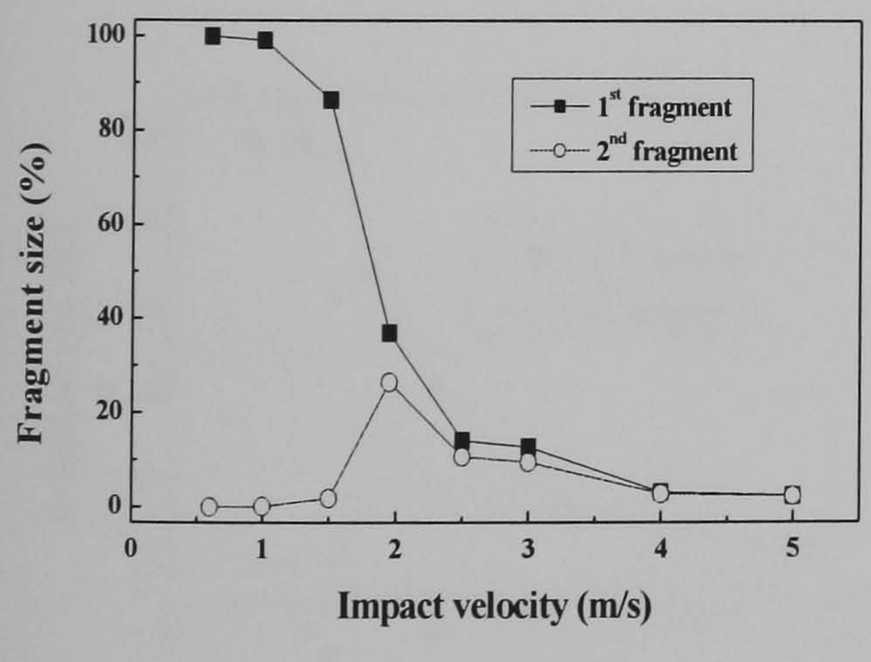

(b2) y-

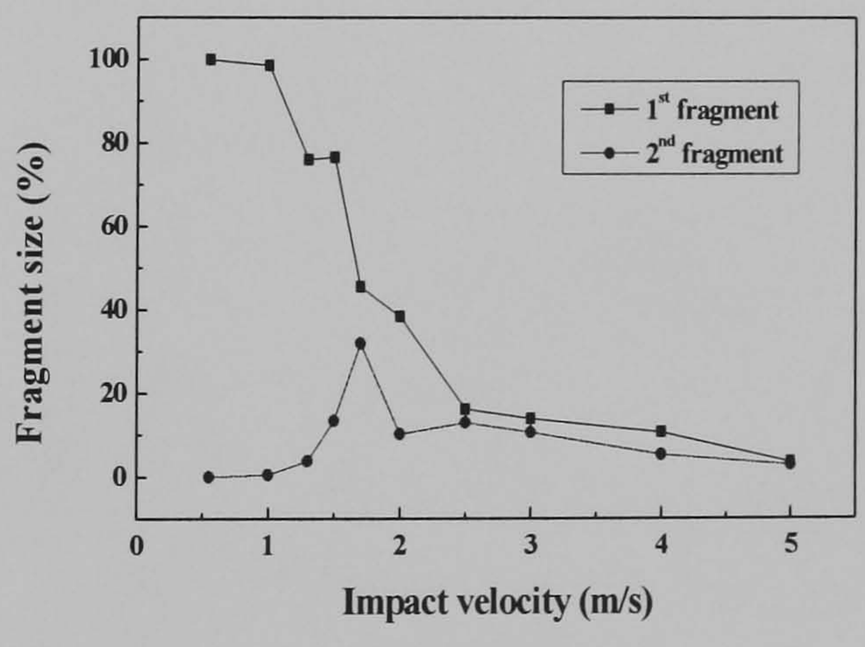

(a3) z-

(b3) z-

Figure 5.5 Variation of the two largest fragments of Agglomerate E and F as a function of impact velocity for different impact orientations. The plots from top to bottom are the results for the cases in which the agglomerates have been impacted on the x, y, and z planes with the impact velocity directed along the x-, y- and z-axes, respectively.

Agglomerate H

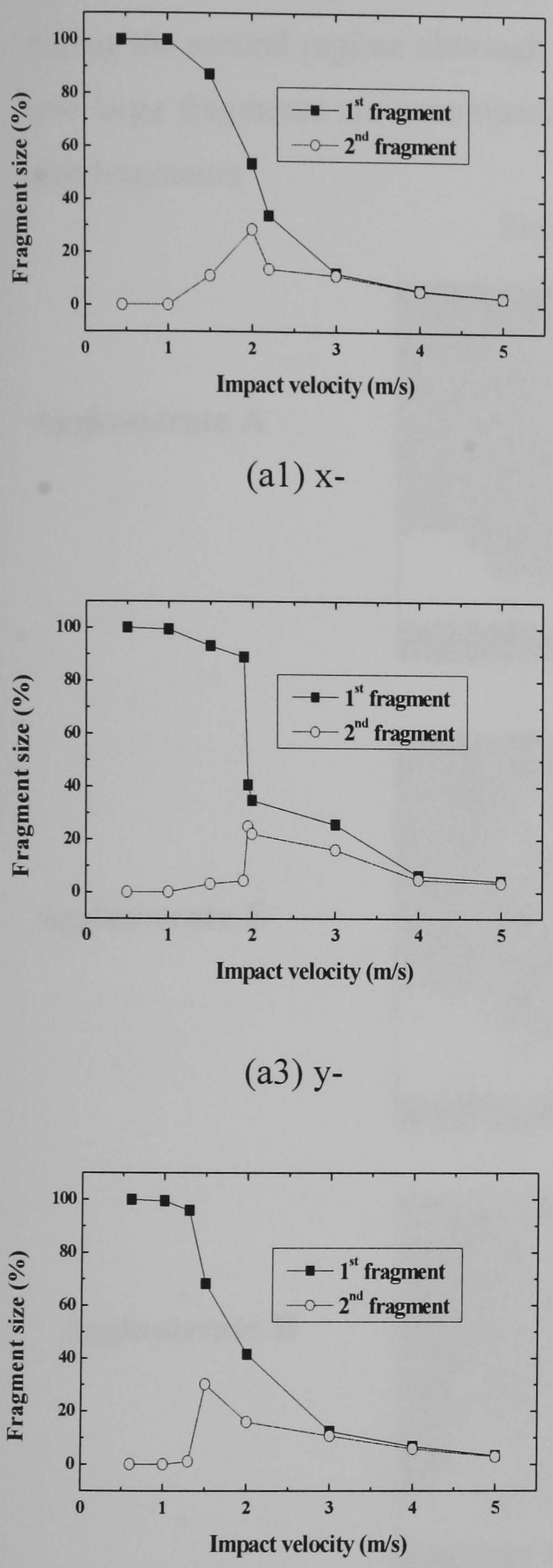

(a1) x-

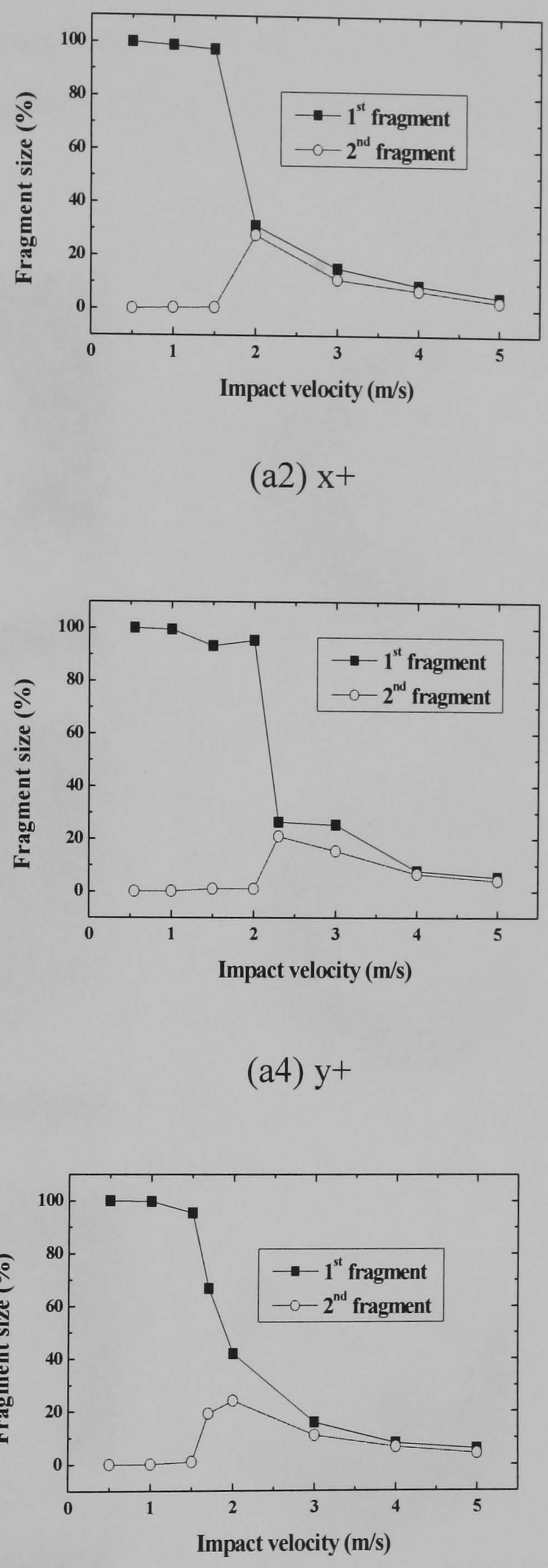

(a2) x+

(a3) y-

(a4) y+

(a5) z-

(a6) z+

Figure 5.6 Variation of size of the two largest fragments of Agglomerate H as a function of impact velocity for different impact orientations along directions x-, x+, y-, y+, z- and z+.

Figure 5.7 shows the breakage pattern of Agglomerates A (500 particles), Agglomerates E (3000 particles) and Agglomerate H (10000) particles. These agglomerates are representative of the behaviour of agglomerates for the same size during the second regime although some exceptions have been found to this rule. The two large fragments are accompanied by small debris in the contact area and medium size fragments.

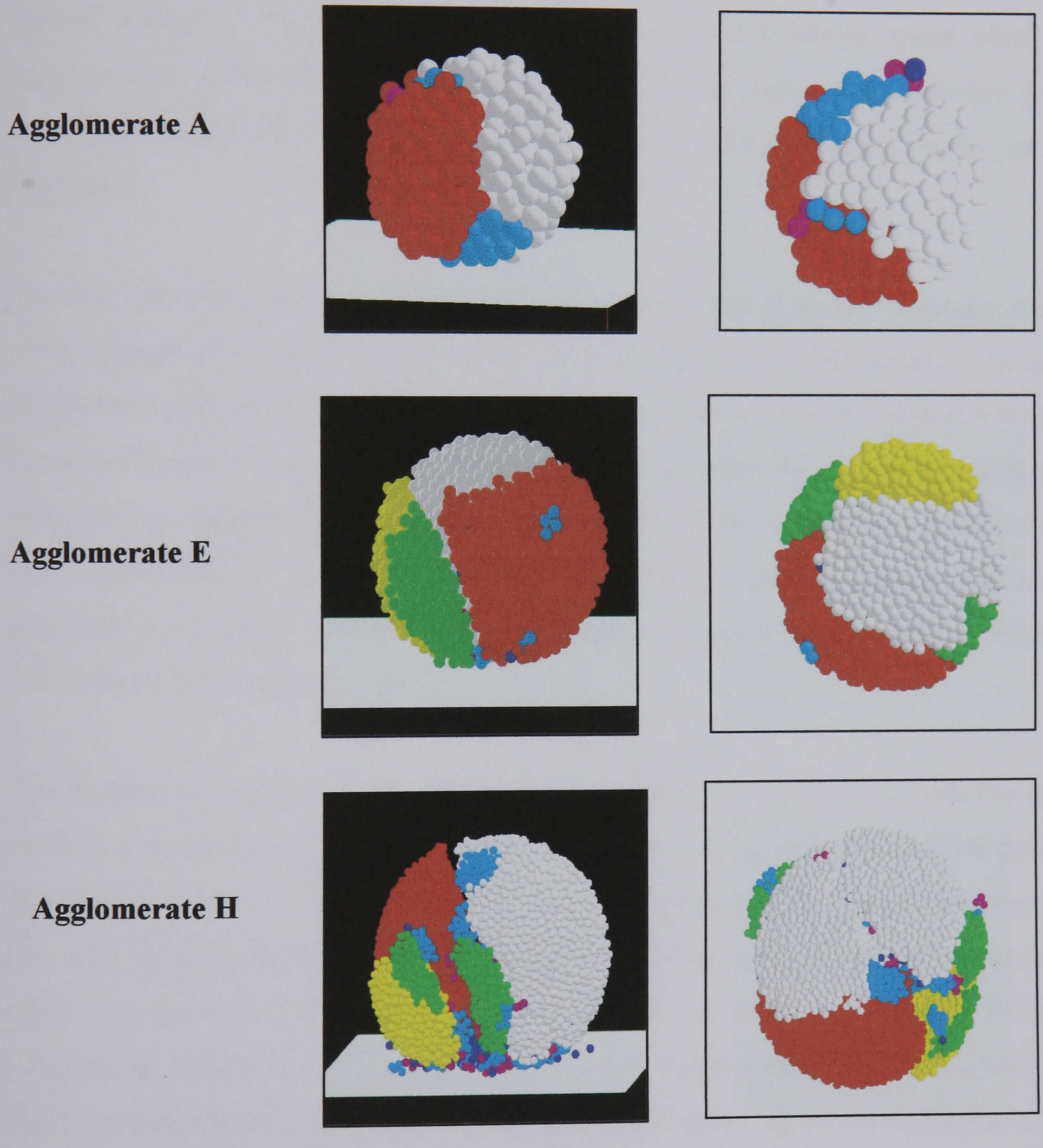

Figure 5.7 Fragmentation patterns of Agglomerates A, E and H viewed from a side direction and from top. Colour coding: grey: corresponds to the largest fragment; red: the second largest fragment; yellow: the third largest fragment; green intermediate clusters between 100 particles and yellow cluster; cyan: fragments between three and 100 particles; pink: doublets; blue; singlets; and white is the target.

Agglomerate H normally breaks into two large fragments but sometimes into three or even four fragments. Figure 5.8a shows the breakage pattern at two different impact orientations and a schematic diagram of the fragmentation pattern. Figure 5.8a shows Agglomerate H divided into four large fragments of comparable sizes. The debris is mainly in the contact area. Figure 5.8b shows the same agglomerate impacted at a different orientation that has fragmented into three large pieces. In case (b) it is also possible to observe the disintegration into small fragments of a side of the agglomerates (green colour). The schematic diagram of Fig. 5.8 shows more clearly the fragmentation patterns described above. None of the above fragmentation patterns have been observed for Agglomerates E and F, which usually breaks into two fragments.

Another important difference is that Agglomerates A and B do not fragment at all for some impact orientations. The reasons are not clear but the influence of the surface roughness could be as important as the volumetric effect since the agglomerate radius is just five primary particle diameters. It seems that when the size of the agglomerate increases, the tendency of fragmentation increases. This is based on the observation that Agglomerates A and B do not fragment in certain impact orientations, agglomerates E and F fragment into two large pieces and Agglomerate H fragments into three or four large fragments.

The number of singlets produced upon impact shows a clear trend with the impact velocity and agglomerate size as shown in Fig. 5.9. The number of singlets produced has a large scatter at low impact velocities but this improves at higher velocities. The data sets for different velocities have been fitted with a power law relationship and the results are given in Table 5.5. The data poorly fit a power law at values of impact velocities of 2.0m/s or less. At high impact velocities the number of singlets follows an approximately linear dependency on the agglomerate size. There are fluctuations in the coordination number especially in the external layers which have less density of particles and contacts. The exponent of the power law as well as the correlation coefficients increase with the impact velocity, indicating a strong dependency on the agglomerate size (Table 5.5).

a)

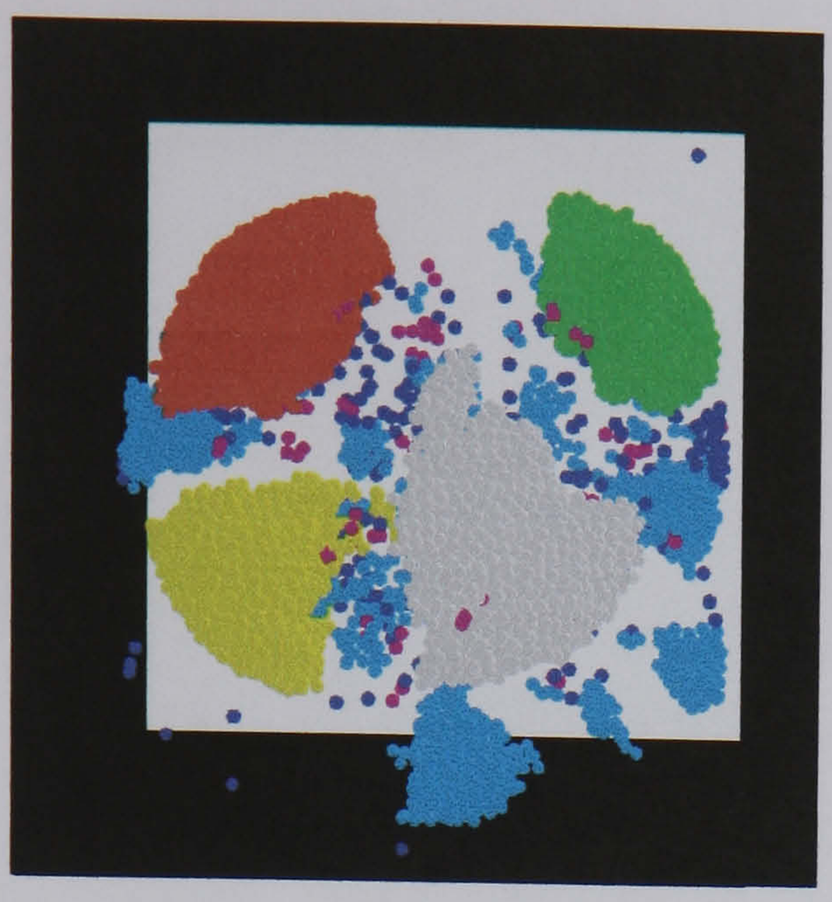

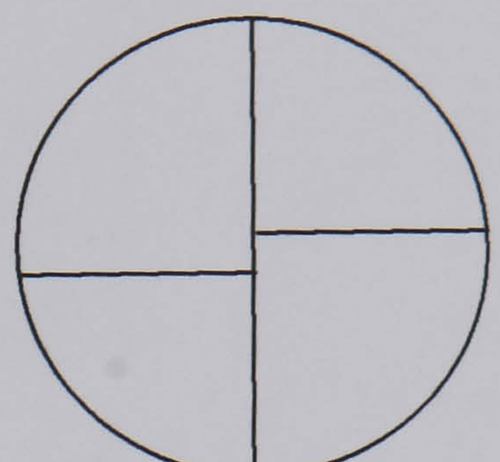

b)

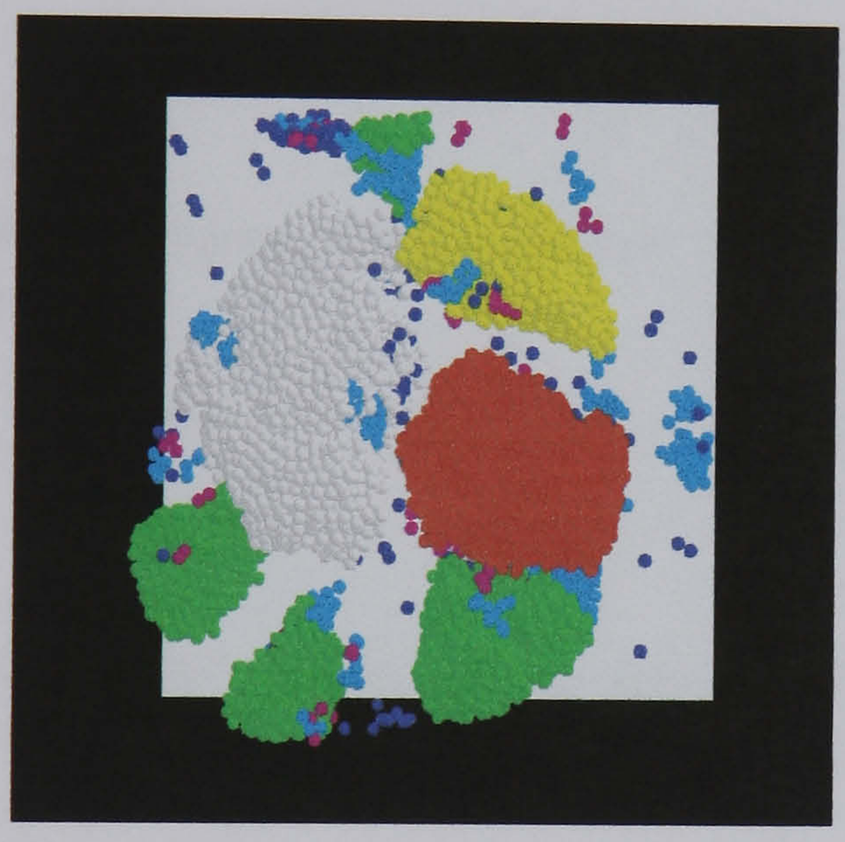

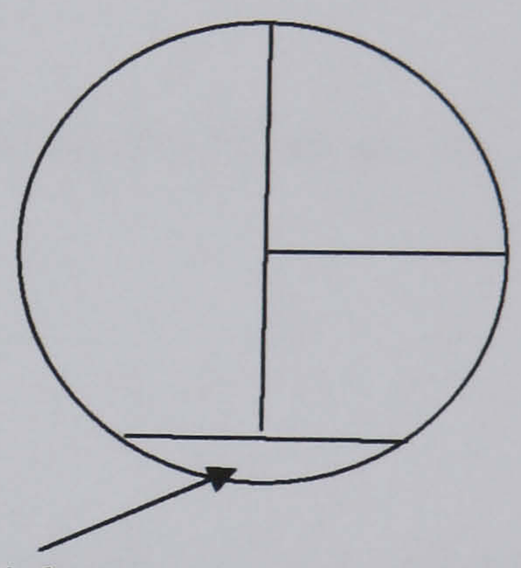

Lateral fragments

Figure 5.8 Top views of two fragmentation patterns of Agglomerate H and a schematic diagram of the fragmentation pattern. Cases (a) and (b) correspond to impact at different orientations. (a) Fragmentation into four large fragments at 2.3 m/s; (b) Fragmentation into three large fragment at 2.0 m/s. Colour coding: white is the target; grey, red and yellow indicate the first, second and third largest fragments, green colour shows smaller fragments, respectively cyan fragments sized between 3 and 100 particles; pink are doublets and blue are singlets.

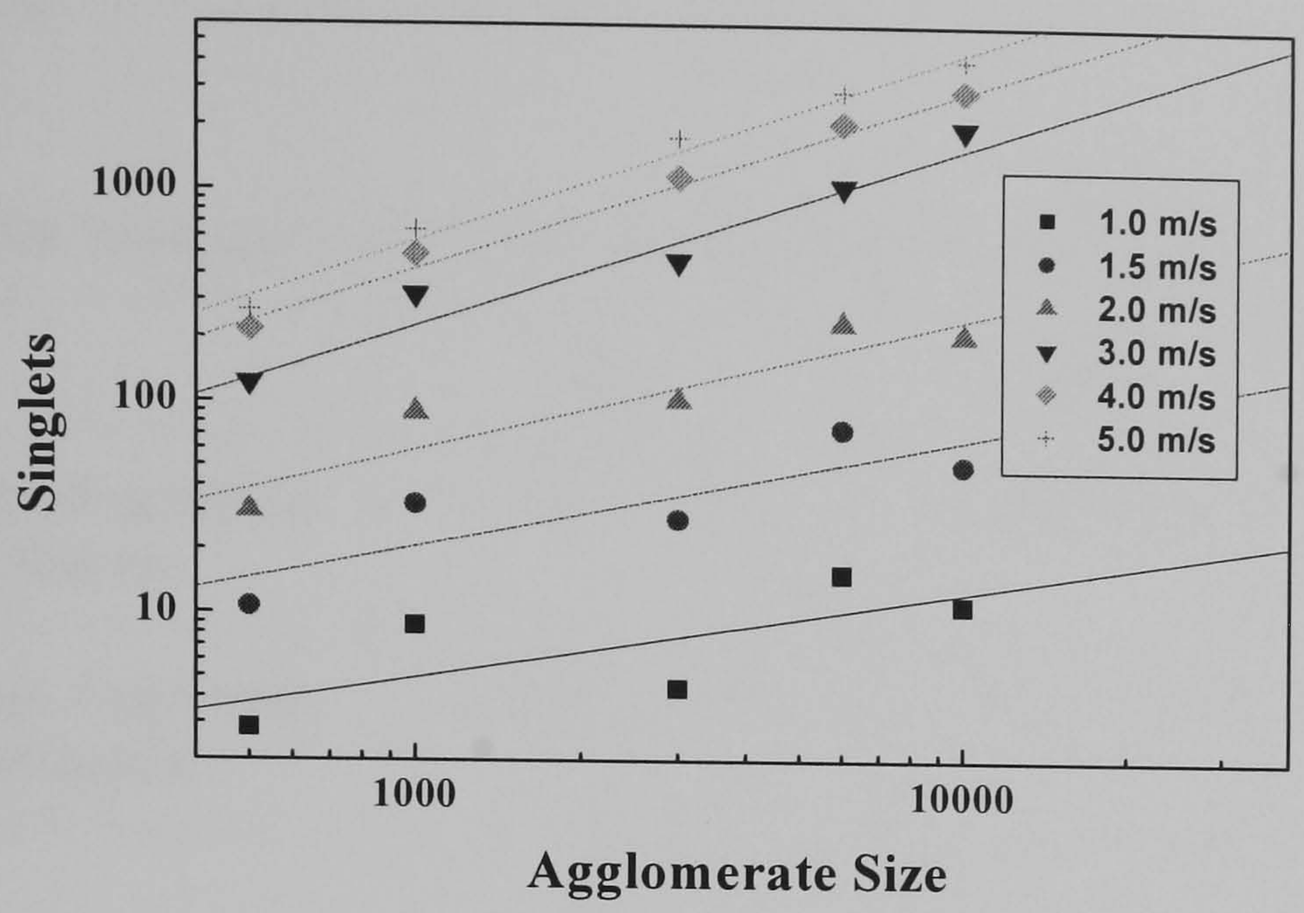

Figure 5.9 Dependency of the number of singlets produced upon impact on the agglomerate size.

Table 5.5 Power-law fitting of the number of singlets, *S*, produced as a function of agglomerate size, *N*, for different impact velocities ($S = AN^{\alpha}$).

Velocity (m/s)	1.0	1.5	2.0	3.0	4.0	5.0
Exponent (α)	0.465	0.507	0.623	0.847	0.846	0.890
Constant (A)	0.301	0.625	0.822	0.695	1.284	1.232
Corr. Coeff.	0.528	0.727	0.870	0.961	0.992	0.985

Table 5.6 shows the mass and size of debris at the impact velocity of 1 m/s for the agglomerates of 500, 3000 and 10000 particles in a normalised way, *i.e.* in terms of mass and size fraction and standard deviation. The results are the average and standard deviation of the data obtained for different impact orientations and different agglomerates with the same size. It is observed that the fractional size and mass of debris decrease with agglomerate size. The fractional mass decreases with agglomerate size since it is mainly in form of singlets and doublets which constitute a relatively

smaller percentage for larger agglomerates. Furthermore, in both cases, the standard deviation of mass and size of debris is comparable with the average value of the same parameters.

Table 5.6 Mass and size of debris detached from the agglomerates at 1 m/s

	500	**3000**	**10000**
Average fractional size of debris	0.036 ± 0.028	0.008 ± 0.009	0.0012 ± 0.0011
Average fractional mass of debris	0.060 ± 0.034	0.014 ± 0.013	0.005 ± 0.004

Table 5.7 shows the cumulative mass distribution undersize of debris as a function of normalised size average for the agglomerates of 500, 3000 and 10000 particles at the impact velocity of 2.0 m/s. The size and mass of the total debris are also given. The comparison of the results for different agglomerate sizes shows clearly that there is no sensitivity of the mass of debris to the agglomerate size.

Table 5.7 Cumulative mass distribution undersize of debris as a function of normalised size for impact velocity of 2 m/s

	Agg. 500	**Agg. 3000**	**Agg. 10000**
Mass fraction	**Normalised debris size**	**Normalised debris size**	**Normalised debris size**
0.05	0.002	0.0006	0.002
0.10	0.006	0.005	0.007
0.20	0.024	0.032	0.027
0.30	0.045	0.056	0.058
0.40	0.062	0.094	0.083
0.50	0.117	0.115	0.134
Average fractional size of debris	0.12 ± 0.05	0.17 ± 0.05	0.20 ± 0.10
Average fractional mass of debris	0.50 ± 0.12	0.44 ± 0.14	0.50 ± 0.24

This is in contrast to the expression given by Ghadiri and Zhang (2002) for solid particle impact, where the fractional mass detached from the particles is proportional to the particle size. The model of Ghadiri and Zhang (2002) is based on the propagation of sub-surface lateral cracks which produces the detachment of a platelet of a solid particle. However agglomerates studied here are far from being solid particles and at low impact velocities the detachment of small fragments (singlets) is due to the breakage of contacts mainly on the external layer of the agglomerates. Due to the discontinuous nature of agglomerates, it is not possible to consider crack propagation at these values of impact velocities.

5.5 Conclusions

The influence of the agglomerate size on its breakage during impact has been addressed in this chapter. The dependency of the number of broken bonds as a function of the agglomerate size has been quantified. It is found that the number of broken contacts follows a trend based on a simple hypothesis that the number of broken contacts is proportional to the input kinetic energy of the agglomerate. The number of broken contacts does not show any sensitivity to factors such as local change of the coordination number.

An analysis of the production of debris reveals that the number of singlets produced on impact varies almost linearly (0.85-0.9) with the agglomerate size at high impact velocities. There is a large scatter in the data at low impact velocities where the power index for the effect of the size is much lower than unity (0.46-0.6). In this velocity range, local variations of the structure of the impact site seem to have a more significant effect than the agglomerate size.

The breakage pattern of agglomerates seems to be influenced by agglomerate size. When the agglomerate size is increased the tendency to fragment into more pieces is increased. Agglomerates containing 500 particles do not fragment at all in certain impact orientations. However, the agglomerate of 10000 particles breaks usually into two large pieces. However, in certain cases breakage is also observed into three or four large pieces.

CHAPTER 6: ANALYSIS OF THE MECHANISMS OF BREAKAGE OF AGGLOMERATES

6.1 Introduction

The analysis of the effect of impact on agglomerates reported in the literature mainly focused on the breakage pattern of agglomerates after impact (Thornton *et al.* 1999, Subero *et al.,* 2001, Subero and Ghadiri, 2001) and how the breakage pattern relates to factors such as impact velocity (Thornton *et al.*, 1996), packing fraction and coordination number (Mishra and Thornton 2002). The relationship between breakage of contacts and packing fraction has been analysed (Kafui and Thornton, 1993). The evolution of the breakage of contacts with time during the impact process has been analysed by (Thornton *et al.*, 1999). However, analyses showing the effect of orientation, contact force distribution and whether the contacts are in compression or in tension are scarce.

Thornton *et al.* (1996) described the impact of an agglomerate in 2-D and analysed the agglomerate behaviour as a function of impact velocity. They showed that the orientation of the broken contacts follows the orientation of contacts in tension. However, they did not report the number of contacts in tension and in compression during impact.

Ciomocos (1996) studied the relationship between packing fraction and the possibility of crack propagation in agglomerates. He observed that agglomerates with high packing fraction fragmented under both impact and compression. In contrast agglomerates with low packing fraction deformed extensively without fracturing. Ciomocos (1996) also analysed the relationship between average contact force and force on the target and found that both followed a similar trend. In addition, he observed that the possibility of rebound of agglomerates was directly related with the strain energy accumulated in the contacts during loading.

Ning *et al.* (1996) described how the interparticle bonds were broken in the impact of weak lactose agglomerates and showed that the broken contacts were perpendicularly

orientated to the lines of maximum compression in the agglomerate. The lines of maximum compression spread radially from the contact of agglomerate with the target.

Subero and Ghadiri (2001) observed in their experiments that within a certain range of impact velocities the agglomerates showed a statistical distribution of breakage patterns despite having been prepared by the same method. Some agglomerates fragmented while others failed by extensive interparticle bond breakage near the contact zone with the wall without any crack propagation. The simulation work of Mishra and Thornton (2001) established the packing fraction as an important parameter responsible for the fragmentation of agglomerates. They also showed three patterns of behaviour of the agglomerate depending on the value of the packing fraction. For intermediate values of the packing fraction, it was observed that the pattern of damage was influenced by the impact site, *i.e.* different orientations gave rise to different patterns. The reason for this observation was unclear but it was suggested that fragmentation can be influenced by the density and orientation of contacts around the impact site. The work highlights the necessity of an in-depth analysis of the influence of contact breakage during the impact process. Therefore, the observation of Subero (2001) could be qualitatively explained by the results of computer simulations of Mishra and Thornton (2001).

The analysis carried out in this work has the objective of quantifying the evolution of the number of contacts in compression and tension during impact, as well as the average contact force. In addition, a detailed analysis of the detachment of a fragment from a side of an agglomerate has been carried out by observing the evolution of the number of contacts on the fragmentation plane to observe crack propagation. A further comparison between the agglomerate behaviour during impact and compression has been carried out in order to establish the differences in the response of the agglomerate during the loading cycle.

6.2 Simulation details

An agglomerate of 3000 particles was prepared. The properties of the single particles and the final structure are given in Table 6.1 and Table 6.2, respectively.

Table 6.1 Single particle properties

Young's modulus (GPa)	31
Poisson ratio	0.3
Density kg/m^3	2000
Surface energy (J/m^2)	3.50
Friction coefficient	0.35
Particle radius (μm)	50

Table 6.2 Agglomerate particles

Number of particles	3000
Agglomerate radius (mm)	0.907
Packing fraction	0.546
Coordination number	5.617

6.3 Impact test

Once the agglomerate was created, it was positioned close to the target and the impact tests were carried at different velocities. From the different breakage patterns observed, the one produced at the impact velocity of 2.4 m/s was selected since a medium fragment size was detached from the agglomerate. At impact velocities lower than 2.4 m/s only a small number of small clusters were detached. At higher impact velocities, the number of contacts broken in the agglomerate increased

considerably which made it more difficult to carry out the analysis and visualisation of the broken contacts on a fracture plane.

6.3.1 Evolution of the number of broken contacts

Figure 6.1 shows the evolution of the wall force and the damage ratio versus time during the impact. As described in Chapter 2, an impact process can be divided into two stages, loading and unloading. The loading stage starts when the agglomerate first contacts the wall and finishes when the wall force reaches its maximum value (Fig. 6.1). The loading period in this case is approximately 4.5 μs. The unloading stage starts after the maximum of the wall force and lasts until the end of the impact at about 310 μs from the beginning of the impact. At this moment, the impact is considered finished since after this time no important changes in the number of broken contacts or detachment of fragments is observed. In the case studied here the agglomerate remained deposited on the target and no rebound was observed. The number of broken contacts during loading is close to 20% of the total number of broken contacts. The remaining 80% of contacts are broken during the unloading stage.

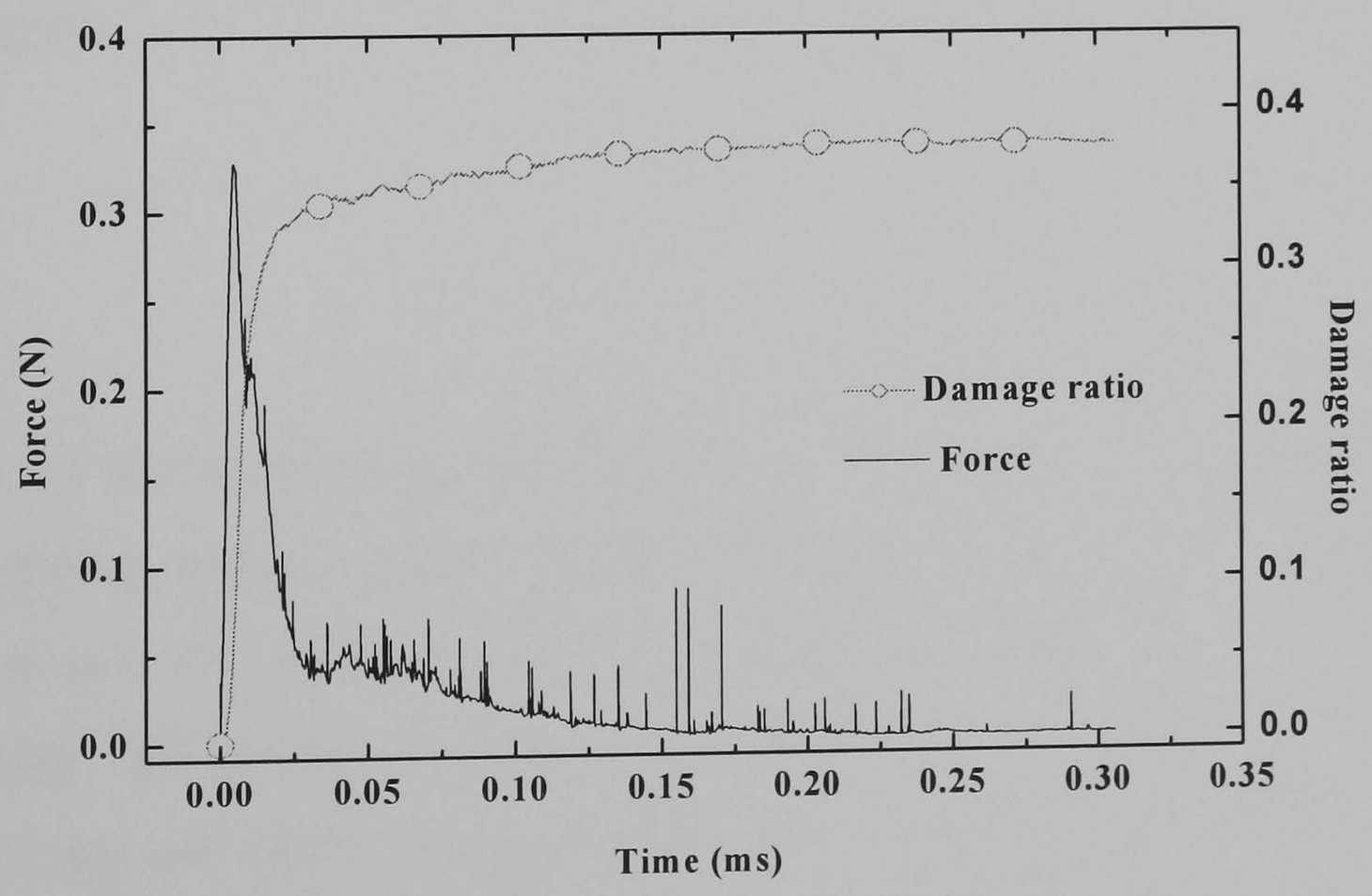

Figure 6.1 Evolution of the wall force and damage ratio during impact.

At the end of the loading stage only one singlet and one doublet are actually detached from the assembly. However, at the end of impact the size of the residual cluster is about 45% of the initial agglomerate size. It is clear that most of the fragments are detached during the unloading period. Figure 6.2 shows the agglomerate after impact. The fragments are coloured as a function of the fragment size. The damage is mainly localised in the contact area and the lateral sides of the agglomerate (Fig. 6.2). The second largest fragment, shown in red colour, is a side platelet which is detached at about 135 μs from the beginning of the impact and its size is around 13% of the initial size of the agglomerate.

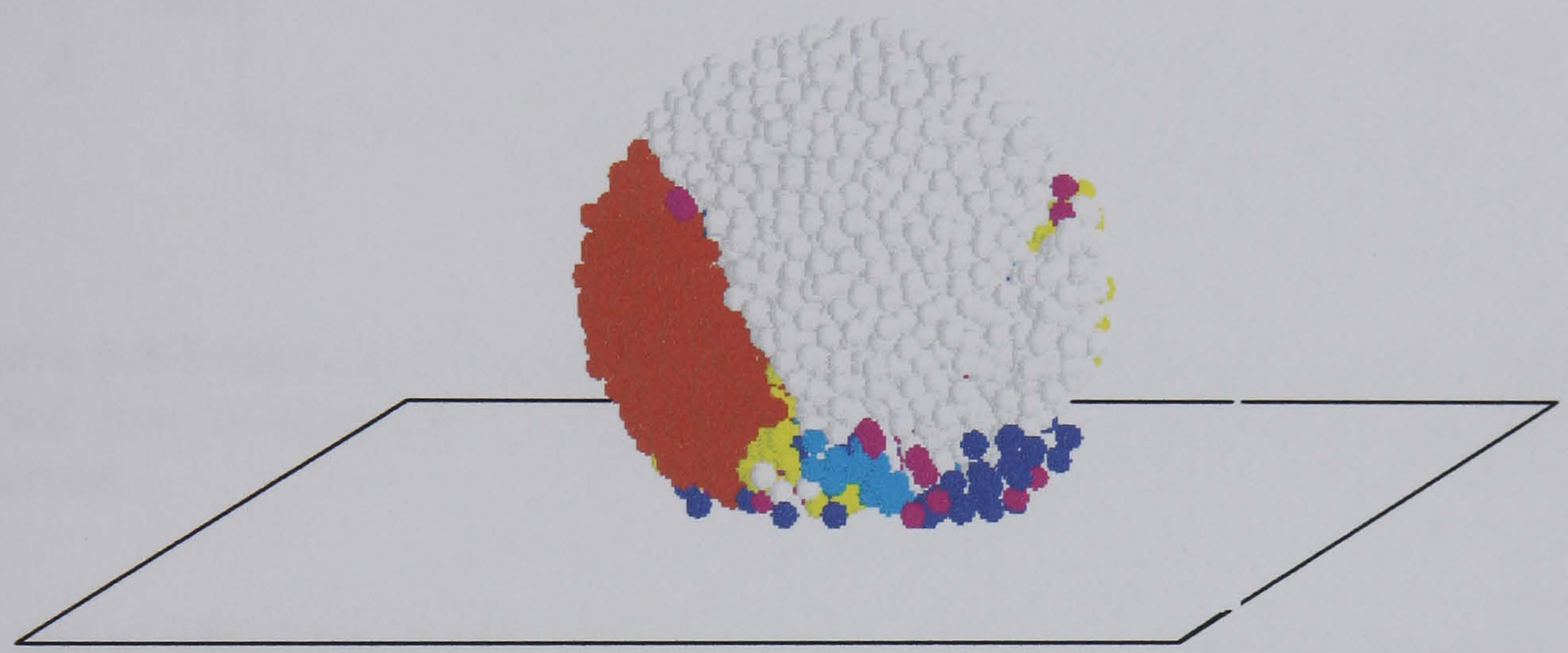

Figure 6.2 Breakage pattern of an agglomerate at the end of an impact at 2.4 m/s. Colour coding: Light grey: residual cluster; red: cluster with 418 particles; yellow clusters smaller than 418 particles and larger than 10 particles; cyan: clusters between three and ten particles; pink: doublets and blue: singlets.

The analysis of the evolution of the number of contacts in the agglomerate can be carried out distinguishing between contacts in tension and contacts in compression. Figure 6.3 shows the evolution of the compressive, tensile and total number of contacts during the impact process. The population of tensile and compressive contacts goes up and down during loading, although the total number of contacts decreases during the whole impact process. The variation of the compressive and tensile contacts is a balance between the new contacts that are formed, the contacts

that are broken and the contacts that change their state from compressive to tensile and *vice versa*.

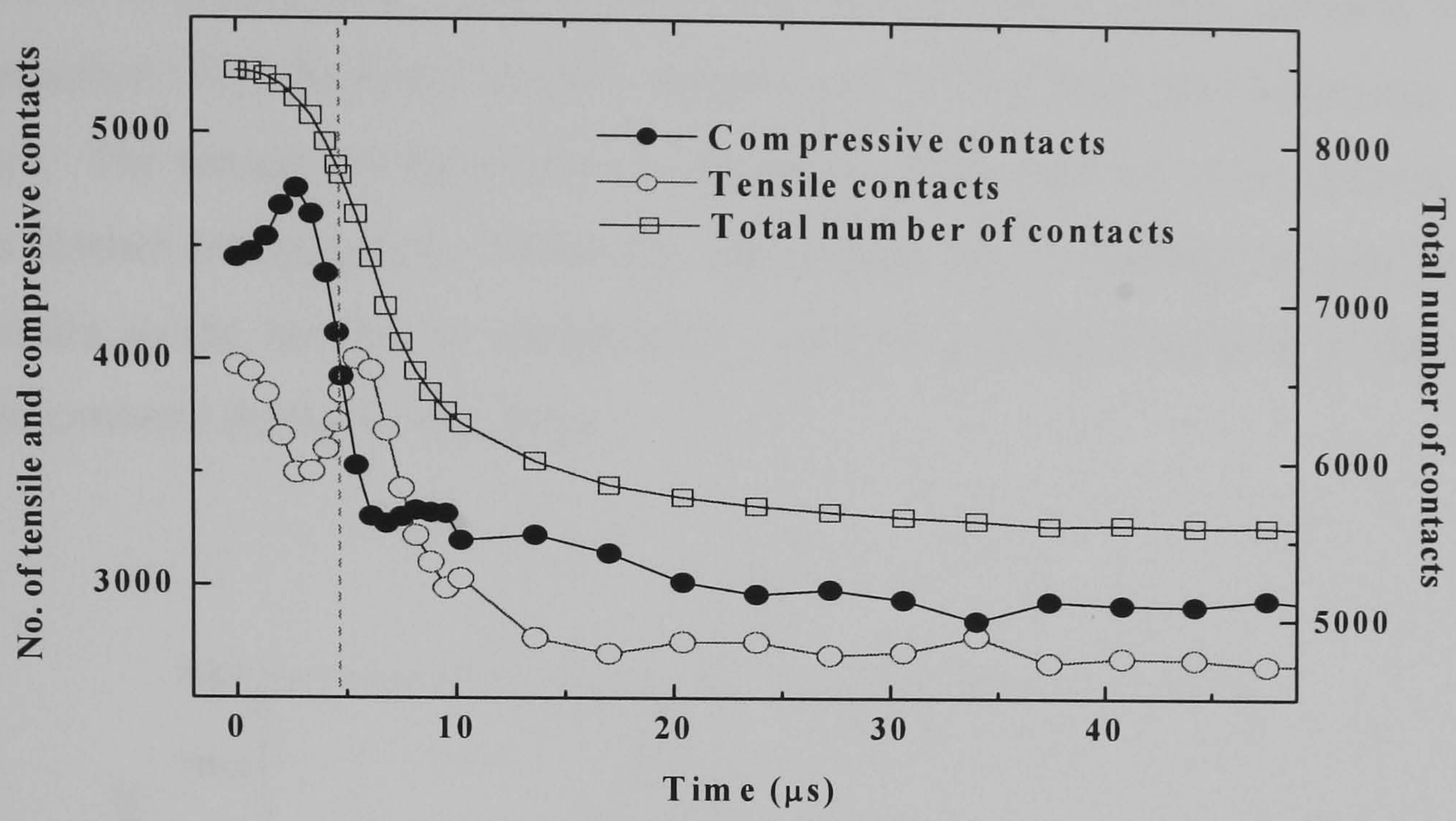

Figure 6.3 Evolution of the compressive, tensile and total number of contacts. The dashed line corresponds to the moment at which the maximum wall force was observed.

The rate at which the tensile contacts become compressive during an interval of time Δt is given by

$$V_{TC} = \frac{\Delta N_{TC}(t, \Delta t)}{\Delta t} \tag{6.1}$$

where $\Delta N_{CT}(t, \Delta t)$ is the number of tensile contacts that become compressive during the interval of time between t and $t+\Delta t$. In the same way, the rate at which the compressive contacts become tensile contacts can be written as

$$V_{CT} = \frac{\Delta N_{CT}(t, \Delta t)}{\Delta t} \tag{6.2}$$

where $\Delta N_{TC}(t, \Delta t)$ is the number of compressive contacts that become tensile during the interval of time between t and $t+\Delta t$.

Figure 6.4 shows the rates V_{TC} and V_{CT} as defined by Eqs 6.1 and 6.2 during loading and beginning of unloading. The velocities V_{CT} and V_{TC} increase during loading and pass through a maximum at different times. The time of the maximum wall force is plotted as a dashed line. The slope of the rate at which tensile contacts become compressive, V_{TC}, becomes slightly negative at 2.7 μs from the beginning of the impact. The reason for the change in the slope of the rate V_{TC} is not known and it needs further investigation. However, this change was coincident in time with the maximum in the number of compressive contacts and the minimum of number of tensile contacts shown in Fig. 6.3.a.

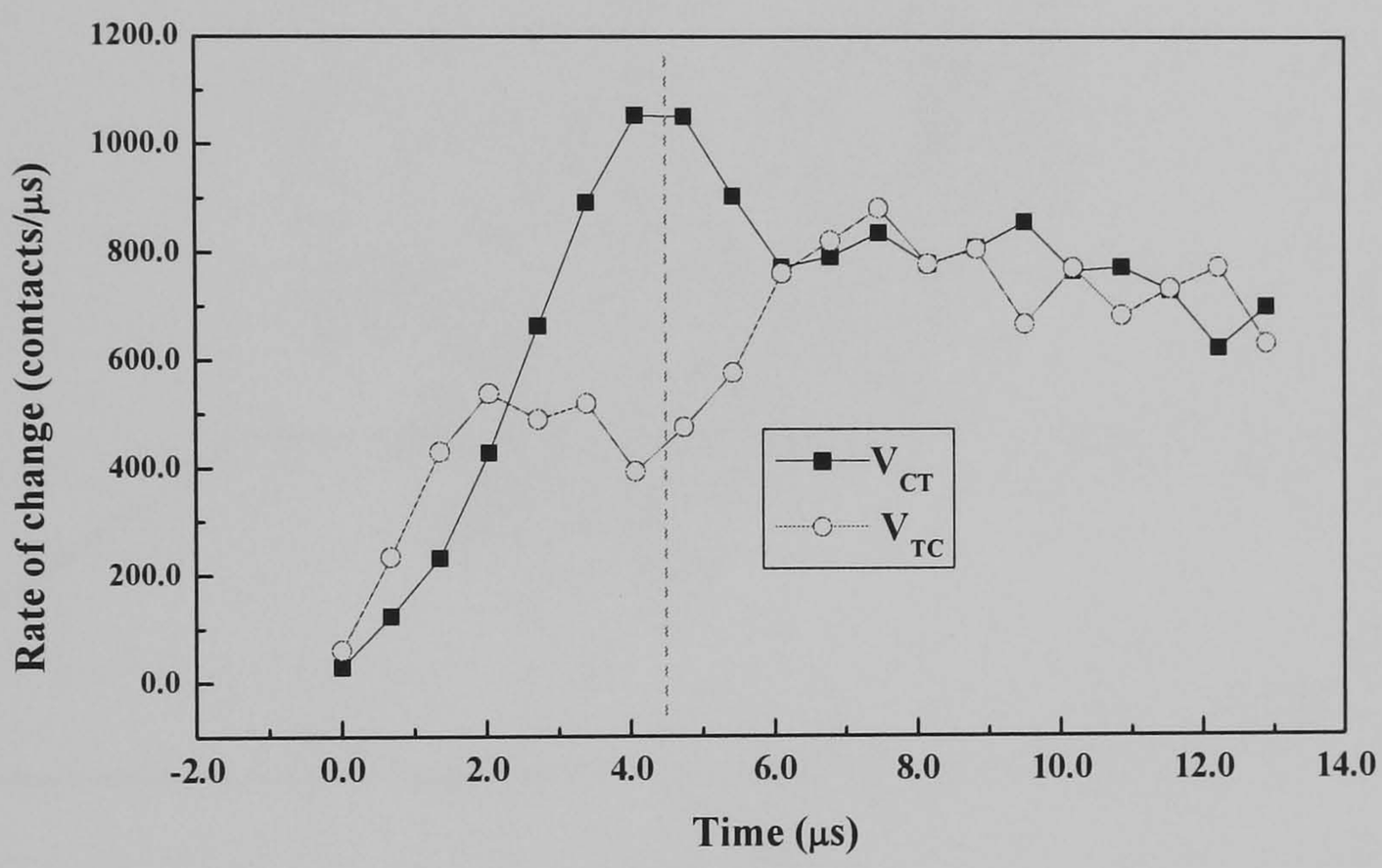

Figure 6.4 Rate of change of contacts from tensile to compressive and *vice versa*. The dashed line corresponds to the moment in which the wall force reaches a maximum.

Figures 6.5a and 6.5b show the tensile contacts that become compressive and the compressive contacts that become tensile during the loading period, respectively. It is possible to observe clearly that the tensile contacts that become compressive during this stage are radially spread from the impact site. In contrast, the compressive contacts that become tensile are perpendicularly orientated to the previous ones (Fig. 6.5b).

In Fig. 6.6 the average compressive and tensile forces are plotted as a function of time. During loading there is a continuous increase of the average compressive force

in spite of the oscillations of the number of compressive contacts as shown in Figure 6.3. However, the average tensile force shows a minimum at the same time as the number of tensile contacts is minimum. Later on, the average tensile force increases until it reaches its maximum at the same time as the average compressive force. This increase in the average contact forces is a direct consequence of the compression of the agglomerate. It is noteworthy that the maximum of the average contact forces occurs after the maximum of the wall force.

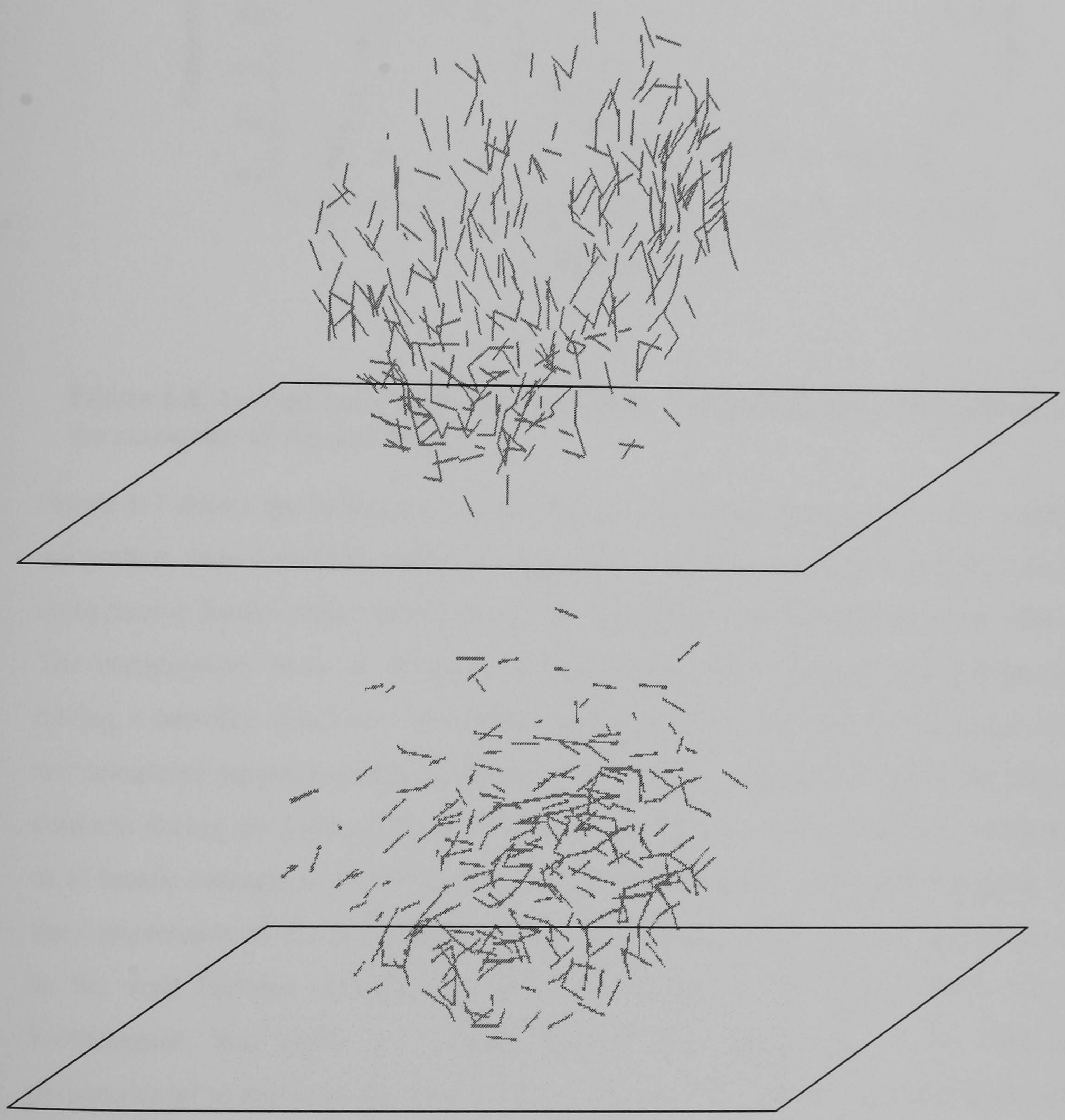

Figure 6.5 a) Tensile contacts that become compressive during loading. b) Compressive contacts that become tensile during the loading stage.

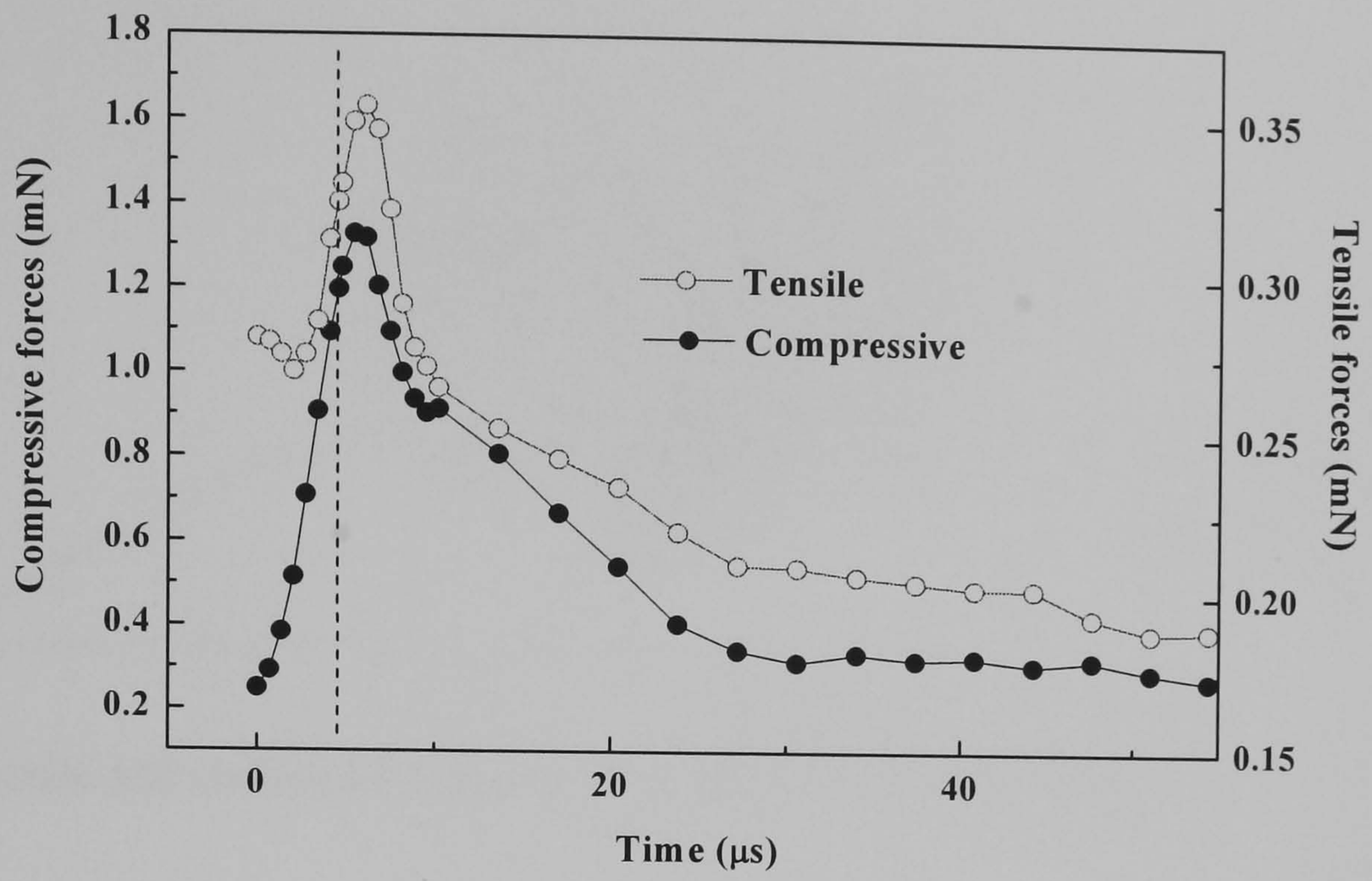

Figure 6.6 Average value of the contact forces. The dashed line corresponds to the maximum of the wall force.

Figure 6.7 shows the propagation of the tensile and compressive forces. To illustrate the pattern, only tensile forces larger than 33% of the maximum tensile force and the compressive forces larger than 0.5% of the maximum compressive force are plotted. The compressive force at the peak of wall force spread through the agglomerate having a tree-like structure. The tensile contacts during the peak of the target force are orientated perpendicularly to the normal contacts. Figure 6.8 shows the broken contacts during the loading period. They are mainly orientated in the same direction as of tensile contacts as shown in Fig. 6.7. Figures 6.5a, 6.5b, 6.7 and 6.8 suggest that the compression of the agglomerate makes the contacts that are almost perpendicular to the wall become compressive and those parallel to the wall become tensile. Furthermore, the larger the compression of the agglomerate in the direction perpendicular to the wall, the larger is the tension in the direction parallel to the wall producing the breakage of the tensile contacts. This mechanism of rupture is in agreement with the results of Ning *et al*. (1996) for the impact breakage of weak agglomerates.

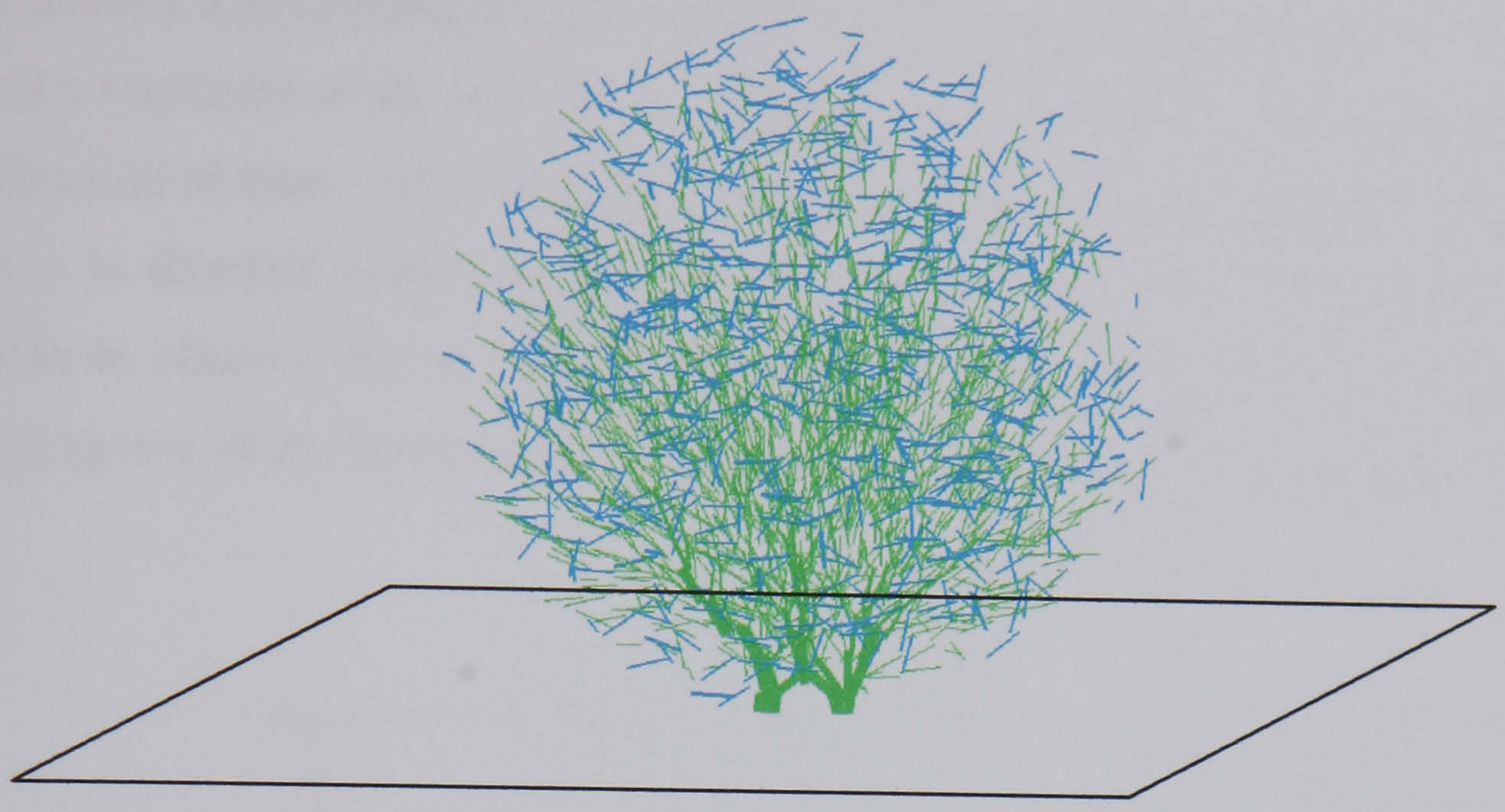

Figure 6.7 Tensile and compressive forces at the peak of the target force.

Figure 6.8 Contacts broken between the beginning of the impact and the peak time of the force on the target.

To explore the effect of velocity on the impact force, the velocity of the particles that make contact with the target is monitored as a function of time. Figure 6.9 shows the normal component of the velocity, V_Y for the first four particles that contact the wall as a function of time. This component of the velocity is defined as negative when the velocity is directed toward the target and positive in the opposite direction. It is possible to observe that at peak of the target force and therefore the beginning of unloading two of the three particles in contact with the wall are rebounding.

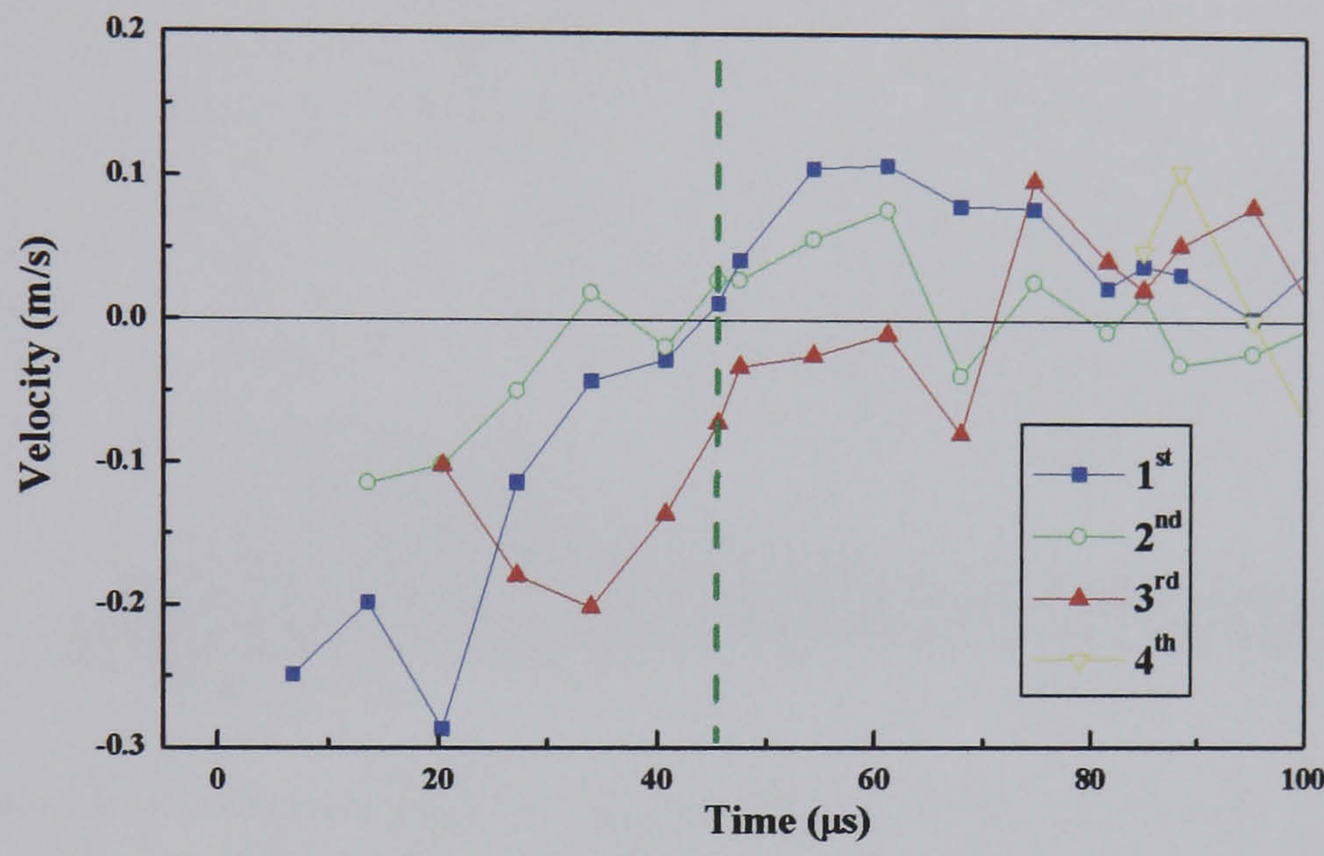

Figure 6.9 V_y of the particle as a function of the initial contact time. In the legend the numeral correspond to the order in which the particles establish the contact with the wall.

Figure 6.10 shows the vertical component of the particle velocity, V_y, as a function of the vertical coordinate component of the position of the centre of the particles, y, at the moment in which the maximum of the wall force is observed. A zoom of the region of the closest particles to the wall is also shown in Fig. 6.10. It is possible to observe that the only particles that are rebounding in the agglomerate are two of the three particles in contact with the wall. Obviously, since the maximum of the wall force is observed at this instant, the rebound of the agglomerate seems to be initiated by the rebound of these two particles. Therefore the increase in compressive and tensile forces within the agglomerate continues until the other particles of the

agglomerate start to rebound. The maximum of the average contact forces is observed after the maximum of the wall force as already shown in Fig. 6.6. This implies that the damage process proceeds after the maximum target force is reached.

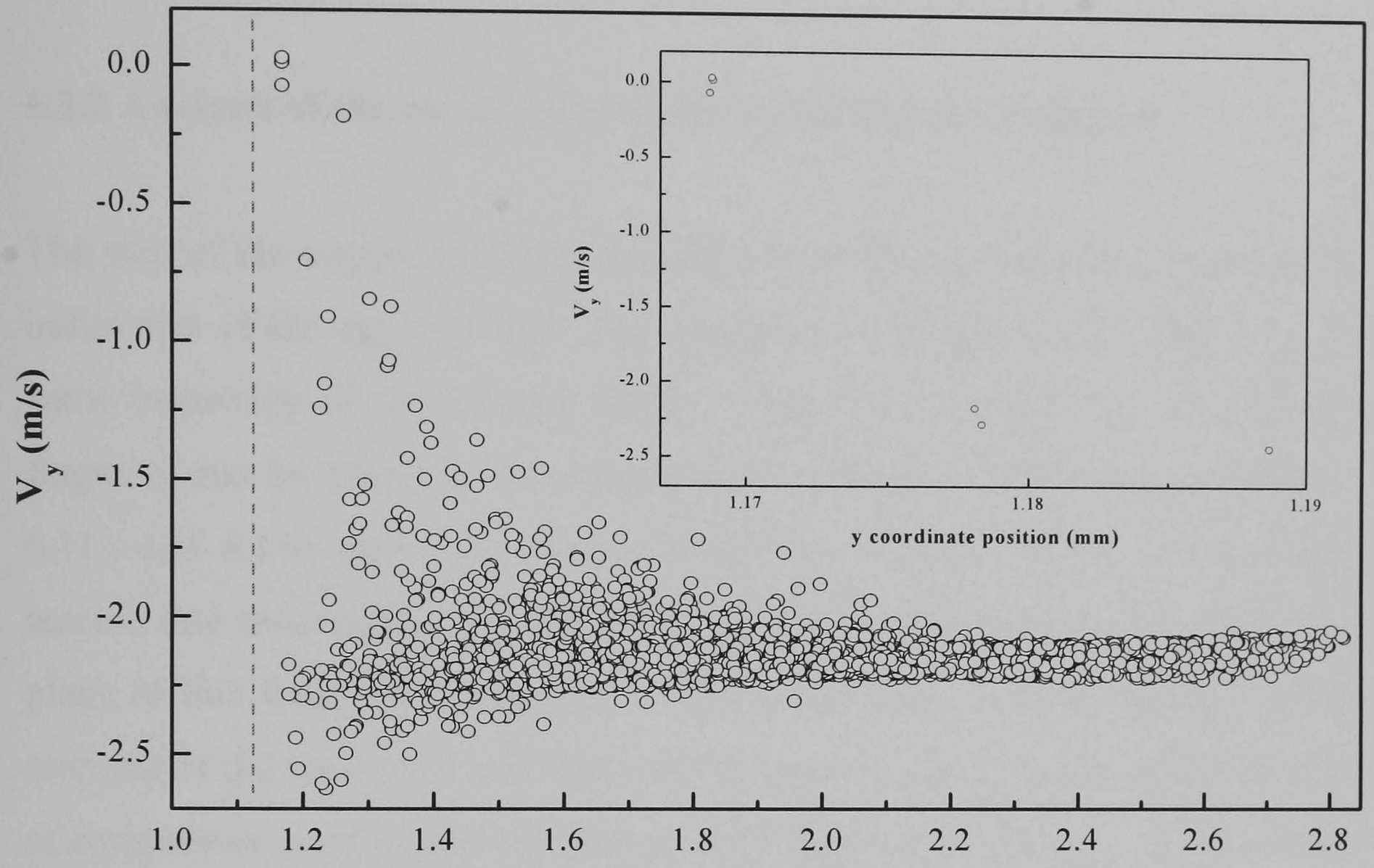

Figure 6.10 Vertical component of the particle velocities, V_y, as a function of the vertical component of the particle positions, y. The green dashed line corresponds to the position of the wall. The inset shows a zoom of the closest particles to the wall.

After the maximum value of the contact forces is reached, the number of contacts as well as the contact forces decrease rapidly. The number of broken contacts is about 10% of the initial number of contacts for the period of time between the moment at which the maximum contact force is reached and 4 μs after it. This corresponds to 30% of all the contacts broken during impact (Fig. 6.1). At this stage the biggest fragment has still 99.0% of the original number of particles but has about 66% of the initial number of contacts.

In this test the impact is considered finished at about 310 μs when no more changes in the size of fragments occur. So for the rest of the impact time (300 μs) no further significant changes in the orientation or values of the contact forces are observed that could explain the breakage of the 30% of all the contacts broken during impact. During this period the residual cluster was reduced from 99% to 45% of the initial agglomerate size. Further work is necessary to elucidate the breakage process in this stage.

6.3.2 Analysis of the detachment of the second largest fragment

The size of the largest fragment detached from the agglomerate is about 16% of the initial size of the agglomerate. The fragment is coloured red in Fig. 6.2. Therefore some inspection of the fracture plane is made in the following. The origin of this fragment can be found in the rupture of 257 contacts of the fracture plane. Figure 6.11a and 6.11b show the evolution of the number of contacts (in compression, tension and total number of contacts) and the average contact forces on the fracture plane of this fragment, respectively. The dashed line in these figures represents the moment of the maximum wall force in the agglomerate. The evolution of the number of compressive and tensile contacts on the fracture plane is quite similar to that of the whole agglomerate shown previously in Fig. 6.3. The number of compressive and tensile contacts oscillates before the agglomerate reaches the maximum target force although the maximum and minimum of the oscillations are less pronounced than those for the whole agglomerate. The average compressive and tensile forces plotted in Fig. 6.11b show more fluctuations than those for the whole agglomerate. It is probably due to a statistical effect since the initial number of bonds on the fracture plane is only 3% of the total number of bonds. The comparison of Figs 6.11b and 6.6 shows that the first maximum of the compressive and tensile forces of the fracture plane coincided with the maximum of the tensile and compressive forces of the agglomerate. The value of the peak of the average tensile and compressive forces on the fracture plane is very close to the value of compressive and tensile forces for the whole agglomerate.

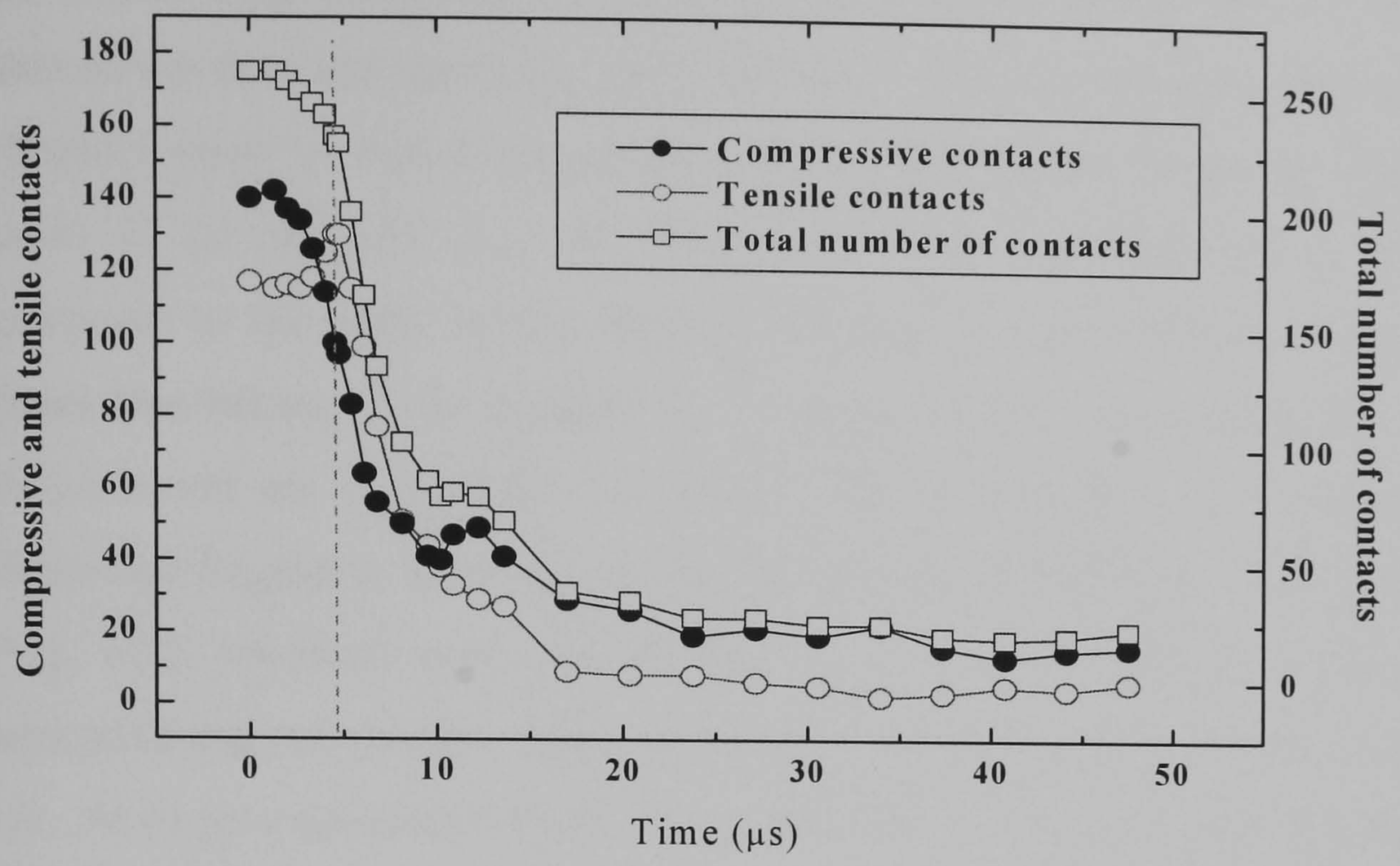

(a)

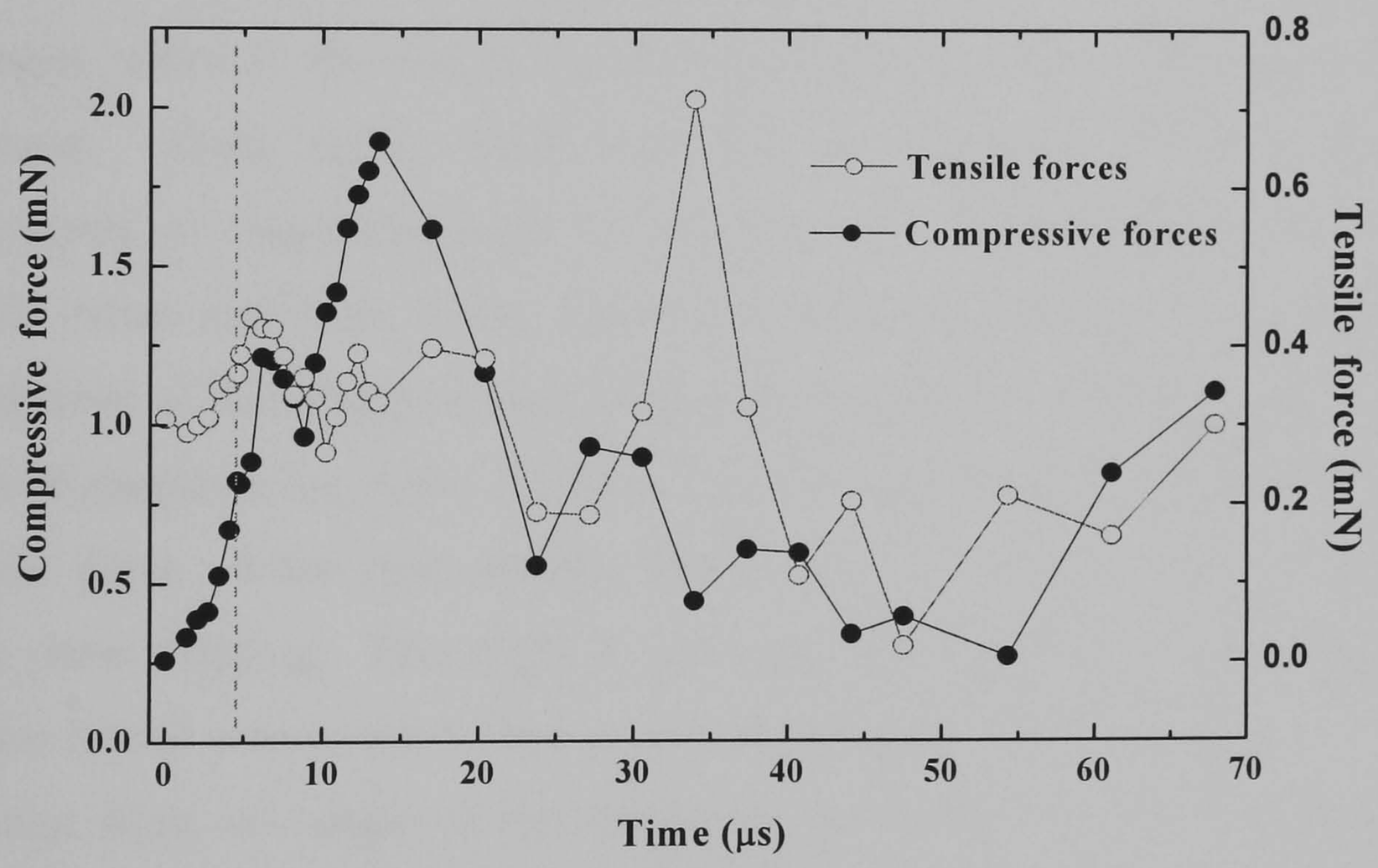

(b)

Figure 6.11 a) Evolution of the number of compressive and tensile contacts on the fracture plane of the largest fragment detached from the agglomerate. b) Evolution of the averages of tensile and compressive forces of the same contacts.

After the maximum of the contact forces is reached at about 5 μs from the beginning of the impact (Fig. 6.11b), the process becomes more complex since the analysis of contact forces does not show any clear behaviour. Figure 6.12 shows the contacts on the fracture plane as well as the particles of the agglomerate in contact with the wall between 27 μs and 129 μs. The thickness of the lines showing the contacts is proportional to the value of the force in the same contact. Blue particles are the particles that belong to the medium-size fragment and are in contact with the wall. Particles in red are all particles in contact with the wall that do not belong to the medium-size fragment. Between 27 μs and 54 μs the contact shown in a yellow circle in Fig. 6.12 becomes more compressive as time passes and then become less compressive and later breaks suggesting that it is subjected to a local rather to a global effect. At 61 μs a new contact with a large compressive force is observed as shown in the yellow square. This large force is not there in the previous frame. At about 102 μs only three contacts remain to be broken on the fracture plane (Fig. 6.12). However at 109 μs new contacts are formed on the fracture plane keeping the fragment joined to the rest of the agglomerate which delays the detachment of the fragment. These local effects introduce an important statistical factor in the detachment of fragments from the agglomerates. Consequently it is difficult to predict when and from where a fragment will be detached. The analysis of the detachment of this fragment also shows that the origin of the fragment is not due to crack propagation but rather the breakage of a large number of broken contacts on a specific plane. When solid particles that fail in a semibrittle mode are impacted they often show chipping. The origin of this type of fragment is the propagation of sub-surface lateral cracks due to the release of residual tensile stresses. This is clearly different from the origin of the fragments detached from the agglomerates which highlights once more the differences between solid particles and agglomerates.

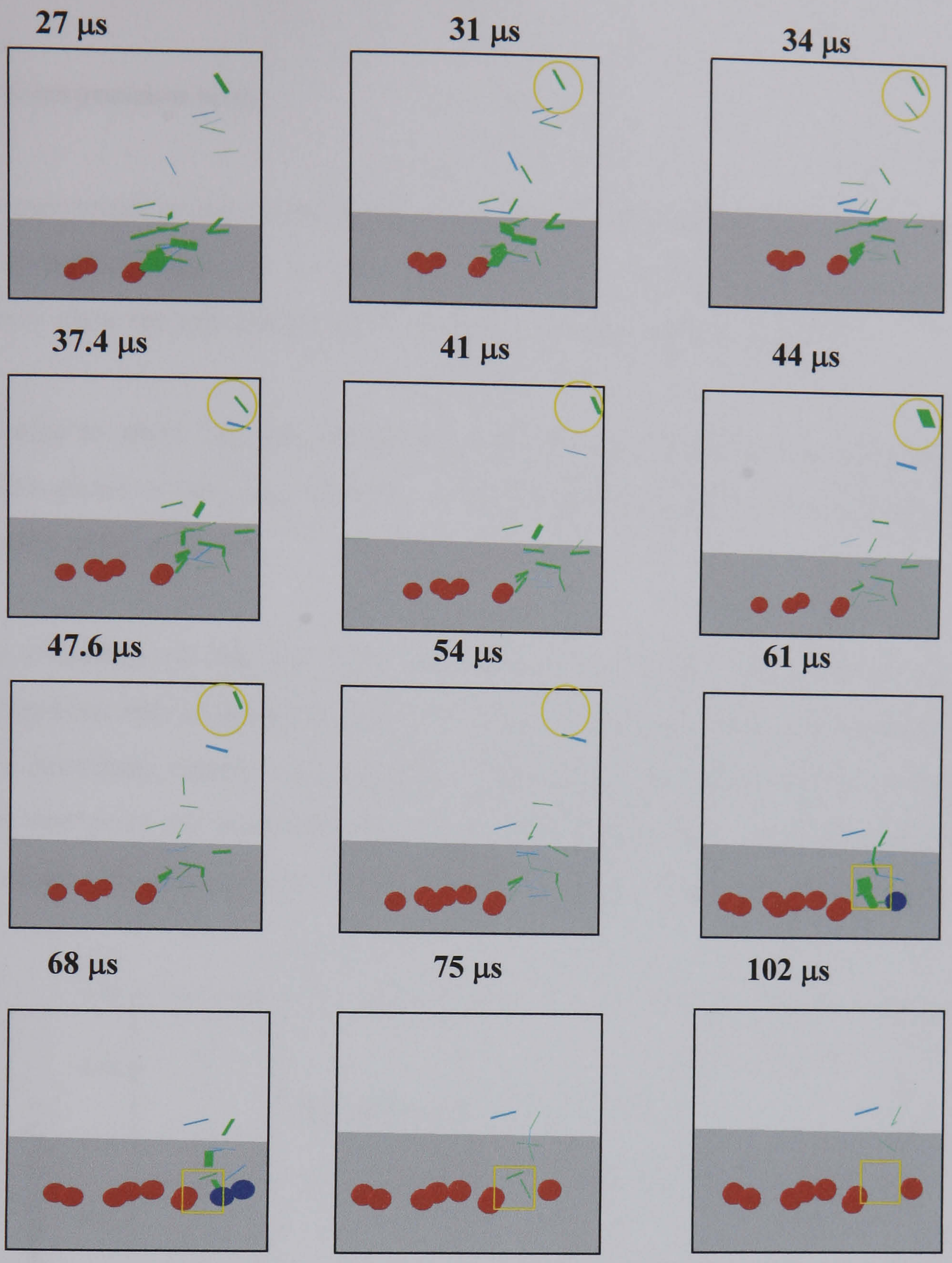

Figure 6.12 Visual observations of the contacts on the fracture plane of an agglomerate showing compressive (green) and tensile (cyan) contacts. Blue balls are in contact with the wall and belong to the cluster that is going to be detached and red balls are in contact with the wall but belonging to other clusters.

6.4 Compression tests

The compression tests reported here have been carried out at velocities corresponding to the impact range, *i.e.* 2.4 m/s and 0.1 m/s. The differences between the two tests merely show the effect of loading configuration and not the strain rate.

In order to carry out the compression test the agglomerate was deposited on the bottom platen at very low velocity. Afterwards the top platen was moved at constant velocity of 0.1 m/s.

The evolution of the top wall force and the damage ratio through the whole compression test is plotted in Fig. 6.13. At the beginning of the compression the wall force increased rapidly and reached a maximum value followed by a sharp drop. After this point the wall force fluctuated considerably with a tendency of increasing with time. The damage ratio also increased during the whole compression test.

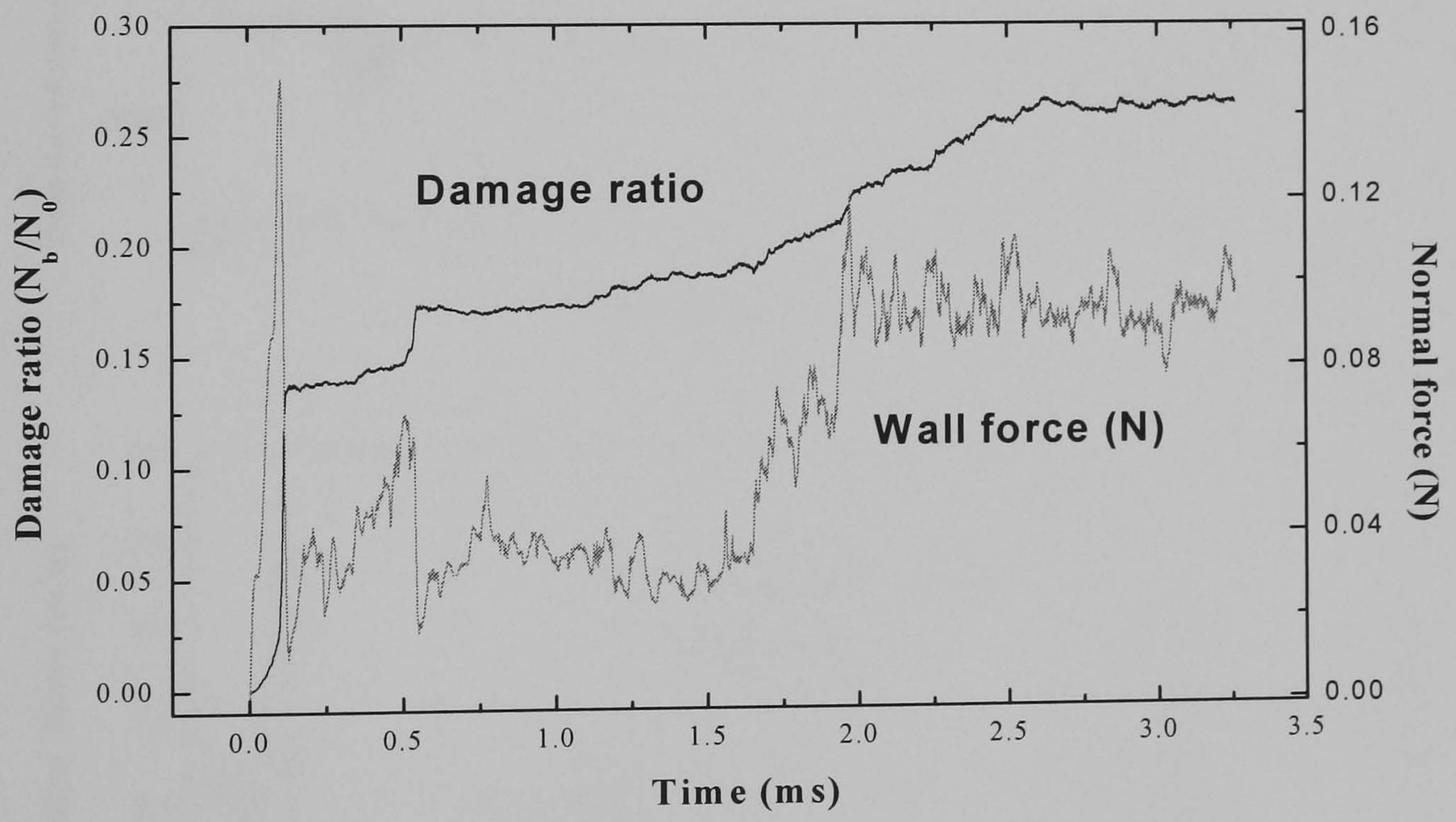

Figure 6.13 Top platen force and damage ratio during the compression test.

Figures 6.14a and 6.14b show the number of contacts in the agglomerate (compressive tensile and total number of contacts) and the average contact forces

(compressive and tensile forces). The dashed line corresponds to the time of the maximum wall force. The number of contacts in compression passes through a maximum at the same time as the number of tensile contacts passed through a minimum before the maximum of the wall force is reached. The oscillations of the number of contacts in tension and in compression are similar to those observed in the impact test which suggests that this type of behaviour could be a common response of the agglomerate subjecting to loading. In spite of the oscillations of the number of contacts in tension and compression the total number of contacts decreases (Fig. 6.14a).

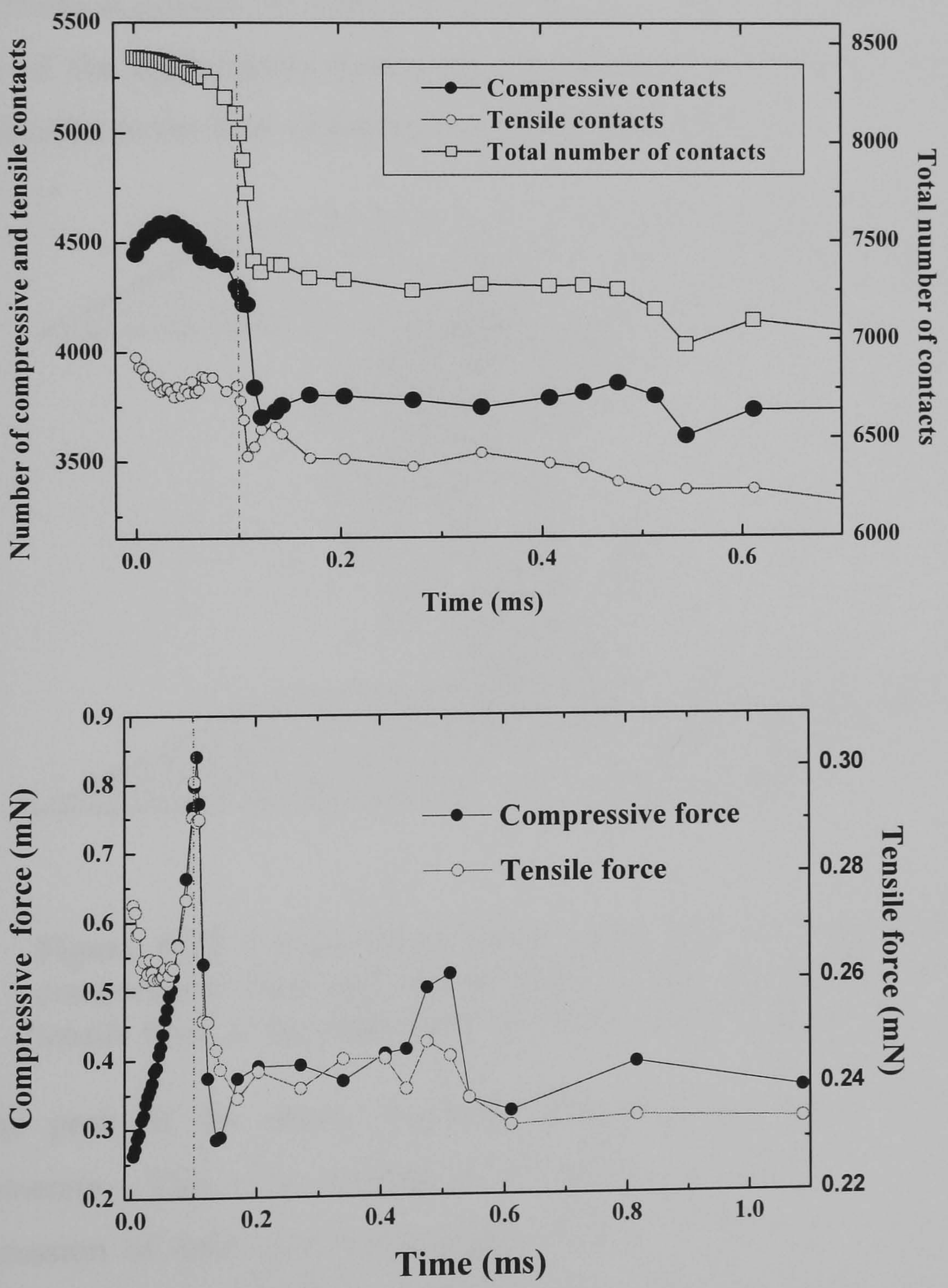

Figure 6.14 a) Number of compressive and tensile contacts during the compression tests; b) average value of the compressive and tensile forces during the compression test.

Figure 6.15 shows the compressive and tensile forces. For clarity of presentation the compressive forces larger than 1% of the maximum compressive force and the tensile forces larger than 50% the maximum tensile force in the agglomerate at the peak of the platen force are shown. It is possible to observe that the lines of maximum compression are trying to percolate the two regions of the agglomerate that are in contact with the platens. The large tensile forces are perpendicularly orientated to the line of maximum compression. Figure 6.16a and 6.16b show the tensile and compressive contacts at about 10 μs after the peak of the wall force and the broken contacts in the agglomerate from the beginning of the compression, respectively. The broken contacts are mainly concentrated in a central region (Fig. 6.16b). These observations suggested the same breakage mechanism of bonds as that observed in the impact of the agglomerate during the loading stage, *.i.e.* tensile contacts that are perpendicular to the lines of maximum compression break.

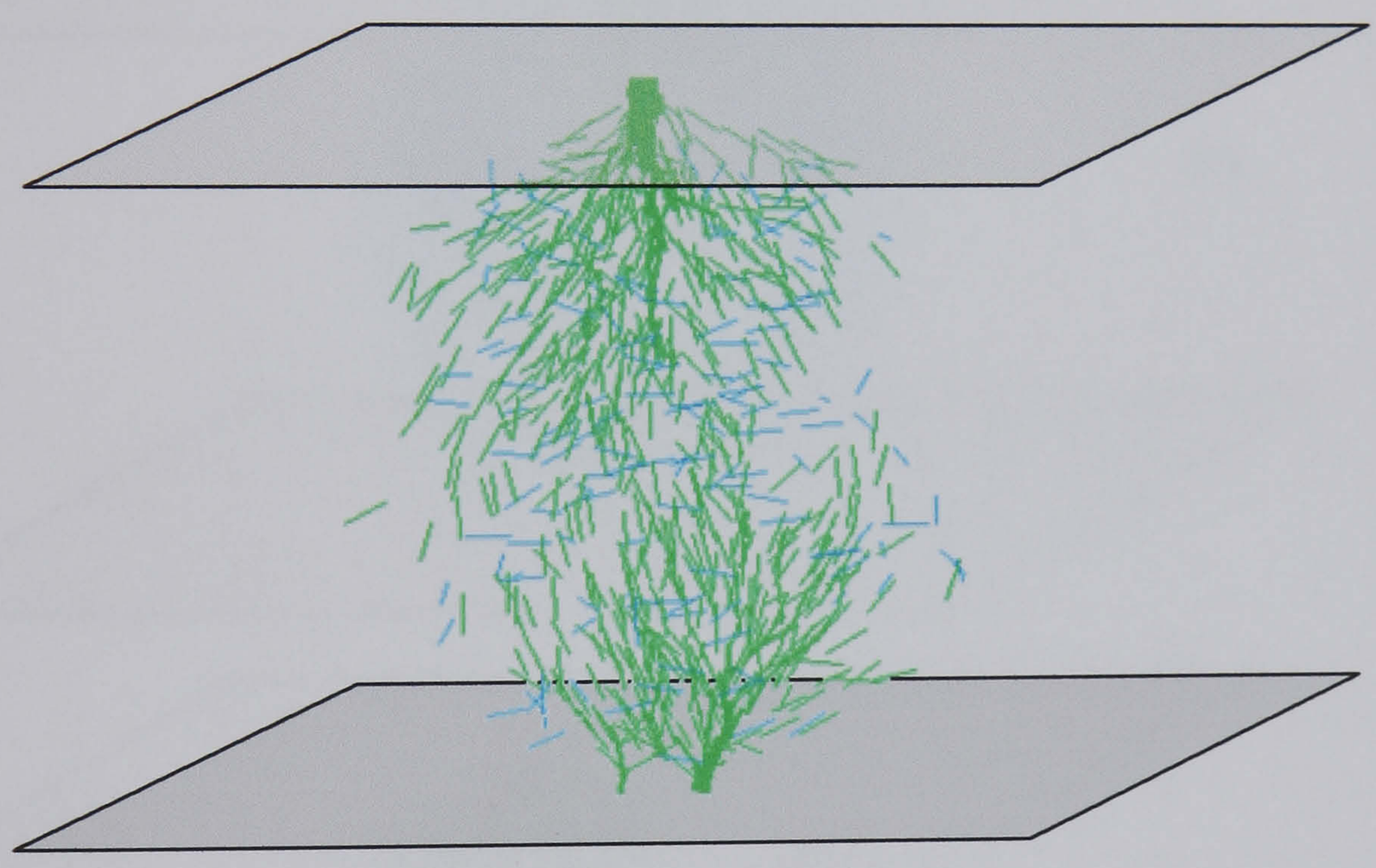

Figure 6.15 Compressive forces larger than 1% of the maximum compressive force and tensile forces larger than 50% of the larger tensile force at the peak of the wall force in the compression test.

At the peak of the platen force no fragments have been detached from the agglomerate. This is in contrast to the results of Thornton *et al.* (2002) on the compression of dense and loose agglomerates. In their case the evolution of the platen force for the dense agglomerate showed a peak with a sharp drop to zero associated with the fracture of the agglomerate into two large fragments. In contrast

the value of the platen force did not drop to zero for the case studied here. The loose agglomerate does not fragment at all during compression but it deformed extensively. The explanation for the difference between the work of Thornton *et al.* (2002) and the work reported here might be found in the value of packing fraction. The agglomerate that is being analysed here has a value of packing fraction of 0.546, which is in between the values of the agglomerates reported by Thornton *et al.* (2002), *i.e.* 0.6525 and 0.4364 for the dense and the loose agglomerate, respectively. Therefore, it is not surprising that the behaviour of the agglomerate here would be intermediate between the behaviour of the dense and loose agglomerates reported by Thornton *et al.* (2002).

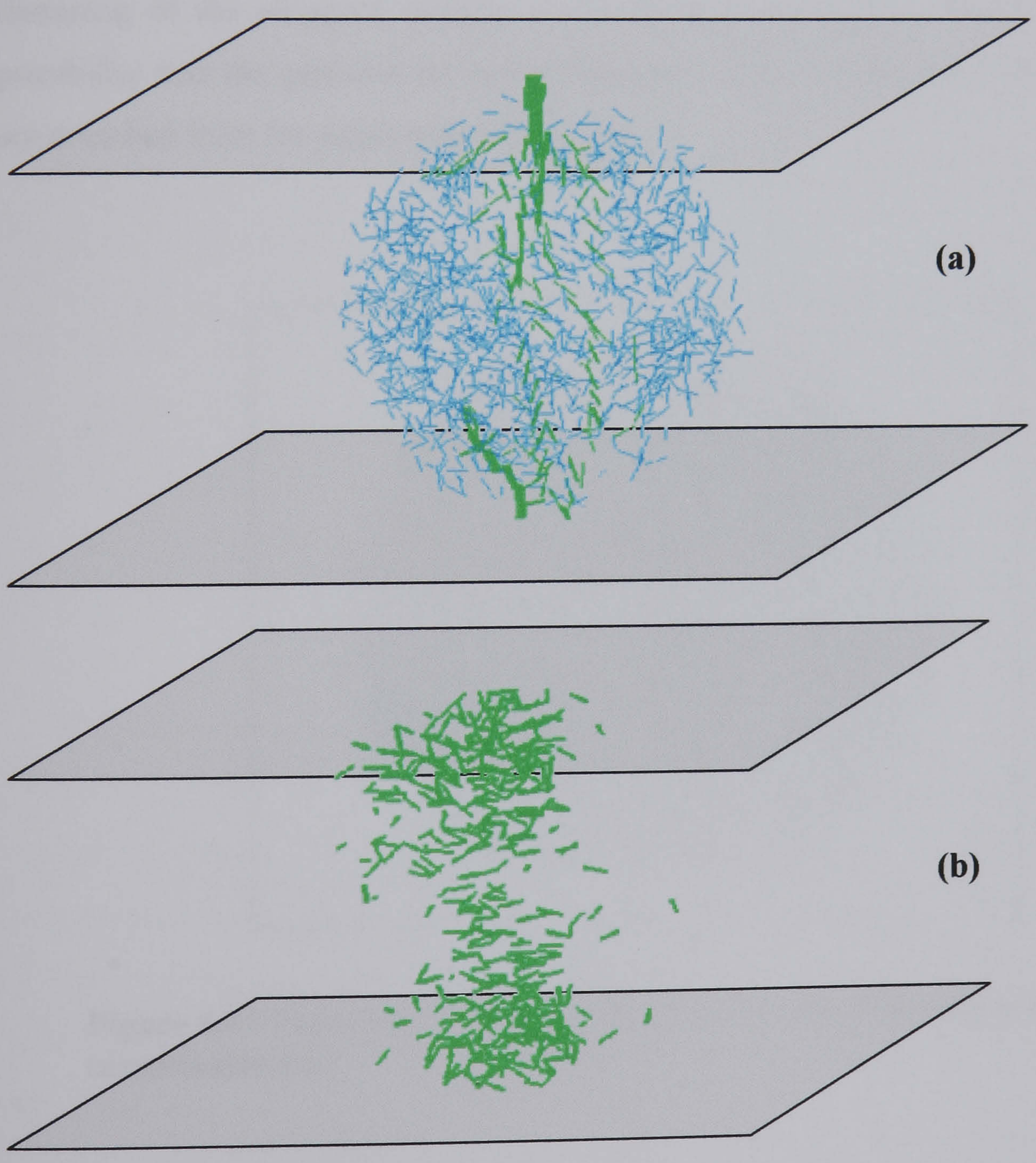

Figure 6.16 a) The tensile contacts larger than 38% of the maximum tensile force and compressive contacts larger than 10% of the maximum compressive force a at about 10μs after the peak of the wall force. b) Contacts broken from the beginning of the compression.

The continuation of the compression between 0.15 and 0.5 ms produces a new increase in the wall force (Fig. 6.13) and a slight increase of the average contact forces (Fig. 6.14b). After the first peak the agglomerate has 15% less contacts than at the beginning of the compression process, and this does not allow further accumulation of high contact forces. A second drop of the wall force is observed associated with the breakage of about 5% of the contacts in the agglomerate.

Between 0.6 ms and 1.6 ms the agglomerate was compressed by 5% of its initial size without an increase in the wall force and with less than 1% of broken contacts. Figure 6.17 shows the agglomerate at 1.6 ms from the beginning of the compression test. The flattening of the agglomerate is clearly observed in this figure. The flattening of the structure without a considerable breakage of bonds suggests the possibility that the particles are being relocated. Figure 6.18 shows the clusters that are detached from the agglomerate at 1.6 ms.

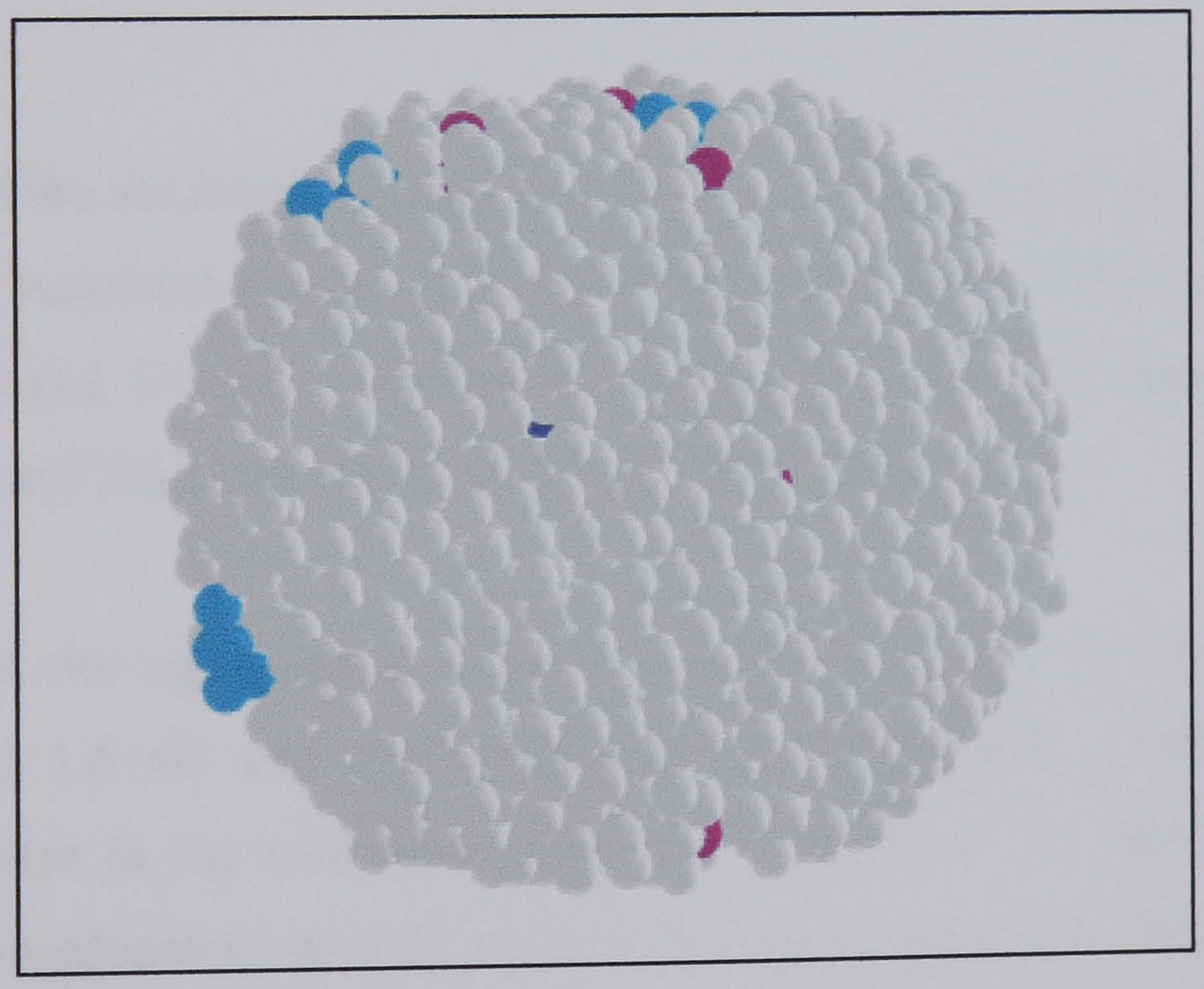

Figure 6.17 Flattening of the agglomerate at 1.6 ms of the beginning of the compression test.

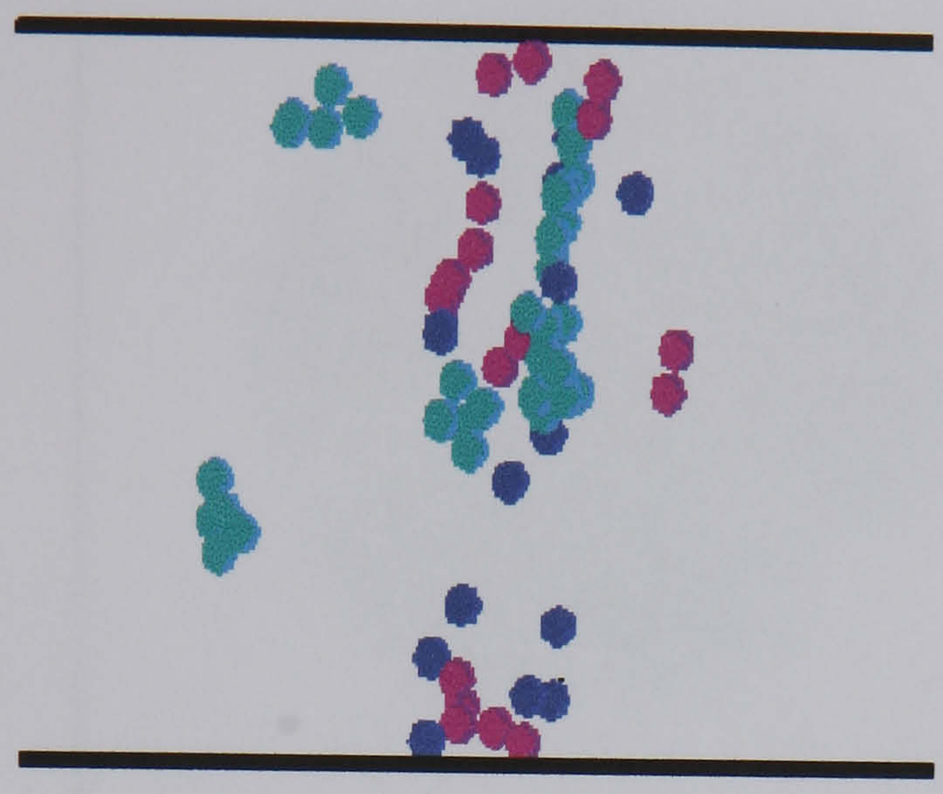

Figure 6.18 Clusters in the agglomerate at 1.6 ms of the beginning of the compression test. Blue are singlets, pink are doublets and cyan clusters with less than 20 particles.

The flattening of the structure without an increase of the value of the wall force can not be endlessly sustained and an increase in the value of the wall force is observed between 1.6 ms and 2.0 ms. During this interval of time the number of broken contacts was around 2% of the initial number of bonds (Fig. 6.13).

At about 2.2 ms the agglomerate enters in a regime similar to the one observed between 0.5 and 1.6 ms and characterised by a compression of the agglomerate without an increase in the wall force (Fig. 6.13). Figure 6.19 shows the contacts remaining in the agglomerate at 3.26 ms from the beginning of the compression. This figure shows the possibility of future fragmentation of the agglomerate into several parts. However, the fragments are not fully detached since there are particles keeping them together.

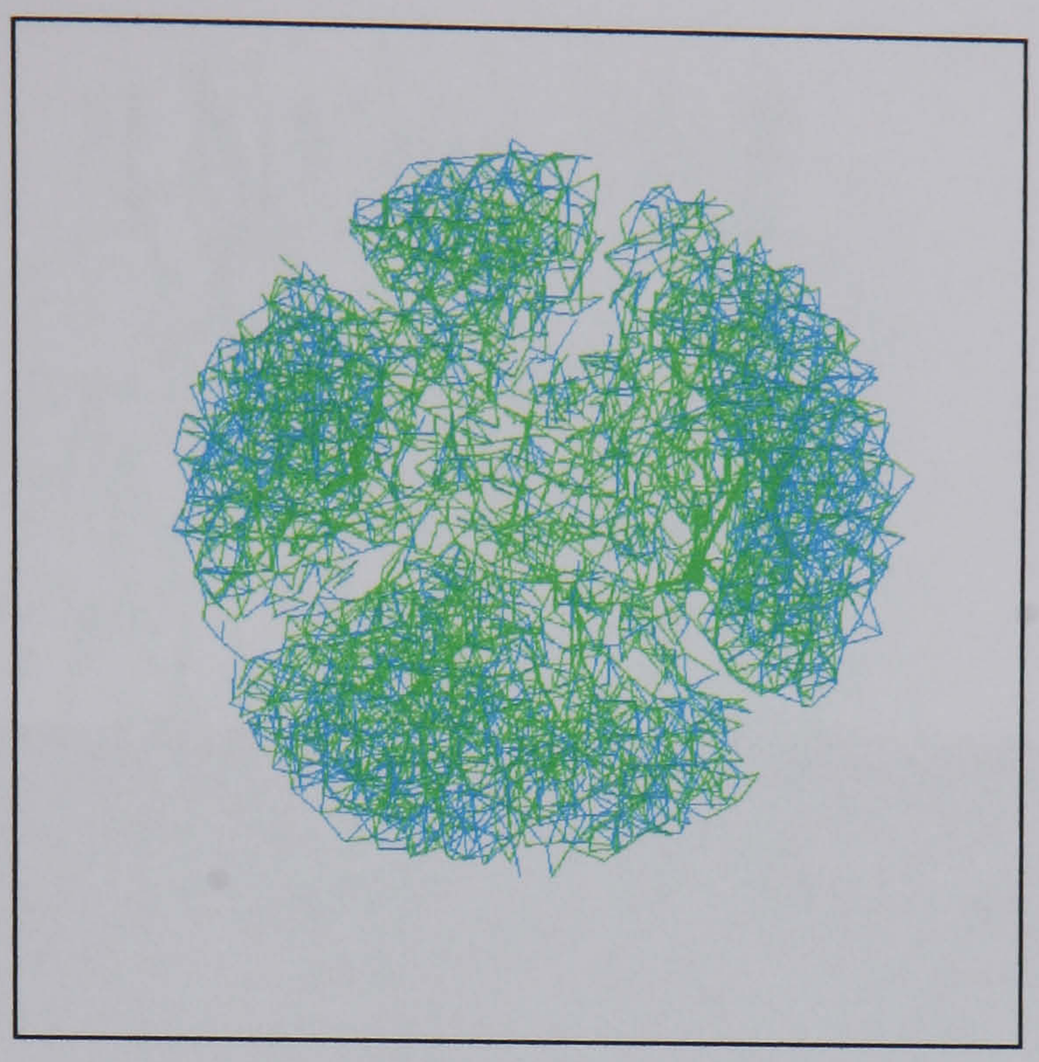

Figure 6.19 Contacts at 3.26 ms of the beginning of the compression (top view). Compressive contacts are plotted in green and tensile contacts are plotted in blue.

Figure 6.20 shows the propagation of the compressive forces within the agglomerate at the value of 3.26 ms from the beginning of the compression test. It is possible to observe the existence of chains of normal forces between the platen. This structure is more similar to the structures observed for the compression of beds of particles than the compression of a single particle agglomerate due to the extensive deformation and flattening of the agglomerate. This has produced an increase in the number of contacts between agglomerate and wall from two contacts at the beginning of the compression to 83 at time 3.26 ms. The compression test of the agglomerate can be considered to be finished since the agglomerate has lost its shape and now is an oval structure flattened at the top and bottom and compressed by about 18% of the initial size (Fig. 6.21). A continuation of the compression test would provide results more related to the new structure that has been formed than related to the initial agglomerate.

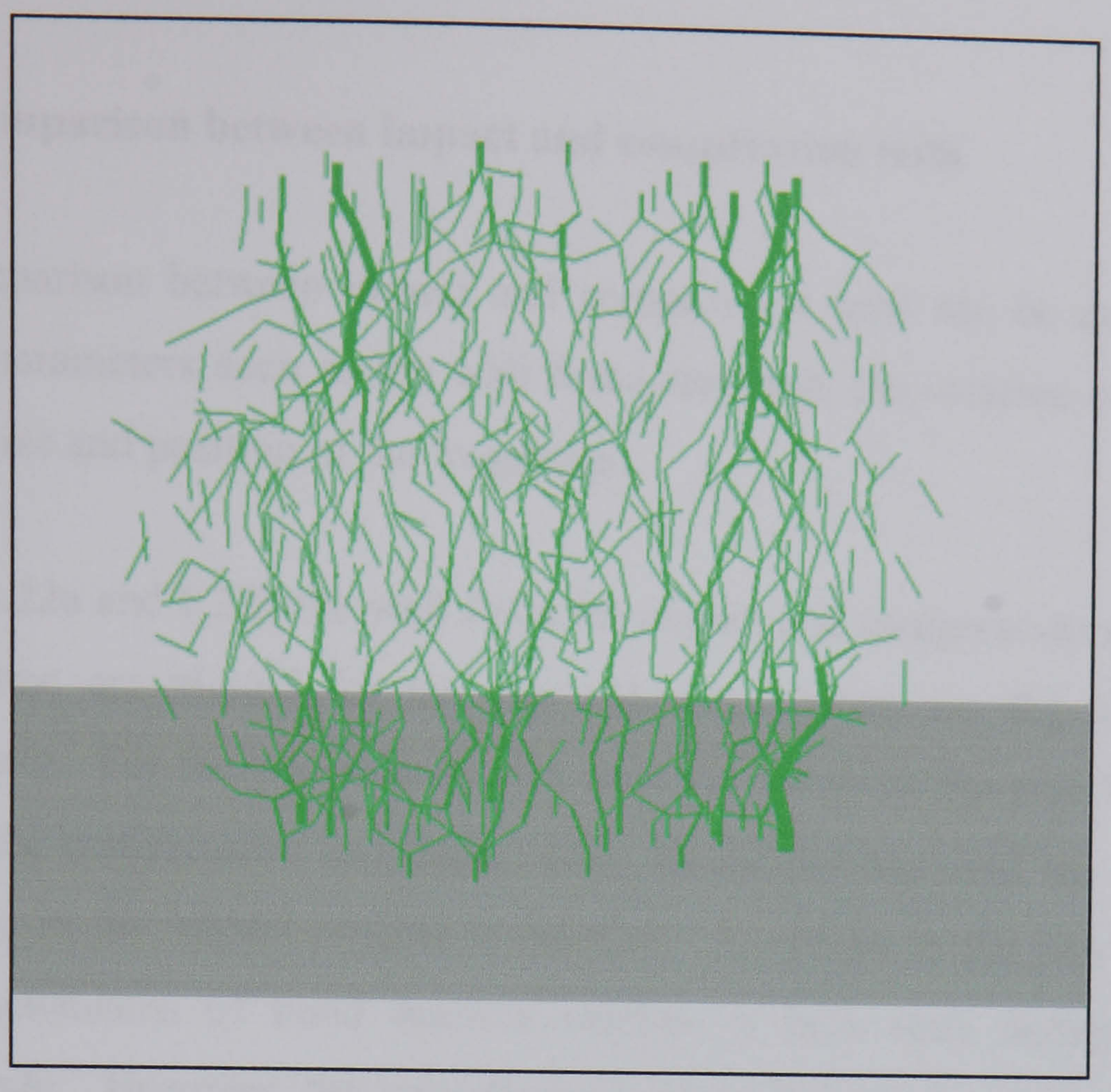

Figure 6.20 Side view of the compressive forces larger than 10% of the maximum compressive force.

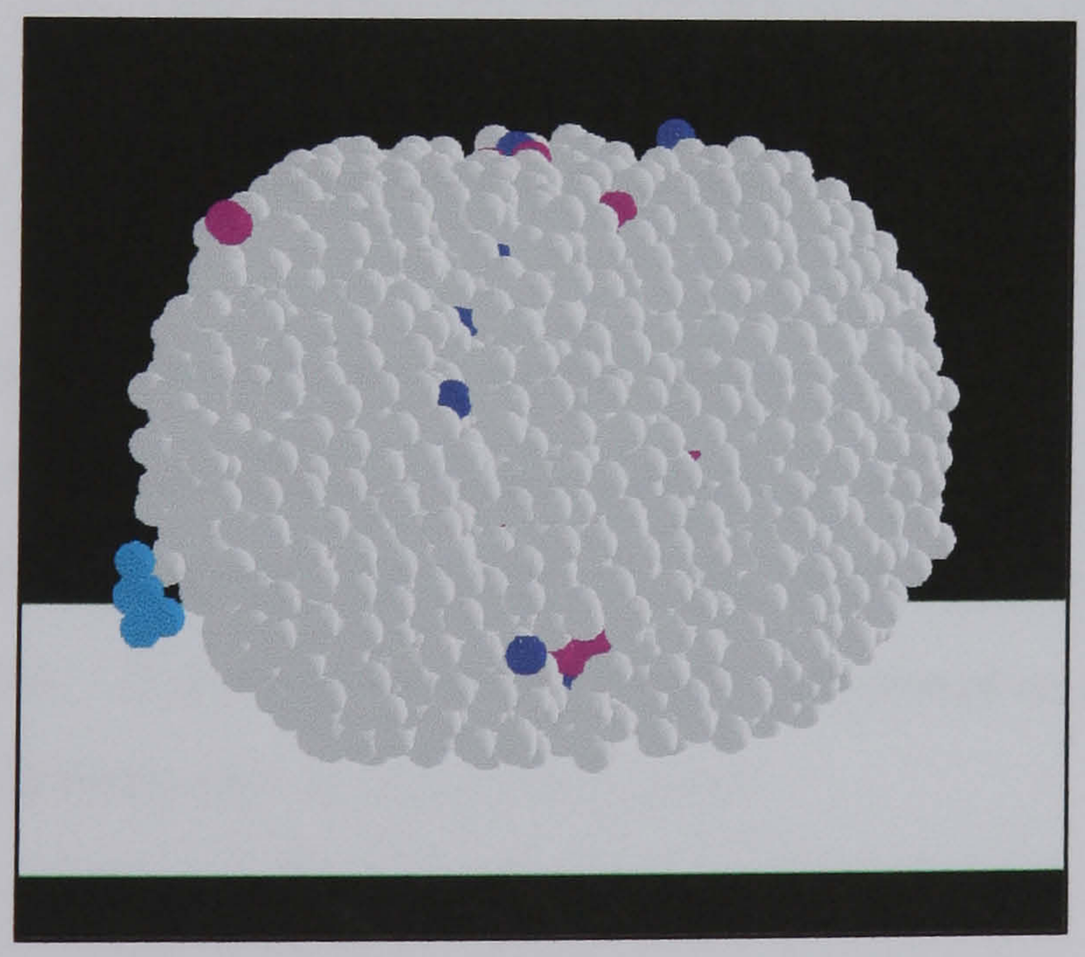

Figure 6.21 Flattening of the agglomerate. Colour coding: Blue singlets; pink doublets; cyan clusters larger than two particles; grey residual cluster; white, the target.

6.4.1 Comparison between impact and compression tests

The comparison between impact and compression tests can be done by evaluating various parameters such as the wall force response, the location of broken contacts and the size and position of the fragments.

In Figs 6.22a and 6.22b the wall force for impact and compression tests as a function of the time are plotted for the two velocities tested, i.e. 0.1 m/s and 2.4 m/s, respectively. For the low velocity (0.1 m/s) the curves of the wall force and damage ratio of the compression and impact tests almost overlap until the maximum of the wall force in the impact process is reached. As shown in the previous sections the same mechanisms of bond fracture operate in both tests during loading of the agglomerate. However, the maximum of the wall force is originated in a different way in impact and in compression. In impact the unloading of the agglomerate is due to the elastic strain energy of the agglomerate. In contrast, in compression the maximum of the wall force is due to a massive breakage of bonds which produces a relaxation of the contact forces and a sharp drop of the wall force. At around 30 μs the rebound occurs in the impact test for impact velocity of 0.1 m/s. The agglomerate reaches the maximum of the wall force in impact at about 15 μs. For compression tests this is reached much later (100 μs) and the value of the force is much higher.

The comparison of the wall force at the impact velocity of 2.4 m/s shows that the maximum of the wall force occurs almost at the same time for impact and compression tests, although the value of the wall force is slightly higher in the compression tests. It is difficult to explain the agreement in the maximum wall force and more work is necessary to clarify this point.

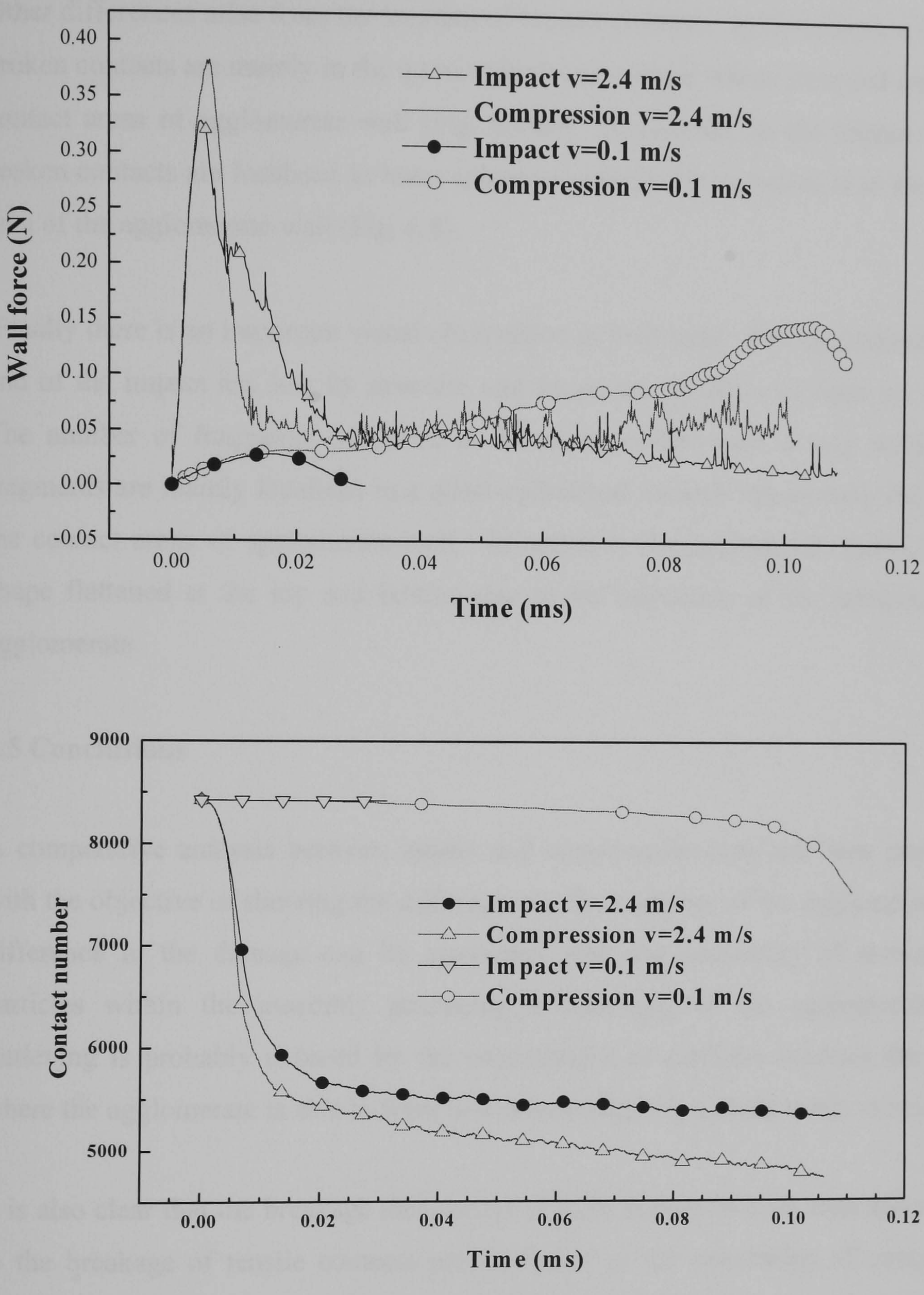

Figure 6.22 a) Comparison of the value of the wall force between impact and compression tests. b) Comparison of the evolution of the breakage of contacts between impact and compression tests.

Other differences arise from the location of broken contacts. In compression tests, the broken contacts are mainly in the quasi-cylindrical volume whose base and top are the contact areas of agglomerate-wall (Fig. 6.16b). In contrast, in the impact test, the broken contacts are localised in hemi-spherical volume whose centre is in the contact area of the agglomerate-wall (Fig. 6.8).

Finally there is an important visual observation in both tests. The agglomerate at the end of the impact has lost its structure and fragments of different sizes are formed. The number of fragments produced in the compression tests is very small. The fragments are mainly localised in a quasi-cylindrical volume whose base and top are the contact areas of agglomerate-wall. In addition, the agglomerate shows an oval shape flattened at the top and bottom due to the relocation of the particles of the agglomerate.

6.5 Conclusions

A comparative analysis between impact and compression tests has been carried out with the objective of showing the differences in the response of the agglomerate. The difference in the damage can be associated with the possibility of relocation of particles within the assembly producing a flattening of the agglomerate. This flattening is probably induced by the confinement of particles between the platen, where the agglomerate is able to form new bonds adopting a more stable structure.

It is also clear that the breakage mechanism is quite similar in both tests and it is due to the breakage of tensile contacts perpendicular to the orientation of compressive contacts. However, in impact tests it is also observed that most of the contacts are broken during unloading (70% of the total contacts broken during impact).

However, the most important feature is that the detachment of fragments is not due to the propagation of a sub-surface crack as is typical of semibrittle continuous solids. The analysis presented was carried out at the same rate for both impact and

compression test. Further work is needed to provide a more detailed analysis of the strain-rate dependency in the compression tests.

CHAPTER 7: CONCLUSIONS AND FUTURE WORK

The effect of the impact on the breakage of agglomerates has been carried out using computer simulation using Distinct Element Method (DEM). The agglomerate behaviour has been compared and contrasted with the behaviour of continuum solids and with the computer simulation and experimental results reported in the literature. In addition, a simple mechanistic theoretical model that predicts the number of contacts broken upon impact has been developed based on the considerations of energy usage that the work for breaking contacts is proportional to the input kinetic energy. This model provides a relationship between the number of broken contacts in the agglomerate and the properties of the primary particles (elastic modulus and density), the bond strength (surface energy), the agglomerate properties (number of primary particles in the agglomerate and coordination number) and the impact velocity. The model predictions are compared by comparison with the simulation results.

The use of DEM in the analysis of agglomerate strength has many advantages with respect to experimental methods. These advantages can be classified into two categories. The first one is the control of the single particle properties. The second one is the possibility of studying internal features which cannot be easily measured in experiments. In order to carry out the investigations presented in this thesis, a total of 12 agglomerates have been prepared and impacted. Some of these agglomerates have the same properties but differ in the random distribution of particle positions. These similar agglomerates were used with the objective of obtaining a certain statistical distribution of results. Therefore, the results correspond to the average of all impacts.

To introduce the friction and cohesion in different stages of the agglomeration process provided a different density and coordination number of the final agglomerate. The friction and cohesion were always introduced once the number of contacts reached a steady state. Therefore, very well-packed agglomerates were used.

Once the agglomerates were created, the mass, contact number and level of stress distribution within the agglomerate was analysed. The agglomeration method provided a

fairly constant value of the above mentioned parameters within layers of the same thickness as the particle radius (50μm). All agglomerates used in this work showed a constant internal density and coordination number. However, in the external layers the density and coordination number were lower than inside of the agglomerates due to the surface roughness. There is no control at present of the properties of the external layers of the agglomerate and it can constitute future work.

A comparative analysis of impact of agglomerates and single particles shows that at low impact velocities agglomerates behave as solid cohesive elastic particles with a size equal to the size of the primary particles of the agglomerate and a mass which is the same as the whole agglomerate. However, when impact velocity increases the breakage of contacts and detachment of particles make agglomerate behaviour very different from solid particles. For this case the dynamics of agglomerate impact can not be analysed based on continuum mechanics.

The analysis of force propagation in the agglomerate provides a method to estimate the elastic modulus of the agglomerate. The comparison of the simulation predictions with the results of the models of Kendall (1988) and Thornton (1993) shows a good agreement with both models.

The effect of the surface energy on the breakage of agglomerates is analysed by paying attention to the influence of the surface energy on the ratio of broken contacts and on the breakage pattern of agglomerates. The mechanistic model developed in this work predicts a relationship between the number of broken contacts and the surface energy in the form of a power law with index of -5/3. This relationship was tested for four different agglomerates in a range of two orders of magnitudes of the surface energy. The simulation results showed a better fit with the exponent to the surface energy -5/3 than to the exponent -1 as predicted previously by the Weber Number which has been extensively used in the literature.

The surface energy also drastically influences the breakage pattern of agglomerates. At low values of surface energy (0.35 J/m^2) agglomerates deform extensively under impact. The agglomerate failure in this case is in the form of the detachment of small clusters

without any evidence of fragmentation. The agglomerate failure seems to be ductile. An increase of one or two orders of magnitude in the surface energy changes the mode of failure of the agglomerates. Agglomerates now show fragmentation but still preceded by the disintegration of the contact area into small clusters. This mode of failure resembles the semi-brittle failure mode of solid particles. It seems that there was a transition from ductile failure to semi-brittle failure when the surface energy is increased. However, it is not clear if this transition is gradual with the variation of the surface energy or in contrast there is a value of the surface energy above which the agglomerates fail in a semi-brittle mode and below which the agglomerates fail in ductile mode.

Other factors such as impact angle also have a strong influence on the agglomerate breakage. The analysis of the influence of the impact angle on the breakage of bonds shows that the number of broken contacts is a function of the normal component of the impact velocity. However, the location of the broken contacts is strongly influenced by the impact angle and therefore by the tangential component of the impact velocity. Obviously, the change in the location of broken contacts produces a change of the location of the clusters produced upon impact. However, it appears that the impact angle influences the location of fragments and also the mode of failure of the agglomerates. For the same number of broken contacts the agglomerates fragment at certain impact angles but only suffer from the detachment of small clusters at other impact angles.

The analysis of the effect of agglomerate size on the extent of breakage shows a linear relationship for impact velocities between 0.1 m/s and 5.0 m/s. The analysis of the effect of the impact velocity shows that at low impact velocities, the number of broken contacts depends on the square of the impact velocity. However, the actual dependency between the number of broken contacts and impact velocity is a sigmoidal function which tends to a constant for high values of the velocity and to a relationship with the square of the velocity at low values of the impact velocity. From this expression has been concluded that the proportionality factor between incident kinetic energy and the work for breaking contacts that appear in the mechanistic model developed in this thesis should depend at least on the impact velocity. However, since the relationship between the number of broken contacts, surface energy and the number of particles in the agglomerate had been

successfully validated by the simulation results, the proportionality factor can not depend on the surface energy and the agglomerate size.

The breakage pattern is influenced by the agglomerate size. Agglomerates made of 500 particles fragment when impacted at certain orientations and do not fragment at other directions. Agglomerates of 3000 particles fragmented into two large fragments within a certain range of impact velocities at all impact orientations. The agglomerate of 10000 particles fragments into two, three or even four large fragments depending on the impact orientation. It is concluded that larger agglomerates have a tendency to fragment more easily than small agglomerates.

The analysis of the evolution of contact forces during impact shows oscillations in the number of tensile and compressive contacts during the loading of the agglomerate. The state of the contacts changes from tension to compression for contacts that are perpendicular to the target and from compression to tension for contacts that are parallel to the direction of compression. The breakage of contacts follows the direction of the tensile contacts. However, during the unloading period no general trend in the breakage of contacts in terms of orientation or location of the broken contacts is observed. The analysis of the detachment of a medium size fragment from the side of the agglomerate showed that no crack propagation produced the separation of this fragment. This process showed once again the differences between agglomerate behaviour and solid particle behaviour in which the detachment of this type of fragment in semi-brittle materials corresponds to the propagation of sub-surface cracks.

A comparison between impact and compression shows that the same mechanism operates in both cases when the agglomerate is being loaded. However, the maximum of the wall force has a very different origin in the two cases. In impact tests the maximum of the wall force is strongly influenced by the rebound of the particles in contact with the wall. However, in compression tests the maximum of the wall force is produced by the decrease in resistance of the agglomerate due to a massive breakage of bonds.

Agglomerate breakage is found to be a phenomenon, which is very difficult to analyse quantitatively and qualitatively. Difficulties arise from the large number of factors that

influence the breakage such as position and orientation of contacts, single particle properties and bond strength. However, the mechanistic model presented in this work has provided an advance in the prediction of the influence of some of the above factors on the breakage of agglomerates.

In future, the influence of factors such as Young's modulus, agglomerate residual stresses, interparticle friction and contact damping on the agglomerate breakage pattern should be addressed since they can have a very important role in the determination of the agglomerate strength. New agglomeration methods should be explored in order to obtain a better control of properties such as level of stresses or surface roughness and if possible a reduction of the computational time required to prepare the agglomerates. It is also recommendable in future to investigate bonds that show a strain rate dependency of the force required to break them. In addition, it is of interest to simulate bonds made of glue which elongate before breaking. Furthermore, a full energy balance during the impact process would help in the understanding of the most important factors that influence the agglomerate breakage and this would be invaluable information for industries.

REFERENCES

Arbiter, N., Harris, C. C. and Stamboltzis G.A. (1969). Single fracture of brittle spheres. *Trans. AIME*, **244**, 118-133.

Antony, S.J. and Ghadiri, M. (2001), Size Effects in a Slowly Sheared Granular Media. *Journal of Applied Mechanics,* **68**, 772-775.

Bitter, J. G. A. (1963). A study of erosion phenomena. *Wear*, **6**, 5-22.

Bowen, W. R. and Sharif, A. O. (1998). Longe-range electrostatic attraction between like-charged spheres in a charged pore. *Nature,* **393**, 663-665.

Chapman, D. L. (1913). A contribution to the theory of Electrocapillarity. *Phil. Mag.,* **25**, (6), 475.

Ciomocos, M. T. (1996). PhD dissertation. Micromechanics of Agglomerate damage processes. Aston University.

Couroyer, C. (2000). PhD Dissertation. Attrition of Alumina Catalyst Carrier Beads. Surrey University.

Cundall, P. A. (1971). A computer model for simulating progressive, large-scale movements in blocky rock systems. *Proc. Symp. Int. Soc. Rock Mech.*, Nancy 2, 8.

Cundall, P. A. and Strack O. D. L. (1979). A discrete numerical model for granular assemblies. *Geotechnique*, **29**, 47-65.

Davies, R. M. (1949). The determination of static and dynamic yield stresses using a steel ball. *Proc. Royal Soc. London A*, **197**, 416-432.

De Bisschop F. R. E. and Rigole W. J. L. (1982). A physical model for liquid capillary bridges between adsorptive solid spheres: The Nodoid of Plateau. *J. Colloid Interface Sci.,* **88,** (1), 117-128.

Derjaguin, B. V. and Landau, L. (1941). *Acta Physicochim.,* **14**, URSS.

Derjaguin, B. V., Muller, V. M. and Toporov, Y. U. P. (1975). Effect of contact deformation on the adhesion of particles. *J. Colloid. Interface Sci.* **53**, (2), 314-326.

Ennis, B. J. and Litster, J. D. (2001). Particle size enlargement. In R. Perry, D. Green (Eds.), Perry's chemical engineers' handbook, *7th ed.* New York: McGRaw-Hill, pp. 20-56 to 20-89.

Evans, A. G. and Wilshaw, T. R. (1976). Quasi-static solid particle damage in brittle solids: I. Observations, analysis and implications. *Acta Metall.*, **24**, 939.

Fisher, R. A. (1926). On the capillary forces in an ideal soil; correction of formulae given by W. B. Haines. *J. Agric. Sci.*, **16**, 492-505.

Ghadiri, M. (1999). Attrition of particulate solids. IFPRI, Annual meeting. Somerset. NJ. 1999.

Ghadiri, M., Antony, S. J., Moreno, R., Ning, Z., (2001), Granular Powders and Solids: Insights from Numerical Simulations. Eds. Roy, Soc. Chemistry, London, 70-81.

Ghadiri, M. and Zhang, Z. (1992). IFPRI Final Report, FRR 16-03, University of surrey, U.K.

Ghadiri, M. and Zhang, Z. (2002), Impact attrition of particulate solids. Part 1: A theoretical model of chipping. *Chemical Engineering Science*, **57**, 3659-3669.

Ghadiri, M. and Subero, J. (1997). IFPRI Annual Report ARR 16-09. University of Surrey, U. K.

Golchert, D. (2003). PhD dissertation, in preparation. Queensland Univ. Australia.

Gouy, G. (1910). *J. Phys.*, **4,** (9), 457.

Griffith, A. A. (1920). The Phenomena of Rupture and Flow solids. *Phil. Trans. Roy. Soc. London*, **A221**, 163.

Hagan, J. T. (1984). Impossibility of fragmenting particles: brittle-ductile transition. *J. of Mat. Science,* **16**, 2909-2911.

Hagan, J. T. and Swain, M. V. (1978). The origin of median and lateral cracks around plastic indents in brittle materials. *J .Phys. D: Appl. Phys.*, **11**, 2091-2102.

Hamaker, H. C., (1937). The London-Van der Waals attraction between spherical particles. *Physica IV*, **10**, 1058-1072.

Hassanpour, A. (2003). PhD dissertation, in preparation. Analysis of bulk compression behaviour of pharmaceutical powders. Leeds University.

Hutchings, I. M. (1981). A model for erosion of metals by spherical particles at normal incidence. *Wear*, **70**, 269-281.

Hutchings, I. M. (1992). Transitions, threshold effects and erosion maps. *Key Engineering materials*, **71**, 75-92.

Hutchings, I. M. (1993). Mechanisms of wear in powder technology: a review. *Powder Technology,* **76**, 3-13.

Hogg, R., Healy, T. W. and Fuerstenau, D. W. (1965). Mutual coagulation of colloidal dispersions. *Trans. Faraday Society,* **62**, 1638-1651.

Israelachvili J. (1985). Intermolecular & Surface Forces. London Academic Press.

Iveson, S. M., Litster, J. D., Hapgood, K., Ennis, B. J., (2001). Nucleation, growth and breakage phenomena in agitated wet granulation processes: a review. *Powder Technology*, **117**, 3-39.

Johnson, K. L. (1954). Surface interaction between elastically loaded bodies under tangential forces. *Proceeding of the Royal Society*, **A230**, 531-548.

Johnson, K. L. (1985). Contact Mechanics. Cambridge University Press.

Johnson, K. L., Kendall, K., and Roberts, A. D. (1971). *Proc. R. Soc. Lond. A*. **324**, 301-313.

Kafui, K. D. and Thornton, C. (1993). Computer simulated impact of agglomerate. *Powders & Grains 93, the proceedings of the 2nd International Conference on Micromechanics of Granular Media.* C. Thornton (Ed.), A. A, Balkema, Rotterdam, 401-406.

Kafui, K.D. and Thonton, C. (2000). Numerical simulations of impact breakage of a spherical crystalline agglomerate, *Powder Technology,* **109**, 113-132.

Kendall, K. J. (1969). PhD dissertation. Cambridge University, England.

Kendall, K. J. (1971). The adhesion and surface energy of elastic solids. *J. Phys. D: Appl. Phys.*, **4**, 1186-1195.

Kendall, K. J. (1988). Agglomerate strength. *Powder Metallurgy*, **31**, 28-31.

Kendall, K. J., Alford, McN. and Birchall, F. R. S. (1987). Elasticity of particle assemblies as a measure of the surface energy of solids. *Proc. R. Soc. Lond. A.*, **412**, 269-283.

Lawn, B. R. (1993). Fracture of brittle solids. Cambridge University Press. 2nd edition.

Lawn, B. R., and Swain, M. V. (1975). Microfracture beneath point indentations in brittle solids. *Journal of material Science*, **10**, 113-122.

Lawn, B. R. and Wilshaw, R. (1975). Review-Indentation fracture: principles and applications. *J. Mater. Sci.*, **10**, 1049-1081.

Lian, G., Thornton, C. and Adams, M. J. (1993). A theoretical study of the liquid bridge forces between two rigid Spherical Bodies. *J. Colloid Interface Sci.*, **161,** 138-147.

London, F. (1937). The general theory of molecular forces. *Trans. Faraday Soc.*, **33**, 8- 26.

Mandelbroot, B. B. (1982). Fractal geometry of Nature. W.F. Freeman. New York

Marshall, D. B., Lawn, B. R. and Evans, A. G. (1982). Elastic/Plastic Indentation Damage in Ceramics: The lateral Crack System. *J. of Am. Ceram. Soc*. **65**, (11),

Maugis, D. (1991). Adhesion of spheres: The JKR-DMT transition using a Dugdale model. *J. Colloid Interf. Sci.*, **150**, 243-269.

Mason, G. and Clark, W. C. (1965). Liquid bridges between spheres. *Chem. Eng. Sci.*, **20**, 859-866.

Maw, N., Barber, J. R. and Fawcett, J. N. (1976). The oblique impact of elastic spheres. *Wear,* **38**, (1), 101-114.

Maw, N., Barber, J. R. and Fawcett, J. N. (1981). The role of the tangential compliance in oblique impact. *Trans. ASME.: Journal of Lubrication and Technology,* **103**, 74-80.

Mazzone, D. N., Tardos, G. I., and Pfeffer, R. (1986). *J. Colloid Interface Sci.,* **113,** 544-556.

Mindlin, R. D. (1949). Compliance of elastic bodies in contact. J. *Appl. Mechanics*. **71**, 259-268.

Mindlin, R. D. and Deresiewicz, H. (1953). Elastic spheres in contact under varying oblique forces. *J. Appl. Mechanics*, **20**, 327-344.

Mishra B. K. and Thornton, C. (2001), Impact breakage of particle agglomerates, *International Journal of Miner. Process.*,**61,** 225-239.

Moreno, R., Antony, S. J., Ghadiri, M. (2003). Effect of the impact angle on the breakage of agglomerates. Powder Technology, **130**, 132 - 137.

Ning. Z. (1995). Elasto-plastic impact of fine particles and fragmentation of small agglomerates. PhD. Dissertation, Aston University.

Ning. Z, Boerefijn, R., Ghadiri, M. Thornton, C. (1996). *Advanced powder technology*, **8**, 15-37.

Ning, Z. and Thornton, C. (1993). Elastic-plastic impact of small particles with a surface. *Powders and Grain, 93, the Proceedings of the 2nd International Conference on Micromechanics of Granular Media,* 33-38.

Overbeek, J. Th. G. (1984). Interparticle forces in colloid science. *Powder Technology*, **37**, 195-208.

Pietsch, W. B. (1969). The Strength of Agglomerates Bound by Salt Bridges. *The Can. J. of Chem. Eng.*, **47,** 403 - 409.

Roberts, A.D. (1968). Ph. D. dissertation, Cambridge University, England.

Rogers, L. N. and Reed, J. (1984). The adhesion of particles undergoing an elastic impact with a surface. *J. Phys. D: Appl. Phys.*, **17**, 677-689.

Rumpf, H. (1962). Proc. Int. Symp. On Agglomeration, (ed. W.A. Knepper) 379

Salman, A.D. Gorham, A. D. and Verba, A. (1995). A study of solid failure under normal and oblique impact. *Wear,* **186-187**, 92-98.

lman, A.D. Gorham, A. D. and Verba, A. (2003), Impact breakage of fertiliser granules. *Powder Technology*, **130**, 359-366.

Samimi, A. (2003). PhD Dissertation. In preparation. Surrey University.

Savkoor, A. R. and Briggs, G. A. D., (1977). The effect of the tangential force on the contact of elastic solids in adhesion. *Proc. R. Soc. Lond. A.*, **356**, 103-114.

Simons, S.J.R. (1996). Modelling of agglomerating systems: from spheres to fractals. *Powder Technology*, **87**, 29-41.

Simons, S. J. R. Seville, J. P. K. and Adams, M. J. (1994), An analysis of the rupture energy of pendular liquid bridges. *Chem. Eng. Sc.*, **49**, (14), 2331- 2339.

Shipway, P.H. and Hutchings, I.M. (1993). Fracture of brittle spheres under compression and impact loading. I. Elastic stress distribution. *Phil.. Mag.,* **A67**, 1389-1404.

Shipway, P.H. and Hutchings, I.M. (1993). Fracture of brittle spheres under compression and impact loading. II. Results for lead-glass and sapphire spheres. *Philos. Mag.,* **A67**, 1405-1421.

Shipway , P.H. and Hutchings, I.M. (1993). *Powder Technology*, **76**, (1), 23-30.

Stern, O. (1924), Z. *Elektrochem.,* **30**, 508.

Subero, J. (2001). PhD Dissertation. Impact breakage of agglomerates. Surrey University.

Subero, J. and Ghadiri, M. (2001). Breakage patterns of agglomerates. *Powder Tech.* **120**, 232-243.

Subero, J., Ning. Z., Ghadiri, M. and Thornton, C. (1999). Effect of interface energy on the impact strength of agglomerates. *Powder Tech.*, **105,** 66-73.

Tardos G. I. and Gupta R. (1996). Forces generated in solidifying liquid bridges between two small particles. *Powder Technology,* **87**, 175 -180.

Thornton, C. (1991). Interparticle sliding in presence of adhesion. *J. Phys. D: Appl. Phys.*, **24**, 1942-1946.

rnton, C. (1993). On the relationship between the modulus of particulate media and the surface-energy of the constituent particles. *J. Phys. D: Applied Physics,* **26**, (10), 1587-1591.

Thornton, C. (1997*). Journal of Applied Mechanics- Transactions of the ASFLE,* **64**, (2), 383-386.

Thornton C., Ciomocos M. T. and Adams M. J. (1998). Proceedings of the 9th European Symposium on Comminution, Albi (France).

Thornton C., Ciomocos M. T. and Adams M. J. (1999). Numerical simulation of agglomerate impact breakage, *Powder Technology,* **105**, 74-82.

Thornton C., Ciomocos M. T. and Adams M. J. (2002). Numerical simulation of diametrical compression tests on agglomerates. 10th European Symposium on Comminution. Heidelberg, Germany.

Thornton, C. Kafui, D. and Ciomocos T. (1995). Numerical simulations of agglomerate attrition, fracture and fragmentation. IFPRI annual meeting. Urbana. US.

Thornton, C. and Ning, Z. (1994). Oblique impact of elasto-plastic spheres. Department of Civil Engineering. Aston University. Birminghan. UK.

Thornton, C. and Randall, C. W. (1988). Applications of theoretical contact mechanics to solid particle system simulation. Micromechanics of Granular Materials. Elsevier Science Publishers B. V. Amsterdam.

Thornton, C. and Yin, K. K. (1991). Impact of elastic spheres with and without adhesion. *Powder Technology*, **65**, 153-166.

Thornton, C., Yin, K. K. and Adams, M. J. (1996). Numerical simulation of the impact fracture and fragmentation of agglomerates. *Journal of Phys. D: Appl. Physics,* **29**, 424-435.

Vervoorn, P. M. M. (1986). Particle attrition. IFPRI. Delft University of Technology, FR13-01, The Netherlands, December 1986.

Verwey E. J. W. and Overbeek J. Th. G. (1948). *Theory of the stability of lyophobic colloids.* Elsevier. Amsterdam. 140-142.

., S., John, W. and Georen, S. L. (1989). Particles on Surfaces (Eds. K. L. Mittal).

Willet, C. D. and Seville, J. P. K. (1998). World Congress on Particle Technology Brighton, U.K.

Wilshaw, T. R. The Hertzian fracture test. *Journal of Applied Physics*, **4**, 1567-1580

PPENDIX A: DISTINCT ELEMENT METHOD AND THE COMPUTER CODE TRUBAL

A.1 Introduction

Distinct Element Method (DEM) is a computer simulation technique initially developed by Cundall and Strack (1979) to study the mechanics of granular assemblies. The method was originally created for 2D systems and the associated computer code was called BALL. This code modelled the contact between particles using a linear elastic relationship between force and deformation. BALL was originally used to study beds of particles subjected to compression and shear deformations (Cundall 1978). The code BALL was later extended to model 3D systems and its name was changed to TRUBAL. The code has been extensively developed by Thornton and co-workers (Eqs A9-A34) for the analysis of the behaviour of spherical agglomerates under impact conditions and packed assemblies under shear deformation. The interactions between particles in the normal and tangential directions for both cohesive and non-cohesive materials have been modelled as detailed below.

The model incorporated in the computer code TRUBAL assumes a relationship between the normal force F_N and displacement, δ_N, based on Hertz analysis.

$$F_N = -K_h(\delta_N)^{3/2} \tag{A.1}$$

This relationship has been extended for the case of adhesive contact substituting the normal force for an effective force P (Jonhson *et al.* 1971).

The contact damping force is given in the form (Ning, 1995),

$$F_{ND} = -D_{mp}(\delta_N)^{1/4}V \tag{A.2}$$

he normal force F_N acts in parallel to the damping force in the contact between particles.

The stiffness of the contact is defined as:

$$k_N = \left|\frac{dF}{d\delta}\right| = \frac{3}{2} K_H \delta_N^{1/2} \qquad \text{(A.3)}$$

and the increment in normal force can be obtained by substituting the derivatives by infinitesimal increments in Eq. A.3.

$$\Delta F_N = k_N \Delta \delta_N \qquad \text{(A.4)}$$

These non-linear relationship between force and displacement is complemented with the Newton's laws, which are used to calculate accelerations, velocities and positions.

All variables in the computer code TRUBAL are updated cyclically starting with the variables related to the motion and continuing with the variables that characterise the contact between particles. An account of the expressions used in TRUBAL is shown below.

A.2.1 Motion laws

DEA updates cyclically particle position, velocity and acceleration using a finite difference version of the Newton's laws.

$$\vec{F}(t) + m\vec{g} - m\alpha_g \frac{\vec{V}(t+\Delta t) + \vec{V}(t)}{2} = m \frac{\vec{V}(t+\Delta t) - \vec{V}(t)}{\Delta t} \qquad \text{(A.5)}$$

$$\vec{M} - m\alpha_g \frac{\vec{\omega}(t+\Delta t) + \vec{\omega}(t)}{2} = I \frac{\vec{\omega}(t+\Delta t) - \vec{\omega}(t)}{2} \qquad \text{(A.6)}$$

where V and ω are the linear and angular velocities respectively, I the momentum of inertia, F and M are the total force and momentum of the force applied to a specific particle and α the global damping coefficient.

Rearranging terms in the expressions A.5 and A.6 the equations for the velocity and position of any particle are:

$$\vec{V}(t+\Delta t) = \left(\vec{V}(t)\cdot\left(1-\frac{\alpha_g \Delta t}{2}\right)+\vec{F}\frac{\Delta t}{m}+\vec{g}\Delta t\right)*\frac{1}{1+\frac{\alpha_g \Delta t}{2}} \qquad \text{(A.7.a)}$$

$$\vec{x}(t+\Delta t) = \vec{x}(t)+\vec{V}(t+\Delta t)\Delta t \qquad \text{(A.7.b)}$$

The equations for rotational motion have a similar form:

$$\vec{\omega}(t+\Delta t) = \left(\vec{\omega}(t)\left(1-\frac{\alpha_g \Delta t}{2}\right)+\vec{F}\frac{\Delta t}{I}\right)\frac{1}{1+\frac{\alpha_g \Delta t}{2}} \qquad \text{(A.8.a)}$$

$$\theta_r(t+\Delta t) = \theta_r(t)+\omega(t+\Delta t)\Delta t \qquad \text{(A.8.b)}$$

Once the positions and velocities have been updated the code checks the contacts between particles.

A.3 Contact between particles

When the position of two particles at the instant $t+\Delta t$ is such that they would deform, the deformation is calculated according to the expression:

$$\Delta\delta_n = V_n(t)\Delta t - R_i - R_j \qquad \text{(A.9)}$$

with V_n being the velocity of approach between the two particles and R_i and R_j the radii of the two particles.

The code calculates the pull off force, P_{off}, for the contact between the two particle using the model of Johnson, Kendall and Roberts (JKR) of 1971 (Johnson *et al.* 1971). The expression used is

$$P_{OFF} = \frac{3}{2}\pi\Gamma R^* \tag{A.10}$$

with R^* being the reduced radius of the two particles in contact and Γ the interface energy. If the contact is non-adhesive the pull-off force is zero.

If a new contact is going to be formed between two adhesive and elastic spheres, the external load in the contact is calculated according to the expression:

$$F_N = \Delta\delta_n \frac{4E^* a_o^{\,2} - 6\sqrt{\pi\gamma E^* a_o^{\,2}}}{2\frac{a_o^{\,2}}{R^*} - \sqrt{\frac{\pi\gamma}{E^* a_o^{\,2}}}} \tag{A.11}$$

with a_0 being the initial contact area radius and defined as

$$a_o = \left(\frac{4}{3}\right)^{2/3} a_{off} \tag{A.12}$$

If the contact is already formed, the stiffness of the contact is calculated. For the no adhesion case the stiffness is given by

$$k_N = 2E^* a \tag{A.13}$$

and for the adhesion case the normal stiffness is given by

$$k_N = \frac{2Ea\left[3 - 3\left(\frac{a_{off}^3}{a^3}\right)^{1/2}\right]}{3 - \left(\frac{a_{off}^3}{a^3}\right)^{1/2}} \qquad \text{(A.14)}$$

(See Yin 1991, and Thornton and Yin, 1991 for more details of the expressions given above).

Then the incremental normal force in the contact is calculated according to the expression

$$\Delta F_N = k_N \Delta \delta_n \qquad \text{(A.15)}$$

The value of the incremental normal force is added to the previous value of the normal force, $F_N(t)$, in the contact being

$$F_N(t + \Delta t) = F_N(t) + \Delta F_N(t, t + \Delta t) \qquad \text{(A.16)}$$

where $\Delta F_N(t, t+\Delta t)$ is the increment of normal force between t and $t+\Delta t$ (previously named as ΔF_N).

After obtaining the value of the stiffness of the contact the expression for the damping force F_{ND} as a function of the damping ratio β_d, the displacement $\Delta \delta_N$, the time step Δt and the reduced mass of the two particles in contact is calculated

$$F_{ND} = 1.8257\ \beta_d \frac{\Delta \delta_n}{\Delta t} \sqrt{m^* k_n} \qquad \text{(A.17)}$$

This value of the contact damping force is added to the previous value of F_N and ΔF_N giving the total normal force F_{TNF}.

$$F_{TNF} = F_N + F_{ND} \tag{A.18}$$

After these calculations the code updates the contact area radius, a, using the effective force defined by JKR model (Johnson *et al.* 1971).

If there is no tangential traction, the contact area radius, a, is calculated according to the expression

$$a = \left(\frac{3}{4} \frac{R^*}{E^*} P_{EFF} \right)^{1/3} \tag{A.19}$$

where P_{EFF} is the effective force defined in the JKR model as:

$$P_{EFF} = F_N + 2P_{off} + \sqrt{(4F_N P_{off} + P_{off}^2)} \tag{A.20}$$

If there is a tangential traction and the particles are not sliding and a peeling process is happening in the contact the expression given by Savkoor and Briggs (1977).

$$P_{EFF} = F_N + 2P_{OFF} + \sqrt{4(F_N P_{OFF} + P_{OFF}{}^2) - \frac{1}{4}\frac{T^2 E^*}{G^*}} \tag{A.21}$$

where G^* is the reduced shear modulus of the two particles in contact and is defined as

$$\frac{1}{G^*} = \frac{(2-\nu_i)(1+\nu_i)}{E_i} + \frac{(2-\nu_j)(1+\nu_j)}{E_j} \tag{A.22}$$

where i and j are the subscript of the two particles in contact.

However, if there is sliding of the particles the model of Thornton (1991) is applied. The model of Thornton established that if the normal force F_N is greater than -0.3P_{off} (P_{off} is defined as the absolute value of the force required to break the contact which is intrinsically negative), the contact area radius is given by

$$a = \left(\frac{3}{4} \frac{R^*}{E^*} P_{EFF} \right)^{1/3} \tag{A.23}$$

where P_{EFF} is given by

$$P_{EFF} = F_N + 2P_{off} \tag{A.24}$$

If the normal force is smaller than -0.3P_{OFF} then the contact area radius is calculated according to Thornton (1991) as:

$$a = \left[\frac{3}{4} \frac{R*}{E*} P_{EFF} \left(\frac{2P_{EFF} + F_N}{3P} \right)^{3/2} \right] \tag{A.25}$$

where P_{EFF} is given by Eq. A.20.

Afterwards, the code calculates the tangential displacement using the values of the tangential velocities at the contacts. Then, the tangential displacement is used to calculate the tangential traction using the model of Mindlin and Deresiewicz (1953) for the non-adhesion case and Thornton and Randall (1987) for the adhesion case. According to Mindlin and Deresiewicz (1953) the state of the tangential contact depends on the loading history, therefore the tangential force is calculated differently for loading, unloading or reloading. The expression for the contact stiffness is dependent on a parameter θ which is calculated by the expressions A.26a-c for loading, unloading and reloading respectively:

$$\theta^3 = 1 - \frac{T + \mu\Delta P}{\mu P} \tag{A.26a}$$

$$\theta^3 = 1 - \frac{T^* - T + 2\mu\Delta P}{2\mu P} \tag{A.26b}$$

$$\theta^3 = 1 - \frac{T - T^{**} + 2\mu\Delta P}{2\mu P} \tag{A.26c}$$

and the stiffness is calculated according to Eq. A.27 in the form (Thornton and Yin, 1991)

$$k^t = 8G^* a \pm \mu(1-\theta)\frac{\Delta F_N}{\Delta\delta_t} \tag{A.27}$$

where the signs plus and minus are applied for loading and unloading conditions, respectively.

The increment in tangential force is calculated as

$$\Delta T(t, t+\Delta t) = k_t \Delta\delta_t \tag{A.28}$$

and this value is added to the previous value of the tangential force

$$T(t+\Delta t) = T(t) + \Delta T(t, t+\Delta t) \tag{A.29}$$

The tangential damping is computed according to the expression

$$F_{DT} = 2\beta_d \frac{\Delta\delta_T}{\Delta t}\sqrt{m^*\left(\frac{\Delta T}{\Delta\delta_T}\right)} \tag{A.30}$$

where m^* is the reduced mass of the two bodies in contact.

The damping force is added to the tangential force in order to obtain the total tangential force in the contact, T_{TSF},

$$T_{TSF} = T + F_{DT} \tag{A.31}$$

When the tangential force is increased the contact area decreases due to a peeling process. This process continues until certain value of the tangential force is reached. This value of tangential force, T_{Peel} cancels the square root in Eq. A.24. It is given by

$$T_{Peel} = 2\sqrt{(4F_N P_{OFF} + 4P_{OFF}^2)\frac{G^*}{E^*}} \tag{A.32}$$

If the value of the tangential force is larger than the one required for completing a peeling process, gross sliding occurs. In this case and with the additional condition that the normal force is larger than the value of $-0.3P_{off}$, the tangential traction during sliding is given by

$$T = \mu(F_N + 2P_{off}) \tag{A.33}$$

If the normal force applied is less than $0.3P_{off}$ the sliding criterion become:

$$T = \mu P\left(\frac{2P_{EFF} + F_N}{3P_{EFF}}\right)^{3/2} \tag{A.34}$$

where P_{EFF} si given by Eq. A.20.

The last step is to add the forces calculated in the contact to the forces applied in the centre of the particles and to initiate the cycle of calculation again.

A.4 Time step

There are three types of waves which can propagate through elastic bodies: (a) dilatational or waves of pressure (longitudinal waves), (b) distortional or shear waves (transversal waves) and (c) waves that can propagate along the surface of an elastic body, which are called Rayleigh waves.

The speed of propagation of the dilatational waves, c_D, the shear waves, c_D and the Rayleigh waves, V_R are functions of the shear modulus G, the density of the material ρ and the Poisson's ratio ν and are given by:

$$c_D = \left(\frac{2(1-\nu)G}{(1-2\nu)\rho} \right)^{1/2} \tag{A.35}$$

$$c_s = \left(\frac{G}{\rho} \right)^{1/2} \tag{A.36}$$

$$V_R = \eta \sqrt{\frac{G}{\rho}} \tag{A.37}$$

and where η is a parameter which depends on Poisson's Ratio, ν, given by the following equation:

$$\eta = 0.1631\nu + 0.876605 \tag{A.38}$$

According to Miller and Pursey, (1955), (see also Johnson, 1985) the energy is mainly transported by Rayleigh waves. Based on the previous observation, Thornton and Randall (1988) considered that the time step should be based on the fact that the transmission of energy through a particle is made by Rayleigh waves. Therefore, the time step should be less than the time required for the wave to travel to the diametrically opposite point of the contact:

$$\Delta t = \frac{\pi R}{V_R} \tag{A.39}$$

with V_R being the velocity of the Rayleigh waves and R the radius of the particle. Substituting the expression for the velocity of propagation of the Rayleigh waves Eq. A.41 is obtained:

$$\Delta t = \frac{\pi R}{(0.1631\nu + 0.8766)}\sqrt{\frac{\rho}{G}} \tag{A.40}$$

It is important to note that the dependency of the time step on the size of the particles is linear, implying that the computational time increases as the particle size decreases. In most of the simulations carried out in this work particles of 50 μm in radius, Poisson's ratio 0.3, density 2000 kg/m^3, and G = 11.9 GPa have been used. Applying the Eq. A.40, the time taken by the Rayleigh waves in propagating along the surface of the single particles is approximately 69 ns. It implies that one second of real time is equivalent to 14 million cycles of calculations.

A.5 Damping

The damping in the computer code TRUBAL has two different forms: global damping and contact damping.

The global damping acts at the centre of the particles as if a drag force is applied. This damping is proportional to the velocity of the particles in the form

$$F_{GD} = -\alpha m V \tag{A.41}$$

This damping is incorporated in the equations of motion as given by equations (A.7.a, A.8.a).

Global damping is used during the agglomeration process in order to help the system to reach a steady state by avoiding a continuous increase of the velocities when accelerated by an external force.

The contact damping is used to account for various energy dissipation processes in the impact event and has the form

$$F_{ND} = -D_{mp}(\delta_N)^{1/4}V \tag{A.42}$$

where D_{mp} is the contact damping coefficient. Damping is applied to both normal and tangential forces.

The damping coefficient, D_{mp}, is defined as a fraction, β_d, of the critical damping, D_c, which is the damping required to convert the oscillatory motion of the particles in to an exponential decay.

$$D_{mp} = \sqrt{\frac{5}{4}}\beta_d D_C = 2\sqrt{\frac{5}{4}}\beta_d m\omega_0^2 \tag{A.43}$$

where ω_0 is the natural frequency of oscillation of the particles.

Substituting the expression (A.43) in (A.42) the expression of the contact damping used in the code is obtained:

$$F_{ND} = -\sqrt{\frac{10}{3}}\beta_d\sqrt{k_N m^*}V \tag{A.44}$$

The ratio β_d between the applied damping and the critical damping is an input parameter in the code TRUBAL. This coefficient is related to the restitution

coefficient, e_n, which is the ratio between the rebound and the incident particle velocity. The relationship between β and e_n can be written as

$$ln e_n = -\frac{\beta_d \pi}{\sqrt{1-\beta_d^2}} \qquad \text{(A.45)}$$

and consequently the relationship between incident and rebound velocity is given by

$$V_r = V_0 e^{-\beta\pi/\sqrt{1-\beta^2}} \qquad \text{(A.46)}$$

A.6 Discussion and conclusions

The computer code TRUBAL is a sophisticated tool in the analysis of the elastic behaviour of solid particles under different types of loading due to the incorporation of models based on the Contact Mechanics.

The original code BALL was tested comparing the network of forces forming in a 2-D bed of particles with the results of photoelasticy of De Joselin De Jong (1971). The network of forces was quite similar in both cases but the comparison was purely qualitative. In this primary code the relationship between forces and deformations were assumed to be linear.

Later on the Hertz model of deformation of an elastic body in normal contact was incorporated in the code substituting the previous linear relationship between forces and displacements.

The model of Johnson, Kendall and Roberts (JKR) (Johnson *et al.*, 1971) for the case of normal contact of an elastic body in presence of adhesion was also added later by Thornton and co-workers. The theoretical model of Johnson *et al.* (1971) was validated comparing the deformation of rubber sphere against a flat rubber surface

and gelatine spheres against gelatine spheres, finding a good agreement between the model and the experimental results.

In the absence of adhesion Mindlin and Deresiewicz (1953) showed that the effect of a tangential force depends on the history of the loading process and on the initial loading. Thornton and Randall incorporated the model of Mindlin and Deresiewicz into TRUBAL. They validated the incorporation of the model into TRUBAL studying the dependency of the tangential force on the loading history. The curves obtained revealed a similarity between simulation data and the theoretical model of Mindlin and Deresiewicz (Thornton and Randall, 1988).

Savkoor and Briggs extended the JKR model to the case in which a tangential force is applied to the contact. They observed a reduction in the contact area when the tangential force was increased. They compared their model with the case of a rubber hemisphere pressed against a flat glass surface. The agreement between experiment and theory was good in a wide range of tangential forces. This model was added to the computer code TRUBAL by Thornton and co-workers.

As described above, in some cases the models of Contact Mechanics have been validated comparing the theoretical predictions with experimental results (Johnson *et al.* 1971, Savkoor and Briggs, 1977). This comparison provided a reliable base for predicting the behaviour of contacts between elastic particles. This, however, needs to be verified by careful comparison with experimental data which are accurately simulated by TRUBAL code.

APPENDIX B: ANALYSIS OF THE BREAKAGE OF CONTACTS OF AGGLOMERATES UPON IMPACT.

B.1 Theoretical approach

In the literature the relationship between interface energy and breakage of contacts has been analysed by the use of the Weber number (Kafui and Thornton, 1993). Weber Number is a dimensionless group, which is defined as

$$We = \frac{\rho D V^2}{\Gamma} \qquad \text{(B.1)}$$

where V is the impact velocity, ρ is the single particle density, D is the diameter of the primary particles that form the agglomerate and Γ is the interface energy. The interface energy for the case of agglomerates made of particles of the same material is 2γ, γ being the surface energy (Israelachvili, 1985).

The above analysis is however empirical and does not unify the simulation results. An alternative analysis is proposed here based on the energy required for breaking each contact.

The input kinetic energy immediately before impact is given by

$$E_K = N\frac{1}{2}mV^2 \qquad \text{(B.2)}$$

where m is the particle mass and V the impact velocity, and N is the number of particles in the agglomerate.

The work, W_C for breaking N_B contacts, assuming that all contact have the same contact area, is given approximately by

$$W_C = N_B \Gamma A_C \tag{B.3}$$

where A_C is the contact area.

Let us consider that the total energy required to break the bonds is proportional to the input kinetic energy

$$N_B \Gamma A_C = k \frac{1}{2} m V^2 N \tag{B.4}$$

where k is the proportionality factor. Rewriting the expression (B.4) as a function of particle density, ρ, and particle diameter D, and rearranging terms,

$$N_B = k \frac{1}{12} \pi N \frac{\rho D V^2}{\Gamma} \frac{D^2}{A} \tag{B.5}$$

According to Eq. B.5 the number of broken contacts after impact depends on the Weber Number $(\rho D V^2/\Gamma)$, the factor D^2/A and the number of particles in the system, N. However, the factor D^2/A depends on the interface energy and mechanical properties of the contact. Therefore, the dependency of the number of broken contacts on the interface energy is not fully determined by the exponent –1 on the interface energy in Eq. B.5.

Let us assume that the contact area is given by the JKR model. This is not strictly accurate since the model of Savkoor and Briggs (1977) is incorporated in the computational modelling. The model of Savkoor and Briggs (1977) establishes a reduction in size of the contact area when a tangential force is applied. The JKR model provides the following expression for the contact area radius, a, which can be expressed as a function of an effective force, P', and the pull-off force, $P_{OFF.}$,

$$a^3 = \left(\frac{3R^*}{4E^*}\right) P_{EFF} \tag{B.6}$$

$$P_{EFF} = P + 2P_{OFF} + (4PP_{OFF} + 4P_{OFF}^2)^{1/2} \tag{B.7}$$

$$P_{OFF} = \frac{3}{2}\pi\Gamma R^* \tag{B.8}$$

where R^* is the reduced radius, E^* the reduced elastic modulus, P the external load to which the particle is subjected, P_{OFF} is minus the force for breaking a contact and Γ the interface energy.

If we suppose that before impact there are no external forces acting in the contacts, the value of the external load, P, becomes zero and therefore the effective force, P', is equal to $4P_{OFF}$.

$$P_{EFF} = 4P_{OFF} \tag{B.9}$$

If the agglomerate is made of monodispersed particles R* = R/2 and if the particles correspond to the same material E* = E/2(1-ν^2), where ν is the Poisson's ratio. Therefore, the contact area, A, can be expressed as a function of the particle diameter and the interface energy.

$$A = \pi a^2 = \left(\frac{3}{4}\right)^{4/3} \pi^{5/3} (1-\nu^2)^{2/3} \left(\frac{D^{2/3}}{E}\Gamma\right)^{2/3} \tag{B.10}$$

Finally, if the value of the contact area A is introduced in the Eq. B.5. and the terms are rearranged, the number of broken contacts on impact can be expressed as:

$$N_B = k \frac{4^{1/3}}{3^{7/3}\pi^{2/3}} N \frac{1}{(1-\nu^2)^{2/3}} \frac{\rho D^{5/3} V^2}{\Gamma^{5/3}} E^{2/3} \tag{B.11}$$

The expression (B.11) relates the number of contacts broken in the agglomerate with the single particle properties (particle density, ρ, particle diameter, D, and particle elastic modulus, E), the interaction between particles, the agglomerate properties (Number of particles in the agglomerate, N) and the characteristics of the test (impact velocity V).

In order to obtain the damage ratio, it is necessary to relate the initial number of bonds in the assembly, N_0 to the number particles in the agglomerate. This can be done using the coordination number, Z:

$$N = \frac{2N_0}{Z} \tag{B.12}$$

Therefore, the expression B.11 can be rewritten in the form:

$$N_B = k\frac{2^{2/3}}{3^{7/3}\pi^{2/3}}\frac{2N_0}{Z}\frac{1}{(1-\nu^2)^{2/3}}\frac{\rho D^{5/3}V^2}{\Gamma^{5/3}}E^{2/3} \tag{B.13}$$

and damage ratio, which expresses the ratio between the number of broken contacts and initial number of bonds, can be given in the form

$$D_R = k\frac{2^{5/3}}{3^{7/3}\pi^{2/3}}\frac{1}{Z}\frac{1}{(1-\nu^2)^{2/3}}\frac{\rho D^{5/3}V^2}{\Gamma^{5/3}}E^{2/3} \tag{B.14}$$

Now it is possible to define a new dimensionless number that incorporates a new exponent for the dependency on the diameter of the primary particles, the elastic modulus and the interface energy.

$$W' = \frac{\rho D^{5/3}E^{2/3}V^2}{\Gamma^{5/3}} \tag{B.15}$$

According to Thornton this number can be written as a product of two primary numbers, the Weber Number, W, and the elastic adhesion index, I_e, which is defined as the ratio of elastic force to bonding force (Kafui and Thornton, 2000),

$$I_e = \left(\frac{ED}{\Gamma} \right) \tag{B.16}$$

Therefore the new dimensionless number adopts the form

$$W' = W_e I_e^{2/3} \tag{B.17}$$

This expression is still dimensionless and it expresses the ratio between the total input kinetic energy to the total energy used in bond breakage.

B.2 Simulation

Two agglomerates have been created and impacted in order to test the previous model. These agglomerates are made of 200 and 3000 single elastic particles whose elastic modulus is 31 GPa, density 2000 kg/m^3 and Poisson's ratio 0.3. The agglomerates are tested for the values of interface energy 0.35 J/m^2, 3.5 J/m^2 and 35.0 J/m^2.

B.3 Results

In Fig. B.1 the number of broken contacts is plotted as a function of impact velocity. The effects of impact velocity, interface energy and agglomerate size are clearly observed.

The number of broken contacts increases with the impact velocity. At low impact velocities the number of broken contacts increases linearly in the log-log plot

(Fig. B.1). At high impact velocities the number of broken contacts approaches asymptotically the maximum number of contacts in the assembly.

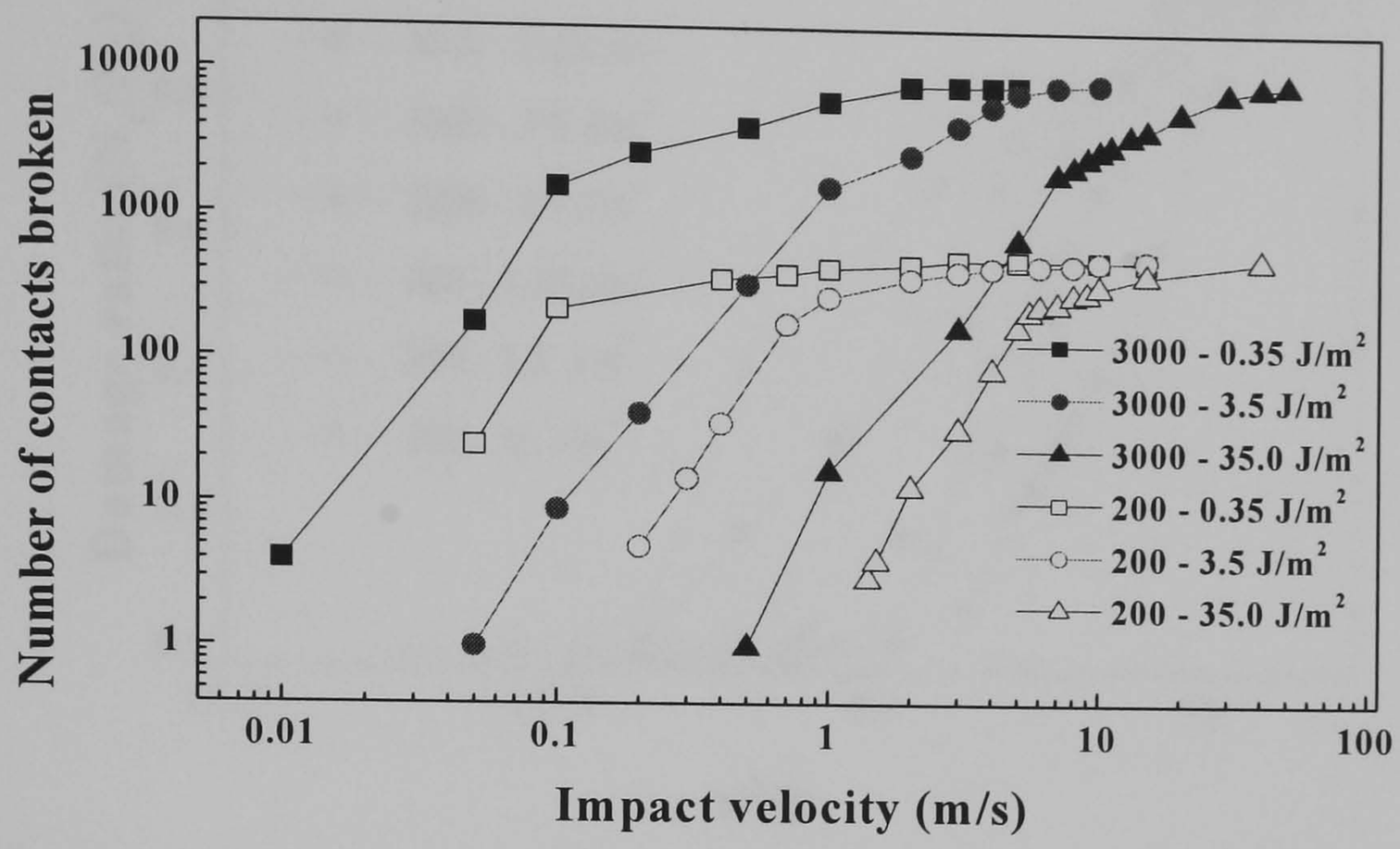

Figure B.1 Number of contacts broken versus impact velocity.

It is also observed that the number of broken contacts decreases when the interface energy increases. The increase in the interface energy of the bonds leads to the point that the work required for breaking a contact is larger. Therefore more input kinetic energy is necessary for breaking the contacts.

In Fig. B.2a, damage ratio is plotted as a function of the ratio V^2/Γ. This is equivalent to plot this as a function of the Weber Number defined in Eq. B.1 since density and particle diameter are constant for all cases presented here. Different authors have claimed that the different curves corresponding to different interface energies can be unified when damage ratio is plotted as a function of the Weber Number. However such unification of the results for different interface energies is not observed in Fig. B.2a.

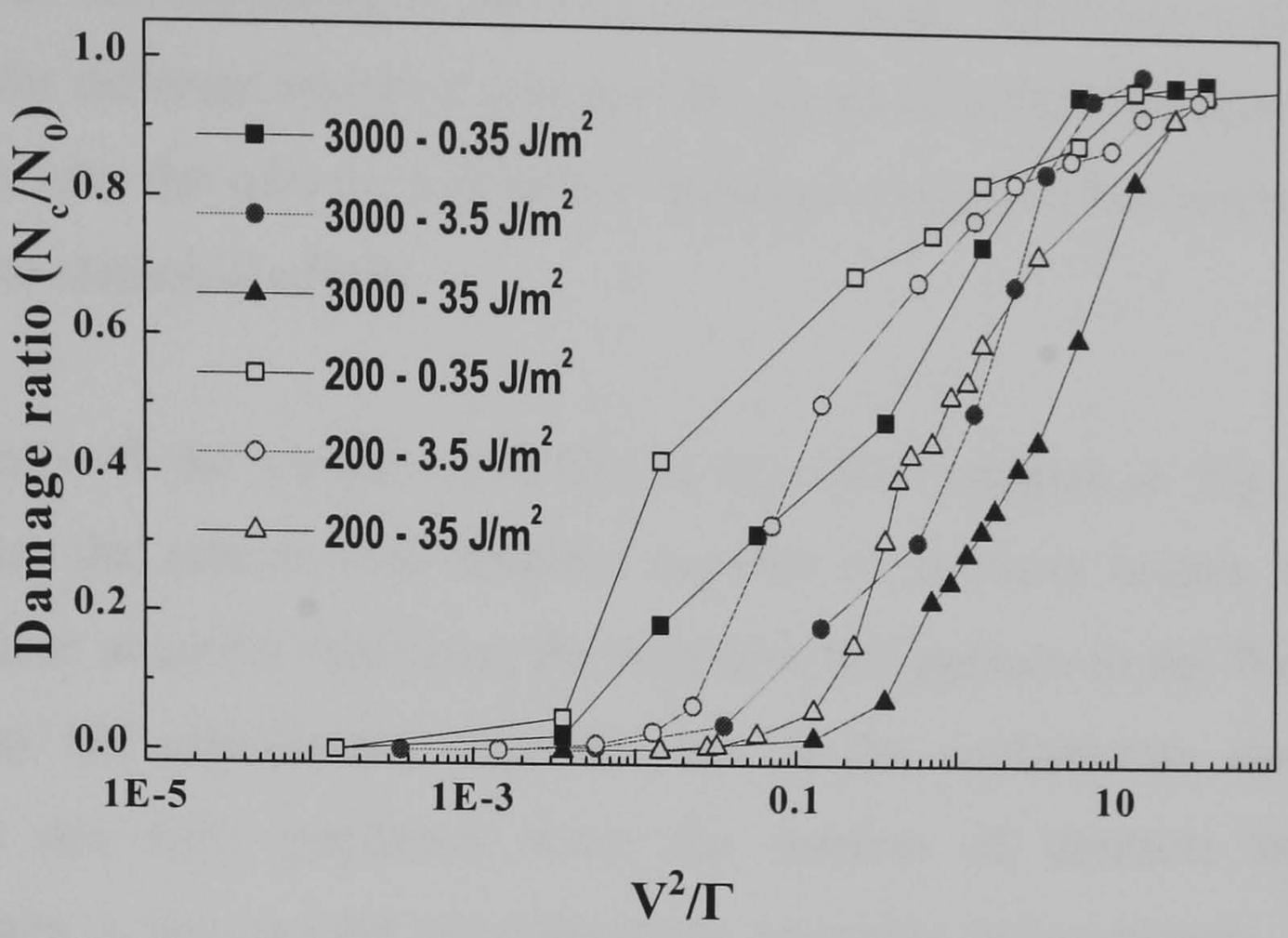

a)

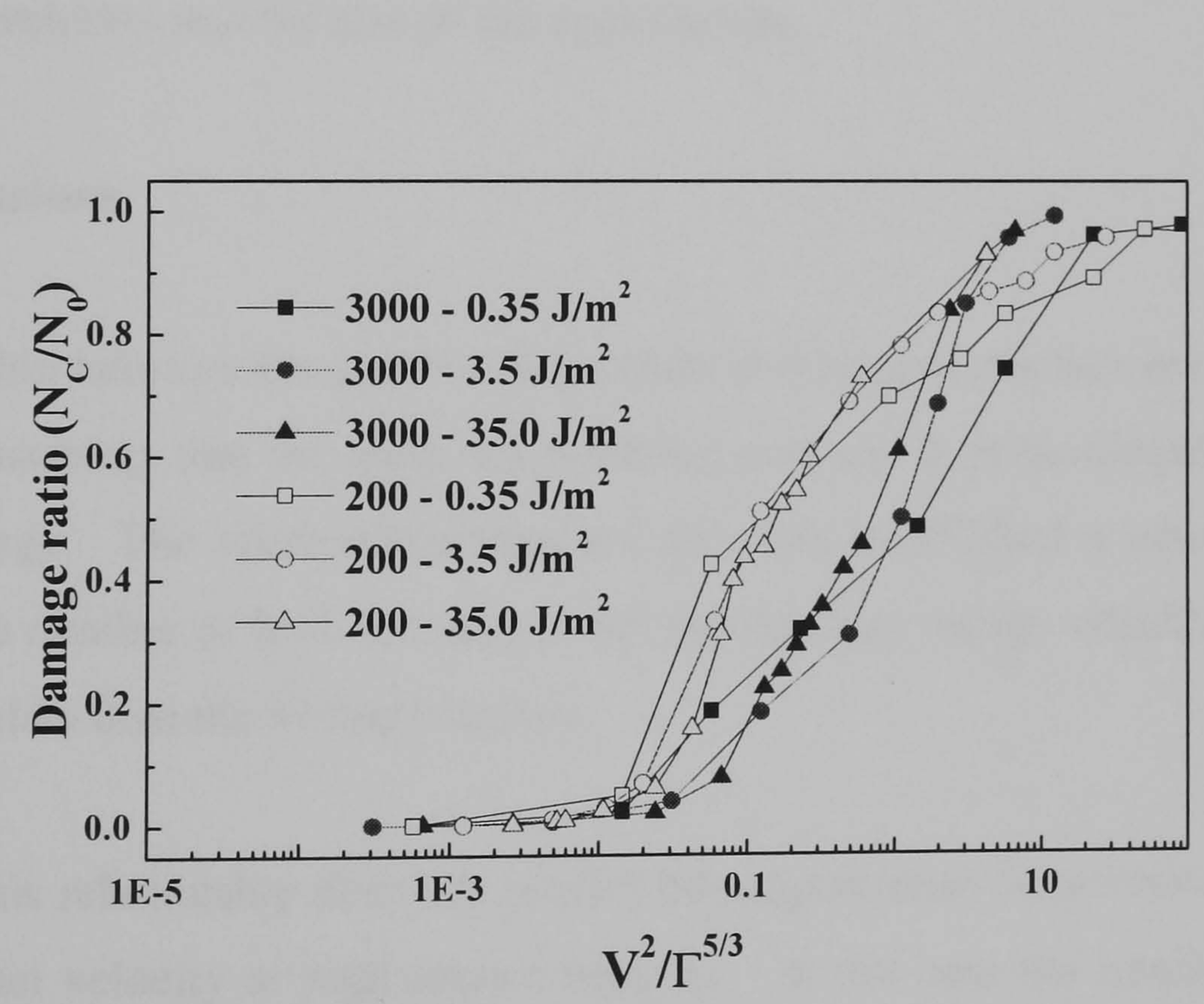

b)

Figure B.2 a) Damage ratio plotted as a function of V^2/Γ b) Damage ratio plotted as a function of $V^2/\Gamma^{5/3}$.

In Figure B.2b damage ratio is plotted as a function of the ratio $V^2/\Gamma^{5/3}$ reflecting the functional dependence as given by Eq. B.12. It is possible to distinguish the two sets of curves corresponding to the two different sizes. However within every set, the curves for different interface energies are closer to each other than in Fig. B.2a. The reasons why the curves of different interface energy do not overlap completely can be due to statistical effects.

The proximity of the curves for different interface energies in Fig. B.2b clearly suggests that the relationship between number of contacts broken and interface energy is more accurate than using the exponent that appears in the Weber Number. Nevertheless the relationship with the size of the agglomerate and the impact velocity is not fully predicted since the number of contacts broken trends asymptotically to the number of bonds in the assembly before impact. The previous observations also suggest that the proportionality factor k accompanying the input kinetic energy does not depend on the interface energy although it could depend on the impact velocity and the size of the agglomerate.

B.5 Conclusions

A relationship between the number of contacts broken and interface energy has been obtained assuming that the work for breaking contacts is proportional to the input kinetic energy. The relationship obtained here has established a new dependency between the number of broken contacts and the interface energy which fits better the simulation data than the Weber Number.

However this relationship does not predict the agglomerate behaviour as a function of the impact velocity at high impact velocity. In this case the number of broken contacts as a function of the impact velocity seems to trend asymptotically to the maximum number of contacts present in the assembly prior to impact. It is obviously due to the finite size of the agglomerate. In future this theory needs to be modified in order to account for the size of the agglomerate.